PREDICTING OLIGOCENE RESERVOIR POTENTIAL IN THE DEEP-WATER WESTERN NIGER DELTA: AN INTEGRATED BASIN MODELLING AND DIAGENETIC STUDY

Obinna Kingsley Chudi

Submitted for the degree of Doctor of Philosophy

Heriot-Watt University
Institute of Petroleum Engineering
The School of Energy, Geoscience, Infrastructure and Society

October 2015

ABSTRACT

This study presents a multidisciplinary integrated approach undertaken in predicting the reservoir potential of an untapped deeper Oligocene succession located offshore of the western Niger Delta. The shallower Miocene sands are known to have excellent reservoir quality with porosities exceeding 30 % and permeability in the Darcy range.

The study revealed a distinctive geometry in the deep marine depositional systems around mud diapirs. Unlike shallower Miocene reservoirs that are characterised by highly amalgamated channel systems, the Oligocene systems' depositional pattern shows a transition from a confined channel to a weakly confined lobate morphology, particularly when the channel system approaches depressions flanked by mud diapirs. High seismic reflection amplitudes suggest they are sand-rich and possibly hydrocarbon bearing.

SEM Photomicrographs reveal a rare presence of quartz overgrowth in the Middle Miocene interval that increases in volume to less than 3% in the Lower Miocene reservoirs, suggesting that the deeper Oligocene reservoirs that are buried under higher temperature conditions are likely to have significant quartz cement. Wireline log evaluation from the single well that penetrated part of the Oligocene succession supports this claim, with estimated reservoir properties, particularly porosity and permeability, being significantly lower in the Oligocene sands compared to the shallower Miocene reservoirs. Of the 7 units of Oligocene sands encountered in this well, 3 sand units are noted to be thin bedded, highly compacted with low porosity.

Results from basin modelling reveal that the Oligocene reservoirs have been subjected to maximum temperatures greater than 70˚ C from Early Miocene to present day and have had around 13 % of the pore space occluded by quartz cement. The results of this integrated approach suggest that the potential Oligocene reservoir within the vicinity of the study area is likely to have its reservoir quality partially compromised by quartz cementation. However, by considering the time of charge versus the time of significant quartz cementation, it is likely that no more than 7% of the Oligocene pore space is cemented. In all 4 modelled hydrocarbon accumulations, peak hydrocarbon saturation was attained between 15 and 8Ma, predating the onset of significant quartz cementation below 7Ma.

ACKNOWLEDGEMENT

I would be forever grateful to Almighty God for seeing me through, and providing all the necessary resources required during this phase of my life. My research would be meaningless without Him.

I am thankful to the Nigerian government under the auspices of the Petroleum Technology Development Fund (PTDF) for funding this research through her scholarship program. I would always be indebted to my great Country. The data used in this project was generously provided by Shell Nigeria (SNEPCO) and for that I am particularly thankful to the Chief geologist – Dan Agbaire, Chike Nwosu (now with Addax Nigeria), Leo Adoghe, Nnaemeka Umeh, Joel Asake, Tunde Adekambi and Chukwueke Njoku, for all their support, ensuring that I had requisite data and information needed at each phase of the research. Special thanks to Andy Bell of Shell Global Solutions International, The Hague, and Sadat Kolonic of Shell Petroleum Development Company (SPDC) Nigeria for their expert advice and reviews.

I am equally grateful to the staffs and authorities of Schlumberger Aachen and Aberdeen for their support and technical advice throughout the course of my work, particularly to Anthony Avu (now with EON), Thomas Hantschel, Daniel Palmowski, Nour Koronful, Cordelia Emeledoh, Jamie Bennett and Claire Jones.

I have gained knowledge that cannot be bought, skills I believe that can never be matched, ideas that have shaped not just my research and my ability to grasp technical concepts but also my disposition and drive for success in life. For this my erudite advisors Dr. Helen Lewis and Professor Dorrik Stow would always be remembered. Their expert guidance, their time and their understanding were invaluable throughout the duration of my study…THANK YOU SO MUCH. I would also like to appreciate Jim Buckman for assisting me tirelessly, willingly and timely with the petrographic aspect of my research – I am truly grateful. The computer support team, the staff admin team, the sweet ladies in the store, the graphic and media group, what would I have done without you all? You sure made life easy for me while studying, thank you. I would like to acknowledge colleagues and friends here in Heriot-Watt University- Mustapha Lamorde, Salako Olarinre, Simeon Agada, Dennis Obidegwu, Alessandro Mangione, Juan Li, Adel Taki, Salem Abdalah, Yiqun Zhang, Haitao Wang, Jiangchen Han, Saeed Ghanbari, Ibimina Esentia, and Antonio Zamarron. They all made my time

in Heriot-Watt enjoyable and stood by me with sweet words of encouragement even though sometimes they also needed to be encouraged!

My dearest family – my wife Patricia, my kids Ivanna, Asher and Neriyah, their love kept me going, their support kept me standing in these 3yrs. I am so glad that I have you all. Finally to my father Chief Nelson Chudi and mother Gladys Chudi – this is what you've always wished for, this is what you've always want me to be…God bless you.

RESEARCH THESIS SUBMISSION FORM

TABLE OF CONTENT

CHAPTER 1

INTRODUCTION

1.1 Introduction to the Thesis

Today's success in hydrocarbon exploration and production is largely attributed to the discoveries made from rocks with good reservoir quality. Reservoir quality here is particularly linked to the measure of pore volume (porosity) that controls the storage capacity of the rocks and pore network (permeability) that dictates the transmissibility of fluid within the rocks themselves and into a wellbore. The quest by scientists to understand how porosity and permeability are distributed in potential reservoir rocks has led to a plethora of research work centred on predicting reservoir quality (Bjørkum et al., 1998, Lander and Walderhaug, 1999, Walderhaug, 1994, Walderhaug, 2000, Taylor et al., 2010, Taylor, 1950, Athy, 1930, Bloch et al., 2002, Rosales and Perez-Garcia, 2010, Schmoker and Gautier, 1988, Ajdukiewicz and Larese, 2012) that stems from early porosity depth trends to recent numerical models. These simulate diagenesis mostly in sandstone reservoirs in which quantitative evaluations of diagenetic processes are considered when constructing quantitative forward models for reliable predictions (Brenner et al., 1991).

Investigating the risk of loss of reservoir quality is principally important for prospects or plays that have as their target reservoirs buried at depth with temperatures above 70^{o} C or those under extreme vertical stress conditions capable of compromising the porosity and permeability of the reservoirs (Taylor et al., 2010). This has become extremely relevant in deep-water exploration where the presence of seismic bright spots forms a significant basis upon which exploration decisions are made. Where successful, these may result in huge hydrocarbon discoveries in relatively shallow reservoirs. However, with increase in burial depth leading to progressive diagenesis and porosity reduction, the acoustic properties of potential sandstone reservoirs are significantly affected so that proper differentiation, for example between reservoir rocks with different fluid types, could be problematic (Taylor et al., 2010). This factor, coupled with the attenuation of seismic signal with depth, downplays the use of seismic signatures for evaluating reservoir quality and finding potential exploration targets at great depths. Hence the need for various techniques that can be integrated to yield a more reliable outcome and

lead to a reduction in the uncertainty gap in reservoir quality prediction in deeper, hotter and more challenging plays.

This thesis presents an integrated workflow in reservoir quality prediction for Niger Delta deep-water sandstones with emphasis on the unexplored, poorly understood Oligocene succession. The study area is situated in the mid to lower slope region of the basin. Present day hydrocarbon exploration has been centred in the Miocene to younger sedimentary sequence that lies at depths of less than 2500m below sea-floor and temperatures of less than 80˚ C, while the deeper sequence remains untapped with little work done in understanding their reservoir potentials.

1.2 Aims and Objectives

Pertinent questions that this research and thesis aim to address and that underpin the key objectives of the study include the following:

1- **What is the depositional style of the Oligocene succession?**

   Understanding the depositional architecture is fundamental to assessing play potential and distribution of reservoir facies (Posamentier and Kolla, 2003). This is particularly important in deep-water hydrocarbon exploration and production where depositional style dictates the development philosophy adopted during the hydrocarbon production phase. In this study, assessing the depositional architecture is achieved by using a high resolution 3D seismic volume calibrated with well logs. These are made more challenging as coverage of the well logs only extends to the Miocene sequence and only a single well, herein referred to as “Well A1” that reached just below the top of the Oligocene.

2- **How does the burial history in this area affect reservoir quality across the region?**

   The degree of quartz diagenesis for the objective Oligocene sandstone is assessed by considering: (1) the interplay between burial history and thermal regime; and (2) the thermal conductivity of the sediments and heat flow in relation to some geologically consistent assumptions. From 2D burial history, the temperature history can be inferred as a time dependent variable; both burial and thermal histories are major controls on diagenetic reaction kinetics. A plot

of temperature versus time is then compared with a time-temperature integral for quartz precipitation to deduce at what stage in the burial history of the Oligocene they were exposed to sufficient time and thermal energy to achieve a given degree of quartz cementation.

3- Is overpressure important in this context?

The hypothesis that preservation of porosity occurs under significant overpressure conditions arising from compaction disequilibrium, where high pore fluid pressure reduces the vertical effective stress (VES) that can normally lead to intense grain to grain contact, is suggested as an important factor in the maintenance of reservoir quality, particularly in sandstones (Athy, 1930, Lundegard, 1992, Taylor et al., 2010). However, where sediments have been subjected to high temperatures conducive for diagenetic reaction (eg. Quartz cementation) prior to the development over pressure, then this process may not adequately preserve porosity. This concept is considered here by comparing time-temperature plots and time-pressure plots for the Oligocene reservoir. With a present day burial depth of the Oligocene sequence within a depth window of possible overpressure, is it then possible that the Oligocene sediments were overpressured prior to being exposed to temperatures suitable for quartz cementation?

4- Can a multi-technique approach be developed to address the above questions?

Four techniques are been considered in this thesis: (a) 3D seismic interpretation is used both for assessing the depositional architecture and for predicting reservoir presence; (b) advanced petrophysical evaluation where suites of well logs are used as input to estimate volumetric composition of rock minerals across the logged interval so that some level of prediction can be made beyond the logged section; (c) high resolution petrographic analysis based on SEM and optical microscopy which are used to differentiate detrital from authigenic minerals through the Miocene succession, where samples exist, and the use of these data to infer possible conditions in the Oligocene section where no cores or samples have been acquired; and (d) development of a 2D basin model that is

adopted to understand the burial and cementation history of the study area leading to a prediction of the present reservoir quality of the Oligocene potential reservoirs. The results from (c) above are used to aid in calibrating the 2D basin model.

5- **Has this approach worked elsewhere in the world for other deep-water systems?**

The integration of all four techniques that results in a holistic outcome is believed to represent a novel approach. An individual technique by itself or a combination of any two of the techniques has been applied in reservoir quality prediction across various tectonic settings and depositional environments. For example burial history has been used based on time-depth index (TDI) to understand the porosity evolution of sandstone reservoirs along the Brazilian continental margin (onshore and onshore) (Sombra and Chang, 1997). Walderhaug (2000) modelled quartz cementation and porosity of the Brent Group Sandstones offshore Norway by integrating temperature history and petrographic parameters from experimental measurements. Seismic attributes are commonly utilized in reservoir prediction, particularly in deciphering reservoir presence (Ahmad and Rowell, 2012, Chopra and Marfurt, 2008). Quantitative use of seismic attributes requires seismic inversion technology and good well control (Pennington et al., 2002, Brown, 2011).

6- **Based on the answers to the above questions can we confidently confirm the likelihood of a new exploration play offshore Niger Delta below the proven Miocene plays?**

If this is proven then it would represent a significant new play that is likely to extend beyond the study area across the western offshore Niger Delta.

1.3 Thesis Layout

This thesis is presented in nine chapters of which 3 chapters form a series of 3 papers, each at a different stage of review to acceptance. These present the principal results of the techniques adopted in resolving the Oligocene as a potential exploration play offshore Niger Delta.

The thesis opens with this introduction chapter (Chapter 1) that sets the scene of the research – the theme, the objectives and overall rationale. Chapter 2 outlines the techniques used and the data base available for this study. Chapter 3 presents the regional geological setting of the area, including general stratigraphy and basin architecture. Sedimentological analysis from interpreted cores and an outline of the main petrophysical evaluation workflows are documented in chapter 4. Chapters 5 to 7 contain the 3 papers which make up a significant part of the thesis. These papers which are linked with a short introduction and summary represent the main techniques adopted in the research and their corresponding results. Chapter 8 contains a detailed discussion that seeks to synthesis the results from previous chapters and puts these findings into a global context. Finally, the conclusion and recommended future work are outlined in the last chapter – Chapter 9. This chapter is followed by conference proceedings and references.

Since the thesis is presented as a series of separate publications, there is some unavoidable duplication particularly related to data collection, the study area, figures and background aims and objectives. All bibliographic references have been removed from these publications and unified into the reference section of this thesis.

CHAPTER 2

DATABASE AND METHODOLOGY

2.1 Introduction

This chapter describes the techniques utilized in the study of deep-water Oligocene sediments of the Niger Delta (Figure 2.1). The techniques represent data analysis at different vertical and horizontal resolution, including: 3D seismic interpretation, petrographic analysis of samples acquired from cores, petrophysical evaluation from well logs and 2D basin and petroleum system modelling. Integrating the results into a better understanding of the Oligocene system is crucial since all this information increases confidence in the resulting predictions and models.

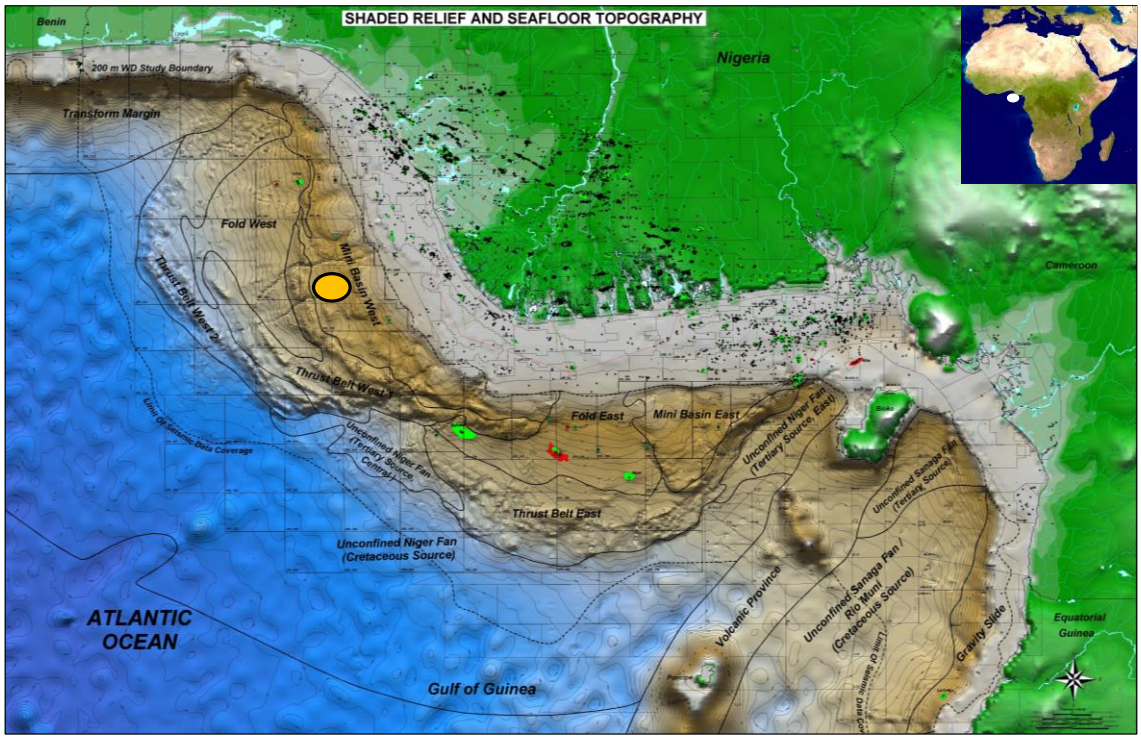

Figure 2.1: Niger delta map showing shaded relief and sea-floor topography. Study area depicted in amber circle (courtesy of Shell Nigeria).

2.2 Seismic Data

Information derived from seismic data is constrained by its vertical resolution. In general it is not possible to resolve formation thickness to less than 10m (Badley, 1985), although this resolution varies as a function of the seismic frequency and the velocity of the rock being investigated. The 3D seismic data utilized in this study covers a 770km^2

(297mi^2) area within the mid to lower continental slope of the study area. The data showcases the structure and stratigraphy within a 6s two way time (TWT) window with crosslines spaced at 12.5m interval and inlines every 25m. The dominant frequency of this survey is 22Hz although the overall frequency ranges from 7-75Hz. The data has been processed as a zero phase wavelet with a negative polarity displayed as a trough that characterises an increase in acoustic impedance.

Three key surfaces were mapped across the seismic volume: the top of the Mid-Miocene, characterised by a strong reflector, and two surfaces within the Oligocene interval – Oligocene-shallow and Oligocene-deep (Figure 2.2). Oligocene-shallow was mapped across a strong reflector representing the top of Oligocene penetrated by well A1, while Oligocene-deep was mapped below the well TD. 3D seismic attribute analysis was used as a key interpretation tool. Root mean square (RMS) and Spectral decomposition-RGB (red green blue) were used for geomorphological studies whereas the Sweetness attribute was adopted for predicting reservoir presence and fluid typing. The choice of these attributes was largely based on the success achieved in their application across other basins and depositional settings (Partyka et al., 1999, Hart, 2008, Ahmad and Rowell, 2012, Dmitrieva et al., 2012). The attributes were applied as interval based attributes. That involves calculating average attribute values over a time window referenced from an interpreted horizon. Since only one well penetrated the Oligocene, interpretation from the Mid-Miocene interval served as an analogue for the Oligocene considering that the Mid-Miocene interpretation was calibrated with good well control. Seismic interpretation was achieved using Petrel^{TM} software package and the results are presented in Chapter 5.

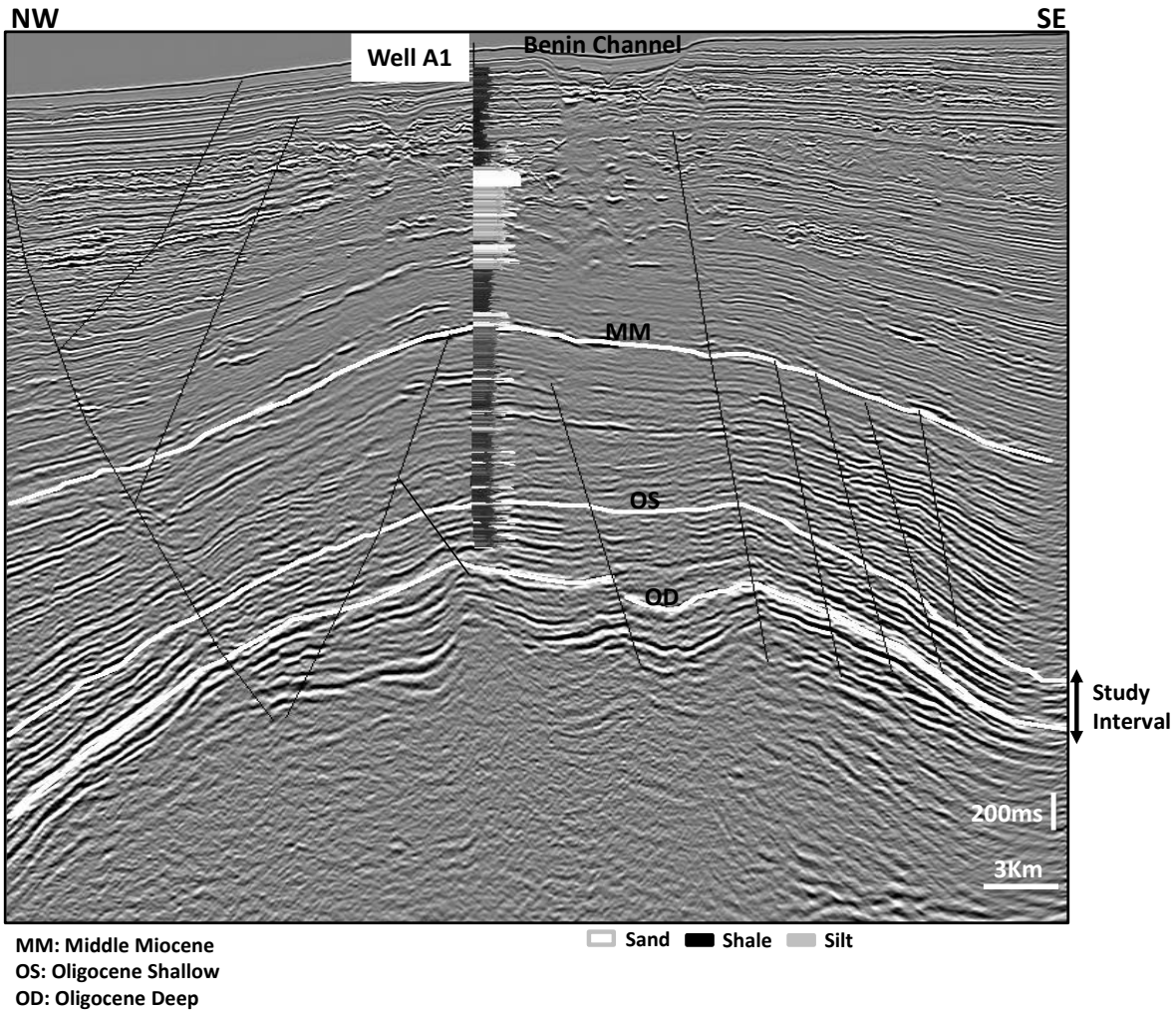

Figure 2.2: Seismic cross-section taken across the study area showing the mapped horizons and interpreted faults (further discussed in chapter 5).

2.3 Petrography

Petrographic analysis was conducted on 17 samples acquired from four wells in the study area. The cored samples were taken within the Miocene interval from Middle Miocene at a depth of 2470m and lower Miocene at 3450m. Samples taken from depths shallower than 3000m were unconsolidated sands. The samples inspected were made into thin-sections and polished blocks.

Techniques used included optical microscopy and Scanning Electron Microscopy (SEM) using Back Scattered Electron imaging (BSE), Cathodoluminescence (CL) analysis and Energy-dispersive X-ray spectroscopy (EDX). Due to the poorly consolidated nature of most of the samples (excluding the Lower Miocene samples),

they were not suited for polished thin-sections; therefore thin-sections with cover slips were made. The samples were dried at 38^{O}C and bulk impregnated under vacuum with epoxy resin to stabilise the samples. Ultraviolet glue was further applied to mount cover slips. For the purpose of SEM studies, samples were also made into polished blocks, drying at 38^{O} C and placing in a 25/30mm diameter mould. The granular samples were filled with epoxy resin, mixed by stirring and placed under vacuum to remove air bubbles.

Optical microscopy was used for mineralogical identification and where optical identification of overgrowths was difficult, SEM was used. Cathodoluminescence (CL) analyses were carried out on the SEM with a Centaurus CL detector. BSE and CL combined analysis was based on the method outlined by Evans et al. (1994) which involves the analysis of pairs of BSE and CL images from polished block samples. A set of 13 samples were selected for analysis. Cathodoluminescence is particularly useful in distinguishing detrital quartz grains from syntaxial quartz overgrowths. SEM analysis was carried out for both the Middle and Lower Miocene intervals to investigate the likely presence of microcrystalline quartz or chlorite rims, as these are likely to impede the nucleation of quartz overgrowth (Bloch et al., 2002, Marchand et al., 2002, Taylor et al., 2010). Chapters 4 and 7 of this thesis showcase the results from the petrographic study and how it ties with petrophysical and basin modelling predictions. The EDX technique was used to investigate the elemental analysis of the Miocene samples. This technology relies on the response to X-rays of the individual elements contained in the rock minerals where unique minerals are excited at different levels so that unique set of peaks are produced on the X-ray emission spectrum (Goldstein et al., 1981).

2.4 Petrophysical Analysis

Wireline log data acquired within the study location were analysed to characterise the porosity and permeability of the reservoir zones penetrated. Of more than 30 wells drilled in the study area, only one well (Well A1) penetrated the Oligocene interval. The density log was used to calculate porosity and these values were calibrated against core porosity where it was available. Permeability was estimated using the neural network technique, where sets of input logs (Gamma ray, sonic, density and neutron logs) were

trained to recognise the core derived, stress corrected air permeability, acquired from routine core analysis (Sonde et al., 2011).

A multi-mineral model based on petrophysical elemental analysis (ELAN) of open-hole logs was used to compute the volume of mineralogical components within the interval of interest. ELAN uses log curves and the response parameters of the tools to compute volumetric constituents of formation minerals and fluid. This method derives the relative quantities, or relative volumes, of the mineral components that would most probably produce the set of measurements recorded by the logging instruments. So, there is a three way triangular relationship among tools (T), response parameters (R) and formation component volume (V). This is well-illustrated in Chapter 7. Given the data represented by any two corners of the triangle the third can be determined. In this study, T and R are used to compute V. For quality control, forward modelling of R and V are used to reconstruct T – the input logs. The reconstructed logs are compared against the input data to determine the quality of the volume results. Four principal minerals (quartz, feldspar, mica and kaolinite) were modelled in ELAN based on their abundances determined in the petrographic study. All petrophysical evaluation conducted in this study was carried out on Techlog^{TM} software package.

2.5 Basin Modelling

Basin modelling is a technique that has been developed since the early 1980's to study the burial and thermal history of a basin, particularly in relation to hydrocarbon generation, expulsion, migration, accumulation and preservation (Welte and Yalcin, 1988b, Wygrala, 1988, Hermanrud, 1993, Underdown and Redfern, 2008). This technique has also been adopted to study diagenetic evolution and its impact on reservoir quality, particularly porosity (Sombra and Chang, 1997, Walderhaug, 2000). Diagenetic reactions are related to burial history with the influence of fluid, stress and temperature changes (Siever, 1983), which ultimately control reaction rates like the transformation of organic matter to hydrocarbon and quartz precipitation from a silica rich fluid. Before the 1980's Arthy's compaction models and similar models are used to relate sediment compaction to porosity (Lundegard, 1992, Paxton et al., 2002), although these are not able to accommodate the effect of porosity loss due to cementation. Other methods that were later adopted, related models of basin history and paleogeotherms

from heat flow model to the temperatures of diagenetic reactions (Siever 1983); inferring temperatures from petrographic study of fluid inclusion, particularly chemical composition and isotopic signatures, (Taylor, 1950, Marchand et al., 2002, Wilkinson et al., 2004) and utilizing time-depth index (TDI) to quantify empirically the influence of burial history on the evolution of sandstone porosity (Sombra and Chang 1997).

Chapter 7 illustrates the integration of basin modelling with petrophysical and petrographic analysis to construct forward models by taking into account quantitative evaluations of diagenetic processes in order to make reliable diagenetic predictions. Of importance is the understanding of the type of diagenetic reactions prevalent in the study area, where they take place and when these reactions occur during the history of the basin. Chapter 6 investigates, using the basin modelling technique, the charge evolution of the Oligocene sediments. In addition, the timing of hydrocarbon charge relative to the time of diagenetic processes, particularly quartz cementation, is also considered. This is borne from the widely accepted concept that early hydrocarbon emplacement in a reservoir can potentially stop or slow down the rate of quartz precipitation thereby preserving porosity (Bloch et al., 2002, Taylor et al., 2010).

In this study, basin modelling was performed using PetroMod^{TM} software which is based on the interpreted 2D seismic line provided by Shell Nigeria (SNEPCO). The 2D transect runs NE-SW for over 160km across the extensional, translational and compressional parts of the Niger Delta basin (Bilotti and Shaw, 2005, Corredor et al., 2005, Deptuck et al., 2007). A one dimensional basin model of Well A1 was constructed for calibration purposes and a 2D model was constructed for analysis and predictive purposes. The progradational characters of the sediment were subdivided into chronostratigraphic units which were further subdivided into discrete layers controlled by well information. A total of seven chronostratigraphic horizons that included the Sea-floor, Lower Pliocene, Upper Miocene, Mid-Miocene, Lower Miocene, Oligocene and Basement were originally interpreted by Shell Nigeria and were subsequently digitized during this study. Each of these horizons were divided into lithologic units using the deepest well in the study area. The lithology was assumed to be laterally continuous updip and downdip from the well location. This was a key assumption that was considered whilst building the model. However, sensitivity analysis was carried out

to assess the impact of lateral variation in facies on predicted cement volume. In addition to the present-day geometry from the 2D line, other basic data requirements for modelling include boundary conditions, calibration data (corrected bottom-hole temperature – BHT, vitrinite reflectance, reservoir pressure, porosity and present-day hydrocarbon accumulation), stratigraphy, rock lithologies and source rock properties, particularly the kinetic parameters that are responsible for the type and amount of generated hydrocarbon. Interpreted faults on the 2D transect were also digitized in the model, with priority given to the most important faults that are likely to have a significant impact on hydrocarbon migration. The selection of these faults was based on the criteria outlined by Derks et al. (2012) which include the following:

a) Regional faults that extend over a great distance cutting across most of the horizons, most especially faults that connect deep seated source rocks to shallow reservoirs.
b) Where two or more faults are parallel to each other and cutting the same horizons, then a representative fault is selected.
c) Faults that are continued by other faults are merged.

Sensitivity analysis was done on the fault property to evaluate the importance of fault behaviour on fluid flow; however, an open fault system was considered as the most preferred since modelled hydrocarbon accumulation matched present day observation only when faults are open.

2.6 Limitations

The target deep-water Oligocene sediments are buried deeper than the Miocene play, generally in the range of 600 – 2000m deep and even deeper in some cases. Similar observation is noted from the seismic volume used in the study that indicates the Oligocene interval is more than two seconds (2secs) deeper than the Miocene reservoirs. The effect of burial depth on quality of data is seen to significantly affect seismic resolution, mostly its vertical resolution. Unfortunately, both seismic frequency and velocity display changes with depth that causes a gradual decrease in resolution (Badley, 1985). Velocity tends to increase with depth in response to compaction and cementation while frequency typically decreases as the seismic waves gets attenuated with depth, mostly the higher frequencies are more prone to attenuation than the lower

ones. Hence, it is likely that with an increase in burial depth of the Oligocene sediments across the study area, vertical and lateral resolution of the seismic signatures decreases thereby resulting in interference of seismic waves across bed boundaries. Interference, relates in the overlap of reflectors from closely spaced acoustic impedance boundaries due to the seismic pulse being longer than the separation between 'bed' boundaries. The seismic pulse length is noted to increase with depth as the frequencies become lower. Lower frequency makes it less likely that a bed thickness will exceed the usually one-quarter minimum wavelength required for top and base of the bed to be resolvable (Badley 1985).

The paucity of data available for both petrographic and petrophysical assessment of the Oligocene is a major challenge in the study. Some of the samples used for petrographic inspection were loose unconsolidated sands. Others were partially consolidated. Samples were only available from 4 wells in the Miocene succession. Unconsolidated sands makes it impossible to assess porosity in thin section. In addition, the data from only four wells might not be representative of the reservoir properties across the entire study area and particularly not sufficient to establish a detailed pre-drill facies model for the Oligocene sequence.

The basin modelling approach adopted in this study heavily relied on a single 2D seismic line. This would likely not honour the entire three dimensional geology of the area in both space and time. In addition model calibration was based on measured data primarily from a single well location which is subject to both systematic and random errors. Furthermore significant uncertainties exist in the facies definition that relied only on this one well so that away from the well, the spatial distribution of the facies and facies properties were assumed. Source rock properties that were used for the charge modelling aspect of this work were literature sourced with no source rock sample available or source rock geochemical analysis undertaken to support the model construction. This has the potential of not capturing the spatial variation in source rock organo-facies and of using properties that are not fully representative of the source rock present in the study area.

This study considers quartz cement as the main porosity occluding diagenetic mineral and it is the only cementation process that can be directly modelled in PetroMod^{TM}

software. No attempt was made to model the occurrence of non-quartz cement. The occurrence of non-quartz cement, however, can reduce the abundance of quartz cement by reducing the available pore space and by subsequently decreasing the net rate of quartz cementation through a reduction of the available surface area (Lander and Walderhaug, 1999). The software used in the study also treats the major porosity dependent processes such as compaction, hydrocarbon charge, cementation and overpressure as independent simulations, for which the various algorithms controlling the numerical simulation of each of these processes are not interwoven. Hence the net effect of one process, say early hydrocarbon charge, over another process, say quartz cementation is not fully considered by the software.

2.7 Alternative Prediction Methods and Justification for Current Approach

Reservoir quality prediction methods are considered to fall within two groups: (1) effect-oriented models, and (2) process-oriented models (Wood and Bryrnes (1994). Effect-oriented models are related to an established statistical relationship between porosity and other variables, for example the degree of clay coating. Such models are well suited to predicting porosity in sandstones with less than 10% cement but breaks down for higher cement percentages (Lander and Walderhaug, 1999). In addition this model is at its best where samples that share similar characteristics such as geological setting, depositional environment, and sand composition are present as calibration parameters. This implies that in frontier settings where no data exist or in deeper intervals outside the depth range of the calibration parameters, this model would not be applicable.

The second group are process-driven models, such as geochemical reaction-path models that are controlled by the kinetics and thermodynamics of rock minerals, aqueous fluid and gases. This approach uses first principles in simulating diagenetic reactions and therefore is considered to produce a better prediction than the effect-oriented process. However, this approach fails to distinguish detrital from authigenic minerals so that comparing prediction with thin section results poses significant challenges (Lander and Walderhaug 1999). Another setback of this method is implementing the right kinetic and thermodynamic models where significant uncertainties exist, particularly as the kinetic models used are based on laboratory-based experimental analysis that might not reflect true subsurface temperature and pressure conditions.

Further to the two distinct methods highlighted above, Tobin (1997) showed how surface outcrop samples can be used to predict subsurface reservoir quality especially in frontier exploration areas that are typically starved of subsurface data. Outcrop data is believed to provide a unique opportunity for observing surface structural features, lateral bedding and facies variations, and three dimensional spatial configurations of these parameters that are less observable in the subsurface (Tobin 1997). Although the use of outcrop in predicting porosity or permeability is posed with significant uncertainties such as: (1) reservoirs rocks exposed at the surface may have been subjected to varying burial and tectonic history different from their subsurface equivalents, which implies that the resulting paragenetic sequence and porosity-permeability evolution for the outcrop data could be different from the subsurface counterpart; (2) The outcrops are prone to recent diagenetic processes, such as leaching and would therefore produce reservoir qualities that are not comparable to those in the subsurface; and (3) both sets of data may have different rock provenance.

The method adopted in this research synthesizes both the effect-oriented and process-driven methods. Even though the software used (PetroMod^{TM}) does not consider a first principle approach in simulating quartz diagenesis, it does utilise a process algorithm with input parameters that have been empirically calibrated to data sets. In addition, the software through simulation predicts compaction and cementation related variables that can be directly compared with results from both petrographic analysis of thin sections and petrophysical evaluation of well logs, so that the predictive accuracy of the simulation results can be easily assessed. A similar approach has been used in the Exemplar^{TM} software for modelling quartz cementation (Lander and Walderhaug, 1999, Walderhaug, 2000). However unlike the Exemplar^{TM} software which is strictly designed for modelling diagenesis (Walderhaug, 2000, Walderhaug et al., 2009), PetroMod^{TM} software is mainly a basin and petroleum system modelling tool. Exemplar^{TM} relies on thermal and burial history data as input parameters, whereas the cementation model in PetroMod^{TM} directly applies the burial and thermal history that is simulated concurrently with its inbuilt cementation simulation process. The integration of both processes in PetroMod^{TM} saves computational time thereby permitting predictive uncertainty scenarios to be efficiently and rigorously evaluated.

CHAPTER 3

REGIONAL SETTING, BASIN EVOLUTION AND TECTONICS

3.1 Regional Setting of the Niger Delta

The Niger Delta is one of the seven sedimentary basins in Nigeria, located in the southern part of the country in the gulf of Guinea (Figure 3.1) and extending more than 300km from apex to mouth (Doust and Omatsola, 1990). The delta owes its development to the separation of Africa and South America in the Late Mesozoic along a series of rift zones that met in a triple junction. The triple junction is located in the area of the present Gulf of Guinea that is now occupied by the Niger Delta (Stoneley, 1966, Burke et al., 1971, Tuttle et al., 1999). True delta development started in the Palaeocene-Eocene when sediments began building outward onto the continental-oceanic lithospheric transition zone and by Oligocene time the delta had spread over a cooling oceanic crust and buried much of the triple junction. Characterised as a regressive sequence of clastic sediments developed in a series of offlap cycles (Doust and Omatsola 1990), the total thickness of the sediments in the delta is about 12km at the basin centre. The Niger delta has prograded into the Gulf of Guinea at an increasing rate controlled by basement subsidence, eustatic sea level changes and evolving drainage area (Whiteman, 1982).

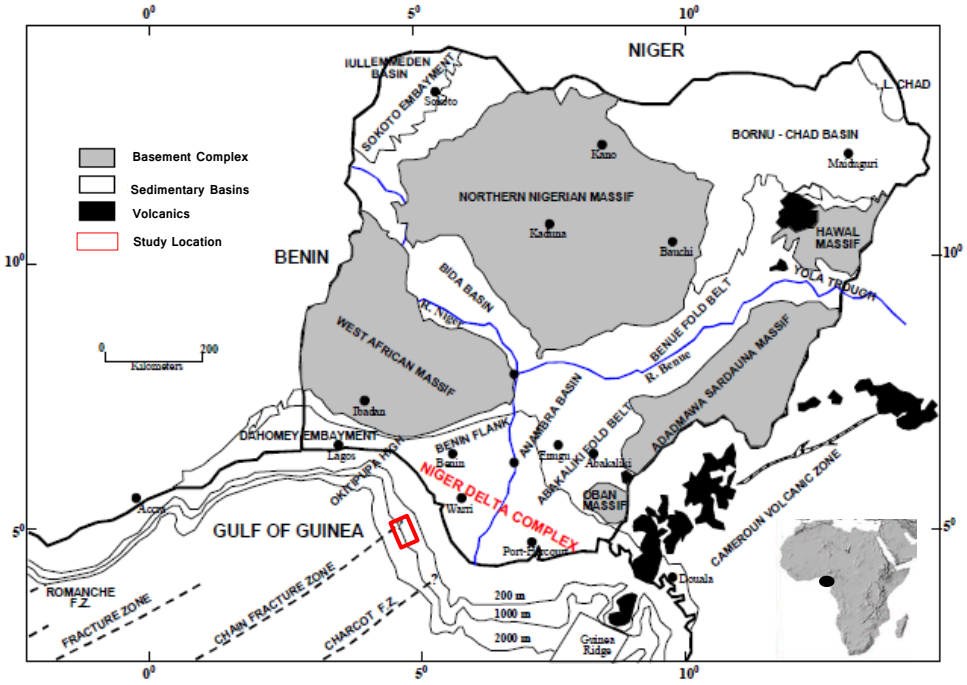

Figure 3.1: Sketch of Nigeria map showing the Niger Delta basin in relation to other sedimentary basins (modified afterAdeogba, 2003). The basin is bounded to the north by the Abakaliki fold belt, to the east by the Okitipupa high that separates it from the Dahomey Embayment and to the east by Cameroon volcanics. The basin's influence extends southward and offshore toward the abyssal plain. The study area is shown in red box.

The morphology of the delta is one of convex-to-the-sea pattern which developed through rapid progradation from Eocene time and a marked increase in sediment input from the Oligocene. It has been classed as a wave and tidal dominated delta, appearing constructive in the centre and destructive at the flanks (Galloway, 1975). The Niger delta overall is divided into six depositional belts, also known as depobelts, that are separated by major synsedimentary faults. These include: the Northern Delta, Greater Ughelli, Central Swamp I, Central Swamp II, Coastal Swamp I and II and Offshore (Doust and Omatsola 1990) (Figure 3.2). The oldest is the Northern Delta while the Offshore depobelt is the youngest. These depobelts are regarded as transient basinal areas that succeeded one another in a punctuated fashion in space and time as the delta built southwards. The development of each depobelt reflects a broad change in tectonic style. On the basis of this distinct tectonic feature, the depobelts have been classified into three groups: (1) Delta Edge - a zone underlain by shallow basement and containing the oldest growth faults that are regularly spaced. This is seen in the

Northern Delta depobelt; (2) Central Delta - the Greater Ughelli and the Central Swamp depobelts fall in this category that is characterised by south dipping rollover structures and associated growth faults; and (3) Distal Delta - a zone that cuts across the Coastal Swamp and Offshore depobelts is noted to have large complex structure that include but not limited to mud diapirs and collapsed crests faults. The interplay of sedimentation, subsidence and growth faulting is largely responsible for the development of these depositional belts. All of these depobelts are currently regions with significant hydrocarbon accumulation.

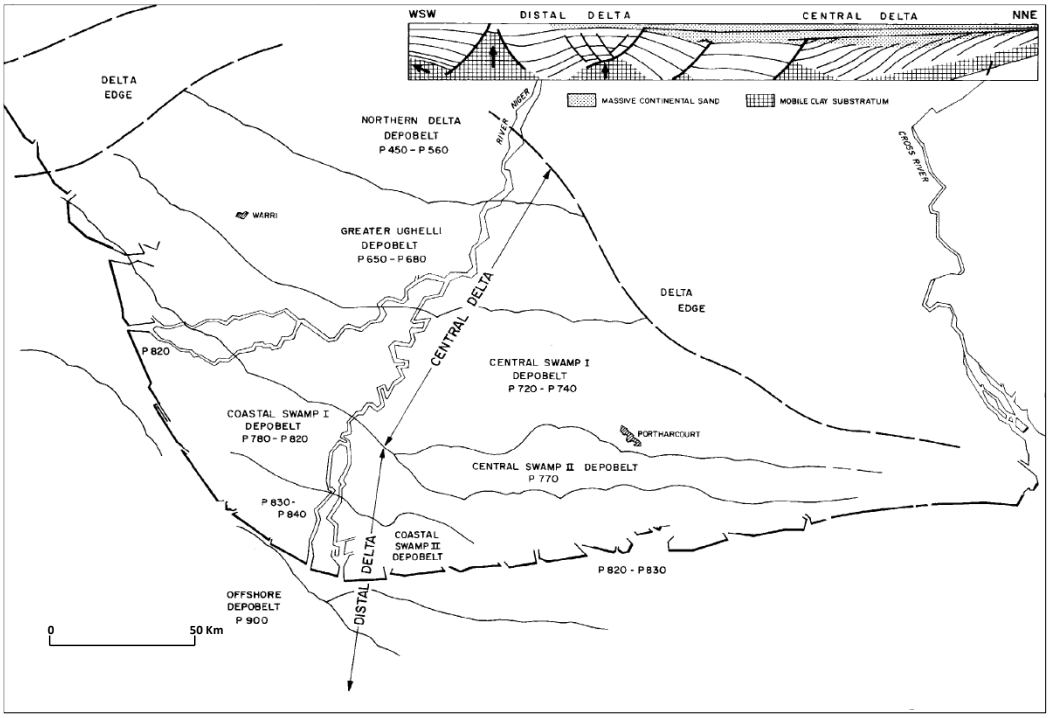

Figure 3.2: Schematic showing the location of the Niger Delta depobelts (Adapted from Doust and Omatsola, 1990).

3.1.1 Stratigraphy

A tripartite lithostratigraphic sequence has been defined based on some of the deep wells that have been drilled in the Niger Delta (Short and Stauble, 1967, Avbovbo, 1978). These three lithological units identified are the Akata, Agbada and the Benin Formation, each unique in its facies distribution, age and depositional environment (Figure 3.3).

The Akata Formation is a marine sedimentary unit that underlies the entire Tertiary Niger delta stratigraphic sequence from onshore to offshore. This Formation is

characterised by pelagic silt, mud and shale with an abundance of fauna and flora that has enabled an age assignment of Paleocene to Recent (Doust and Omatsola 1990). The thickness of this sequence is not definitive as no well has been drilled to its bottom, however, it is thought likely to be about 7000 m in the central part of the delta (Doust and Omatsola 1990) and may extend into the late Cretaceous. The marine muds crop out offshore in the form of mud diapirs that have developed as a result of smectite – rich sediment deposited underneath a rapidly prograding Eocene to Miocene delta complex (Whiteman 1982). This has further resulted in an overpressured condition in the marine sediments (Cohen and McClay, 1996). Diapiric movement of the Akata muds is still active and significant distribution of diapirs has been visible around the continental slope and sea-floor where they are revealed as mud volcanoes (Graue, 2000). The Akata Formation is thought to be the primary source rock in the Niger Delta petroleum province (Evamy et al., 1978, Ekweozor and Daukoru, 1984, Lambert-Aikhionbare and Ibe, 1984, Bustin, 1988, Haack et al., 2000, Samuel et al., 2009).

Overlying the Akata Shales is the deltaic/paralic sand and shale sequence of the Agbada Formation. This forms one of the principle hydrocarbon prospective sequences in the Niger Delta, due to the inter-bedded sands and shales forming excellent reservoir-seal couplets (Frankl and Cordry, 1967). The Agbada Formation is the main deltaic portion of the sequence that was deposited in a delta front, delta topset and fluvial deltaic environment (Short and Stauble 1967, Doust and Omatsola 1990). The paralic sequence is present in all depobelts with an age that ranges from Eocene to Recent. Considering that most exploration wells in the Niger delta were drilled to the base of the Agbada unit, it is confirmed to exceed 3000m in thickness (Doust and Omatsola 1990).

The Benin Formation is progradational across the delta lithostratigraphic sequence, with a thickness of about 2000m onshore, thinning seawards. This lithological unit are mostly of continental sand origin deposited in an alluvial or upper coastal plain environment. The lack of fauna has made it impossible to date the Benin Formation accurately, however, a probable age of Oligocene to Recent has been assigned to this lithofacies (Doust and Omatsola 1990).

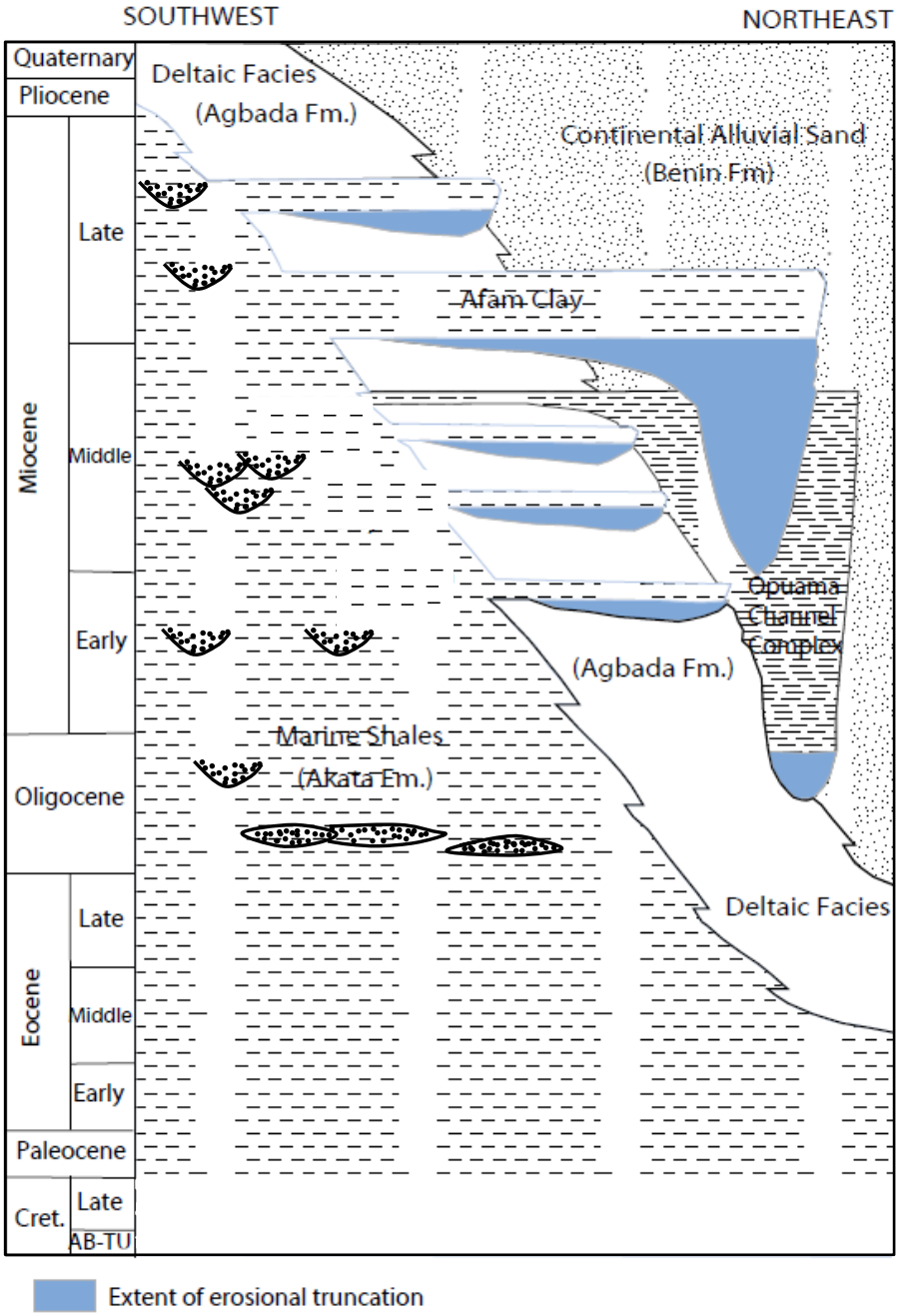

Figure 3.3: Stratigraphic column of the Niger delta showing the three major lithostratigraphic units (adapted from Tuttle *et al.*, 1999). Clay filled erosional features induced by canyons and channels are well illustrated. Turbiditic reservoir sands are noted to occur within the Akata shales.

Most important to this thesis and to the distribution of sediments offshore, across the delta slope and into deeper water, is the development of erosional canyons of Oligocene to Recent age. These canyons are believed to have developed in response to sea level low-stands (Doust and Omatsola 1990) but are then active through several eustatic

cycles. They extend from the shelf break and upper slope into deep-water as channels. Sediments that are funnelled through these canyons and channels are principally supplied by two drainage systems – the Niger-Benue fluvial system responsible for supplying sediments to the western part of the Niger delta and the Cross river system feeding the eastern flank of the delta. Some of the major canyons recognised so far are Lagos, Avon, Mahin, Opuama, Escravos, Benin, Dodo and Ramos located in the Western Niger Delta; the Niger canyon feeding the central part of the delta while the Kwa Ibo and Calabar Canyon are both located in the East part of the delta (Burke, 1972, Petters, 1984). Figure 3.4 illustrates the canyons located in the central and western parts of the Niger Delta. Most of these canyons are linked to deepsea fans through submarine channels that are downslope extensions of erosional submarine canyons (Damuth, 1994). Of all the canyons in the western Niger delta, the Opuama canyon was active in the Oligocene (Petters 1984) and therefore likely to have channelled sediments towards the vicinity of the study area. The Benin canyon also located in the vicinity of the study area is classed as a Recent submarine canyon (Deptuck et al., 2007) and therefore unlikely to have transported sediment to the study area during the Oligocene.

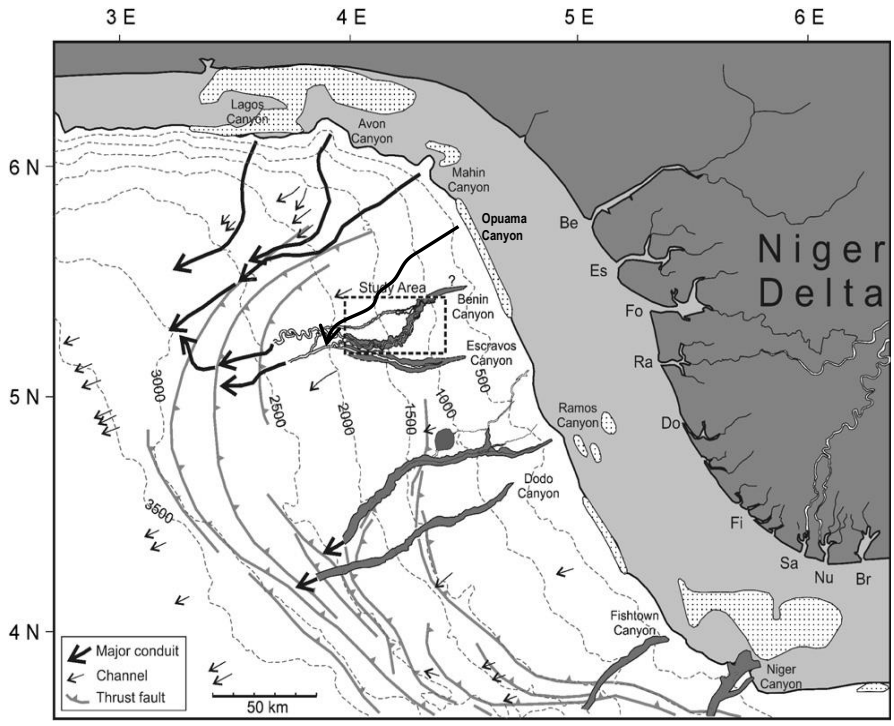

Figure 3.4: Locations of some of the canyons in the central and western Niger delta (modified after Deptuck et al., 2007).

3.1.2 Tectonics

Damuth (1994) describes the tectonic structure of the Niger delta in terms of three different zones: (1) an upper extensional zone that occurs mostly onshore and across the shelf to the upper slope region; (2) a translational zone in upper and mid – slope region; and (3) a lower compressional zone in the lower continental slope and rise.

The extensional zone is one that is characterised by extensive seaward dipping growth faults. These faults are known to develop in response to rapid seaward progradation and loading of delta sediments over mobile, under-compacted and overpressured ductile mud (Doust and Omatsola 1990, Damuth 1994). Faults flatten with depth into a detachment plane at the top of the mobile substratum. Hanging wall rollover anticlines also develop in association with growth faults. These anticlinal structures form as a result of listric fault geometry and differential loading of deltaic sediments above ductile shales (Doust and Omatsola 1990).

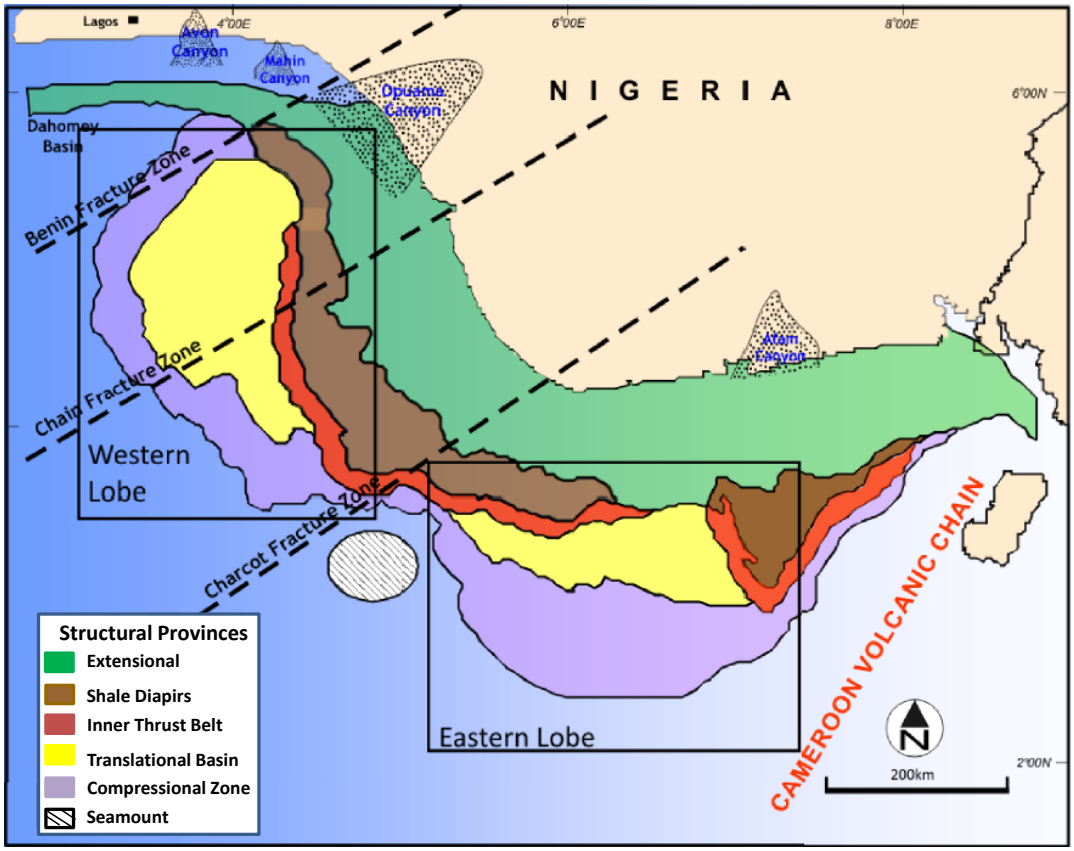

Figure 3.5: Structural provinces across the Niger delta (adapted fromMatthew et al., 2010).

Seismic profiles interpreted across the translational zone of the delta illustrate a widespread distribution of mud diapirs and ridges of the Akata Formation with varying orientation and burial depth. The growth and the upward movement of the diapirs have resulted in faulting and folding of the overlying Agbada sequence leading to erosion at the sea-floor (Damuth 1994). Diapir movement of the Akata mud has also led to the formation of intraslope mini-basins between diapir walls within which sediments up to several kilometres thick are ponded. Further seaward of the translational zone, the deformed strata of the compressional zone reveal linear toe thrust structures forming a fold and thrust belt that indicates that the sediments of the lower slope and upper continental rise are being squeezed upward and outward onto the sea-floor. The deformation noted in this zone is thought to be triggered by downslope movement of sediment due to gravity gliding resulting in major thrust features and forming a fold and thrust belt (Bilotti and Shaw, 2005, Corredor et al., 2005, Deptuck et al., 2007).

3.2 Study Area: Bonga Field

The study area includes the deep-water Bonga field within the translation zone in the north western part of the Niger delta slope. The Bonga Field is located some 120km off the coast of Nigeria in water depths of 800 (2600ft) to 1200 m (3900ft) and is currently operated by Shell on behalf of the Nigerian government (Chapin et al., 2002). This field is the first deep-water discovery offshore Nigeria. First oil production began in 2005 from stacked Upper to Lower Miocene reservoirs through several producer/injector well-pairs. In the space of four years the Bonga field has produced more than 275MMbbl from five main reservoirs located within a depth range of 1800 (6000ft) to 3350m (11000ft) subsea floor (Okoh et al., 2010). Over 30 wells have been drilled in Bonga region to date with only one well, the exploration well herein referred to as Well A1, that was drilled beyond the Miocene reservoirs encountering about 180m of Oligocene succession. The well A1 was drilled to total depth (TD) of about 4000m (Figure 3.6).

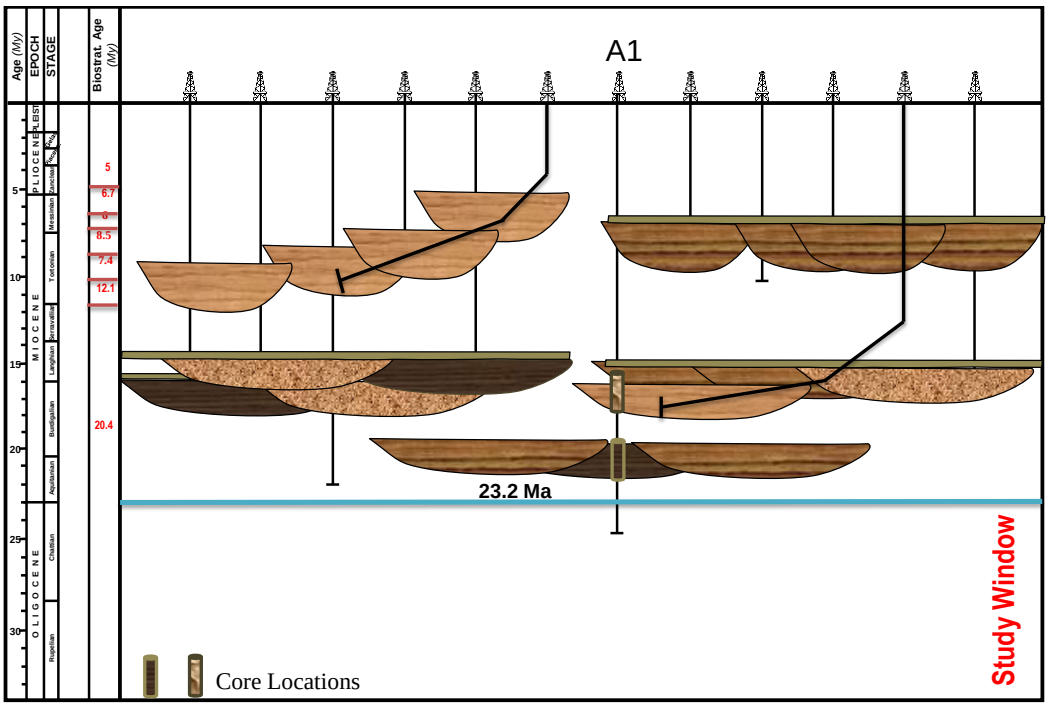

Figure 3.6: Schematic illustration of the distribution of some of the wells across proven reservoirs.

3.2.1 Structure

The Bonga field is located in the translational part of the Niger Delta slope system. The area is characterised by a south-plunging anticline cored by mud diapiric structure (Chapin et al., 2002, Fehintola et al., 2009). Normal faults are also present at the crest of the structure and are also prevalent towards the north close to the mud diapirs. Mud diapirs in the north western Niger delta are believed to have been active since late Oligocene to early Miocene time and are exposed on the sea-floor in places as mud volcanoes (Whiteman 1982, Graue 2000). Syn-sedimentary faults are common and are believed to have influenced turbidite deposition and hydrocarbon emplacement, particularly by modifying the slope topography and serving as fluid conduits from deep seated source rocks. The Bonga field itself is divided into four main compartments (Figure 3.7): Bonga North, Bonga North West, Bonga Central and Bonga South West. The Bonga Central, also referred to as Bonga 'Main', has been the focus for current oil production, while the remaining compartments are at exploration or early appraisal phase.

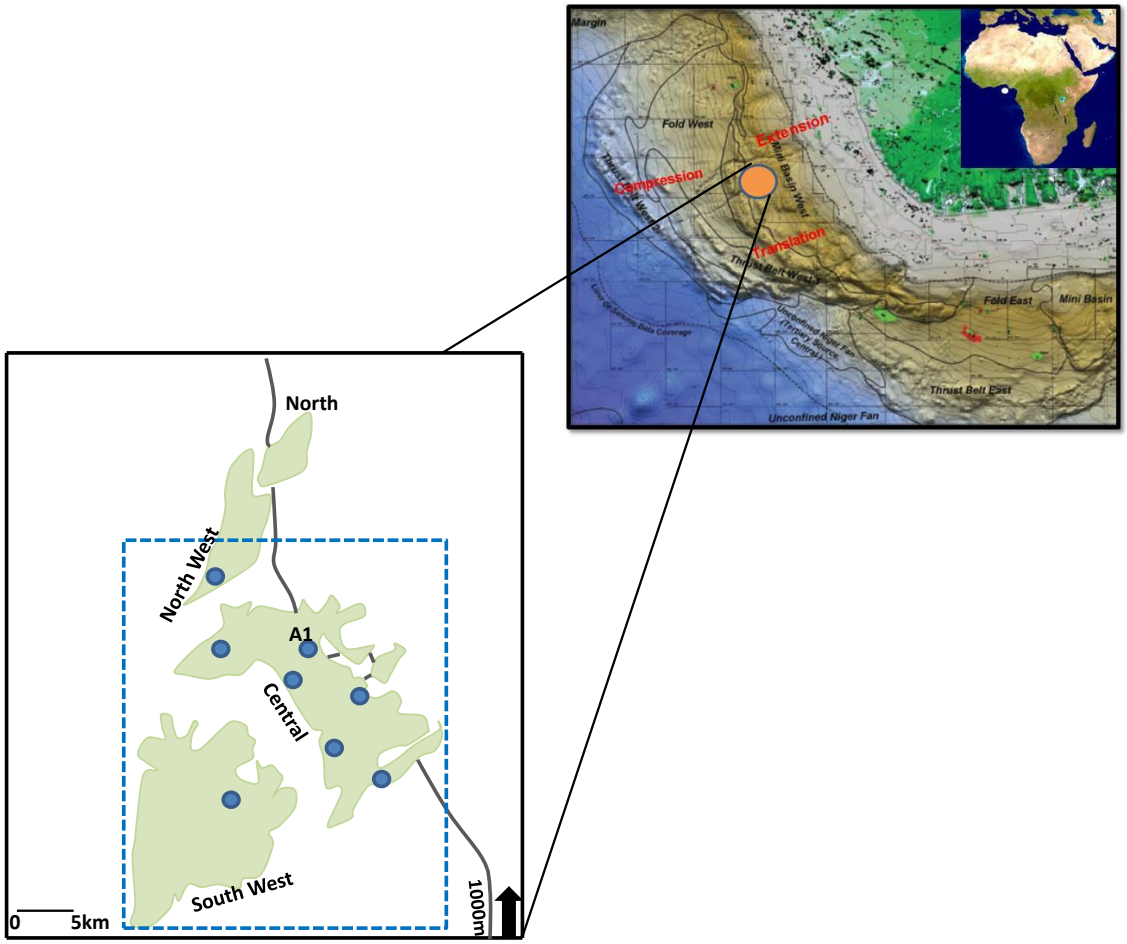

Figure 3.7: Map showing the location of the Bonga field and the main compartments. Note the location of some wells in blue circle, particularly Well A1. The blue dashed square box indicates the coverage of the 3D seismic volume used in this research.

3.2.2 Reservoir characterization

The Bonga hydrocarbon accumulations are predominantly stratigraphically trapped; however structural trapping associated with rollover anticlinal features is also present (Fehintola et al., 2009). Seismic amplitude mapping reveals that the principle reservoirs are within deep-water channel sands. These channels are sinuous and coalesce to form channel complexes. Well penetration in Bonga confirms that the reservoirs are mostly channelized with associated levees and overbank deposits. The overall system is mud dominated forming good reservoir seals and compartmentalising individual reservoirs with poor fluid communication. Cores acquired from some of the wells indicate that the reservoirs are typically unconsolidated massive sands exhibiting no vertical trend and characterised by high net-to-gross. Areas outwith of the main channel axis sands are

noted to have thin bedded and thinly laminated sands. Overlying the main channel deposits there is typically a fining upward section indicating channel abandonment. The Miocene reservoir sands have excellent reservoir quality and diagenetic modification is not significant. Measured sand porosities range from 20-35% and are associated with high permeabilities of up to 4 Darcy (Chapin et al., 2002).

3.3 A Review of the West Africa Deepwater Hydrocarbon System

Offshore oil and gas exploration in the West African region, from Angola to the Ivory Coast, began in the early 1960s with exploration success offshore of the Niger Delta, Congo and Gabon. Oil and gas production in the shallow offshore (< 200m) region of the Niger Delta took the centre stage in 1965, later followed by production in the shallow waters in other neighbouring West Africa countries (Cameron and White, 1999, Leffler et al., 2011). Major deep-water discoveries came into the limelight in 1995 with the discovery of Zafiro field operated by Mobil offshore Equatorial Guinea on the eastern flank of the Niger Delta. Oil production was from channelized deep-water reservoirs (Leffler et al., 2011).

In 1996 the Bonga field was discovered by Shell offshore western Niger Delta, followed by Mobil's Bosi field and Ehra field in 1998. The Chevron – operated Agbami field was also discovered in 1998. The discovery of these fields in deep-water offshore the Niger Delta placed the Niger Delta Basin as the major prolific basin in West Africa and also along the South Atlantic margin (Chapin et al., 2002, Leffler et al., 2011).

The Girassol field was also discovered in 1996 by Elf Aquitaine within the Angolan arm of the Lower Congo Basin. Elf further struck significant hydrocarbon accumulation in the Dalia field in 1997 plus other smaller discoveries. Exxon drilled the Kissanje discovery in 1997, later followed by Hungo, Dikanza, Marimba and a chain of smaller discoveries. Chevron encountered hydrocarbon in the Kuito field of the Lower Congo basin (Cameron and White, 1999, Westwood and Knight, 2001, Raisson and Temple, 2004).

Most of the discoveries cited above were major finds with each having about a billion barrels of recoverable reserves, thus establishing two main petroleum systems – one in the deep-water Niger Delta basin and the other in the Lower Congo basin. For both

regions, the principle source rocks are Tertiary and Cretaceous in age. Figure 3.8 shows the locations of some of the major deep-water fields along the West African margin

The discovery of the giant Jubilee field (1.5bboe) by Tullow oil in 2007 opened up new Cretaceous hydrocarbon play along the West African Transform Margin (WATM). The Jubilee field located about 60km offshore Ghana in 1100m water depth has an estimated recoverable reserve of over 600MMbbl. In 2011, Anadarko announced another major discovery offshore Ghana located in a water depth of approximately 884m (2900ft) from a well drilled to a total depth of 3400m (11185ft) (Mitchell, 2012, Dailly et al., 2013).

The notable success and prolific nature of the West African deep-water systems can be linked to a number of key factors: (1) thick and laterally extensive oil prone source rocks, (2) availability of good quality reservoir facies, (3) early formation of traps, and (4) active hydrocarbon generation (Cameron and White 1999). The following section examines in more detail the geologic controls on deep-water plays along the West African margin, particularly the events that are responsible for placing some basins as key targets for exploration and production of hydrocarbon.

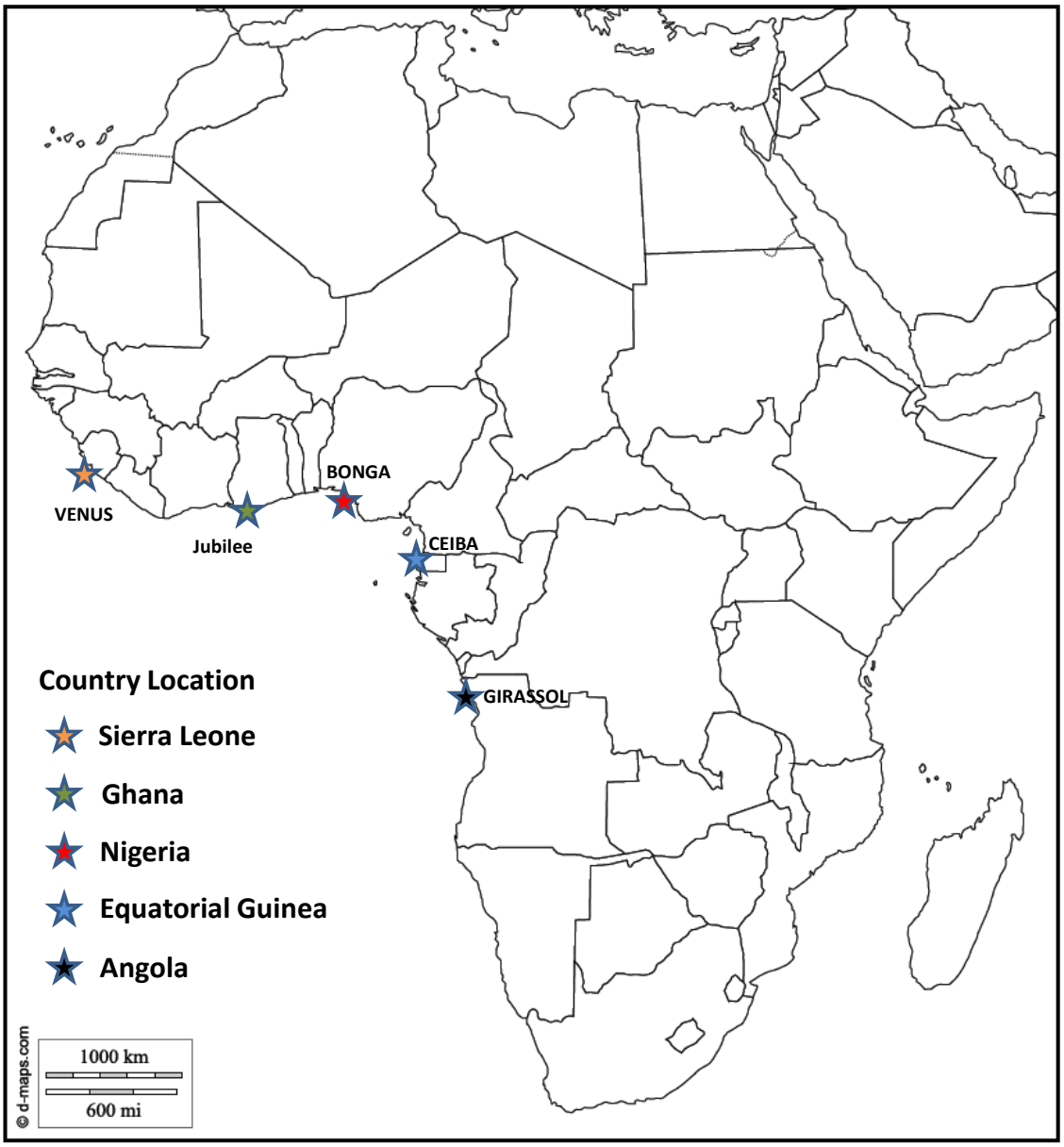

Figure 3.8: Names and Location of some of the major deep-water fields in West Africa. The Jubilee and Venus field were discovered in 2007 and 2009. The Bonga, Ceiba and Girassol were mid to late 1990's discoveries.

3.3.1 Implication of plate tectonics on hydrocarbon exploration along the South Atlantic Margin

Offshore West Africa and the East coast of Brazil are considered as two of the world's most attractive regions for deep-water hydrocarbon production. It is not surprising as both margins have many geologic features in common. Both continents were part of a super continent known as Gondwana (Burke et al., 2003). In the Early Cretaceous (145Ma), due to plate tectonic forces, Gondwana broke up as the South American plate

separated from the African plate. The rifting or synrift phase resulted in the development of rift basins where lakes and fluvial systems formed with a variety of sediments deposited, ranging from clastics to carbonate rocks including source rock facies of algal rich organic deposits (Short and Stauble, 1967, Genik, 1993, Jian-Ping et al., 2008, Beglinger et al., 2012) (Figure 3.9). These rift basins progressively developed from south to north along the South Atlantic margins as the plates separated.

This phase was followed by a phase of subsidence in the Late Aptian to Early Albian. Continued extension and separation of the African plate from South America resulted in rupturing of the continental crust due to extensive stretching and thinning marking the early development of south Atlantic oceanic basin, incursion of seawater from the south followed by a local accumulation of Aptian evaporites. These salt deposits are seen in some basins such as the Campos Basin off Brazil and the Kwanza Basin off Angola. Underlying these are the pre-salt hydrocarbon targets and major discoveries off Brazil. Thick sediment deposition over the salt results in plastic deformation, flow and diapiric intrusion. This, in turn, deforms the overlying sedimentary layers upward forming ridge or dome like structures that today contain some of the giant accumulations in the Angola and Brazil offshore (Jian-Ping et al., 2008).

The post-rift or drift stage in Late Albian to Recent was characterised by several significant episodes of global rise and fall in sea level. In late Albian to Turonian, organic-rich muds and marls were deposited during global oceanic anoxic events that promoted the development of organic-rich source rocks. By Late Santonian to Early Campanian, both the African and South American plate were totally separated with previous sedimentary layers in the rift basin deformed by extensional and compressional forces (Beglinger et al., 2011). On both sides of the Atlantic, deep-water oceanic conditions had developed; river systems from onshore channelled sediments from the hinterlands to shelf canyons and slope channels and into the deep ocean basin. Uplift of the African continent that was associated with mantle plumes, especially in East Africa promoted the transportation of large amount of sediment into the West Africa basins and ultimately into deep-water as channels and deep sea turbidite fans (Jian-Ping et al., 2008).

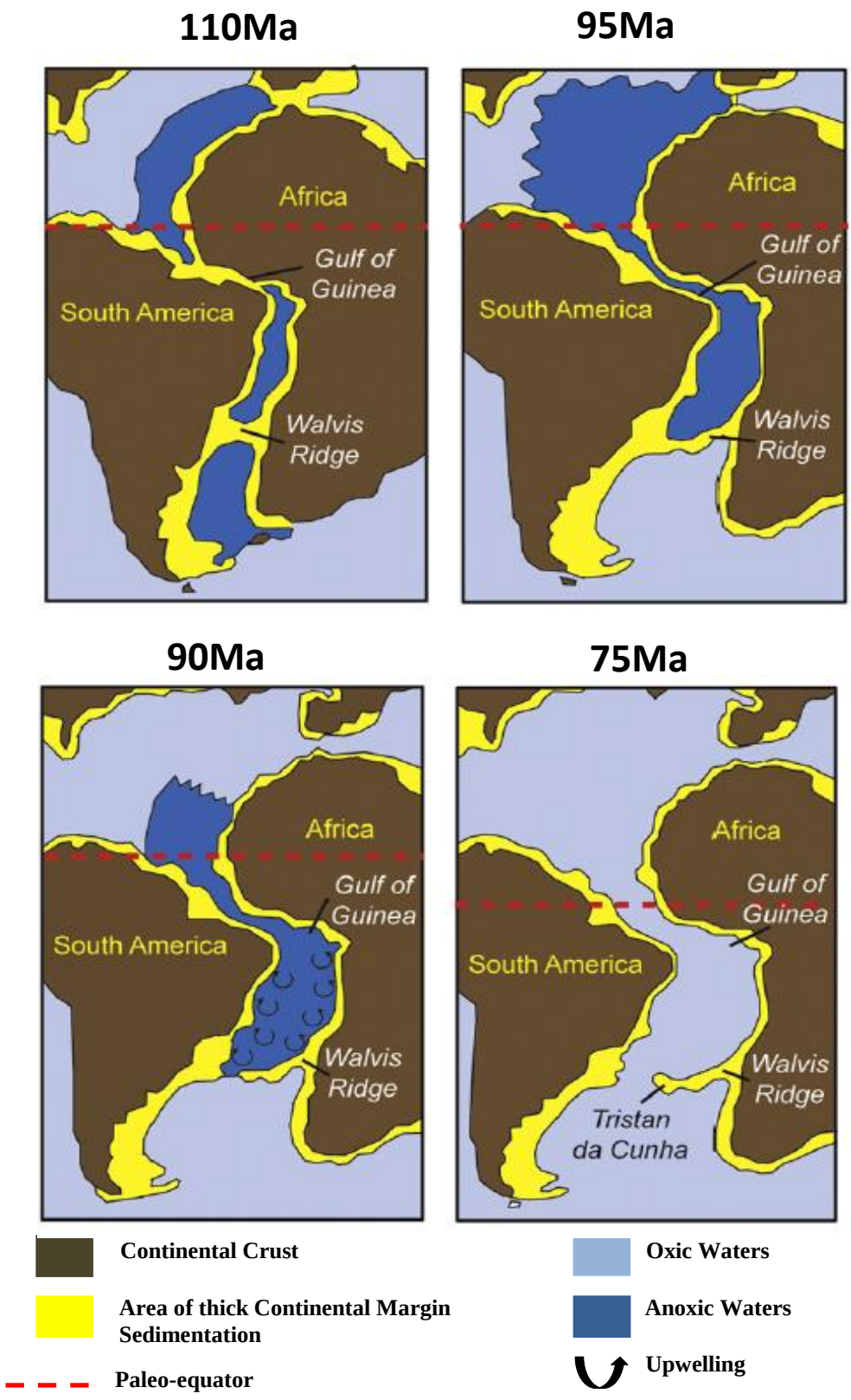

Figure 3.9: Palaeogeographic maps of the Cretaceous break-up of South America and Africa (after Beglinger et al., 2011).

Through a reconstruction of the plates prior to break-up, sedimentary basins discovered on one margin of the South Atlantic appear to be conjugate to basins on the other side. For instance the geology of the Brazil Campos basin is similar to that of the Kwanza Basin of Angola, the Niger Delta in West Africa corresponds to the offshore Ceará/Potiguar Basins on the Brazilian Margin, the Tano Basin of West African Transform Margin (WATM) matches with the IIha de Santana Platform on the Brazilian Side.

The principle proven hydrocarbon petroleum systems in the basins of the West Africa margin include the following (Jian-Ping et al., 2008):

a) Fluvial and lacustrine source rocks deposited in the Early Cretaceous in the Syn-rift phase, responsible for charging the pre-salt source reservoirs sealed by the Aptian evaporites.

b) Post-salt clastic and carbonate reservoirs that are charged by pre-salt source rocks via faults that have cut through the salt serving as excellent migration conduits.

c) Cenomanian and Turonian post-rift source rocks that have generated hydrocarbon for the deep-water turbidite reservoirs via fault conduits with trapping systems of both structural and stratigraphic origin.

d) Deltaic systems that have supplied ample sediment to the Congo fan and the Niger Delta offshore slope and fans. In the Congo, the Oligocene-Miocene turbiditic reservoirs, trapped by salt induced structures, were charged mainly from the Late Cretaceous source rocks with minor contributions coming from the Paleogene source facies (Da Costa et al., 2001). The Niger Delta offshore on the other hand is characterised by the Eocene marine source rocks which are responsible for hydrocarbons trapped in Miocene turbidite reservoirs (Doust and Omatsola 1990).

Figure 3.10 below is a schematic of an integrated chronostratigraphic chart offshore of some of the basins across the West African Margin showing key petroleum system elements.

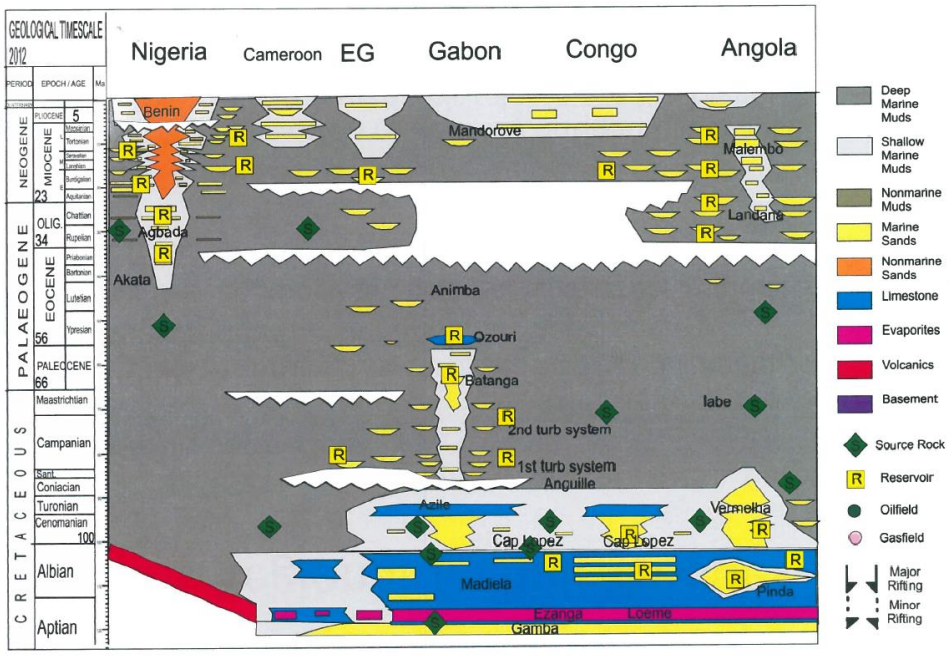

Figure 3.10: Chronstratigraphic Chart: Offshore Nigeria to Angola (Post Salt) (After Macgregor 2013).

Across the West African margin the Niger Delta, the Lower Congo and the Gabon Basins are the largest and with the most promising hydrocarbon finds (Anderson et al., 2012). The Jubilee discovery in the Tano basin of Ghana (Dailly et al., 2013), the Equatorial Guinea's Rio Muni Basin and the Douala Basin of Cameroon are also important. Other sedimentary basins in the West Africa Margin, such as the Kwanza Basin in Angola, the Sierra-Leonean Basin, the Abidjan Margin and Tano Basin in Cote D'Ivoire are still being explored with only sub-commercial finds (Jian-Ping et al., 2008). The table below shows an overview of some of the hydrocarbon reservoirs offshore West African Margin (Chapin et al., 2002, Beglinger et al., 2011, Dailly et al., 2013).

Region	Formation	Age	Lithology	Field	Water Depth (m)	Reservoir Depth (m)	Reservoir properties		
							Ø (%)	K (mD)	Th (m)
Angola	Malembo	Oligocene	Clastic	Girassol	1400	2450	30-40	6000	50-100
Gabon	Anguille	L.Cretaceous	Clastic	Anguille	30	2426	9-24	300-700	10-100
Ghana	Mahogany	U.Creaceous	Clastic	Jubilee	1700	2100	>20	200	90
Niger Delta	Agbada	Miocene	Clastic	Bonga	1000	2500	25-35	1000-3000	80

Table 3.1 Reservoir properties of some of the major deep-water fields in the West African margin (compiled from extensive publicly available data).

One main interesting fact from this table is that the Miocene reservoirs of the Niger Delta have been buried to a depth of about 2500m, similar to or even deeper than the Oligocene and older reservoirs of the other sedimentary basins. One main reason is linked to the significantly higher sedimentation rate seen in the Niger Delta (Figure 3.11), which has resulted in deeper burial of the sediments compared to sediments of the same age in other sedimentary basins. Hence it is imperative that through this study the reservoir potential of older and deeper strata offshore Niger Delta is investigated. The high sedimentation rate seen in the Niger Delta can result to disequilibrium compaction giving rise to overpressured intervals. The impact of overpressure on reservoir quality is considered in this study.

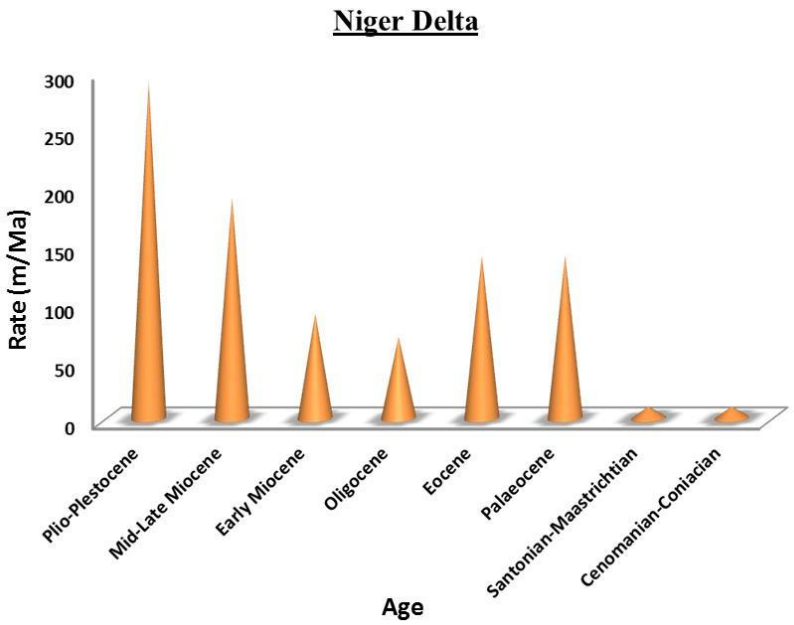

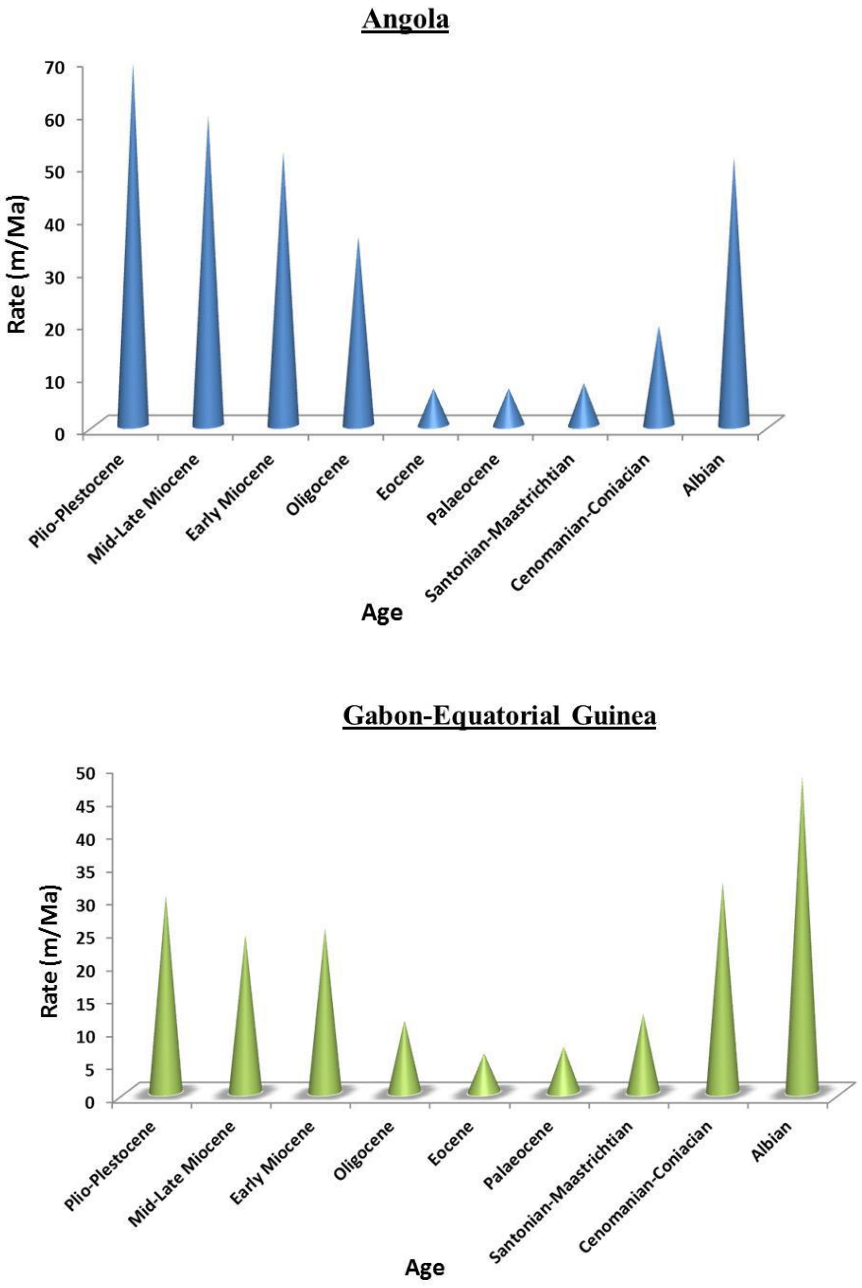

Figure 3.11: Sedimentation rate profile for some West Africa Basins. Note the high sedimentation rate particularly from the Tertiary for the Niger Delta compared with to the other basins. This has led to higher rates of subsidence and deeper burial of its sediments relative to similar age sediments in other basins having lower sedimentation rates (modified after Macgregor, 2013).

3.4 Basin Modelling, Evolution and Tectonics

3.4.1 Introduction

Basin modelling is utilised by the geoscientist to study the dynamic processes of a sedimentary basin, and to investigate if these processes or conditions were suitable for hydrocarbon generation, migration and entrapment in a potential reservoir rock (Al-Hajeri et al., 2009, Yalcin, 1991, Welte and Yalcin, 1988a). The fundamental approach of basin modelling is the transformation of a geological paradigm into numerical form or concept to allow an explorationist to: (1) make quantitative and qualitative predictions regarding non-drilled, often deeper parts of a sedimentary basin accessible only by seismic data; and (2) construct through time if necessary a three dimensional view of a sedimentary basin (Welte and Yalcin, 1988a). Considering that a basin is formed by complex interrelated processes driven by plate tectonics, the evaluation and prediction of the hydrocarbon potential of a basin requires an accurate reconstruction of these key processes. Therefore, valuable insight into overall processes of basin evolution can be acquired from a general consideration of various plate tectonic settings.

This section describes firstly, the mechanism of basin formation and types of sedimentary basin in relation to plate tectonics. Additional processes at work in sedimentary basin such as compaction, fluid flow and overpressure are also briefly discussed. Lastly the concept of basin modelling in relation to types, data requirement and modelling workflow would form the concluding part of this section.

3.4.2 Mechanisms of basin formation

Sedimentary basins are regions of the earth surface where sediments are seen to accumulate and eventually become sedimentary rocks owing to physical, chemical and biological processes. Basins form if there is a significant bathymetric depression, appropriate sediment supply and a suitable depositional environment. Bathymetric depressions are triggered by processes like cooling and contraction, loading, and thinning. These processes are associated with isostasy (Blundell, 1991). Topographic lows created in basement rocks as a result of either tectonic or sedimentation subsidence usually lead to the formation of sedimentary basins. Tectonic subsidence is the subsidence of the basement rock that takes place in the absence of sedimentation, for

example the deep ocean basins. While sedimentation subsidence is subsidence of the basement – sedimentary rock interface induced by rapid sedimentation typically found in river deltas such as the Niger and Amazon Deltas (Deming, 1994).

Based on different lithospheric process the mechanisms that control subsidence and uplift can be linked to the following:

Isostatic mechanism - This process relates to increase in thickness of the crust and lithosphere as a result of thermal cooling of the lithosphere, particularly when new oceanic lithosphere moves away from the spreading centre. Mechanical thickening of the crust and lithosphere as seen during continental convergence would generally cause isostatic uplift, while thickening of the lithosphere by cooling causes subsidence.

Loading - Lithospheric loading can take place either sub-aerially or sub-aqueously. It may result from the emplacement of volcanoes or, seamounts or, on a much larger scale, of whole mountain belts. This leads to crustal flexure and hence subsidence. In addition, loading can be driven by sedimentation.

Dynamic effects of mantle convection, plumes, and asthenospheric flows. These are buoyancy effects due to temperature change in the mantle that are transmitted by viscous flow. They are manifested as subsidence or uplift (Allen and Allen, 1990).

3.4.3 Burial and compaction in clastic rocks

The properties of sedimentary rocks are typically altered as burial depth increases. Shallower sediments mostly near the surface are characterised by loosely packed uncemented fabric, high porosities and high interstitial water content. With increase in total thickness of the sedimentary column in subsiding basins, older sediments are buried by younger sediments to deeper burial depths. Such burial is usually associated with physical and chemical changes in the sediments in response to increase in temperature and overburden weight. Hence, loosely packed sediments are finally consolidated into a sedimentary rock (Boggs, 1987). The degree to which the properties of sediments such as porosity, permeability etc. change is a function of grain texture, mineralogy and chemical processes. The dissolution of minerals permit a closer packing of grain framework while the precipitation of minerals (cements) around sediment grains alter the pore spaces, thereby giving the sediments a more brittle quality. The

transition from uncemented sediments to cemented rocks takes place at varying depth and temperature depending on the mineralogy and textural properties.

This section reviews and integrates theories of rock mechanics with diagenetic models for compaction (mechanical and chemical). The integration of these disciplines is necessary to understand rock properties and fluid flow in a sedimentary basin.

Compaction of siliciclastic sediments

During burial, as the overburden load increases, pore water locked up between rock grains is expelled. This results in a decrease in pore spaces and layer thickness, and the sediment is said to be compacted. In general, mechanical compaction starts out rapidly, but reduces as the depth of burial increases (Barker, 1996). The main effect of mechanical compaction is grain rearrangement with expulsion of water and the corresponding reduction of porosity; hence the porosity trend with depth can provide a means of monitoring compaction in sediments (see Figure 3.12). Several mathematical relationships between porosity and depth have been proposed. One of the earliest was that of Athy (1930), which was put forward for shales and has the expression:

$$\phi_z = \phi_o e^{-cz} \qquad (3.1)$$

where ϕ is porosity, z is depth, c is compaction constant which varies for different lithologies and e is exponent. Equation 3.1, however, is not appropriate for shallow – buried sediments, buried to within a few tens to a few hundred feet (Barker, 1996). Hence, other forms of porosity – depth relationship have been proposed to accommodate other factors, like time (eq. 3.2), or "solidity" – a complement of porosity (eq. 3.3).

$$\phi = A(M)^B \qquad (3.2)$$

where A and B are lithology – dependent constant and M is a measure of thermal maturity expressed in TTI (Time Temperature Index) or vitrinite reflectance.

$$Z = 6.02 \times S^{6.35} \qquad (3.3)$$

where Z is burial depth, S is solidity.

The expression above (eq. 3.3) assumes that porosity continuously decreases with depth under normal hydrostatic burial. However, if the pore pressure becomes greater than the effective overburden pressure/stress, the rock with lack of sufficient permeability would be able to withstand the overburden pressure and so would not compact. This results in a condition known as undercompaction or over-pressure. Rocks in this state generally show porosity values that are anomalously high for the depth of burial. The equation below is preferentially used for such abnormal pressure conditions (Barker, 1996).

$$\delta = (1-P/P_{ob})/(1- P_e / P_{ob}) \qquad (3.4)$$

where P is actual pore fluid pressure, P_{ob} is overburden pressure and P_e is hydrostatic pressure. δ is equal to 1 and the porosity depth equation is same as equation 1, If pore fluid pressure is equal to hydrostatic pressure (P_e). δ is less than 1.0 and the rate of porosity with depth diminishes when pore fluid pressure is greater than the hydrostatic pressure (Barker, 1996).

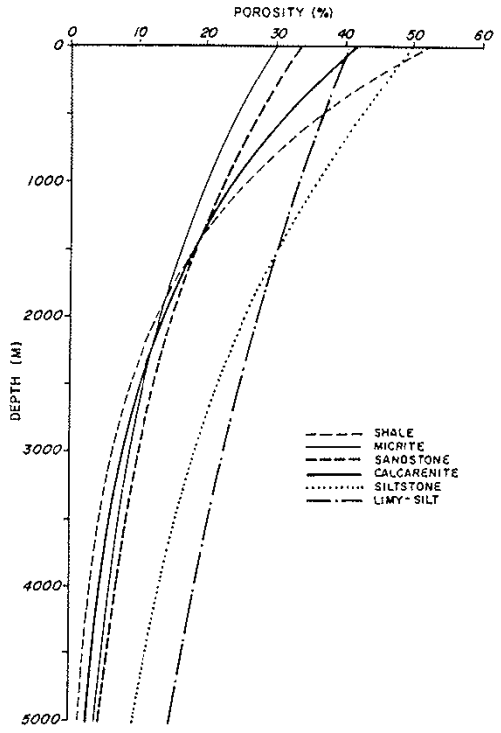

Figure 3.12: Porosity versus depth curves for different lithologies (AfterHegarty et al., 1988).

Mudstone

The degree of compaction of mud as a function of burial depth varies greatly, which is dictated partly by the magnitude of effective stress. The magnitude of effective stress itself is a function of rate of burial and pore fluid overpressure. In addition, grain size distribution and mineralogical composition are key controlling components. The rate of compaction is a function of permeability that controls water escaping out of the pore network.. The permeability is in turn related to grain size distribution. Coarser, silty mudstones are generally more permeable, whereas very fine, clay-rich mudstones are less permeable. Furthermore, smectite-rich mudstones have very low porosity and permeability and hence compact very slowly.

Figure 3.13 is a porosity depth trend for different lithologies. Mudstone with low quartz or carbonate cement content behaves as a porous and soft material up to burial depth of 2km (e.g., in the North Sea), resulting in a low shear strength with low deformation and low seismic velocity (Bjørlykke and Høeg, 1997). Such mudstones are commonly noted to have open fractures when subjected to pressures above their lithostatic/fracture pressure making them highly conductive to fluids (Bjørlykke and Høeg, 1997). Also, at the depths below 2km mineralogical changes are controlled by temperature and mineralogical composition instead of effective stress. Of particular importance in mudstones is the varying temperature of clay mineral diagenesis. For example the transformation of smectite to illite occur at a temperature range of 80-120^{0}C while at higher temperatures of 120-140^{0}C kaolinite converts to illite most especially in a potassium feldspar rich – environment (Bjørlykke and Høeg, 1997).

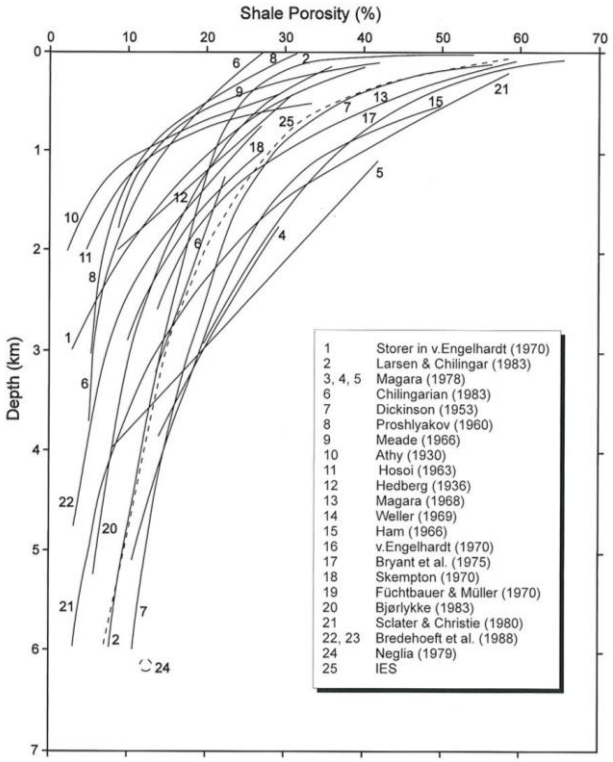

Figure 3.13: Porosity depth trend for shales from various sources (After Welte et al., 1997).

Sandstones

The compressibility of sands depends on factors such as, initial grain packing, shape, size and sorting and particle composition. Initial porosities of loosely packed sands are controlled by sorting, grain shape, grain size and sedimentation rate. These initial porosities can range in values from 25 -55% (Welte et al., 1997). Hence sands with different porosities at deposition compact at different rates, leading to non-uniform porosity loss relative to depth of burial (Boggs, 1987). Figure 3.14 shows a porosity depth trend for sandstones from different sources. In most cases porosity due to copactionon is associated with porosity loss due to cementation. This is particularly true for deeply buried sediments where temperature conditions are suitable for diagenetic processes to occur and vertical effective stress are high to promote mechanical compaction (Gluyas and Cade, 1998). It is therefore challenging to determine the importance of porosity reduction by mechanical compaction alone. As mechanical compaction increases with depth, tighter packed grains may undergo physical changes, so that hard brittle grains may be fractured at shallower burial depths, but with increase

in burial and higher temperatures, they tend to yield plastically by bending or flowing. Sometimes at much greater depths quartz grains undergo solution at grain contacts owing to increase in solubility of the grains and higher pressure imposed at the contact point. This process, known as pressure solution, is responsible for a significant reduction in porosity by bringing grains in closer contact (Houseknecht, 1984, Tada and Siever, 1989, Bjorkum, 1996).

Chemical processes have a significant impact on sediments during burial. Minerals may dissolve due to contact stresses and new minerals may precipitate in pores between existing grains thus yielding to stress during compaction. Fractures may be sealed by cementation. In all, sediments may exhibit ductile behaviour if subjected to gradual strain rate during burial. On the other hand, during uplift, sedimentary rocks may display a more brittle behaviour and fractures are likely to remain open to fluid flow as a result of drop in cementation rate with decrease in temperature.

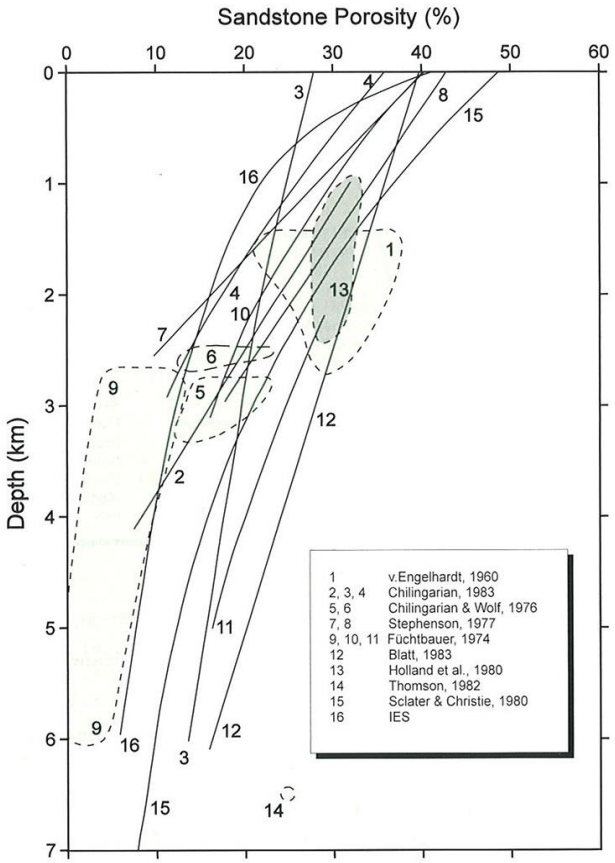

Figure 3.14: Porosity depth trend for sandstone from various sources (After Welte et al., 1997).

Stress regime during burial

Compaction of sediments ultimately leads to volume reduction and the sediment becomes consolidated. The fundamental factor that drives compaction is the weight of the overburden (Allen and Allen, 1990). In simplest term vertical stress is expressed as

$$\sigma v = Pgh \qquad (3.5)$$

where σv is the effective stress, *P bulk* density of the overburden, g is acceleration due to gravity and h is height. In a dry system mechanical response of sediments (granular materials/unconsolidated) is very complex ouside the scope of this thesis. Hence a simplified assumption of equation 3.5 is a starting point that focuses on effective stress via pore pressure evolution.

Sediments are considered to be normally consolidated if it has a high or higher vertical effective stress at present burial depth than any time earlier in its geologic history. But overconsolidated sediment is one that has at any time in the past experienced higher effective vertical stress than at present as seen in sediments below an erosional unconformity. These sediments are overcompacted and will not compact further mechanically until overburden weight has exceeded the previous overburden prior to tectonic uplift and/or erosion. This invariably implies that sediments can undergo cycles of loading, unloading and reloading during its burial history. Normally both consolidated and overconsolidated sediment with similar grain size distribution, mineralogical composition and the same present vertical effective stress would have different geomechanical properties given that they have different degree of consolidation. Hence, the behaviour of normally consolidated sediment is different during loading and unloading (Figure 3.15). In addition the modulus (stiffness) for unloading and reloading is much higher than the modulus for virgin loading. This is why fractures are least likely to develop during virgin loading as seen in a basin experiencing continues subsidence and sedimentation (Bjørlykke and Høeg, 1997).

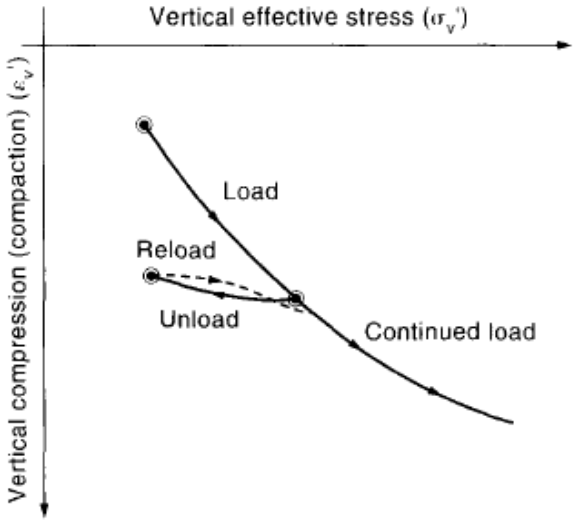

Figure 3.15: Stress-strain behaviour for a uniaxial strain situation during loading, unloading and reloading (After Børlykke and Høeg, 1997).

Overpressure

In basins with high sedimentation rates and low sediment permeability, pore pressure is seen to build up, giving rise to over pressure conditions. The difference between the pore pressure and hydrostatic pressure (where pore pressure is greater than hydostatic pressure) is the overpressure. The pore pressure in most cases lies between hydrostatic and lithostatic pressure (see Figures 3.16 and 3.17). Pore pressure can also be lower than hydrostatic pressure. This would occur when sediments undergo uplift coupled with erosion so that they are now connected to near surface pressure arears along permeable layers (Hantschel and Kauerauf, 2009b). So, when effective stresses are high, sediments experience a reduction in porosity. Conversely, when vertical effective stresses are low relative to pore pressure, minimal effect on porosity is noted. This therefore, suggests that the key controlling factor that causes overpressure would be the rate of fluid expulsion. Fluid expulsion in turn is controlled by one of, low fluid potential gradient, low absolute permeability, high fluid viscosity or low relative permeability (Waples and Couples, 1998). Low absolute permeability and high fluid viscosity are probably the most common means by which fluid flow is impeded and ultimately lead to an overpressured condition. The role of hydrocarbon generation in source rocks is another process which could contribute increments of overpressure to the fluid systems (Bredehoeft and Hanshaw, 1968).

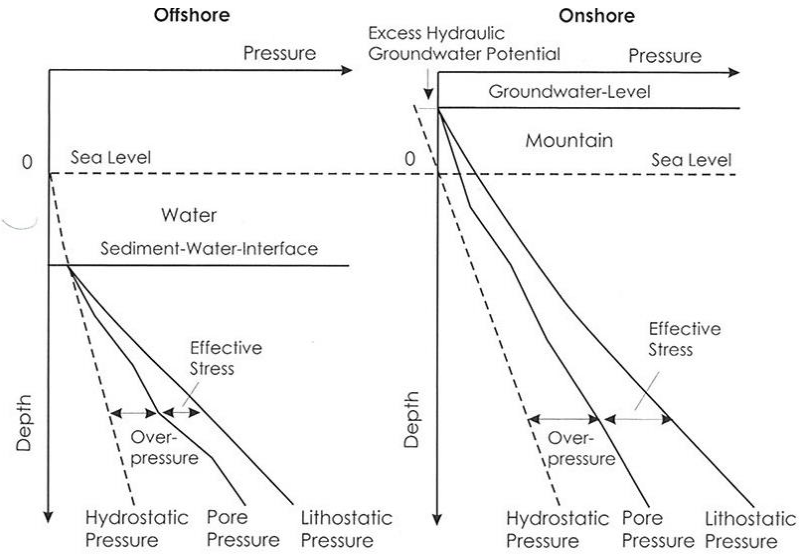

Figure 3.16: Pressure versus depth curve indicating overpressure profile in offshore and offshore environment (After Hantschel and Kauerauf, 2009)

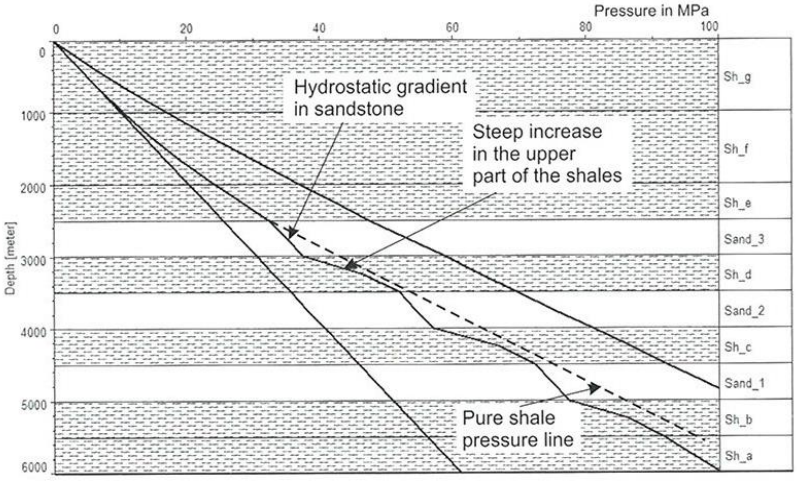

Figure 3.17: Overpressure profile in alternating sand and shale sequence (After Hantschel and Kauerauf, 2009).

3.4.4 Basin modelling

Basin modelling seeks to understand the geological, geophysical, chemical and physical processes at work during the evolution and formation of a sedimentary basin (Nielsen, 1996, Welte et al., 1997). This subject applies algorithms to seismic, stratigraphic, paleontologic, petrophysical, geochemical and other geologic and engineering data to temporally reconstruct the evolution of a sedimentary basin (Al-Hajeri et al., 2009). These suites of data, although used primarily to reconstruct a model of present day

conditions can also provide insight into the past conditions, events and processes that had prevailed in a sedimentary basin. Of particular interest to the explorationist are processes and conditions that lead to the generation and accumulation of hydrocarbon. Basin modelling in this sense aims to calculate the location, type and amount of hydrocarbon accumulations by connecting the past – a basin, the sediment and fluid that fill it, and the dynamic processes acting on them – to the present: hydrocarbon discoveries (Al-Hajeri et al., 2009). A good basin model depends on a well-defined conceptual model, which in itself is based on the integrated sum of all available geological data. The simulation is then performed on a numerical representation of the conceptual model. Output of the simulation is compared with the input and with independent calibration parameters, and if necessary the conceptual model is adjusted to lead to a better match between the simulation and the calibration data. The computer simulation requires the quantification of all defining parameters, and the conceptual model provides the platform needed to structure the input data. For all basin modelling the generation of a conceptual model of the basin history is the first and vital step. It has to be based on the interpretation and integration of conventional geological, geophysical and geochemical observational data placed in a temporal framework. The final model describes the geologic evolution of the basin (Welte et al., 1997)*;* it is related to and includes the concept of a petroleum system and also, provides the history of source rocks, reservoir rocks and seals.

From a geological point of view, four main types of models are considered in basin modelling when predicting hydrocarbon occurrence:

1- Basin-fill models: these simulate the sedimentation and the stratigraphy of a sedimentary basin. In most cases they are stochastic forward models.

2- Tectonic models: these are deterministic models that simulate structural components of a sedimentary basin, from small scale faults and folds to large scale crustal deformation.

3- Fluid flow models: these are concerned with hydrodynamics and hydrogeology as applied to fluid flow in porous media.

4- Thermal models: these simulate the thermal history of a sedimentary basin for a given depositional history and associated with it, the timing, volume, migration and accumulation of hydrocarbon generated. These models are deterministic forward models (Welte et al., 1997).

All model types listed above could either be classed as a 1D-maturity model or as 2D and 3D fluid flow modelling. The following section provides a brief overview of each of these types of model.

Model types

1D Model

1D models are much utilised in predicting maturity and hydrocarbon generation and also the types of products, usually for a specific well. These models are also referred to as maturity models as they encompass 1D heat flow simulation and subsequent geochemical models to construct petroleum generation and expulsion maps for the evaluation of source rock maturity (Hantschel and Kauerauf, 2009a). In addition, calculation and calibration of temperature histories and pore pressure prediction form major components of 1D maturity modelling.

2D basin model

Two dimensional models provide information about the petroleum system in a cross section. The ability to model a series of cross sections of a basin allows some insight into how hydrocarbon fluids migrate; their trapping mechanism and seal break through. Input data are similar to that of 1D models, however, 2D models require incorporation of lateral changes in rocks, source rocks and thermal properties. Lateral changes in these properties imply that each point along the cross-section undergoes a different burial and thermal history. So in the same formation, though at different depths and thermal properties, a source rock could be generating hydrocarbon at different times.

3D models

They permit a more realistic spatial analysis of migration and trapping. This technique is used in reconstructing a petroleum system at reservoir and basin scales and has the ability to display the output in 1D, 2D or 3D (Al-Hajeri et al., 2009). Three-phase darcy flow models can also be performed in 3D modelling. Various processes that affect

petroleum systems model and are observed to change through time are better modelled in 3D (Higley et al., 2006). For example salt or mud movement that are three dimensional in nature can be well captured in space and time using a 3D model as opposed to a 2D model.

Through 3D modelling the statistics of calibration, risk analysis and the considerations of extensional and compressional tectonics have seen significant improvement when compared to 2D modelling.

Data structure

The input data for basin modelling includes data that relates to the following: present day geometry, depositional environments, plate tectonics, rifting events, location of the basin, paleobathymetries and global climate. These suites of data have been assigned to the following categories:

Present day model

The data required for the present day model represent the stratigraphic and the structural elements of a sedimentary basin that includes horizons, facies maps and fault surfaces. Horizons are usually interpreted from seismic reflection surfaces. Individual horizons subdivide layers of distinct properties. Parts of layers with similar property values of geological bodies are termed facies. Layers can consist of different facies. So to adequately capture different facies in a layer, a facies map per layer is required and it is based on well data information and sedimentological analysis. Fault surfaces are constructed from interpreted seismic data and dipmeter logs.

Age assignment

Ages are assigned to all present day layers in association with major geologic events such as deposition, hiatus and erosion. Erosion events require maps depicting the amount of erosion and are combined with the corresponding water depth to capture the related uplift of the basin.

Paleo-geometry data

Knowledge from historical and regional geology, sedimentology and tectonics form the primary sources for paleo-geometry data. Paleo-water depth maps are derived from isostasy considerations of crustal stretching models. Where salt diapirs exist, paleo-

thickness maps for the main phases of salt doming are required. Erosion thickness can be re-calculated by decompaction of present day thickness to the supposed time of erosion and subtracting from an assumed relatively uniform depositional map. So the interplay of paleo-water depth, salt thickness, erosion and other paleo thickness maps determines the paleo-geometries (Hantschel and Kauerauf, 2009a).

Boundary conditions

Boundary conditions include the type and location of the sedimentary deposits that determines the paleobathymetry; and sediment-water interface temperatures throughout geologic time that are required in combination with estimates of paleo-heat flow for calculating the temperature history of a sedimentary basin (Al-Hajeri et al., 2009).

Facies properties

In basin modelling two groups of facies types are considered: the rock facies, also known as lithofacies and the organic facies, commonly referred to as organofacies. The properties that are used to define the lithofacies are dependent on porosity, temperature, thermal conductivities, heat capacity, radiogenic heat, permeability, compressibility and capillary entry pressures. Organofacies relates to all kinetic parameters required for the generation and cracking of hydrocarbon. Examples of such parameters are total organic carbon (TOC), hydrogen index (HI) and Arrhenius-type activation energy (Hantschel and Kauerauf, 2009a).

Seismic data

Seismic data can be in the form of seismic attribute cubes or maps which can be used to improve the facies maps. Seismic cubes could come with two-way-time or depth scales.

Basin modelling workflow

The overall process of basin modelling can be viewed as an iterative process, with most of the steps interrelated. Two key steps make up basin modelling workflow: (1) model building, and (2) forward modelling (Figure 3.18). Model building involves constructing a structural or a conceptual model and identifying the chronology of deposition and physical properties of the stratigraphic units. Forward modelling performs calculations on the model to simulate sediment burial, pressure and temperature changes, kerogen maturation and hydrocarbon expulsion, migration and

accumulation (Al-Hajeri et al., 2009). These processes are further discussed in the sections below.

Model building

The first step in basin modelling is building a present geometric model by creating a depth base structural model of the area of interest, which may aggregate a single or multiple petroleum system depending on the scale. For this initial step input data are formation tops and layer thickness which can come from seismic, from well logs or from out-crop. The modeller then establishes a basin history that is subdivided into an uninterrupted series of stratigraphic events with specific ages and duration. Each event represents a time of deposition, non-deposition or erosion. Syn- and post-depositional episodes of folding, faulting, salt tectonics and diagenetic alteration can also be defined. The entire process is achieved by analysing the present day geometric model to describe the depositional chronology and the properties of the basin fill alongside post-depositional processes. The selection of the critical moment – the time of generation, migration and accumulation of most of the hydrocarbon – is done at this stage based on the discretion of the modeller (Hantschel and Kauerauf, 2009a).

The absolute age for each layer that can be obtained from paleontologic, apatite-fission or radiometric data is important for determining the timing of generation, migration and trapping of hydrocarbon. To better define the potential reservoir or carrier bed, the lithology and depositional environment of each layer is defined when building the geometric model. Source rock characterization is required by describing the depositional environment and essential properties such as total organic carbon (TOC), hydrogen index (HI) and kinetic parameters, all of which contribute to determine the type and volume of hydrocarbon generated (Al-Hajeri et al., 2009).

Several other properties such as porosity and permeability in the reservoir and carrier layers must be specified and are important for fluid-flow computation and hydrocarbon volumetric estimates. Permeability for source rock is also defined and this determines the expulsion efficiency of source layers. Heat capacity and thermal conductivity are inferred from lithology and mineralogy and are needed for thermal calculations that model processes such as kerogen maturation and petroleum generation. In addition, compressibility and density data are needed inputs to model compaction and burial. The

burial history of sediments provides information about burial depth and preservation of organic material. The main inputs for building a burial history are sedimentation rate, compaction, erosion, depositional environment and tectonics. Modelling the petroleum potential of a basin requires the reconstruction of the temperature through time and this is achieved through thermal history modelling. So in addition to model properties, boundary conditions such as paleobathymetry, sediment-water interface temperatures through geologic time and paleo-heat flow must be defined in the model (Al-Hajeri et al., 2009).

Forward modelling

After the structural or conceptual model has been built with the properties of all layers defined, a forward simulation can be done starting with the oldest layer and progressing to the youngest. The following steps are a summary of the workflow as obtained in PetroMod^{TM} modelling software and as used in this research.

Deposition: in this module, depositional thickness can be calculated either by porosity-controlled backstripping starting with present day thickness, imported from structural restoration programs, or estimated from sedimentation rate and depositional environment

Pressure calculation and compaction: here a one phase flow of dewatering driven by overburden due to sedimentation is considered. Processes that cause pressure build up like gas generation, quartz mineralization is also taken into consideration.

Heat flow analysis: as heat flow controls important processes like thermal maturation of source rocks, all sources of heat such as emissions from radioactive minerals and igneous intrusions must all be taken into account. Boundary condition with inflow of heat from the base of the model should be defined. Present day heat flow can be estimated using temperature and thermal conductivity data from wells. The temperatures measured as a function of depth can be used to determine the geothermal gradient.

Petroleum generation: primary cracking (generation of petroleum from kerogen in source rocks) and secondary cracking (breakdown of oil to gas in source or reservoir rock) are considered. PetroMod^{TM} software utilizes a database of reaction kinetics to

predict the phases and properties of hydrocarbon generated from source rocks. By considering absorption models in PetroMod^{TM}, hydrocarbon generated from kerogen are released into free pore space of the source rock, a process also termed primary migration.

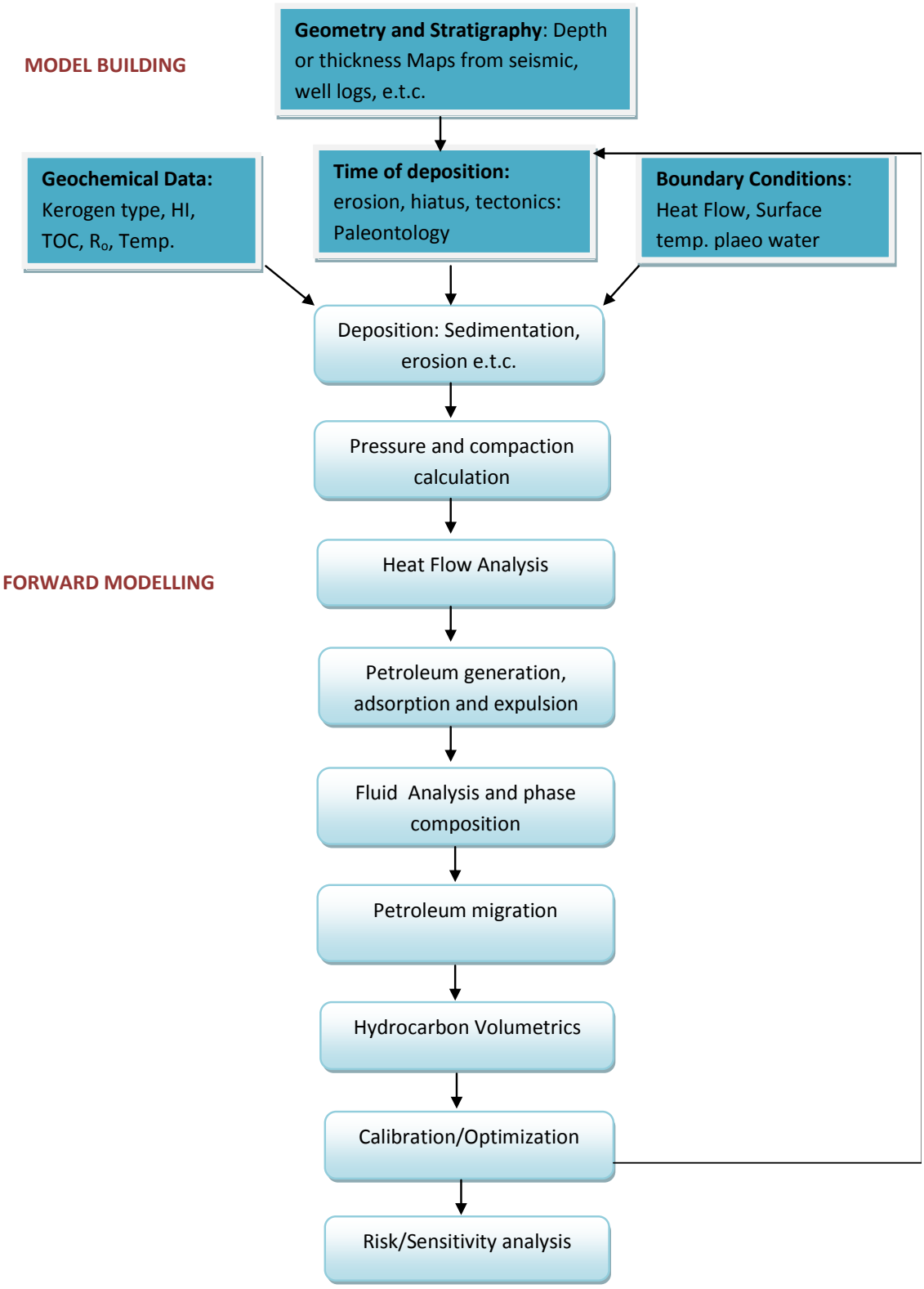

Figure 3.18: A typical basin modelling work flow for petroleum system analysis.

Fluid analysis: this step examines temperature and pressure dependent dissolution of hydrocarbon components in fluid phases to determine the fluid properties such as

viscosity and density, which would serve as input to fluid flow calculations, migration modelling and hydrocarbon volumetric calculations.

Fluid flow calculation: in PetroMod three different methods are used to model fluid flow: (1) darcy flow of multi-component three phase flow based on relative permeability and capillary pressure that permits the calculation of migration velocities and saturation of accumulated hydrocarbon; (2) flow-path analysis that carries out simplified fluid flow calculations mostly across high permeability carrier beds aimed at predicting the locations and the composition of accumulations; and 3) invasion percolation that models migration and accumulation. These methods assume that on geologic time scales, petroleum moves instantaneously due to capillary pressure and buoyancy. They are also utilised in modelling fluid flow in faults and for single phase flow.

Reservoir volumetrics: due attention is given to entry pressure of seal overlying potential reservoir and the spill point at the base of the reservoir since they both control the height of the hydrocarbon column in the reservoir.

Calibration/Optimization: the conceptual model of basin evolution, which forms the basis for the input data must be calibrated by comparing calculated results with measured data (Welte et al., 1997). The calculated result could have flaws; for example, the assumed heat flow may be wrong, unconformities may have been missed or missing section over or underestimated, hence it is of utmost importance to test the predicted maturity history against observed trends in maturity indices. The model can then be adjusted by iteration until the best fit solution is obtained. Information useful for optimizing the predicted model is derived mostly from wells; these data include:

(1) Present day temperature, that is, bottom hole temperature (BHT).

(2) Maturity distribution from different maturity indices like vitrinite reflectance, spore colour index, sterane and hopane isomerization (Welte et al., 1997).

(3) Apatite fission track analysis (AFTA)

(4) Fluid inclusions.

(5) Porosity of the layers (used in decompaction).

Risk/Sensitivity analysis: After optimization of conceptual model a sensitivity analysis can be performed by changing selected input parameters within geologically reasonable ranges and simulating again the basin evolution with these values. The use of sensitivity analysis in maturity modelling is vital in order to have a clear knowledge of the geological system, and for knowing how well results can be trusted (Waples et al., 1992); it can also be used to determine what new type of data would provide the greatest improvement to the model. In other words, sensitivity analysis provides a way to determine how much the output from a model or a calculation is altered by varying the values of the input data. Sensitivity analysis is of importance because there are many uncertainties in the input data used for any type of geological modelling (Waples et al., 1992). Recognizing these uncertainties could be very useful in two ways: the modeller can focus his or her attention on acquiring more data to help reduce the greatest uncertainty, and the modeller can establish to a greater extent the level of the uncertainty in the modelling results (Waples, 1998). Use of modelling results to reduce risk in exploration requires that quality measures be assigned to quantitative predictions. For example, what ranges of model predictions are possible for a given variability in the input parameter values? In principle, this question can be determined by repeating the forward calculation of the basin model for a different parameter set within the desired range of variability and observing the scatter of the results (Nielsen, 1996).

CHAPTER 4

BONGA FIELD: SEDIMENTOLOGY AND PETROPHYSICS

4.1 Introduction, Data and Methodology

The Bonga field was the first deep-water discovery offshore Nigeria at present-day water depths of 800-1200m. Although more than 30 wells have been drilled to date into the Miocene-age reservoir section of Bonga, there is minimal published material on the sedimentology. Internal reports (Shell, pers.comm., 2014) indicate a series of stacked and separated channel bodies of early to late Miocene age. The reservoir sands extend over a wide depth range of 1800 - 3350m (5000 – 11000ft) subsurface (Fig. 3.6). Based on a limited dataset, this study aims to provide a preliminary description and interpretation of the Miocene sedimentary section only. This will help with prediction of likely facies and characteristics of the deeper Oligocene succession that was not cored.

The data base from the discovery well (A1) includes:

a) Three conventional cores logged by Shell in April 1996 and re-examined by the author in 2012.

- 2468 – 2481m (8100 – 8143ft): Late Miocene (Cores 1 and 2)
- 3444 – 3500m (11300 – 11480ft) : Early Miocene (Core 3)

b) Seventeen samples selected for subsequent laboratory analysis

c) Conventional core analysis data.

e) Core photographs.

A summary of the analytical techniques used is given in Chapter 2.

4.2 Sediment Facies

Much of the core material examined shows a low degree of consolidation, especially from the more sand-prone sections and for the late Miocene succession. There also appears to have been significant core disturbance, either during the coring process and/or subsequently. This made visual description and interpretation quite challenging.

The deeper sections and those that were more mud-prone were more consolidated and better preserved.

The principal sediment facies identified are as follows (Fig. 4.1):

Unconsolidated sand: disturbed sections of loose, unconsolidated sand, in some cases contaminated with other debris; no clear bedding; no internal structures; fine-medium grained.

Structureless sand: weak to moderate consolidation; beds 0.1 – 1 m thick, with some sections up to 4m thick without apparent bedding; structureless; fine-medium grained, moderately well sorted.

Graded sand and sand-mud units: weak to moderate consolidation; beds 0.1 – 2 m thick; normal grading, rare reverse-graded bases; partial Bouma sequences of structures common (Ta, Tab, Tabc, and Tabcd), erosive bed bases common; grading from medium-grained sand to silt/mud, moderately well to poorly sorted.

Non-graded sand and sand-mud units: weak to moderate consolidation; beds 0.1 – 0.5 m thick; parallel-lamination, rare cross-lamination; medium-grained sand to silt/mud, moderately well sorted.

Interbedded silt/sand and mud: moderate consolidation; beds < 0.1 m thick, mostly < 0.05 m thick; normal grading from fine sand to mud in some cases; partial Stow sequences of structures common (T0-8 divisions represented), some sand/silt units are distinctly lenticular, some mud units are apparently structureless and/or bioturbated, micro-erosive bed bases common; fine sand to silt grade and interbedded mud, moderately poorly to poorly sorted.

Disturbed units: a range of disturbed structures evident, especially in the finer-grained sections (silt/mud units); these include: (a) contorted convolute lamination, (b) contorted slump-fold lamination, (c) cross-cutting injected sands, and (d) micro-faulting, some faults with millimetric displacement.

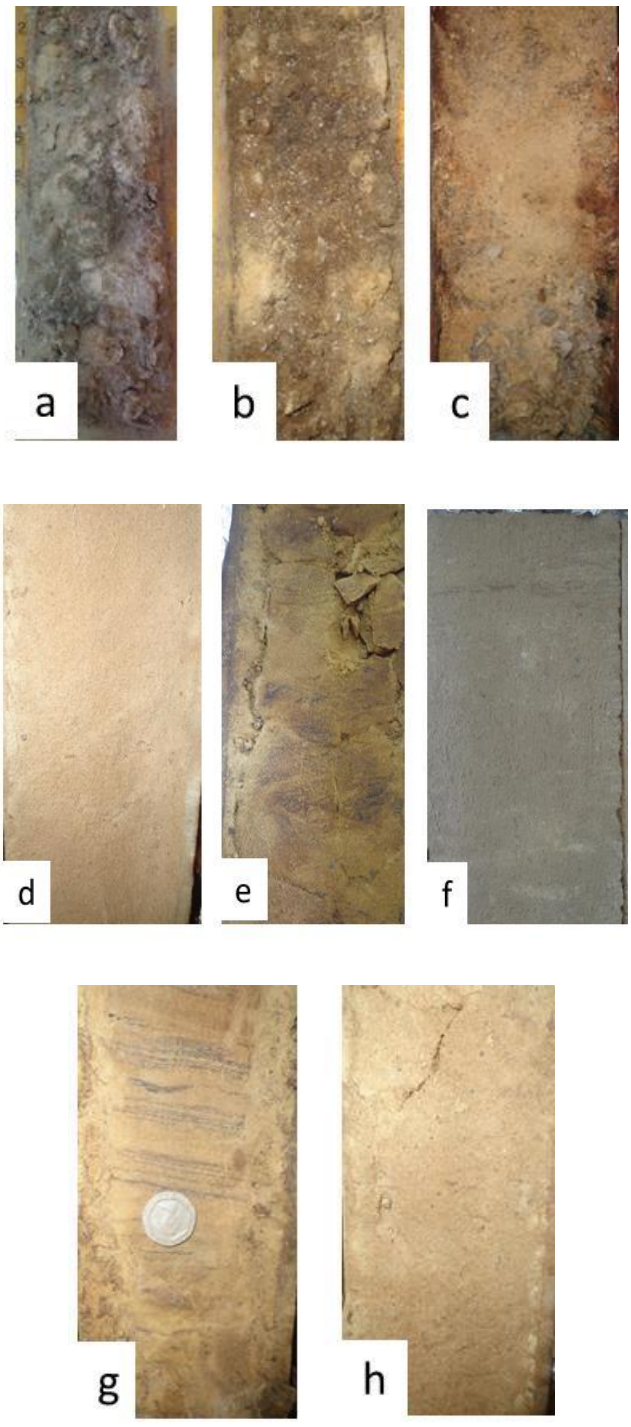
a
b
c
d
e
f
g
h

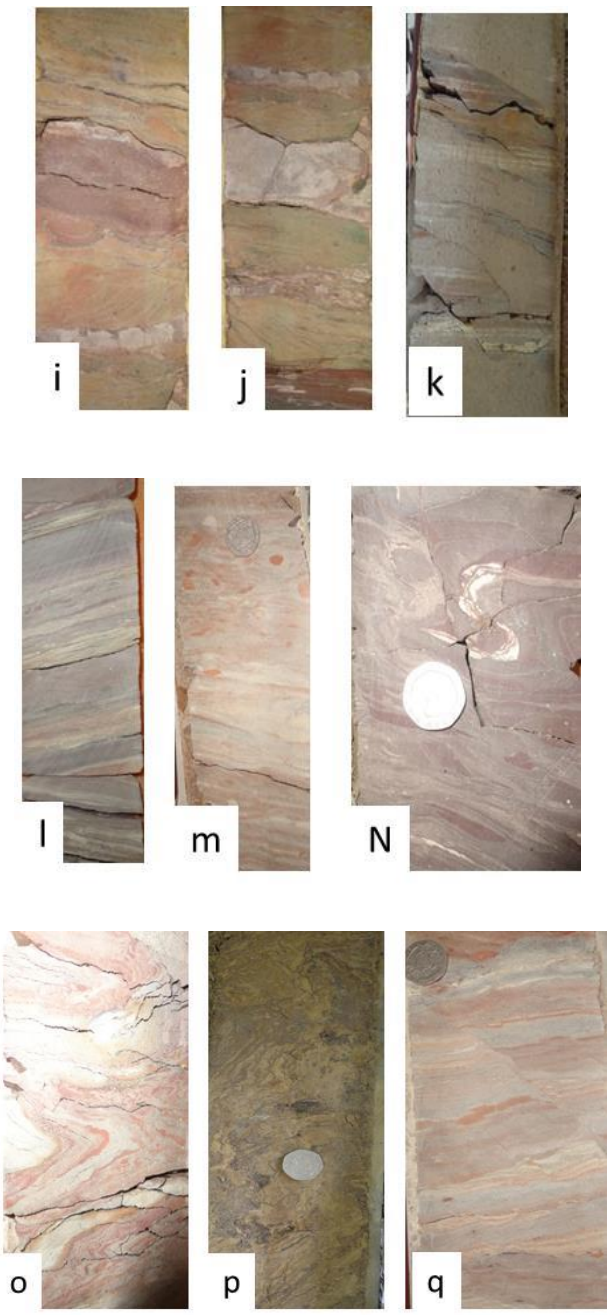

Figure 4.1: Sedimentary facies interpreted from whole core data. Cores a, b and c = loose, highly unconsolidated sands with no clear sedimentary structures; d, e and f = moderately consolidated massive sands with brownish to grey colour. Brown colour noted in core-e is due to oil staining; g and h core showing normal and reverse grading respectively; I, j and k = sand and silty facies characterised by parallel and cross laminations. Erosive base is also a common boundary surface; l, m and n = interbedded silt and sands, in some cases lenticular with some slump folding (core photo-n); o, p and q = highly disturbed units. These cores are also characterised by contorted convolute laminae (o), injectities (p), and micro faulting (q). (

4.3 Sediment Attributes

4.3.1 Colour and hydrocarbon staining

The sands and silts are mostly pale grey to brownish in colour, where the brown colours are due to oil staining. This oil staining only affects the medium to very thick-bedded sands, and has not affected the thinner-bedded sandstones and contorted beds.

4.3.2 Sediment texture

Thin section petrography reveals that the cored sands show remarkably consistent sediment textures throughout. The sand samples all show a dominant grain-size which is borderline between fine and medium sand (217 - 281 microns) and maximum grain sizes ranging from coarse (upper) to very coarse (upper) (710 - 1480 microns). The sands are mainly moderately sorted and grains are dominantly sub-rounded. The sands all show loose packing with a dominance of point contacts and very friable aspect.

4.3.3 Sediment composition

Detrital mineralogy: Thin section analysis in conjunction with SEM data indicates that the detrital mineralogy of the sand-rich samples is dominated by quartz with moderate proportions of feldspar and heavy minerals. They can be classified as quartzarenites since they are dominated by quartz with <15% feldspar.

A brief summary of the main detrital minerals are given below. Mineral percentages refer to estimates from SEM images. Scandium^{TM} software package was utilised in providing an estimate of percentage distribution of detrital mineralogy. The software works by defining the range of grey levels of the individual minerals identified. These are then converted to colour and automatically quantified based on the thresholded colour images. In addition, porosity was also estimated, particularly for the lower Miocene samples which were consolidated. Appendix A shows BSE photomicrographs of the Lower Miocene reservoir showing the distribution of the minerals. The percentage distribution of the detrital minerals in the Upper Miocene reservoir was not quantified because of the nature of the samples, which were mostly sands and would not be representative of its in-situ condition.

Quartz (86%) is the dominant framework grain component. It is present mainly as monocrystalline grains with straight to slightly undulatory extinction, together with minor polycrystalline grains including strained metamorphic types.

Feldspar (4%) is present in most of the analysed samples, with potassium feldspar as the dominant feldspar type that show simple twinning under x-polars. In thin sections, most feldspar grains appear fresh or only slightly leached and degrading to clay.

Accessories (1%) are present in minor amounts in most samples. Low amounts of heavy minerals likely zircon, tourmaline or garnet are noticeable. Detrital opaque minerals are seen in most samples possibly pyrite.

Diagenetic mineralogy: The sand samples from Well 1 are characterized by very low proportions of diagenetic minerals. The only significant diagenetic phase present is authigenic quartz, with very rare kaolinite and pyrite.

Quartz (1 - 4%) is the dominant diagenetic phase in all samples. In general quartz is present as thin syntaxial overgrowths, which slightly occlude primary intergranular pores. Other authigenic phases are not present in sufficient quantities to determine the relative timing of the quartz overgrowth development.

Kaolinite occurs in minor amounts (less than 5%) in only three samples. Observed kaolinite is present as microporous partly pore-filling patches of booklets, typically <15 microns in size.

Siderite is noted in one sample only as thin discontinuous laminae/lenses and as a rare coating of quartz grains.

Figure 4.2 are photomicrographs of optical microscopy and SEM that illustrates some of the minerals highlighted above.

Porosity: Porosity was estimated from the polished blocks (Figure 4.1 C and D) using the Scandium software was about 21 % (21 porosity units – p.u) for the Lower Miocene. This is close to the 25% average porosity calculated from wireline log (see next section).

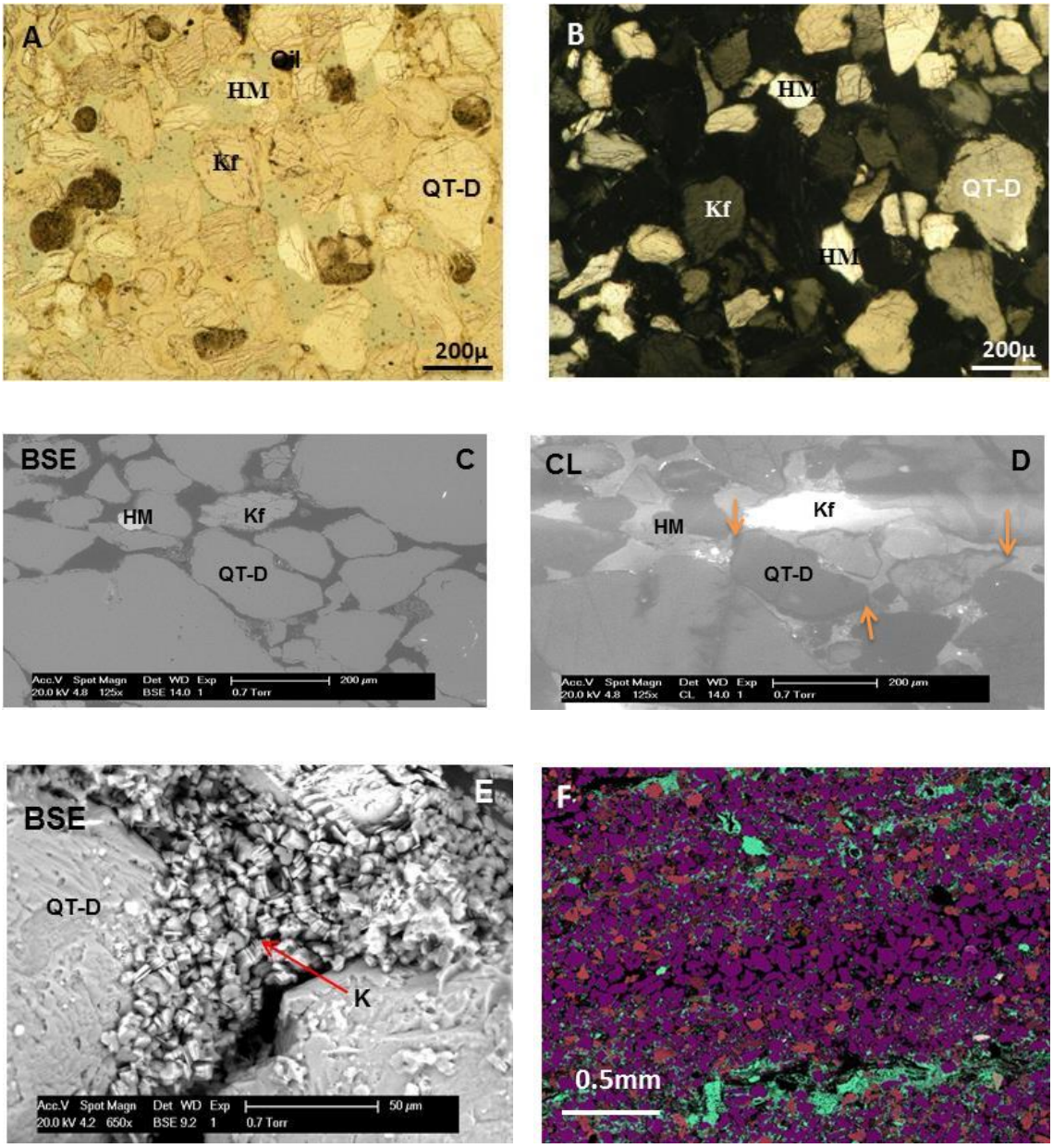

Figure 4.2: Photomicrographs of thin sections, polished blocks and whole grains taken from the Miocene succession. A and B are plane polar and cross-polar thin section images, showing mostly detrital minerals – quartz, feldspar and heavy minerals. The plane polar image also clearly shows weathering of feldspars characterised by dirty brown patchy occurrences. C and D are Backscattered Electron (BSE) and Cathodoluminescence (CL) plates from polished blocks that reveal the presence of quartz overgrowth indicated by the amber coloured brown arrows. E is a BSE image of whole grain showing pore space filled with kaolinite crystals. F is an elemental dispersive X-ray (EDX) map, illustrating the rare presence of siderite laminae (green) in Miocene reservoir.

4.4 Preliminary Sediment Interpretation

The features and sediment facies observed in the cores are interpreted as the result of normal deep-water depositional processes. There is clear evidence of thin and medium-bedded turbidites, with partial Bouma sequences (Bouma and Ravenne, 2004), and of very thin-bedded turbidites, with partial Stow sequences (Stow and Shanmugam, 1980). The thicker structureless sand units are interpreted as deepwater massive sands of turbidite or debrite affinity. Disturbed facies with slump-fold laminae are probable slump deposits. Other disturbed sections may result from post-depositional and/or coring disturbance. The sands are texturally and mineralogically mature to sub-mature. The finer-grained facies (silts and muds) are mainly hemipelagic in appearance.

Diagenesis is weakly developed throughout. The upper cores are very poorly consolidated with compaction and minimal cementation. Diagenesis with weak cementation is better developed in the deeper samples.

4.5 Petrophysical Properties

This section aims to investigate the potential implication of the sedimentological and mineralogical assessment of the Miocene sequence on key petrophysical properties, particularly porosity and permeability. This was achieved through an integration of core and log based petrophysical evaluation. Results from the evaluation were then used to make both qualitative and quantitative assessment of the reservoir quality of the un-cored Oligocene sediments. Petrophysical evaluation conducted on well A1 – the only well that penetrated the top of the Oligocene succession formed the basis of the estimated rock properties for the Oligocene reservoir.

4.5.1 Data availability and quality control

Data availability

Nearly all the wells provided for this study were evaluated with full suite of modern logs. All wells were logged with both gamma ray (GR) and resistivity tools. Of the 20 wells available for evaluation, complete suite of conventional logs, including sonic logs plus check shots survey, were available in only 10 wells. Core data were provided for three of the wells, including core porosity and core permeability measurements from routine core analysis (RCA). The core measurement provided "ground truth" references

for calibrating rock properties computed from well log data and most importantly helped minimise uncertainty in the evaluated parameters.

Quality control/data preparation

Where poor data quality exists, data editing such as de-spiking (clipping erroneous values) was carried out to ensure that the recorded data respected true formation response. In addition, when correlated with other suites of data, recorded information was checked to ensure consistency across all data type. For example, where there are missing data due to acquisition issues or intervals where poor bore hole conditions existed due to fluid invasion or washouts, highly sensitive tools like the density log would typically record abnormal readings. The density log in such case was flagged as poor data with low confidence when calculating rock properties. Core depth matching was also carried out, so that cores that were acquired and referenced to the driller's depth were corrected to the wireline logger's depth. The gamma ray log served as a reference for qualitative core depth adjustment. The core measurements were provided as stressed corrected data (Shell, pers.comm., 2014) to reflect reservoir properties at *in-situ* condition.

4.5.2 Evaluation of reservoir rock properties

Volume of Shale

The volume of shale which is a key input in calculating porosity and defining net thickness was carried out based on two different methods: (1) a single log method using only the gamma ray log – a lithology identification tool (Equ. 4.1); and (2) a combination of two logs – the density and the neutron porosity logs (Equ. 4.2) (Rider, 1986, Asquith and Krygowski, 2004). The integration of both methods is necessary for the shortcoming of the individual tools, most especially the effect of radioactive sands on the gamma ray tool. Radioactive sands or hot sands would typically have a significantly higher gamma ray value than actual clean sands (Chudi and Simon, 2012), which would result in a higher than expected volume of shale and ultimately compromise the net sand thickness. Hence, the density-neutron combination for shale volume assessment was the preferred model adopted to compensate for the effect of radioactive sands since both density and neutron logs are not affected by radioactive minerals.

$$GR_{index} = \frac{GR - GR_{matrix}}{GR_{shale} - GR_{matrix}} \qquad (4.1)$$

Where GR_{index} = indicator of shaliness, GR = recorded gamma ray value from log, GR_{matrix} = gamma ray value in a clean sand, GR_{shale} = gamma ray value in shale

$$V_{shale} = \frac{(X_1 - X_0)}{(X_2 - X_0)} \qquad (4.2)$$

$$X_0 = NPHI_{MA}$$
$$X_1 = NPHI + M_1 \times (RHOB_{MA} - RHOB)$$
$$X_2 = NPHI_{Sh} + M_1 \times (RHOB_{MA} - RHOB)$$
$$M_1 = \frac{NPHI_{FL} - NPHI_{MA}}{RHOB_{FL} - RHOB_{MA}}$$

where NPHI = neutron porosity log, RHOB = density log, MA = Matrix, Sh = Shale, FL = fluid

Porosity

Reservoir porosity was determined from the density logs using the density equation (Equ. 4.3). An average matrix density of 2.65g/cc for quartz was used. This was based on the grain density measurement from routine core analysis of the cored wells. In addition fluid density (ρ_{fl}) of 1.01g/cc was used as the density of mud filtrate in the flushed zone at near well bore region. This was a reasonable estimate considering that the reservoirs encountered by the wells are not gas bearing.

$$\phi = (\rho_{ma} - \rho_b)/(\rho_{ma} - \rho_{fl}) \qquad (4.3)$$

where

ρ_{ma} = matrix density

ρ_b = bulk density

ρ_{fl} = apparent fluid density

Water Saturation (S_w)

Water saturation (S_w) was estimated using Archie water saturation model (Equ. 4.4). The choice of the model was guided by the relatively clean nature of the hydrocarbon bearing sands seen both from logs and core data. The main aim of calculating water saturation was to use estimated irreducible water saturation as an input to the Wyllie and Rose permeability equation.

$$S_w = \left(\frac{a * R_w}{R_t * \phi^m} \right)^{-n} \qquad (4.4)$$

where

a = tortuosity exponent

R_w = formation water resistivity

ϕ = formation porosity

R_t = formation resistivity

m = cementation exponent

n = saturation exponent

The tortuosity exponent (a), cementation exponent (m) and the saturation exponent (n) are all electrical properties of rock that are typical measured from core samples. Where no measurements was conducted on core then values of 1, 1.8 and 1.8 which are typical values for siliciclastic sediments (Asquith and Krygowski, 2004) are assumed respectively for each of these properties.

Permeability

The reservoir permeability was estimated from the Wyllie and Rose equation which is dependent on porosity and irreducible water saturation (Sw_{irr}). The irreducible water saturation was calculated by employing the Archie water saturation equation across pre-production wells. The Wyllie and Rose model was adopted because it considers the irreducible water saturation which is a reflection of grain size – a key control on permeability. Where large grain sizes would are characterized by low irreducible water saturation and therefore a high permeability value. On the other hand smaller grain size would be reflected as having high irreducible water saturation and a corresponding lower permeability values. So there is a strong relationship amongst grain size, permeability and irreducible water saturation. Smaller grain sizes are prone to lower permeability and have a higher affinity to water due to exposed larger surface area, hence higher irreducible water saturation.

$$k = \frac{C\,\phi_{eff}^{6}}{S_{wirr}^{2}} \qquad (4.5)$$

where

k = permeability

C = empirical constant with values of 62500 for oil or 6500 for gas reservoir

ϕ_{eff} = effective porosity

S_{wirr} = irreducible water saturation

Multi-mineral core-log integration

A multi-mineral model based on petrophysical elemental analysis (ELAN) of open-hole logs inversely calculates the volume of mineralogical component of a formation. This technique is at its best when the minerals have been identified from petrographic study

of core samples. In this study the volumetric estimate of quartz is pertinent across the intervals logged, that is, from the Miocene to deeper Oligocene succession. The results from ELAN would be integrated with other methods applied in this study to assess the volume change of quartz and the factors that are likely responsible for this change observed in younger sediments and further deeper into the Oligocene interval.

ELAN uses log curves and the response parameters of the tools to compute volumetric constituents of formation minerals and fluid. This method derives the relative quantities, or relative volumes, of the mineral components that would most probably produce the set of measurements recorded by the logging instruments. So there is a three way relationship; tools, response parameters and formation component volume, as depicted in Figure 4.3.

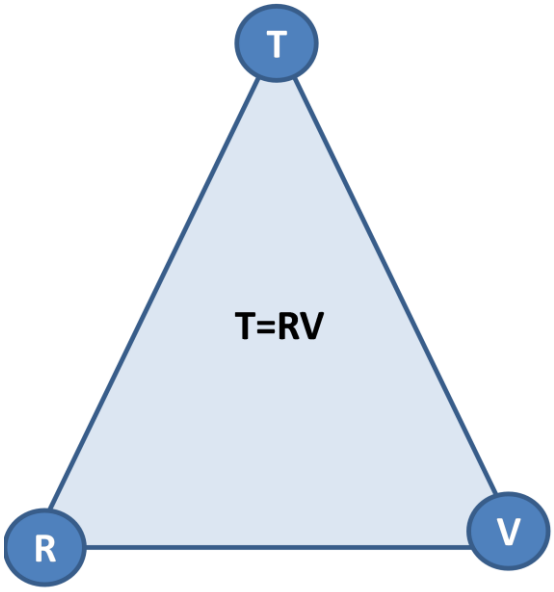

Figure 4.3: Schematic illustration of ELAN. T represents the tool vector in this case the input log data (gamma ray, resistivity, neutron, density, and calculated porosity logs), R is the response matrix, that is, a pre-defined value for the reading each tool would give for 100% of each formation component. R values were determined based on the known mineralogical responses to the physics of the different tools (Reeder *et al*. 2013) as defined using the Schlumberger ELANPlus programme in Techlog software package. V is the volume vector – the volume of the formation components.

In the inverse model, T and R are used to compute V. The solution of the inverse model is considered the main objective of the ELANPlus program.

The forward model, known as log reconstruction, uses R and V to compute T. A log reconstruction model is computed for each inverse model. The reconstructed logs are compared against input data to determine the quality of volumetric results from the inverse model

Using T and V to compute R also called model calibration. Here the question would be 'what response parameter value(s) should be used to obtain the best fit between the observed logging instrument readings and the likely formation component volumes (possible core results)?'

Electrofacies Analysis

In the absence of core data in the Oligocene succession, an electrofacies model was built through an integration of the density-neutron cross-plot (Figure 4.4).

In the density-neutron crossplot, the density log values are plotted on the y-axis with values displayed in a reverse order (values increasing downward) and the neutron values are plotted on the x-axis with its values increasing from left to right. The location of points on the plot can discriminate underlying mineralogy and reveal trends such as shaliness or porosity. Each pure mineral will plot as a single point. The power to discriminate depends on the independence and uniqueness of log responses to the lithologies of interest. The density-neutron crossplot includes calculated overlay points and lines. The points locate various lithologic endpoints of interest, while the lines track the simultaneous solution of the response equations for the two logs over a range of variable such as porosity, or percentage of one mineral vs. another. These response equations are simply the linear mixing-law response equations discussed in the sections above on the individual logs. With only two variables—the two logs—only two unknowns can be extracted. For example, one could determine matrix type (and its associated endpoint-log readings) and the amount of water-filled porosity. Ideally, because both are porosity logs, points of a given porosity in a pure lithology will fall along a diagonal line. Such a line represents the simultaneous solution of the density and neutron mixing laws as a function of varying porosity. Three such lines are generally plotted as overlays on this crossplot. They correspond to a calcite, dolomite, or quartz matrix with water-filled porosity. Examination of the density-neutron

crossplot serves as a major steps in reconnaissance log analysis. The crossplot is been used to identify rock types and porosity ranges and guide the selection of facies and zones.

The facies classes were modelled to honour the variation in density-neutron value principally controlled by rock type and fluid content. There is no gas present in the reservoir that can result in anomalously recorded values of both density and neutron logs. The influence of oil would be minimal considering that both oil and formation water have near similar density values. So the facies discrimination was mostly affected by rock properties.

The density-neutron crossplot,was chosen because the nuclear logs (density and neutron) have an advantage over sonic or resistivity laws. Nuclear logs generally obey simple, linear, bulk mixing laws that have a firm basis in physics. The mixing laws for sonic and resistivity measurements are not only nonlinear but also largely empirical, with only weak connections to theory. Nonlinear terms in a mixing law show up on crossplots as curved lines.

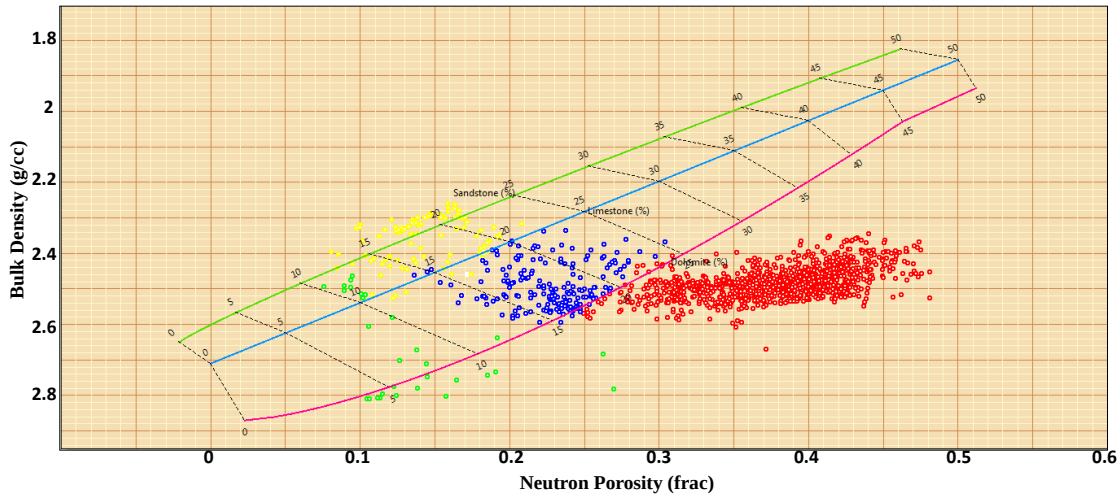

Figure 4.4: Density-neutron cross plot of the logged Oligocene interval showing colour coded data based on the log values which reflects four classes of electrofacies. Yellow = clean sand facies, blue = shaly sand facies, green = tight sand facies, and red = shale.

4.5.2 Results

Shale Volume

The volume of shale estimated across the wells indicates that the Miocene reservoirs have very minor shale content that is unlikely to have a significant effect on the computed total porosity from the density logs (see Figure 4.5). This is also supported by the observation from both core description and thin section were minor clay mineral (kaolinite) is seen between rock grains. Therefore the Miocene reservoir is described as clean sandstone with an average clay content of about 5%. The estimated volume of shale within the Oligocene reservoir shows a lesser volume of shale compared to the Miocene reservoir.

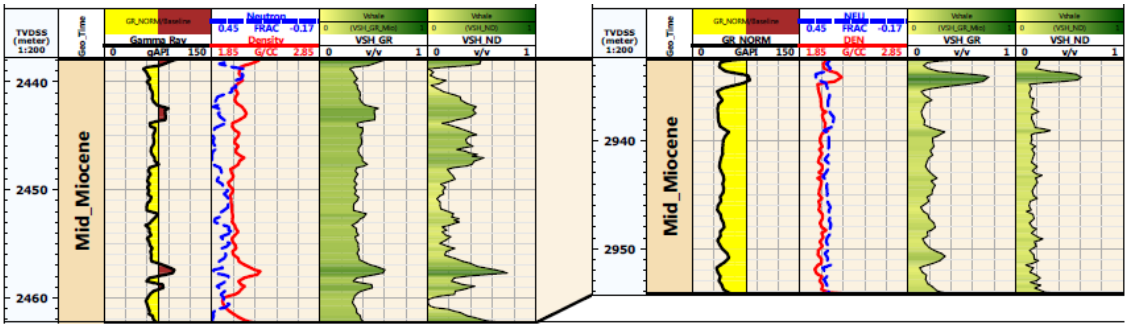

Figure 4.5: Volume of shale computed from gamma ray log (track 5) and density-neutron combination (track 6) for the Mid Miocene reservoir in two wells. Note the slightly higher volume of shale computed using the gamma ray log compared to the volume of shale from the combination of density-neutron logs. The gamma ray shows sandstones in yellow colour and shales in brown. The calculated volume of shale is based on equations 4.1 and 4.2 above.

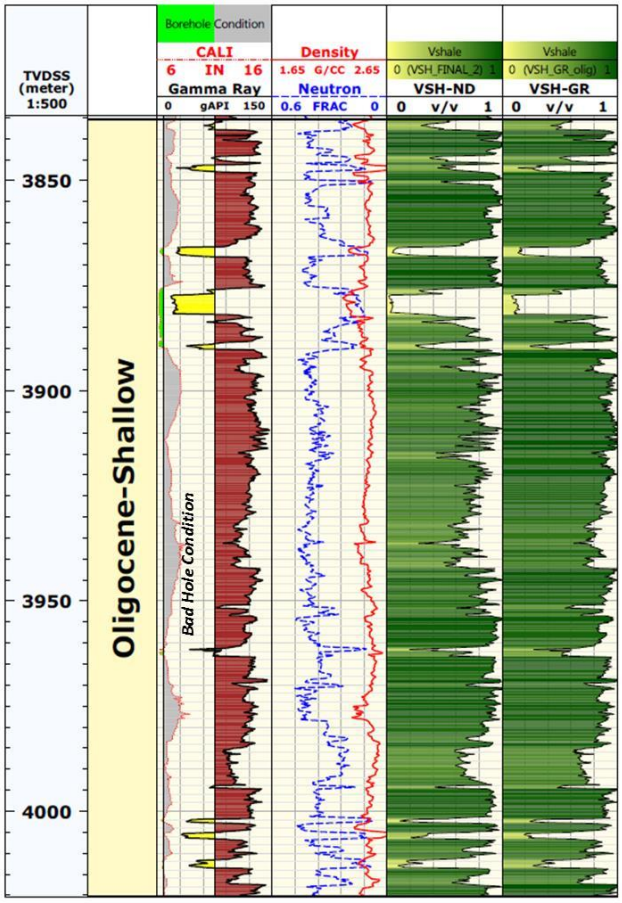

Figure 4.6: Volume of shale computed from density-neutron (track 5) and gamma ray log (track 6) for the Oligocene section in Well A1. The gamma ray shows sandstones in yellow colour and shales in brown. Note the bad hole condition (grey shaded area in track 3) reflected as the calliper log records larger bore hole size in comparison to the drill bit size (black straight line).

Porosity

The Miocene sediments generally show good porosity distribution that ranges from 25-37% with the higher values from younger aged reservoirs to Mid-Miocene and decreases to about 25% in the Lower Miocene reservoir. The porosity depth plot thus reveals high porosity values from Mid Miocene to Lower Miocene (1500m – 3200m) and drop significantly from Lower Miocene into the Oligocene interval (3200 – 4000m). The high porosity values is likely attributed to early oil charge that has the potential of halting porosity reducing diagenetic reactions and creating a localized overpressured condition suitable for preserving porosity. Beyond 3200m the reservoirs encountered by well A1 are not hydrocarbon bearing, hence they are susceptible to diagenesis resulting to lower porosities.

Cross plot of porosity against depth shows porosity values decrease steadily into the Oligocene reservoir to total average value of about 20% (Figure 4.7). Since there are no cores acquired in the Oligocene interval which can be used for calibration, it is therefore likely that the porosity decrease is attributed to combination of both compaction and cementation. An increase in both density and neutron values across some the penetrated sands reflects the possibility of a highly compacted reservoir (e.g. reservoirs located at 3847m, see Figure 4.6). The resistivity logs responds to compaction by a positive excursion to the right, however, this could also be attributed to the presence of hydrocarbon.

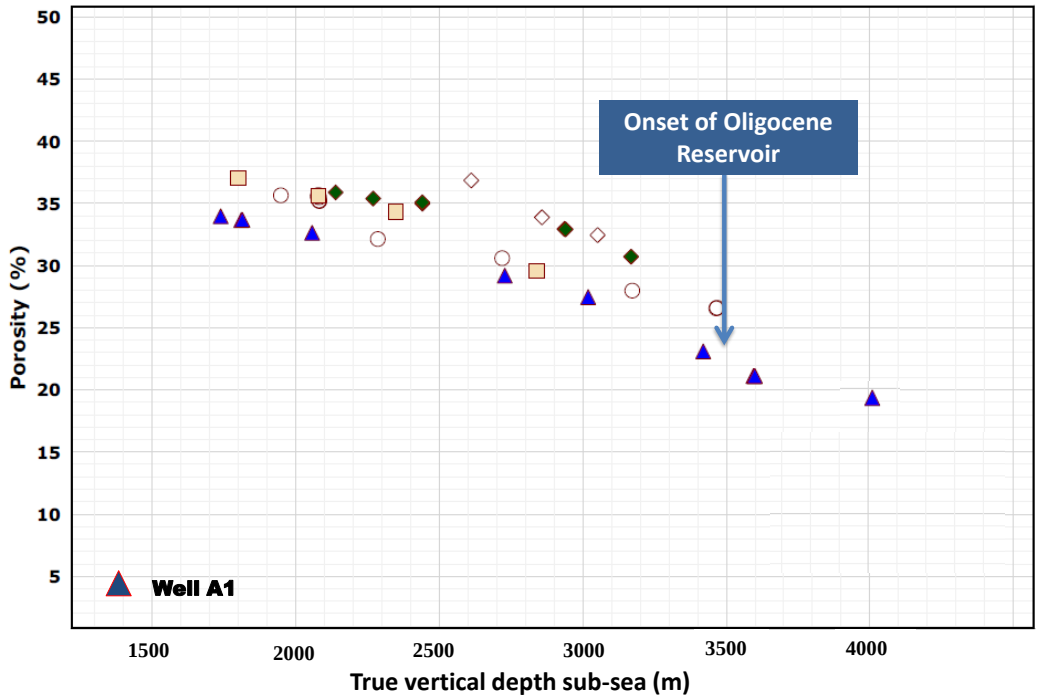

Figure 4.7: Average porosity versus depth showing reduction in porosity for several stacked reservoirs plotted against depth for 5 wells. Well A1 the deepest well in blue triangle with Oligocene porosity starting at 3500m. The other data are from four wells located not more than 500m away from Well A1.

Permeability

Core permeability values of the Miocene reservoir range from 10-10000mD with an average value of about 2000mD. A good correlation exists between core permeability and porosity, suggesting a dependency of permeability on porosity across the Miocene

sediments (Figure 4.8). Hence, it was suitable to use the Wyllie and Rose equation in estimating log based permeability. The Log based permeability also showed good agreement with the core permeability as illustrated in track 7 of Figure 4.9.

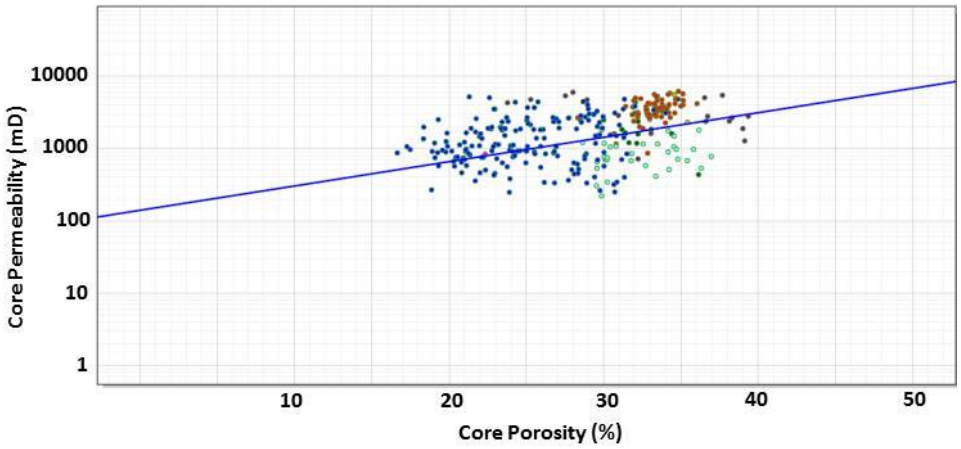

Figure 4.8: Cross plot reveals the correlation of core porosity and core permeability. The colours represent data from four different wells.

Saturation

Average Sw_{irr} for the Miocene reservoir was estimated at 12% (Table 4.1). The Oligocene units indicate to be significantly water bearing with computed average water saturation close to 65%. Since only a single well encountered the Oligocene succession the computed average water saturation might not be representative of the Oligocene reservoir across the entire study area. Hence there exists a significant uncertainty in saturation estimates. The calculated water saturation was used in computing permeability (Figure 4.10). The permeability across the Oligocene interval was not calibrated since no core was acquired from the Oligocene interval. However, a good core to log calibration for both porosity and permeability was archived in the shallower Miocene reservoir (Figure 4.9).

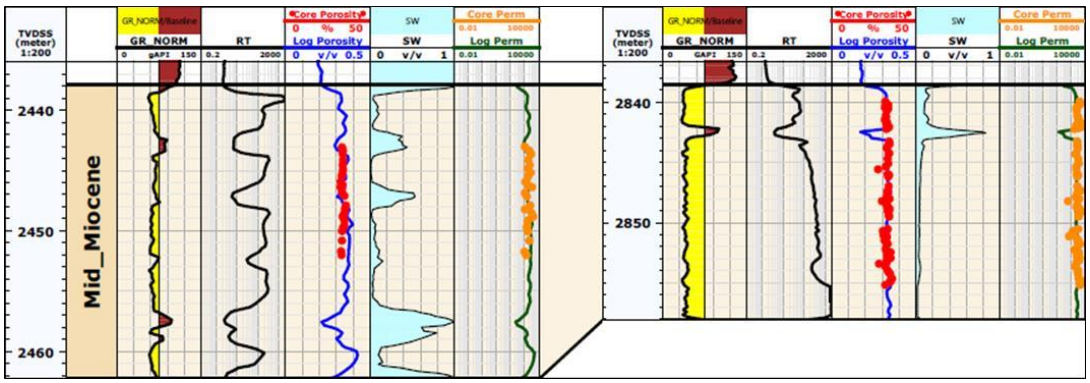

Figure 4.9: Composite log panel for two wells with core measurements showing log and core porosity (track5), estimated water saturation (track 6) and core permeability (track 7). A good match is seen between core porosity (red dots), core permeability (amber dots) and the log-derived porosity and permeability in blue and green curves respectively.

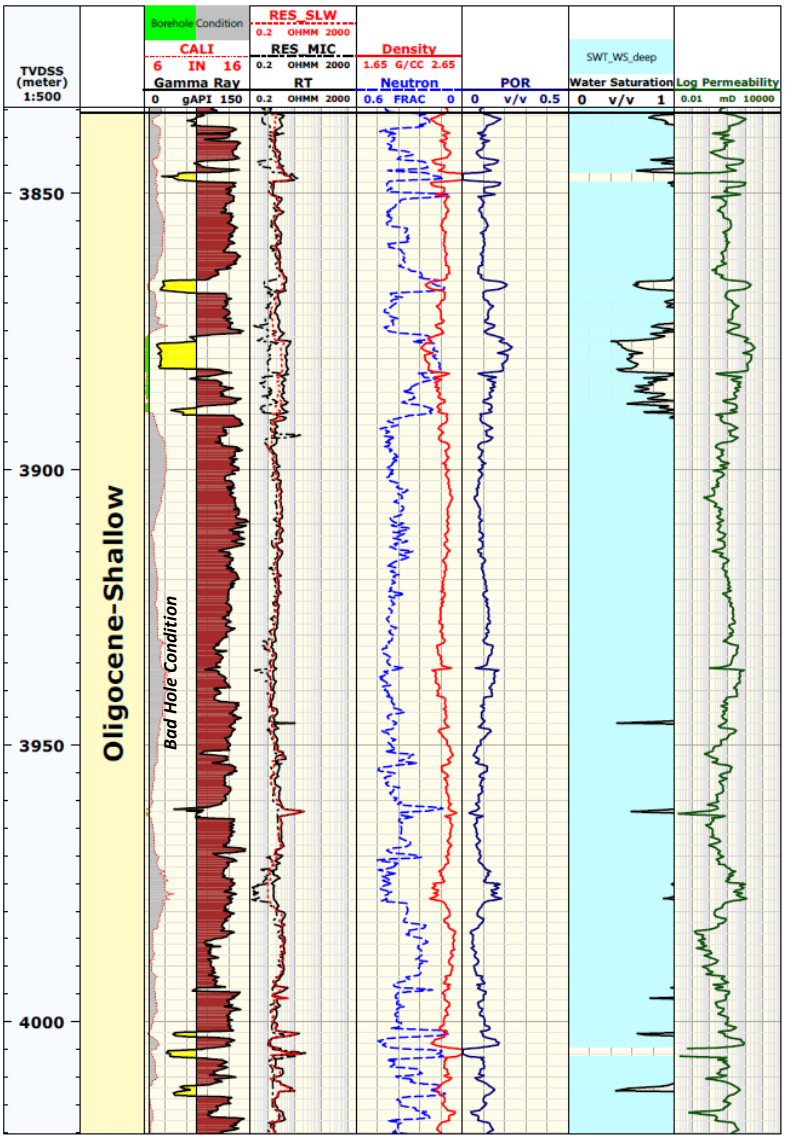

Figure 4.10: Composite log for the Oligocene logged section showing raw logs (Tracks 3 – 5: track 1 = gamma ray and calliper; track 4 = shallow, mid and deep resistivity logs; track 5 = density and neutron logs) and evaluated logs (Tracks 6 – 8: track 6 = porosity, track 7 = water saturation, and track 8 = log-derived permeability).

Average reservoir rock properties were calculated across the Miocene reservoir and the logged Oligocene intervals (Table 4.1). The volume of shale was used as a cut-off parameter in discriminating reservoirs from non- reservoirs. This also formed the basis for calculating the average porosity, water saturation and permeability across the net reservoir sections. Of all the calculated reservoir properties, only average net-to-gross that is noted to increase from Miocene to Oligocene by 8% (0.08 frac). This is likely linked to the lower shale content in the Oligocene compared to the Miocene.

Reservoirs	Thickness (m)	N/G (Frac)	Porosity (%)	Hydrocarbon Saturation (%)	Permeability (mD)
Oligocene	**6**	**0.98**	**20**	**44**	**180**
Mid-Miocene	**25**	**0.9**	**35**	**88**	**2300**

Table 4.1: Average rock properties for Mid-Miocene and Oligocene reservoirs. A dramatic reduction in most of the average rock properties is seen from Miocene to Oligocene reservoirs.

Multi-mineral analysis

The results of the multi-mineral analysis are displayed in Figures 4.11 and 4.12. Tracks three to eight of Figure 4.11 shows the input logs while the track 8 illustrates the multi-mineral model derived from the input data. With the key mineralogical component of the formation defined based on the core analysis done on the Miocene interval, the volume of quartz mineral was well predicted. This is particularly true where a good match was achieved between the input log and the reconstructed logs (green curves), most especially across the reservoir unit (coded yellow in GR log). A match was not achieved across the shales most likely due to poor bore hole condition, attributed to shale washout.

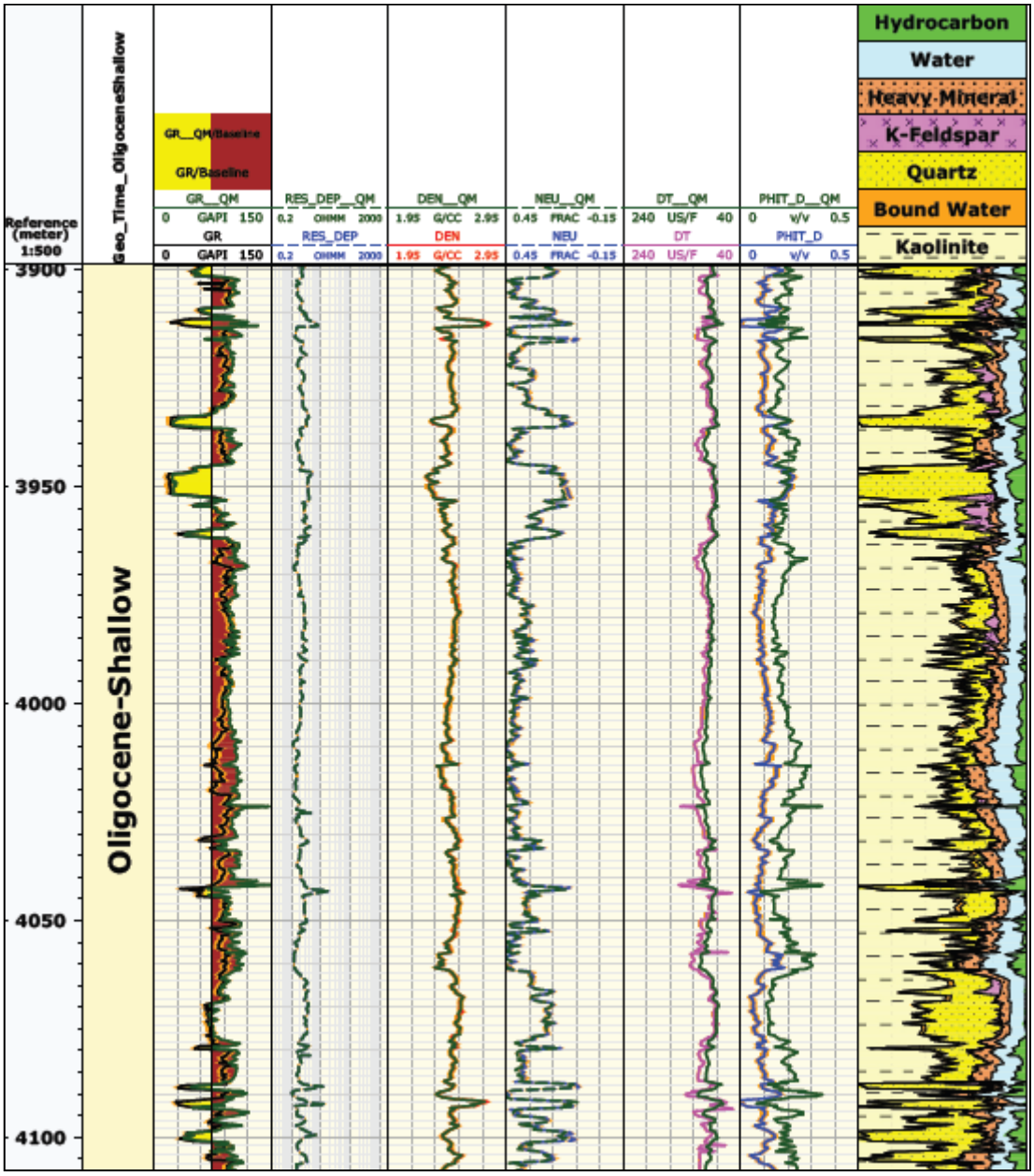

Figure 4.11: Modelled mineral volumes across the Oligocene interval illustrated in track 8 (quartz = yellow, feldspar = pink, heavy mineral = dotted amber, kaolinite = cream with dash).Track 3 = Gamma ray, track 4 = resistivity, track 5 = density, track 6 = neutron and track 7 = porosity. Logs with suffix of 'QM' represents back calculated logs.

The modelled quartz volume is seen to increase with depth as observed from the cross plot of quartz volume as a fraction of the total reservoir component (mineral, fluid and rock) plotted against depth (Figure 4.12) with two trend lines seen. The first trend line (a) indicates a steady increase with depth in quartz volume of close to 60% volume

fraction from the Upper Miocene to the Middle Miocene reservoirs. An offset is seen in the second trend (b) representing quartz volume for Lower Miocene down to the Oligocene with estimated quartz of close to 80% in the Oligocene aged reservoir. The separation (C) between the two trend lines is the additional volume increase most likely due to both compaction and cementation.

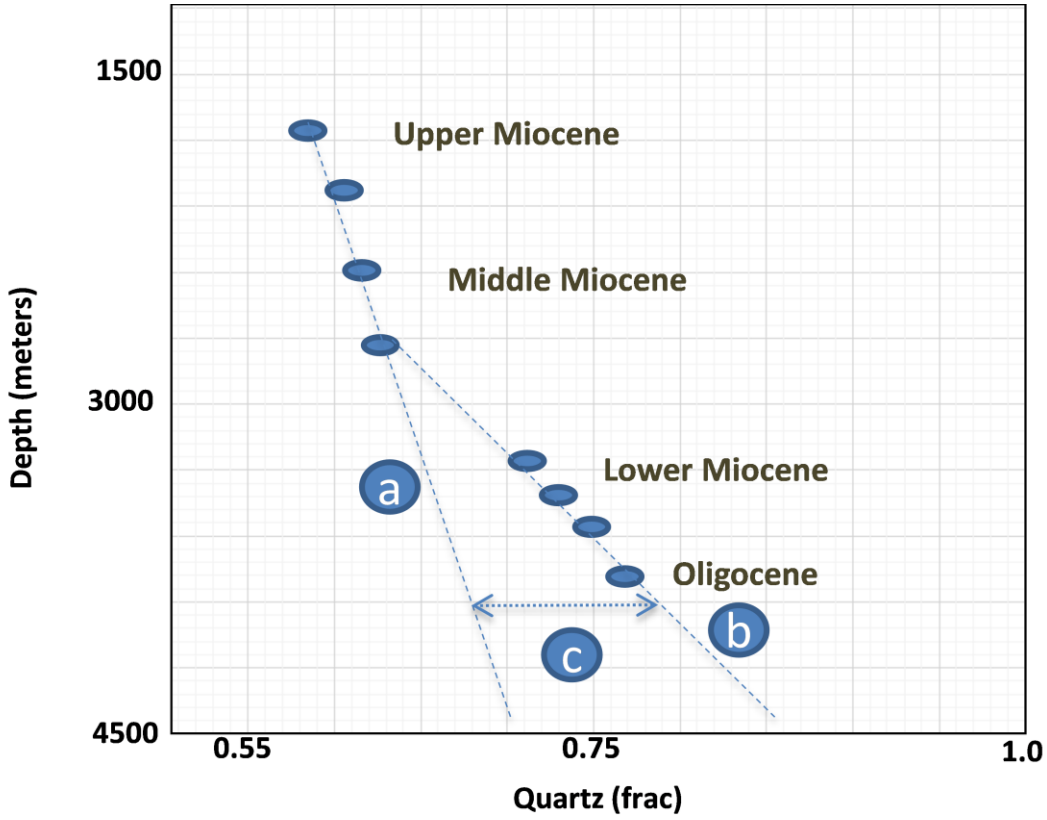

Figure 4.12: Cross plot of modelled quartz volume against depth

Electrofacies

The electrofacies classification based on the density-neutron cross-plot reveal the presence of four facies – clean sand, shaly sand, tight sand and shale. Each facies is characterised by a unique set of data clusters as noted in the density-neutron cross-plot. Clean sands are plotted across the density neutron sand line and would represent the best reservoir units. Shaly sands are characterised by a gradual increase in both density and neutron values. The data cluster in this case, plots mostly between the limestone and dolomite region of the plot. Since the depositional environment in this study is not prone to carbonate sedimentation, any departure of data away from the sandstone line and towards limestone line is largely influenced at least by the presence of shale. The data coded in green indicates highly compacted sands with low neutron values and high

density. The low neutron value is a reflection of low hydrogen atom due to low or absence of formation fluid (the neutron tool measures number of hydrogen atoms). While an increase in density value responds to a high grain density. Shales indicated in red are characterised by high density and high neutron value in response to bound water. The electrofacies model defined from the combination of density and neutron logs is displayed in track 5 of Figure 4.13. Same colour code represents the interpreted facies as depicted in the cross-plot (Figure 4.4).

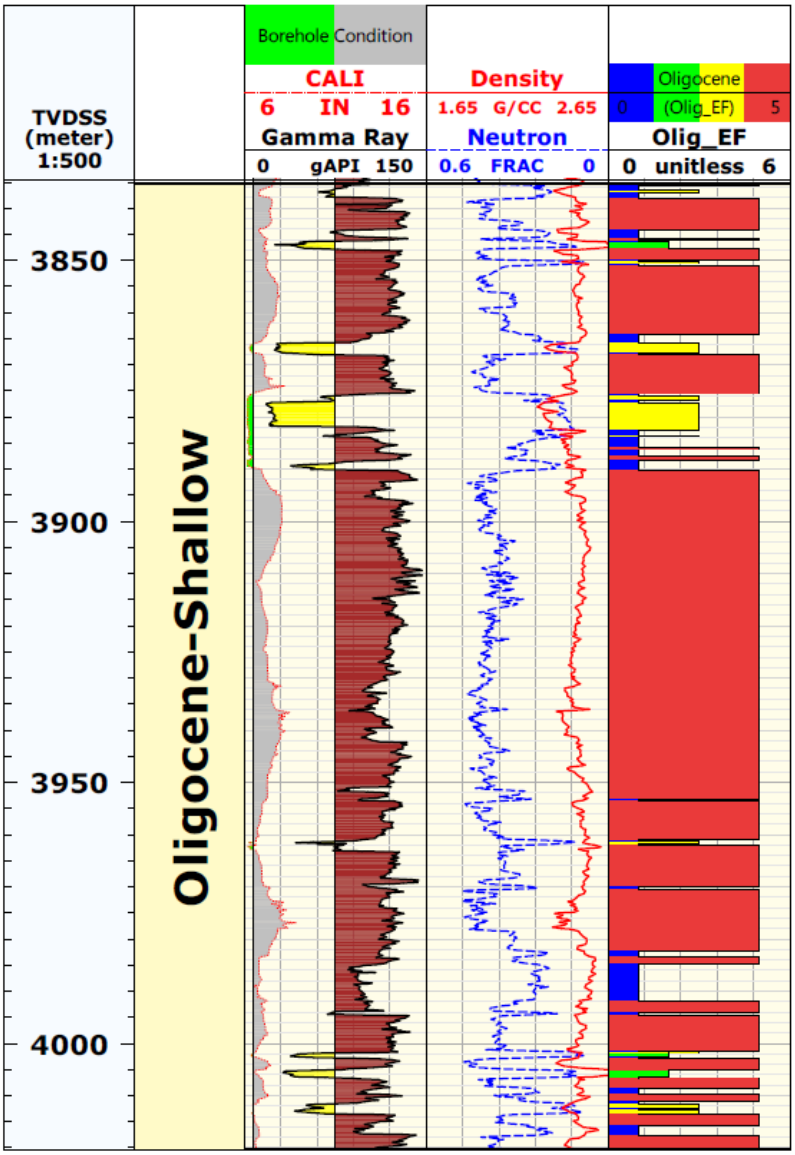

Figure 4.13: Petrophysical log plot showing raw logs in tracks 3 and 4 and electrofacies log in track 5. Track 2 = calliper (CALI) with poor hole condition in grey colour, track 4 = density and neutron logs, and track 5 = electrofacies logs (EF) across the Oligocene interval.

CHAPTER 5

3D SEISMIC INTERPRETATION

This chapter comprises Paper 1 of the thesis: “Predicting Oligocene Reservoir Potential in the Deep-Water Western Niger Delta: An integrated Basin Modelling and Diagenetic Study”.

It is based on 3D seismic interpretation in the study area of the western Niger Delta. The paper has been submitted to the American Association of Petroleum Geologist (AAPG) and it is currently been reviewed.

It is reprinted here in full, although figure numbers have been replaced by chapter figure numbers (e.g. Figure 1 becomes Figure 5.1), and the references are included in the main reference list at the end of the thesis.

There is necessarily some overlap and repetition with other parts of the thesis in presenting the ‘introduction’ and ‘geological setting’. The discussion is developed further in Chapter 8.

The authorship includes my two supervisors, but the work and principal findings are entirely my own.

5.1 Paper 1

3D Seismic Interpretation of Depositional Architecture and Reservoir Potential of Deep-water Untapped Oligocene Sequence of the Western Niger Delta

Obinna Chudi, Helen Lewis and Dorrik Stow
Institute of Petroleum Engineering, Heriot-Watt University, EH14 4AS, Edinburgh, UK

This Paper was submitted to the American Association of Petroleum Geologists Bulletin (AAPGB) and it is currently being reviewed

Abstract

The deep-marine Oligocene succession in the western Niger Delta-Slope region is still largely unexplored. On the basis of 3D seismic interpretation, we propose a depositional architecture characterised by a complex channel-lobe system and intervening mud-diapir ridges. There is strong influence of sea-floor morphology on depositional architecture, in which channels are deflected by and lobes ponded against the mud ridges. Syn-sedimentary ridge growth has affected the position of weakly confined channel conduits and partially unconfined lobate depositional bodies. These are particularly evident where the channel system approaches depressions flanked by mud ridges. In the study area, channels are up to 1km wide and 10-15km long, feeding lobes that are 3-5km wide and 6-8km long. Based on the high seismic reflection amplitudes that characterise both channels and lobes, we suggest they are both sand-rich and possibly hydrocarbon bearing. Seismic attribute analysis, particularly RMS amplitude and spectral decomposition-RGB blending, were both adopted for constraining the depositional architecture, while the sweetness attribute was useful in predicting sand presence and fluid typing within the study area. Although not yet penetrated by drilling, we are confident that these Oligocene lobes represent a viable petroleum play.

Introduction

The Niger Delta sedimentary basin is noted for its hydrocarbon prolific nature with significant discoveries made both onshore and offshore across Miocene and Younger intervals of the delta system. Until the mid 1990's exploration and production had been concentrated in the onshore and shallow offshore regions within a water depth of less than 100m (328ft). Following the giant discoveries such as the Agbami, Akpo, Bonga,

Bosi and Ehra fields located in the continental slope of the basin (Cameron and White, 1999), significant attention has now been given to deep-water exploration in water depth greater than 500m which has culminated in major studies undertaken in this part of the basin. The Miocene and younger turbidite deposits have been the primary reservoir target, in most cases taking the form of stacked channel complexes with associated overbank and levee systems. Single channel width of up to 500m and complexes of over 1300m wide have been encountered having excellent reservoir quality with an average porosity and permeability of up to 35% and 2000mD respectively (Ofurhie et al., 2002). Such reservoir properties typify the Miocene reservoirs in the study area located in a water depth of 800-1200m. As oilfield development in the basin becomes more mature, the quest for additional reserves has caused a focused attention on stratigraphically deeper plays.

This study focuses on the deeper, poorly understood Oligocene sequence with emphasis on the effect of tectonically-induced seabed topography and its corresponding influence on depositional architecture, facies distribution and associated sand presence. Other studies have documented the influence of growing structures such as salt and mud diapirism, folds and faults on deep-water channels and associated facies in both Oligocene and Miocene sequences (Anderson et al., 2000, Broucke et al., 2004, Hempton et al., 2005, Gee and Gawthorpe, 2006, Wood and Mize-Spansky, 2009, Dunlap et al., 2010, Mayall et al., 2010, Dmitrieva et al., 2012). From these studies it has been well established that the geometry of deep-water channels is seen to change both where a decrease in gradient of the continental slope is encountered and as channels approach constriction points flanked by mud-wall structures. Such topographic effects result in changes in channel width and sinuosity producing a change from confined to unconfined channel systems.

Three dimensional (3-D) seismic data from the study area have been useful in understanding the reservoir potential of Oligocene deep-water depositional settings. Over thirty wells have been drilled in the study location but only the exploration well (Well A1) penetrated the top of the Oligocene succession. Of importance in this study is the integration of varying suites of seismic reflection attributes for seismic geomorphological studies. With the advent of this technique, detailed depositional elements can be interpreted and lithology predicted. The spectral decomposition-RGB

(red, green, blue) blend technique integrated with the RMS (root mean square), as amplitude visualised on map view images, formed the core attribute utilized for depositional architecture. The sweetness attribute tied to well logs was used for predicting lithology and hydrocarbon presence.

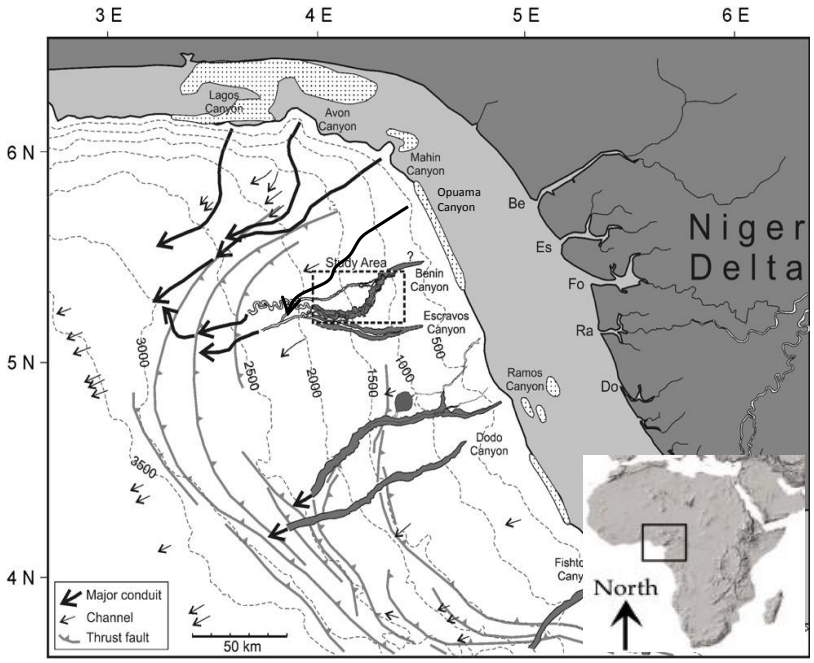

Figure 5.1: Location of the Western Niger Delta showing bathymetry, major submarine canyons and study area in dotted rectangle (modified after Deptuck *et al*. 2007).

Geologic Setting

The study area is located in the mid to lower slope deep-water setting, offshore Niger Delta in the Gulf of Guinea, which is situated along the West Africa passive margin (Figure 5.1). The basin evolution is attributed to the breakup of the South American and African plate in the Mid to Late Cretaceous (Burke et al., 1971, Whiteman, 1982). The end of rifting in the Late Cretaceous was followed by a post rift sedimentation phase in the Tertiary, progradation of the delta seaward from the Eocene. Significant sediment influx from the hinterland into the basin via the Niger-Benue fluvial system in the west and the Cross River in the East was seen from the Late Oligocene and increased steadily up to Plio-Pleistocene times (Whiteman, 1982). A series of canyons developed during the Tertiary that incised into the shelf margin and extended basinwards. These canyons formed major point-sourced conduits for sedimentation in the deep-water environment. Major canyons in the western part of the delta around the study area include, the Mahin,

Opuama, Benin, Escravos, Lagos and Ramos Canyons (Burke et al., 1972, Petters 1984) (Figure 5.1). The Opuama canyon is thought to be of Oligocene age (Petters, 1984) and based on its present day location and time of development, it is most likely the canyon that channelled sediments to the slope region around the study location. Although the Benin Canyon is also seen to traverse the study location, the works of Deptuck et al. (2007) assigned a Pleistocene age to this canyon. These northeast-southwest orientated canyons or the equivalent paleo-canyons actively fed sediment from the delta front and shelf to the slope and deeper basin from the onset of delta formation and ocean formation up until the present day. The principle mode of downslope transport was by turbidity currents and associated mass transport processes. During the Miocene period, in particular, slope canyons and channels acted both as transport conduits and sites of deposition of sand-rich turbidites. These form the principle reservoirs and plays for active hydrocarbon exploration and production today (Bandele and Claudel, 2010, Chapin et al., 2002, Piovesanel et al., 2013).

A tripartite lithostratigraphic regressive sequence has been penetrated by most of the deep wells drilled across the basin (Short and Stauble 1967, Reijers 2011). The three elements from top to bottom are (Figure 5.2): (1) continental sands of the Benin Formation, (2) a paralic to shallow marine sand and mud sequence of the Agbada Formation, and (3) deep marine muds, silts and isolated sands of the Akata Formation. The sands and muds of the Agbada Formation form the highly prolific deltaic reservoir and seal couplets from the onshore to offshore Niger Delta. The isolated slope channel sands of the Akata Formation form the Miocene deepwater reservoir and play, while the deeply buried Akata muds and shales are the principle source rocks (Evamy et al., 1978, Nwachukwu and Chukwura 1986, Doust and Omatsola 1989). The Akata muds are typically overpressured and are hence the main unit leading to mud daipiric activity.

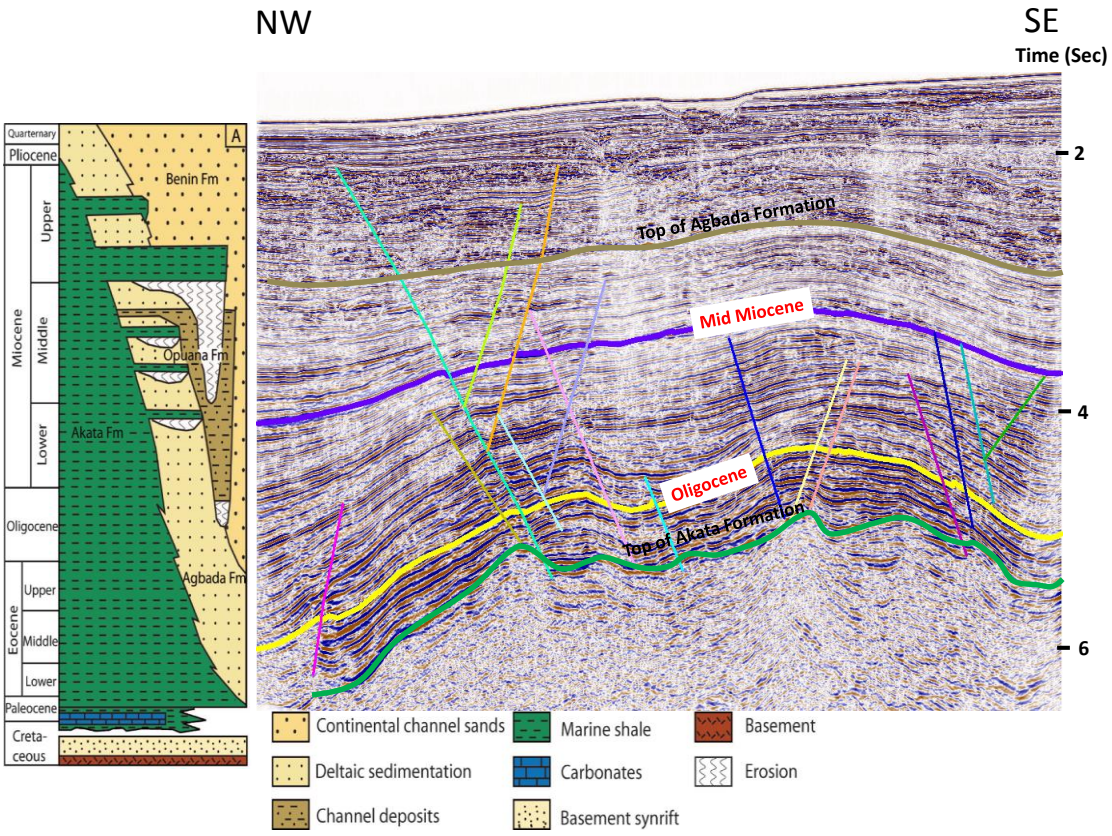

Figure 5.2: Schematic diagram of the regional stratigraphy of the Niger Delta and seismic amplitude cross-section with main horizons mapped in the study area that includes: (1) speculative top of Agbada Formation, (2) top of Oligocene and (4) speculative top of Akata Formation (Modified after Corredor et al. 2005). Line of section is shown in Figure 5.6A.

Three structural provinces have been identified in the Niger Delta from onshore to offshore (Damuth 1994) (Figure 5.3). (1) The extensional zone extends from onshore to the shelf and part of the upper slope. Extensional features are dominant, with large-scale growth fault structures. (2) The upper to mid slope lies within the translational zone, characterised by active mud diapirs with associated folds and faults that formed as a result of rapid sedimentation over undercompacted mud. These mud diapirs are known to express themselves at the sea-floor as mud volcanoes (Graue, 2000). (3) Following gravitational remobilization of the sediments further downslope, the lower slope region experienced significant folding and thrusting forming a fold and thrust belt, which is defined as the compressional zone (Morley et al., 2011). The study area lies in the translational zone of the delta-slope system.

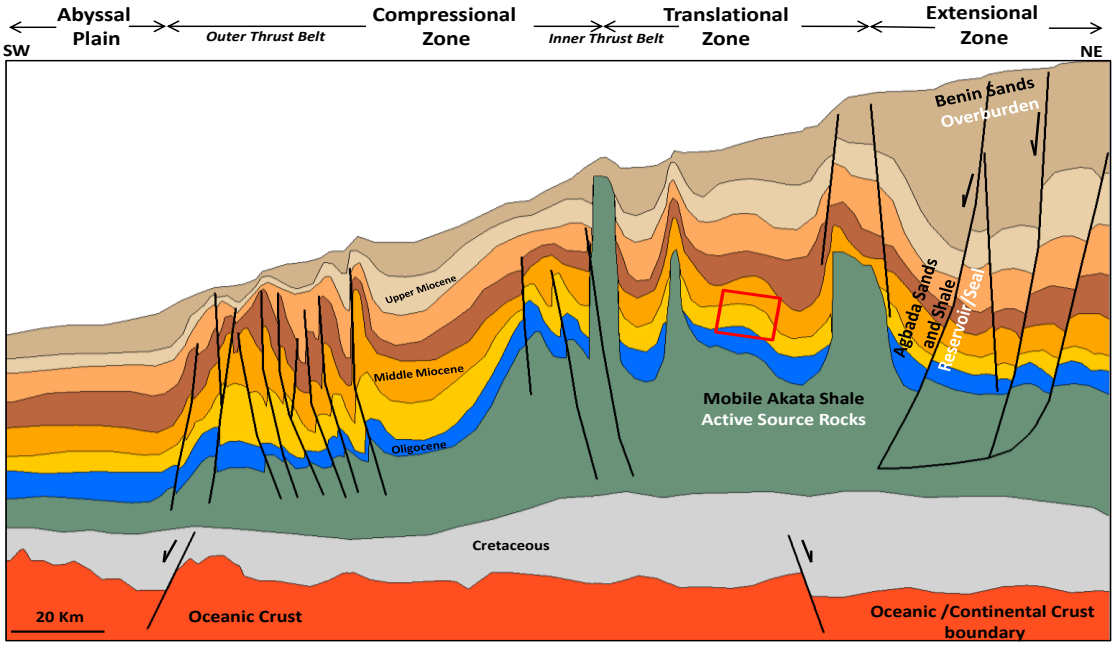

Figure 5.3: Regional cross section of the Western Niger Delta illustrating the structural provinces. The study area is shown in red square. Structural complexity increases basin-wards with the development of mud diapirs, fold and thrust features. The main lithostratigraphy is also represented and the corresponding petroleum system element. (Chudi *et al.*, 2015).

Data and Methodology

The 3D seismic data utilized in this study covers a 770km^2 (297 mi^2) area within the mid to lower continental slope (Figure 5.1). The data showcases the structure and stratigraphy within a six seconds two way time (TWT) window with crosslines spaced at a 12.5m interval and inlines every 25m. The dominant frequency of this survey is 22Hz, although the overall frequency ranges from 7-75Hz. The data has been processed as a zero phase wavelet with a negative polarity displayed as a trough that characterises an increase in acoustic impedance.

Three key horizons have been identified and mapped, corresponding to the top of the Mid-Miocene sequence and two surfaces within the Oligocene interval. These latter are called Oligocene-shallow and Oligocene-deep (Figure 5.5). Oligocene-shallow was mapped using a fairly continuous reflector representing the top of Oligocene, as penetrated by well A1, while the Oligocene-deep was mapped on a strong reflector below the well TD. Seismic geomorphological studies carried out were based on RMS

and RGB attribute maps computed across time intervals (zero to + 25ms/95ms) underlying the mapped horizons. Sweetness attribute formed the bases for inferring the likely lithology within the Oligocene succession.With only a single well penetration into the Oligocene succession, interpretation of the Mid-Miocene interval served as an analogue for the Oligocene. The Mid-Miocene interpretation has been calibrated with very good well control. Detailed seismic methods are outlined in the following sections. Appendix B provides further description of the seismic attribute used in the study.

Well to Seismic Tie

The well to seismic tie process is an integral part of the seismic interpretation workflow that was adopted in this work. Well ties provided a means to (1) correctly identifying horizons that were mapped, and (2) placing the seismic wiggles in geological context, so that reflection amplitude measured by seismic in time can be correlated to lithological information measured from the wells in depth domain. This is achieved by matching a synthetic seismogram generated at the well location to real seismic trace, so that features from the well are correlated to the seismic data. Below is an outline of the procedure for tying well logs to seismic data (White and Simm, 2003):

1- Sonic and density logs were edited and calibrated. The sonic and density logs were edited to remove spurious signals largely due cycle skipping and poor borehole conditions which are observed on the logs as spikes.

2- A synthetic seismogram was constructed from the calibrated well logs by choosing an appropriate reflection series and constructing the reflection series in two-way time.

3- Performing the match by determining the best match location and estimating the wavelet and its accuracy.

Figure 5.4 shows a comparison of the synthetic trace and seismic data in time for well A1 that was used in performing well-to seismic tie. Seismic trace is extracted from each 3D survey at the reservoir penetration and compared to the appropriate synthetic seismogram. The tie is seen to be good particularly at 3400 and 4000msec.

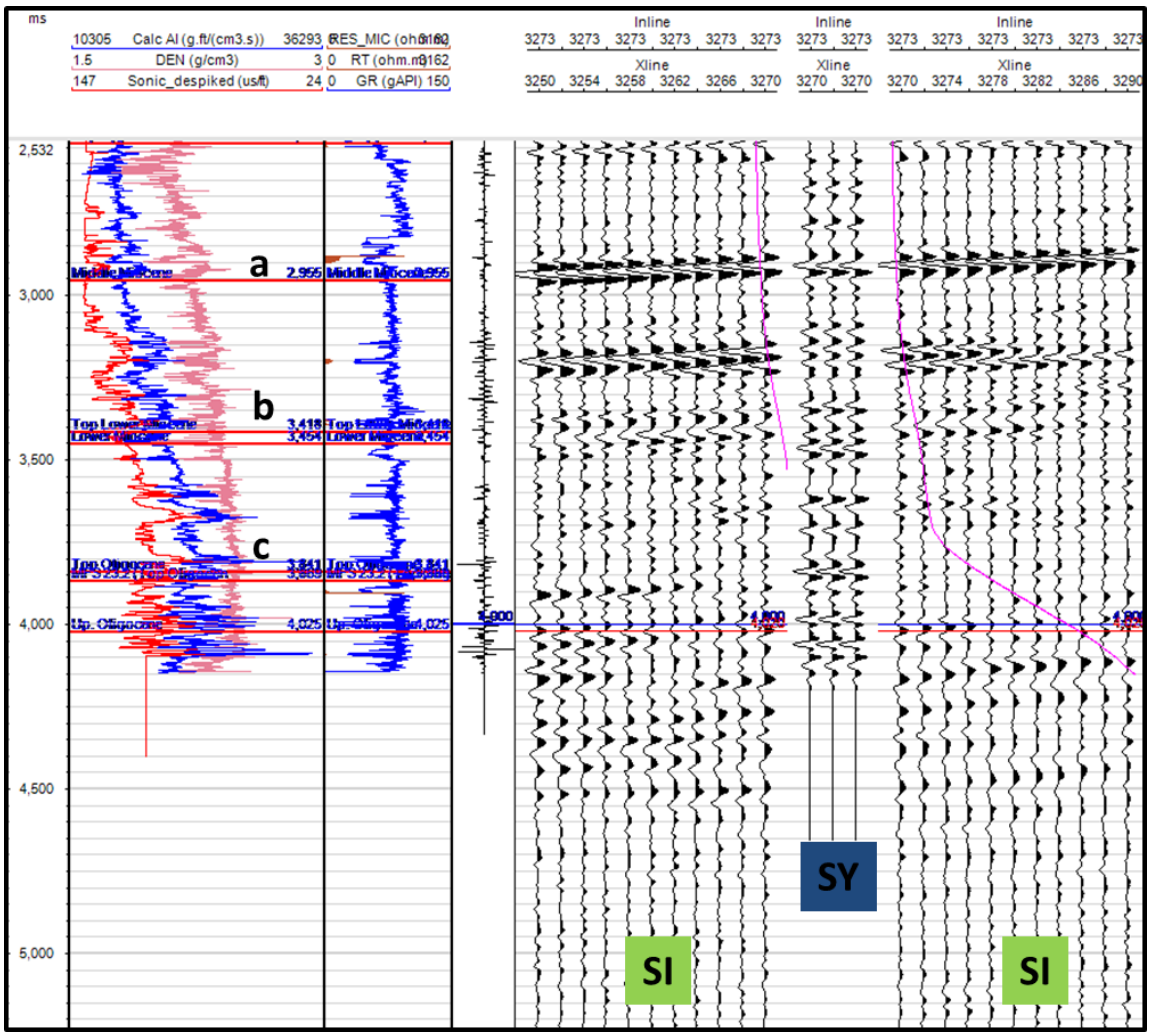

Figure 5.4: A correlation panel showing seismic data (SI) tied to synthetic seismogram (SY) from well A1 with age boundaries were near good match was performed (a = Mid Miocene, b = Lower Miocene and c = Top of Oligocene.

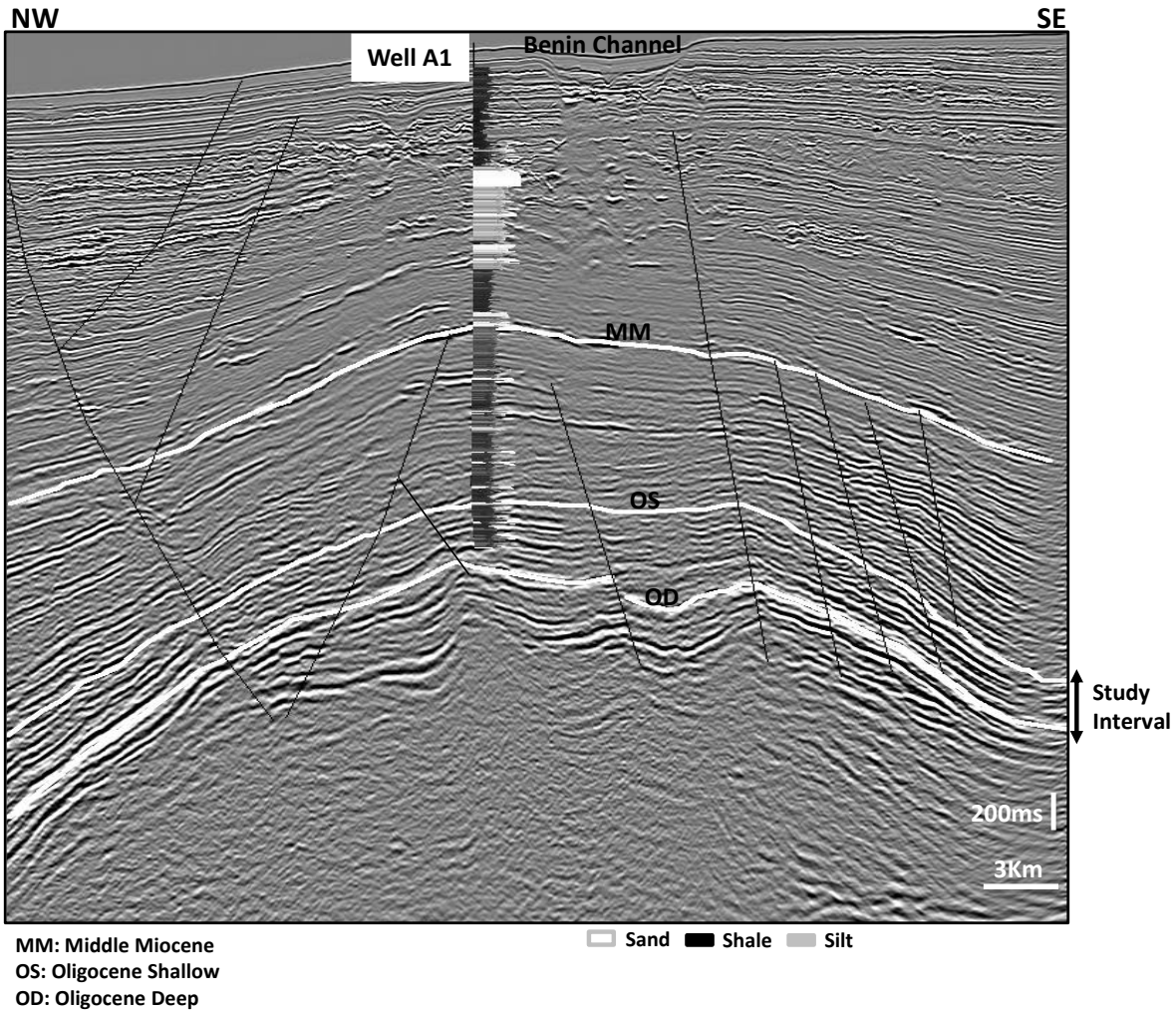

Figure 5.5: Seismic cross-section passing through well A1 in the study area, showing the mapped horizons and interpreted faults. Line of section is shown on Figure 5.6A.

Depositional Architecture

This section outlines the architectural elements and geometry of the turbidite system encountered in the Miocene and in the target Oligocene sequence, as revealed from the interpreted 3D seismic data. The main depositional elements that have been encountered are: amalgamated channel complexes, overbank sands and sandy lobes. These are interpreted based on the classification scheme of Posamentier (2003) and Posamentier and Kolla (2003). To characterise the turbidite depositional bodies, two attribute techniques have been adopted: (1) root mean square (RMS) amplitude, and (2) spectral decomposition-RGB (red, green and blue) blending. These attributes are draped on interpreted horizon slices or computed across a time window.

RMS amplitude is a measure of reflectivity within a time window. It is used for detecting amplitude variation within a depositional body, such as channels, based on the change in amplitude relative to the surrounding amplitude (Chopra and Marfurt, 2008) (Figure 5.6A). Hence it is well suited for bright spot detection and where depositional features like channels show anomalous amplitude signatures. In such cases, RMS amplitude can also help reveal stratigraphic features (McDonnell et al., 2008).

The spectral decomposition-RGB blend was utilized in imaging geologic features and as a direct hydrocarbon indicator (DHI) (Chopra and Marfurt, 2012). Spectral decomposition involves decomposing a seismic volume into discrete iso-frequency domains via an algorithm such as Discrete Fourier Transform (DFT) (Partyka et al., 1999, Brown, 2011). This technique is widely used for imaging and mapping bed heterogeneity, boundaries, and thickness variability, by spatially analysing frequencies that reveal such geologic features (Brown, 2011, Ahmad and Rowell, 2012).

In this study three iso-frequency volumes -10, 20 and 30HZ were generated and converted to an amplitude volume using "envelope". Envelope allows amplitude to be studied independent of phase, hence is an indicator of reflection strength. The conversion of the seismic volume to envelope allows only amplitudes associated with the respective central frequencies (10, 20 & 30Hz) to be analysed through the RGB colour blending technique, so that geologic features are better exposed and interpreted. The 10Hz low frequency was assigned the red channel while the 20Hz is green and blue for the 30Hz frequency volume. For geomorphological studies, features with a dominant red colour indicate significant contribution from the low frequency and blue would be high frequency. This colour distribution also provides information on relative temporal thickness where amplitude contours move from thick to thin packages as you advance from low (10Hz-red) to high (30Hz-blue) frequency amplitude anomaly. The work of Partyka et al., (1999) fully describes the use of this blending technique in understanding or mapping temporal bed thickness. In Figure 5.6B, features highlighted in white reveal an area with high amplitude response from all three colours, while features like faults appear as black lineaments due to a low response from all three frequency volumes, allowing them to be easily identified when compared to the upthrown and downthrown fault blocks (Chen et al., 2010, Wei, 2010, Cooke et al., 2014).

Miocene sequence

An acoustically strong Mid-Miocene reflector that is laterally continuous throughout the study area was mapped across the 3D seismic volume and subsequently used to study the depositional elements of the Mid-Miocene reservoir (Figure 5.5). This sequence is characterised by amalgamated, moderate to low sinuosity channel complex systems with associated lobe and oxbow features (Figure 5.6A, B and C). Attribute maps generated from a 25ms (two-way travel time) window referenced from the Mid-Miocene horizon were used for interpretation. The RMS amplitude map reveals that some of the channel complexes have high amplitude seismic signatures that have been confirmed by well penetration to be sand-prone and hydrocarbon bearing. Gamma ray and other lithological identification logs also show that the channel sands have very high N/G (net-to-gross) of up to 85% with only rare mudstone intervals (Figure 5.7). These channels are orientated northeast-southwest with lengths ranging from 1 to 5km within the study area. Each individual channel system is less than 500m wide, whereas channel complexes are up to 1300m in width. Some of the Miocene channels are shale-prone or water bearing with no amplitude anomalies and are seen to bypass and erode older depositional bodies (see Figures 5.5A and B).

The RGB blend draped on the Mid-Miocene horizon slice (Figure 5.6B) complements the RMS amplitude map. The blended interval clearly images the depositional features and structures better than the RMS map. In some cases the channels transit downdip into lobes with associated distributary channels bypassing and incising underlying strata, as illustrated in Figure 5.6B and vertical seismic profile 'C3'. Similar features have been identified offshore Niger Delta and described by Adeogba et al. (2005) as a transient fan system. Posamenteir et al. 2003 identified similar features in the Makassar Strait, offshore Kalimantan, and defined them as frontal splays. Shanmugam and Moiola (1991) attributed such features as lobes, which is the terminology adopted here. The downdip lobate element, located south-west in Figure 5.6, is elongate in dip direction and ranges from 3-7km in length and 2-4km in width. The bright colour seen in some of the depositional features reflects sand fill and clearly matches high amplitude zones on the RMS amplitude map, which has also been calibrated against log information. Shale-fill channels most likely indicate channel abandonment or deposition dominated by pelagic or hemipelagic fallout. These are observed as dark grey to black

in colour. Structural features like faults and diapir ridges, which do not tune into any of the frequency channels, are also black in colour.

A

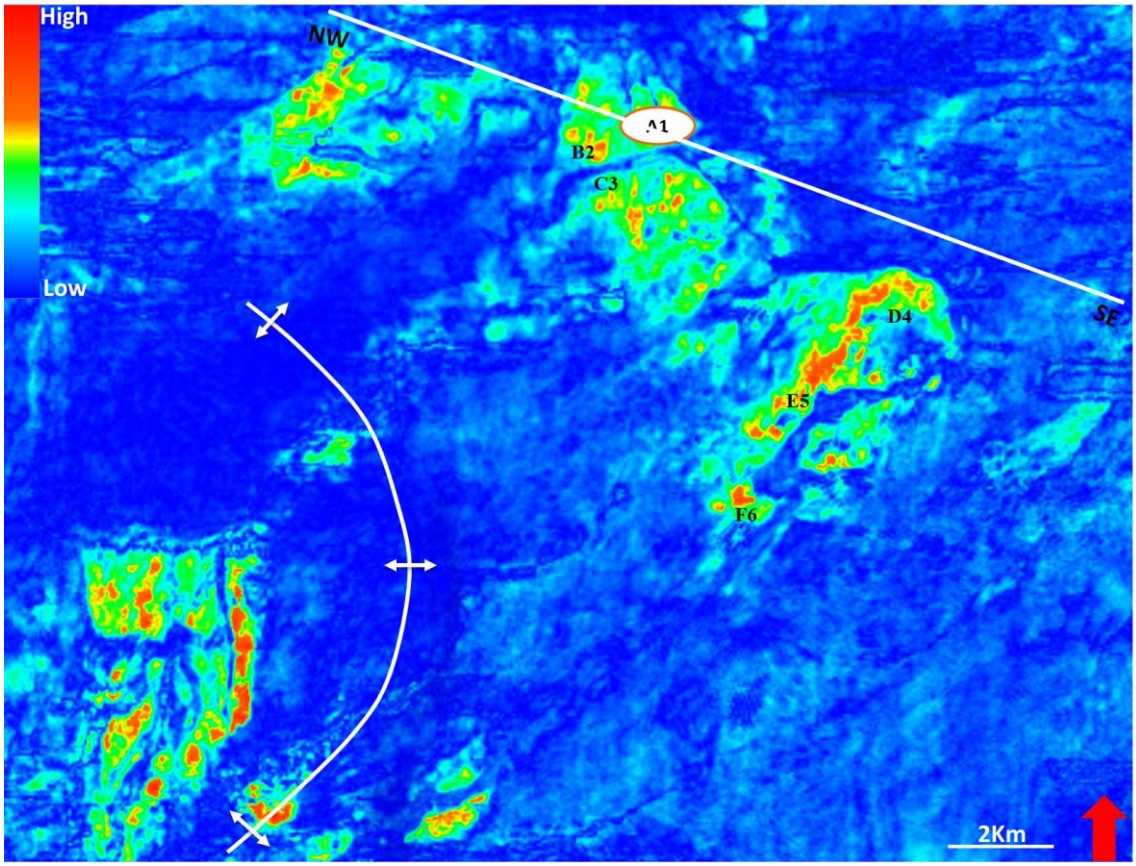

B

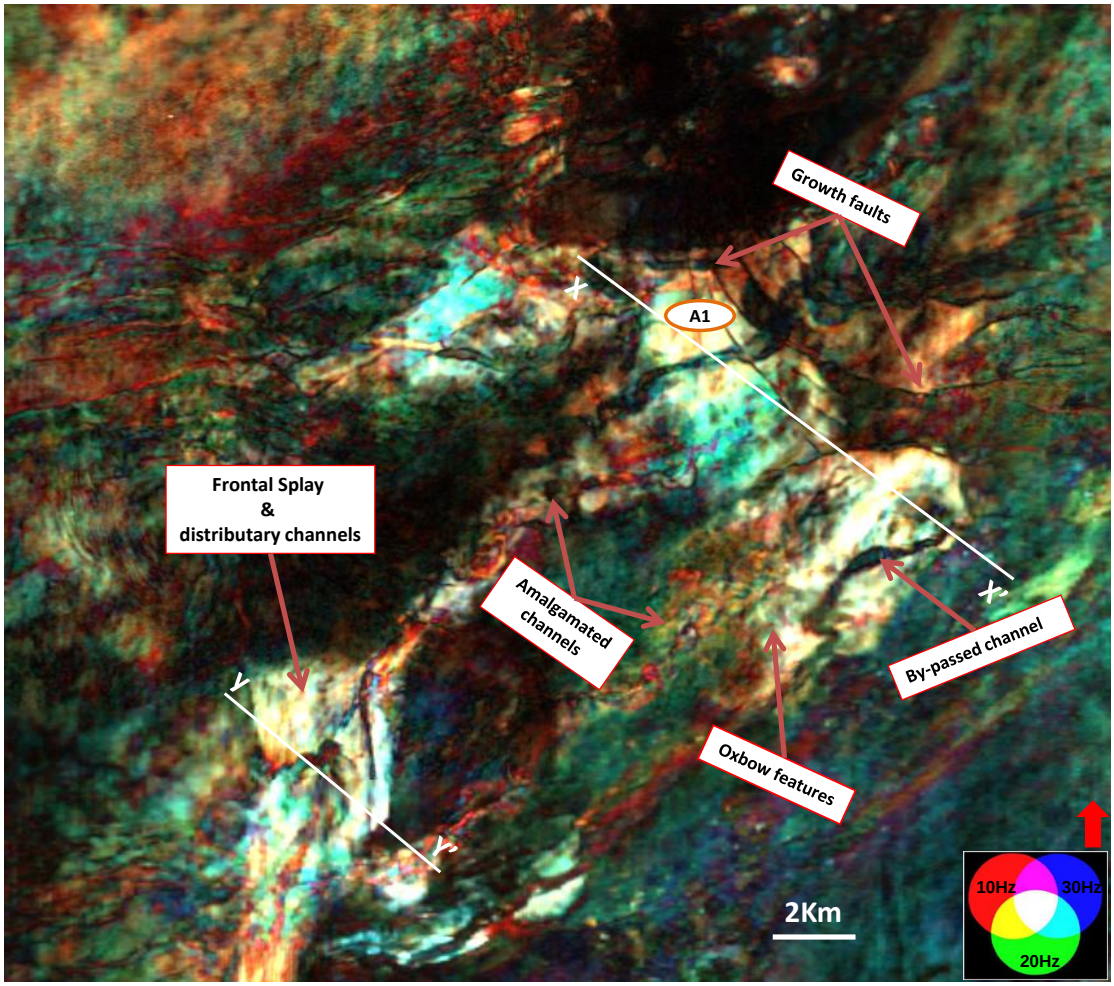
Growth faults
X
A1
X'
Frontal Splay
&
distributary channels
Amalgamated
channels
By-passed channel
Y
Oxbow features
Y'
2Km
10Hz
30Hz
20Hz

C

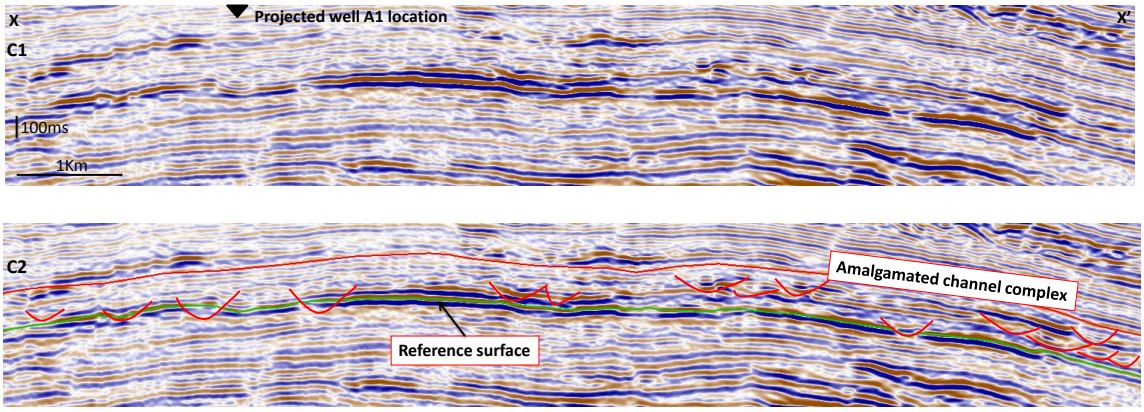
X
Projected well A1 location
X'
C1
100ms
1Km
C2
Amalgamated channel complex
Reference surface

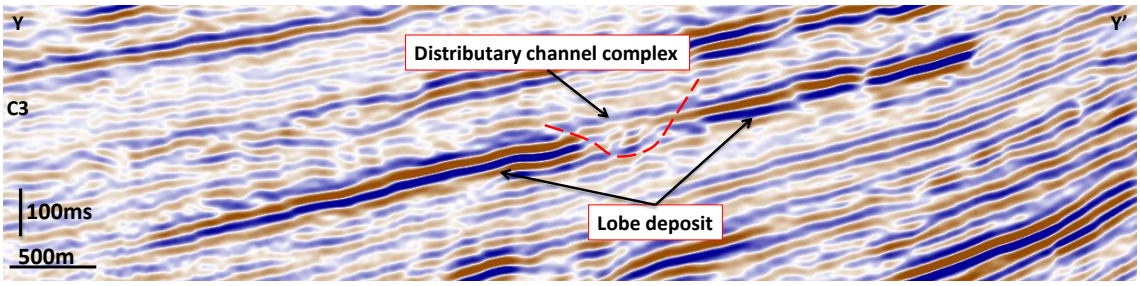

Figure 5.6: A = amplitude map-RMS amplitude extraction in approximately 25ms TWT window. High amplitude hydrocarbon bearing zones are shown together with well locations. B = RGB blend map draped on structure illustrating some depositional and structural features with high amplitude (white) and low amplitude (black). C1 = NW-SE seismic cross section and interpretation. C2 = mapped Mid-Miocene reference horizon (green) with interpreted faults and channel complex. Line C3 showing frontal splay and associated distributary channel profile.

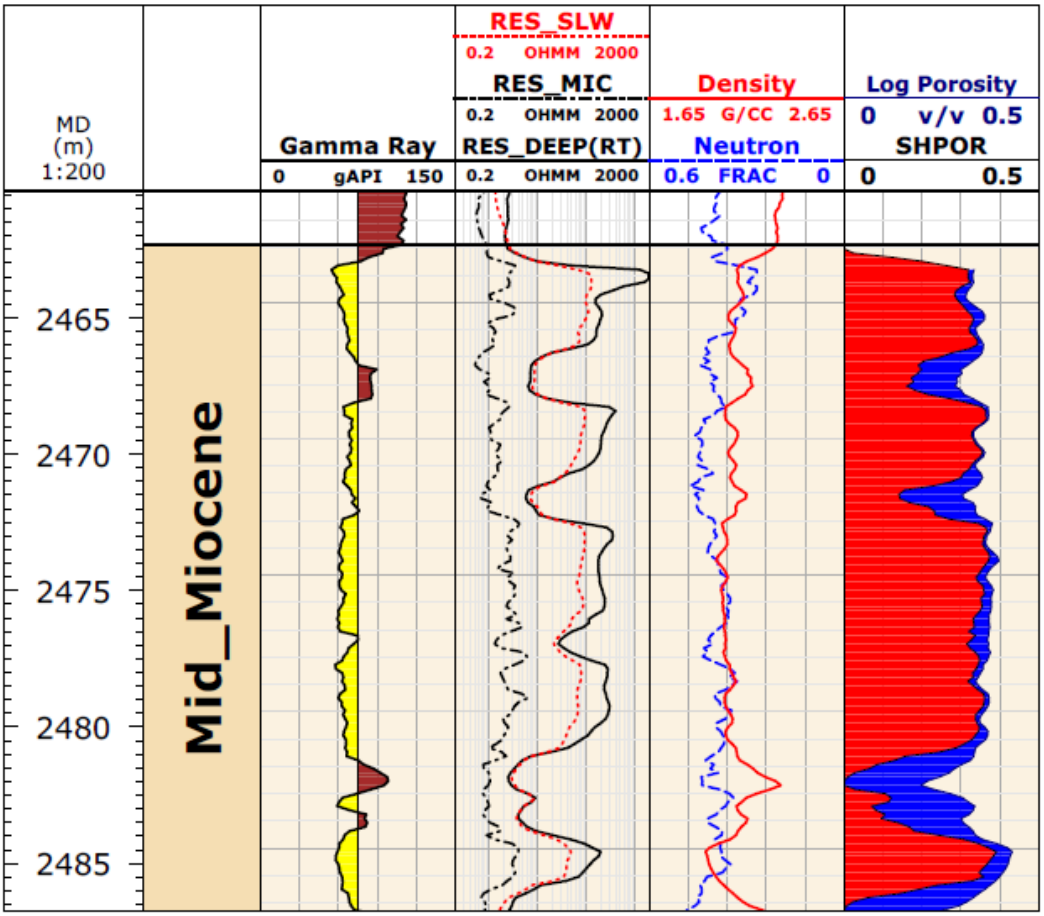

Figure 5.7: Conventional log display from well A1 illustrating hydrocarbon bearing relatively clean stacked channel sand: track 1 = gamma ray log, track 2 = micro (RES_MIC) shallow (RES_SLW) and true formation resistivity (RT) logs, track 3 =

density-neutron logs, track 4 = combination of porosity (POR) and hydrocarbon saturation log depicting fraction of pore volume filled with hydrocarbon (SHPOR) represented in red and fraction of water filled pores in blue.

Oligocene play

Considering that only one well penetrated the top of the Oligocene sequence, seismic to well calibration was not sufficiently achieved for depositional architecture or facies analysis. This was particularly so for the two horizons (Oligocene-shallow and Oligocene-deep) mapped across the Oligocene succession. In particular, the Oligocene-deep horizon was below the well TD (total depth) of 4100m. Hence, the Mid-Miocene interpretation, where a good seismic to well tie was achieved, was adopted as an analogue for the deeper Oligocene stratigraphy, specifically the amplitude reflection character in relation to depositional style and sand presence.

The RMS amplitude draped on the Oligocene-shallow horizon slice (Figure 5.8) indicates that the amplitude signatures at the well location appear to be low or entirely absent. This could be attributed to either poorly resolvable thin sandstone units of less than 10m thick or water bearing sands, both of which would result in weak amplitude anomalies. This is supported by the well data that show low resistivity values across thin units (Figure 5.9). However, downdip of the well in the southeast and southwest section of the mapped horizon, high amplitude values are seen. The southeast high amplitude signature reveals a single straight to low sinuous channel associated with a lobe-shaped feature. The width of the channel itself is about 700m and it extends for up to 14km in length within the study area. The channel in the northwest direction deflects around the mud ridges and then flows parallel to the ridge and terminates as two lobate features. These appear indicative of episodes of fill and spill (Figure 5.8). This typically occurs when available accommodation space fills to its spill point so that the subsequent turbidte system bypasses the earlier filled mini-basin and fills into a downslope adjacent basin.

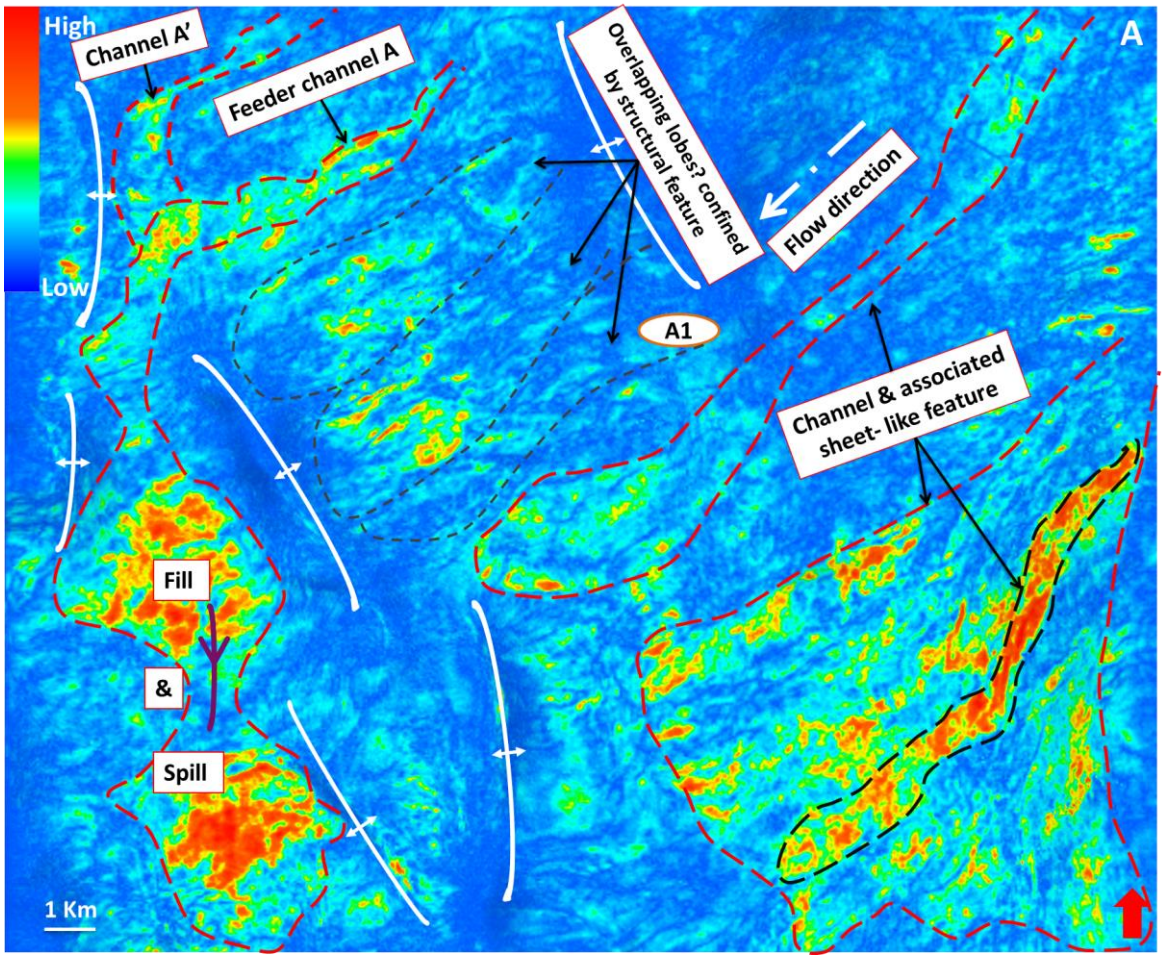

Figure 5.8: Horizon slice of RMS amplitude for Oligocene-shallow showing depositional features, particularly channel with associated lobe-like features. Mud structures are shown as white lines with double facing arrows. Main channel A is adjoined by another minor channel A'.

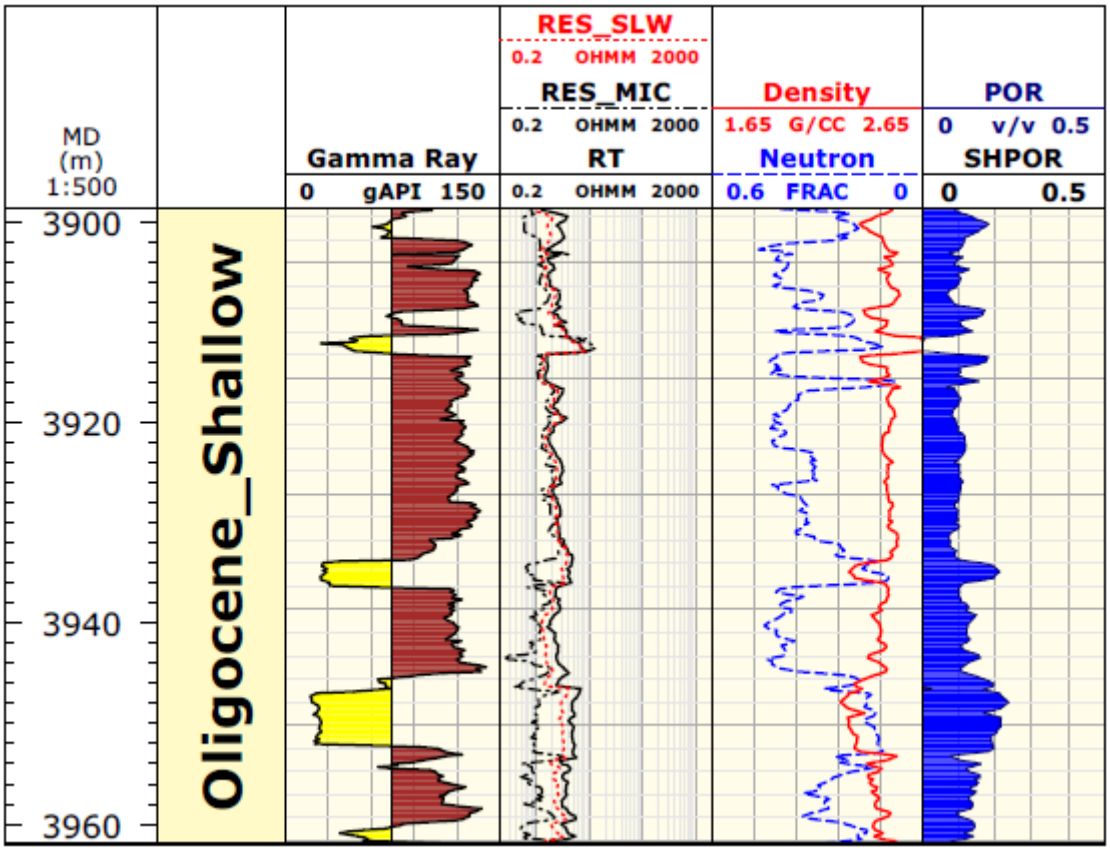

Figure 5.9: Conventional log display from well A1 showing water-wet thin sand of Oligocene age: track 1 = gamma ray log, track 2 = micro (RES_MIC) shallow (RES_SLW) and true formation resistivity (RT) logs, track 3 = density-neutron logs, track 4 = combination of porosity (POR) and saturation log depicting fraction of pore volume filled with fluid indicating water-wet sand.

Similar features as were observed in the Oligocene-shallow were also interpreted in the deeper Oligocene horizon mapped below the well TD. This is particularly evident in Figure 5.10 where the northwest channel and lobe features deposited within mini-basins flanked by mud ridges down-dip of the study area are noted, both in Oligocene-shallow (Figure 5.8) and Oligocene-deep (Figure 5.10). This indicates that the thickness of the depositional body likely extends across both horizons. However, for the southeast area of the Oligocene-deep (Figure 5.10), well developed fan lobe complexes with associated feeder channels have been interpreted. In plan view, attribute maps (Figure 5.10A-C) reveal channels that are weakly confined and oriented NE-SW. These pass downslope into lobes. Some of the lobes appear to overlap, forming lobe complexes (lobes 6-8) as illustrated in Figure 5.10A, while lobes 1 to 5 appear to be deposited as isolated lobes.

Each lobe appears to be limited in width, largely controlled by the lateral extent of the mini-basin into which the sediments pond. Generally the lobes range in width from 3-5km and in length from 6-8km. The associated feeder channels, most especially the well-imaged channel ‘D’ located in the south-east, extend up to 1.5km in width and 14km in length in the study area. The geometry of the Oligocene fan system is also well imaged in the RGB blend map (Figure 5.8B), with the white patches clearly defining the depositional geometry of weakly confined channels and terminal lobes.

A

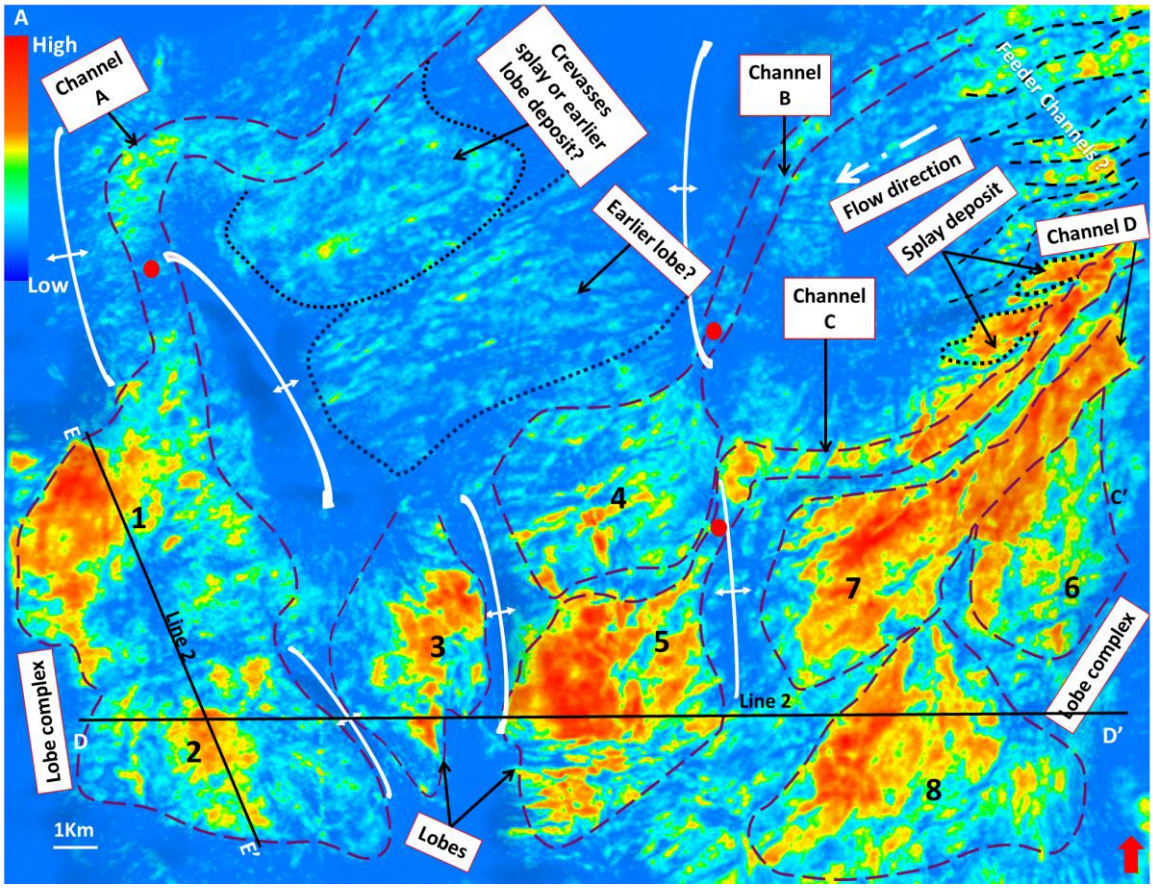

B

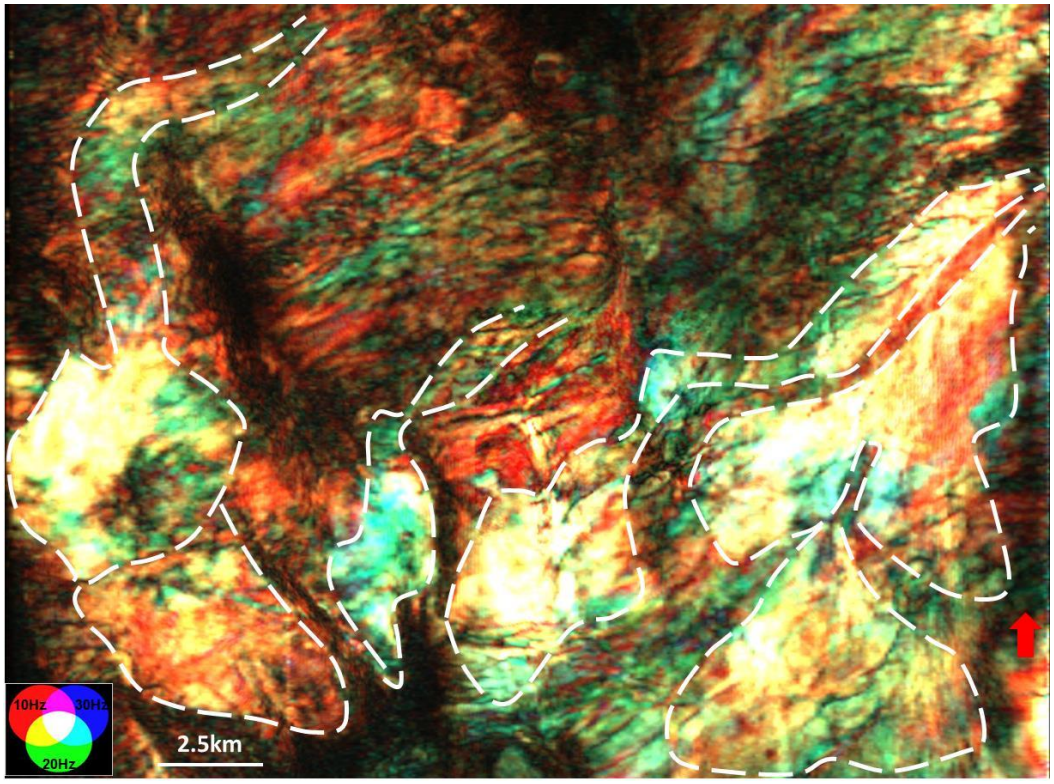

C

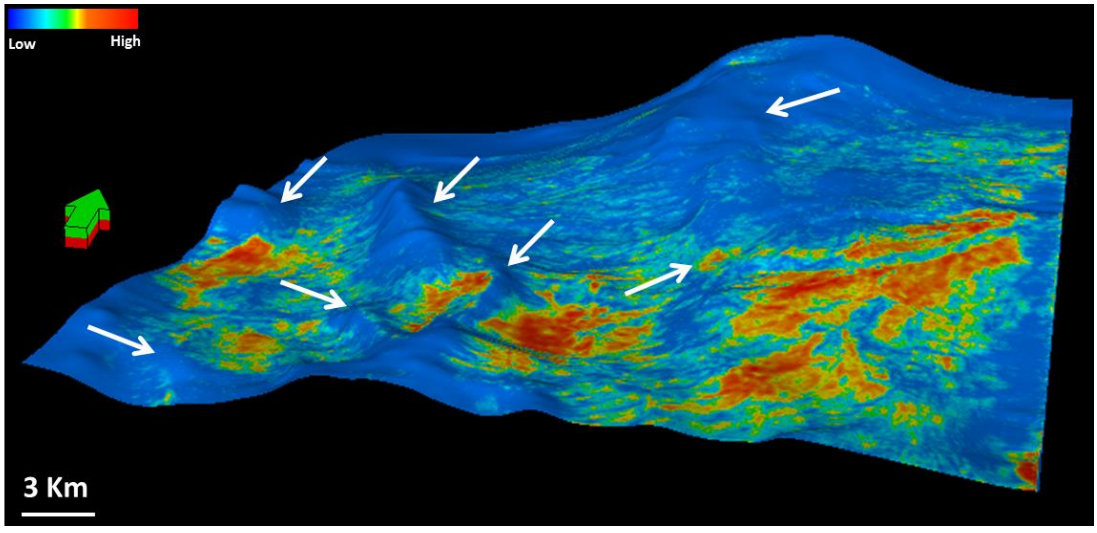

Figure 5.10: Oligocene-deep depositional elements controlled by mud highs. (A) RMS interval amplitude mapped below the Oligocene-deep Horizon (0 to +90ms). (B) RGB Blende map of amplitude in narrow frequency bands (10Hz- red, 20Hz-green and 30Hz-blue) draped on the Oligocene-deep horizon also showing key depositional elements. (C) RMS amplitude map in 3D view clearly showing the interplay of structural highs and depositional lobes, arrows pointing at some of the mud highs.

Lithology and Hydrocarbon Prediction

A qualitative approach of using the sweetness seismic attribute has been adopted in predicting lithology, particularly sandstone, and also hydrocarbon presence. Sweetness is an integration of envelope (reflection strength) and instantaneous frequency attributes. It is derived by dividing the envelope by the square root of the instantaneous frequency. Generally the sweetness attribute has been recognised for its use in differentiating sands from shales, and hence is reliable in detecting sand-filled channels surrounded by shales (Hart, 2008). Sweetness is particularly useful when there is a strong acoustic impedance contrast between lithologies. High sweetness value is usually associated with high amplitude and low frequencies. For example sands that are encased in shale would have a high amplitude that corresponds to a high acoustic impedance contrast with the shale. But if the acoustic impedance contrast is small or negligible, especially in thin beds where sands and shale beds are closely spaced and produce destructive interference of reflections from bed boundaries, then the reflection strength would be weak and therefore the sweetness value would be low. This means that pore fluids like hydrocarbon that can significantly affect the acoustic impedance contrast can result in changes in sweetness values and be treated as an indicator of hydrocarbon bearing sands.

In this study, where there are well penetrations mostly within the Miocene and younger succession, sweetness is compared with the gamma ray log for lithology identification and with the resistivity log for fluid typing. Figure 5.11 is a vertical transect of sweetness attribute displayed at well penetrations. For each well, both the gamma ray and the resistivity logs are shown. Excursions to the left for the gamma ray log represent low gamma ray values and therefore sands and a deflection to the right represents radioactive shales. Based on the petrophysical evaluation of the logs integrated with core description, there are no hot (radioactive) sands, so high gamma ray values are interpreted as shales. The resistivity logs, which are principally fluid indicators, should have high values in the presence of hydrocarbon and low values for formation water. Note how the low gamma ray response representing channel sands

corresponds to high sweetness, while shale-rich zones with high gamma ray corresponds to low sweetness.

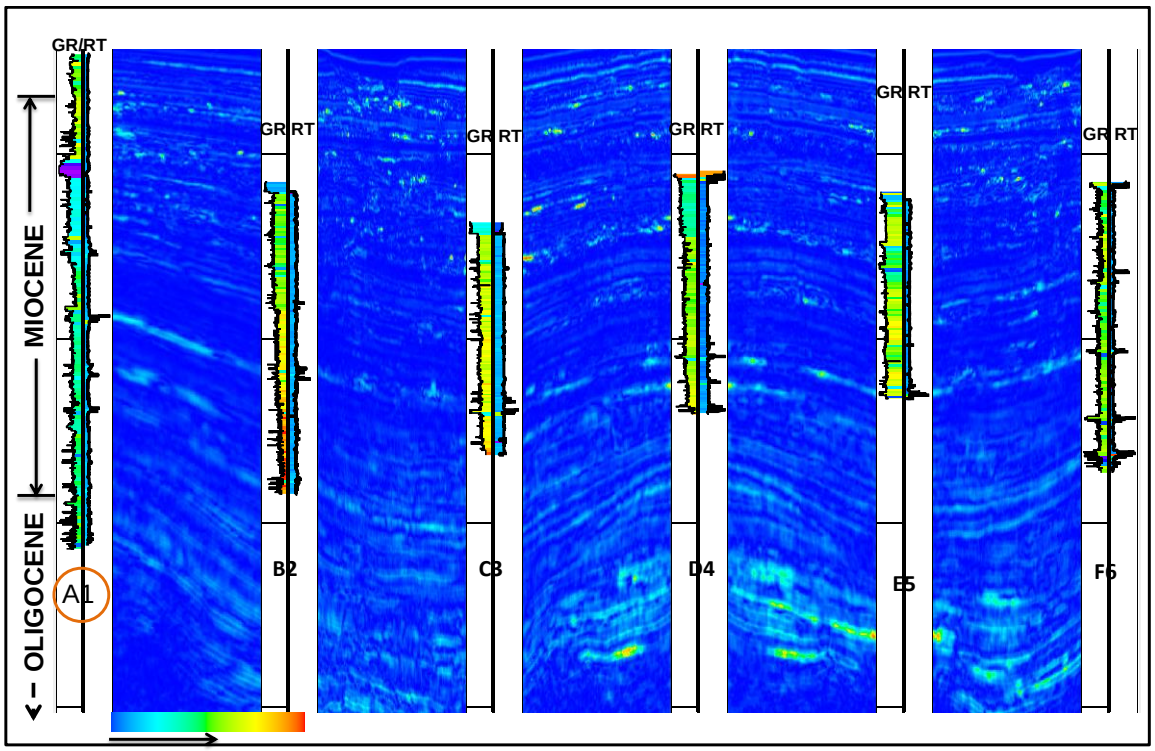

Figure 5.11: Vertical seismic profile of sweetness attribute tied at well location illustrating the good match between sweetness values and gamma ray (GR) plus resistivity (RT). High sweetness values increase to the right of the scale and low values (blue) to the left. Six of the wells shown are approximately 1-7km apart. The approximate well locations are depicted in Figure 5.6A.

The resistivity logs also appear to correlate with sweetness, since the low gamma ray-sand-prone intervals that are oil bearing with high resistivity values correspond well with sweetness. To further confirm the relationship between fluid content and sweetness, Figure 5.12 is an extract from Figure 5.11 highlighting only two of the wells (Well A1 and E5). The intervals with red markers indicate some water bearing sand units with low gamma ray and low resistivity. These water bearing sands are seen to have good correlation with low sweetness which thus suggests that sweetness is not only a good predictor of lithology but also of fluid type.

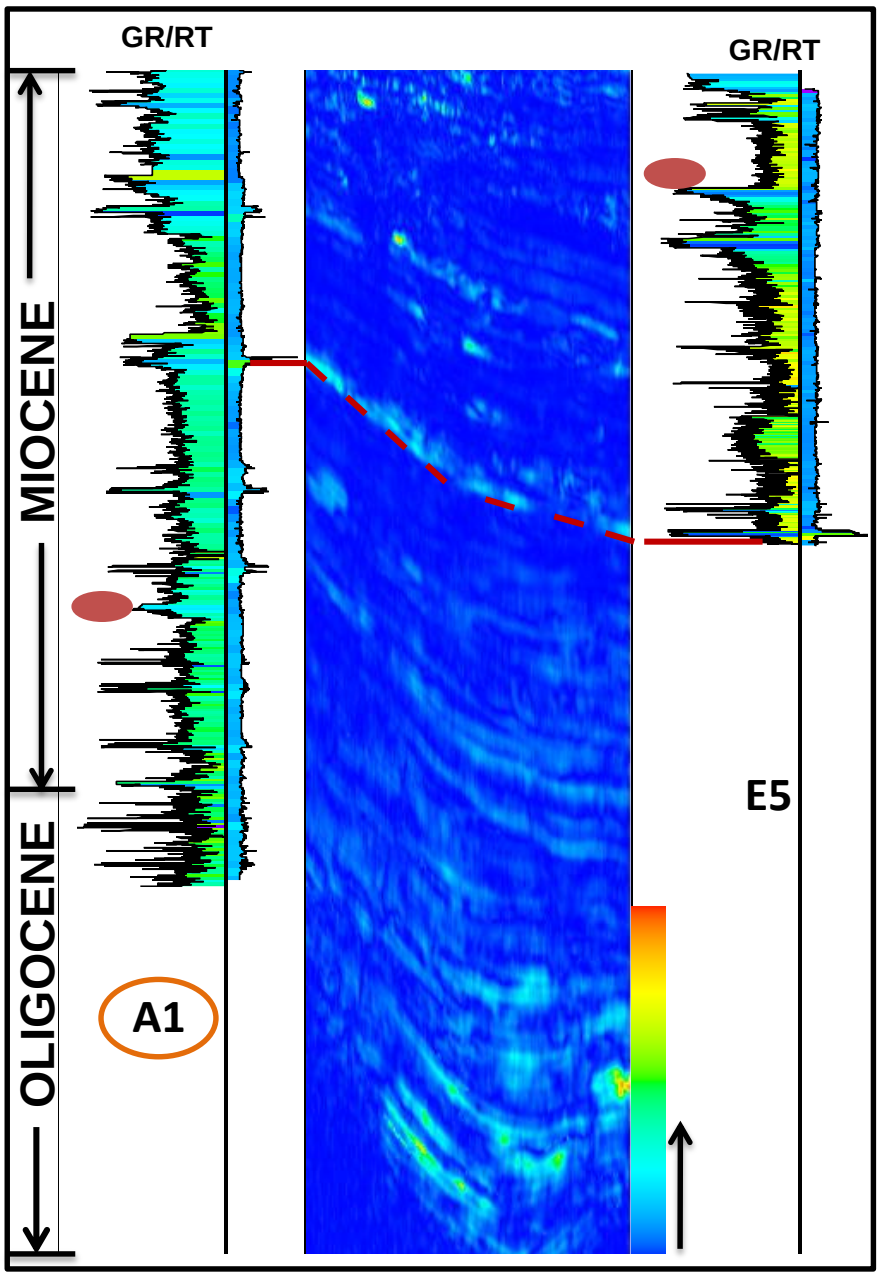

Figure 5.12: A cross section of sweetness tied to two wells showing the correlation of resistivity log to sweetness values (dashed lines). Both wells and cross section view are displayed in TWT. Good correlation of hydrocarbon bearing sands with sweetness illustrated in dash lines while water bearing sand correlating with low sweetness is marked with red circle.

Discussion

This study provides an in-depth analysis of the spatial and temporal distribution of untapped Oligocene deep-water sediments of the Niger Delta slope system. Using

seismic data and well data, we have mapped a series of depositional units and demonstrated how their depositional patterns have been influenced by sea-floor morphology. The interplay of sea-floor topography and sedimentation is seen to have a strong effect on the geometry, nature and distribution of deep-water facies (Broucke et al., 2004, Gee and Gawthorpe, 2006, Wood and Mize-Spansky, 2009, Mayall et al., 2010) and this has been observed in the Oligocene succession of this study. The top of the Oligocene was penetrated by a single well within the study area and this well encountered a water bearing sand unit less than 10m in thickness (Figure 5.9). The well log responses also confirm the seismic signatures in the vicinity of the well-bore, which show weak or poor amplitude anomalies (Figure 5.8). However, amplitude signatures based on the RMS attribute displayed in a plan-form view reveals the presence of subtle channel and ponded sedimentary lobes downslope of the well location. Another horizon mapped deeper, designated as Oligocene-deep, reveals high amplitude depositional facies of primarily lobes with associated channels (Figure 5.10).

Controls on Oligocene Deep-water Depositional Patterns

Across the Niger Delta slope mud diapirs are seen to impose significant control on structural development and sedimentation (Whiteman 1982, Doust and Omatsola 1990). They are well expressed particularly offshore in the mid to lower continental slope where the sediments are much younger and have severe overpressure development, whereas upslope and across the shelf diapirism is negligible or entirely absent. This is most likely because the equivalent formation is older and therefore would have considerably dewatered over time (Whiteman, 1982). The 3D seismic data within the study area reveals the presence of mud highs. Their development has been attributed to rapidly prograding delta-fan complex overlying undercompacted mud, coupled with downslope gravity gliding or sliding of thick sedimentary packages (Whiteman 1982, Morley et al., 2010).

In this study, the sea-floor is interpreted to have been deformed before the accumulation of Oligocene sediments, particularly in the downdip direction of well A1. The deformed sea-floor has resulted in complex flow pathways of turbidity currents, causing considerable non-uniformity in reservoir facies distribution and architecture. The seismic volume clearly images the interplay between tectonics and channel

development, particularly as channels approach depressions or mini-basins flanked by mud ridges (Figures 5.7 and 5.9). Prather (2003) suggested that mini-basins are most likely the products of a mobile mud or salt substrate withdrawal that ultimately forms a ponded accommodation space. These take the form of a linear to arcuate, doubly-plunging syncline in the case of mud based withdrawal. Whereas in salt withdrawal the ponded accommodation space is circular to semi-circular. The depressions or intraslope mini-basins are characterised by a localised reduction in slope gradient and are capable of accommodating good quality hydrocarbon reservoir sands.

Mini-basins induced by salt withdrawal are notably responsible for trapping hydrocarbon reservoir sands in the Gulf of Mexico (Beaubouef and Friedmann, 2000) Channel flowing into such depressions are likely to have their profile change from a confined system to unconfined fan-lobe morphology. We have discovered similar features prevalent in the Oligocene succession in the study area where channels are seen to be significantly affected in geometry by topographical modification due to mud withdrawal. Some of the lobes are connected upslope to narrow feeder channels (Channels A, B, C and D) that serve as sediment conduits to the ponded accommodation space. These channels appear to be weakly sinuous with a length of about 10-15km across the study area (Figure 5.8 and 5.9).

Channel A appears to be well-developed at the shallower stratigraphic level with significant bright amplitude that characterise the lobe deposit. However, deeper in the succession at the level of the mapped Oligocene-deep horizon, the seismic amplitude is slightly reduced indicating a likely decrease in sand development with depth. Flowing downslope, channel A approaches two mud-cored folds, gets deflected and flows parallel to the larger 12km long fold before resuming its regional downslope course. As it approaches a topographic low, it opens into a less confined space and forms two lobe deposits (lobes 1and 2), each having a length of about 5.5km in the dip direction and width of about 3km.

Channel B is characterised by low seismic amplitude in both interpreted Oligocene horizons. However, the lobate deposit (lobe 4) formed at the channel end is seen to have a high amplitude signature, possibly linked to a higher percentage of sand compared to its updip feeder channel. This lobe is also laterally extensive with a length and width of

about 5km. The size of the lobe appears to reduce in the Oligocene-shallow horizon possibly indicating a reduction in accommodation space or decrease in sand input through time.

Channel C on the other hand is observed to be well-developed in the deeper horizon where it is particularly expressed by a high-amplitude well-imaged geometry. The plan view of the mapped Oligocene-deep horizon (Figure 5.10) shows significant variation in seismic amplitude of channel C as it is traced downslope over a growing structural high and into a topographic depression. This channel, with a width of about 600m, is initially characterised by high seismic amplitude but as the channel is traced downslope over a mud ridge the seismic amplitude decreases. The decrease in amplitude is significant as it transits into the depression. The weak amplitude may be related to erosional flow behaviour typical of the hydraulic jump region of turbidity currents (Prather 2003, Gee and Gawthorpe 2006). Similar weak amplitude features (see location of red marker in Figure 5.10) are also seen in channels A and B as they transit into lobes. As channel C passes into a slope depression flanked by mud ridges, its seismic amplitude increases significantly. Within this depression, variation in geometry is observed appearing with the development of a broad and possibly stacked depositional lobe system (lobe 5). The width of lobe 5 is close to 5km and onlaps against the mud-wall indicating that the lobe post-dates the structural highs.

In addition to the mud ridge control on sand distribution, the lobe complexes that characterise the Oligocene sequence are also controlled by sediment supply and localised changes in slope gradient led to the development of cone-shaped sand bodies that broaden and fan out into the mini-basins. The lobe complex associated with channel D, located towards the south-east of the study area, illustrates the above controls (lobes 6-8, Figure 5.10). This lobe complex has been interpreted to have three depositional lobe units that together form a complex. Lobe 6 is seen to breach out of the upslope feeder channel as a result of high flow momentum breaching or overtopping the main channel wall. The process responsible for the formation of this lobe is akin to the depositional process responsible for a fluvial crevasse splay (Posamentier and Kolla, 2003). Just beyond the breach, the channel terminates into a lobe deposit (Lobe 7) where a marked reduction in slope gradient is observed. Due to slope topography and sediment supply, channel avulsion is seen with sedimentation prograding further

downslope leading to the development of lobe 8. The individual lobes range from 3-6km in length and 2-5km in width. These lobes (6-8) are observed to be draped on a growing structural crest that has been modified by north-south trending growth faults with faults, throws of less than 70ms (< 120m) (Figure 5.13).

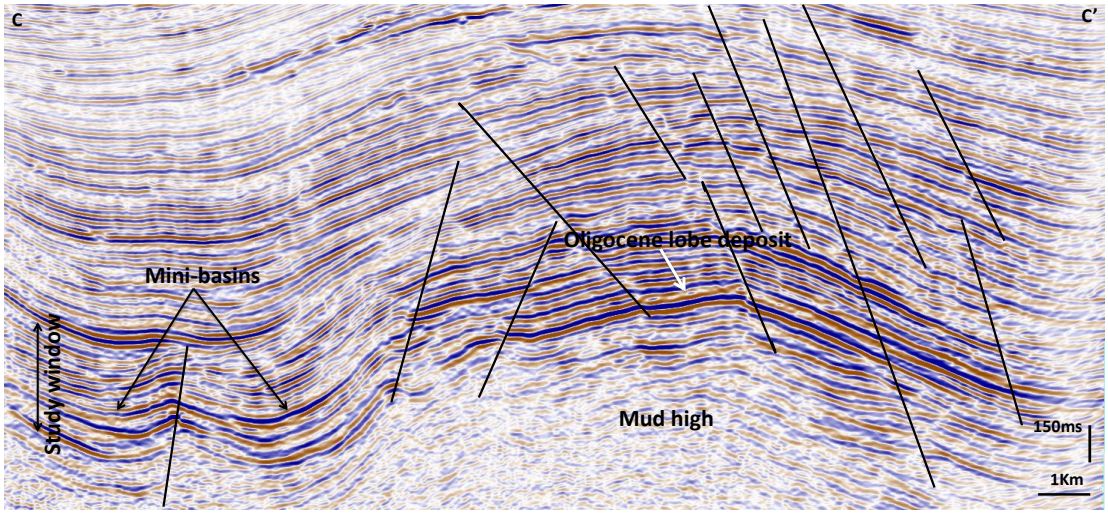

Figure 5.13: Seismic section illustrating the present-day structural pattern and lobe complex location. See Figure 5.10A for location of seismic line.

Oligocene Lobe Model

Although no wells have penetrated any of the Oligocene depositional features interpreted in this study, we have made inferences on the lobe characteristics based in part on seismic attributes and in part on comparison with other lobe studies from analogous sedimentary basins analogous to the Niger Delta with respect to their tectonic setting and depositional style. Shanmugam and Moiola (1991) proposed four main types of lobes: suprafan lobes, depositional lobes, fan lobes and ponded lobes, all of which are distinct in depositional process, geometry and reservoir properties. The Oligocene lobes interpreted in this study appear to fit into the depositional and ponded lobe types of Shanmugam and Moiola (1991), and closely match the ponded accumulations of Prather (2003) from the Gulf of Mexico slope region.

Depositional lobes develop at or near the mouths of submarine channels. Lobes 6, 7 and 8 depicted in Figure 5.10 appear to be of this type. Ponded lobes are deposited in partially confined accommodation space. Lobes 1, 2, 3, 4 and 5 are a close match for this type, as they appear to have developed in direct response to the deformed slope

topography created by local mud tectonics. Figures 5.7 and 5.9 show that ponding of the Oligocene sediments is significantly controlled by mud withdrawal. This is even better imaged in the 3D view of Figure 5.10C.

It is not easy to infer the likely sediment facies that make up the Oligocene lobes of this study. Seismic attribute analysis would suggest that they include sand-rich turbidites. Comparison with the overlying Miocene channel facies would imply a good sand-rich source, at least during the Miocene. The Gulf of Mexico ponded lobes documented by Prather et al. (1998) are characterised by a lack of channels and dominance of relatively fine-grained turbidite facies (Bouma D type), interbedded hemipelagites and a more chaotic facies. According to Shanmugam and Moiola (1991), depositional lobes are typically composed of thin and medium-bedded sand-mud turbidites (Bouma C type) with a grain size that ranges from medium to fine sands. However, without further drilling it is impossible to be more specific about the types and facies of the lobes documented in this study.

Implications for Hydrocarbon Exploration and Production

The plan-view attribute maps from RMS and RGB spectra decomposition indicate that the depositional patterns of sandswithin the interpreted Oligocene sequence have a channel feeder and lobate geometry. Although there are no wells drilled downslope of well A1 or deeper into the Oligocene-deep interval, we infer the presence of sand and possibly hydrocarbon bearing sands based on the bright seismic reflection amplitude from the RMS and RGB maps. In addition, from the sweetness attribute map, which was calibrated to well logs across the hydrocarbon bearing Miocene proven play, high sweetness values correspond to both low gamma ray and high resistivity log values reflecting the presence of hydrocarbon bearing reservoir sands. Applying this interpretation to the Oligocene interval we suggest that the Oligocene lobes that are characterised by high sweetness values are likely to be hydrocarbon bearing sands. Lobate sands are typically known to amalgamate upon deposition (Shanmugam and Moiola, 1991, De Ruig and Hubbard, 2006) thereby developing thickening upward and laterally extensive sequences. This is most likely the case for the lobes of the Oligocene sequence interpreted in this study. These lobe depoists, which are likely sand prone, have the potential to enjoy good fluid communication across individual sand units,

hence making them potential exploration targets. Future production can be optimised by drilling horizontal wells and their placement aided by the attribute maps utilised in this study. Reservoirs from fan lobes deposited in intra-slope mini-basins have been discovered in the mid-slope area of the Gulf of Mexico where they are major exploration targets (Prather, 2003).

Conclusion

The offshore Oligocene sequence of the Niger Delta slope system is still poorly known has been poorly understood as current exploration and production in the sedimentary basin has concentrated on the well-studied Miocene and younger sedimentary succession. This has proved to be a highly prolific hydrocarbon play. For example, in the study location a seismic horizon was mapped across the Mid-Miocene sequence and based on RMS and RGB blend attributes draped on structure, the Miocene is seen to be characterised by medium to low sinuous amalgamated channels systems. In some cases, the channels transit downslope into lobes (Figure 5.6). High seismic amplitude also typifies these sediments which are noted to be sand prone and hydrocarbon bearing confirmed by well penetrations (Figure 5.7).

On the basis of 3D seismic data, the depositional architecture and reservoir potential of the deep-water Oligocene sequence has been documented. Three suites of seismic attributes have been utilised in this study including: root mean square (RMS) amplitude, spectral decomposition-RGB (red, green and blue) blend and sweetness. RMS and RGB blend attributes were both used to image the depositional bodies prevalent in the Oligocene interval. Unlike the Miocene sequence that is characterised by mostly amalgamated channel complex with proven reservoir potential based on well penetrations, the Oligocene succession has been interpreted to be dominated by lobes, which are clearly revealed in the planform displays (Figure 5.8 and 5.9). The presence of these lobe deposits is significantly controlled by sea-floor topography that has been modified by mud-induced highs. These mud highs are most probably linked to mobile mud withdrawal, thereby resulting in the development of mini-basins, and hence accommodation space in which sediments pond. The morphology of the depositional bodies indicates that the structural highs are likely to predate the depositional elements.

Since a single well penetrated only the top of the Oligocene, the interpretation of the type of sediment deposited in the mini-basins and the feeder channels was based on the consideration of lobe deposits elsewhere. The seismic amplitude characteristic seen in the Miocene reservoir confirmed by well penetrations was also useful. The Miocene sands showed high sweetness values correlating nicely to low gamma ray and high resistivity logs indicating the presence of hydrocarbon. High sweetness values coupled with high amplitude seismic reflection suggest that the deeper Oligocene lobes are most likely sand prone and possibly hydrocarbon bearing and are therefore a future potential exploration target.

Acknowledgement

We wish to express our appreciation to Shell in Nigeria for providing the data, particularly to Daniel Agbaire whose expert advice and resolution in seeing this project through was of immense benefit. Also, special thanks to Schlumberger UK for their technical advice, which had greatly enhanced this work and for generously providing Petrel™ and Techlog™ software to Heriot-Watt University. This project is part of Obinna Chudi's PhD which has been generously sponsored by the Petroleum Technology Development Fund (PTDF), Nigeria.

CHAPTER 6

PLAY POTENTIAL OF THE OLIGOCENE SEDIEMNTS

This chapter comprises Paper 2 of the thesis: “Predicting Oligocene Reservoir Potential in the Deep-Water Western Niger Delta: An integrated Basin Modelling and Diagenetic Study”.

It is based on basin and petroleum systems modelling across the study area of the western Niger Delta. The paper has been submitted to the Journal of Marine and Petroleum Geology and it is currently in the first review stage.

It is reprinted here in full, although figure numbers have been replaced by chapter figure numbers (e.g. Figure 1 becomes Figure 6.1), and the references are included in the main reference list at the end of the thesis.

There is necessarily some overlap and repetition with other parts of the thesis in presenting the ‘introduction’ and ‘geological setting’. The discussion is developed further in Chapter 8.

The authorship includes my two supervisors, but the work and principal findings are entirely my own.

6.1 Paper 2

Assessing the play potential of untapped Oligocene sediments Deepwater Niger Delta: A basin modelling approach

Obinna Chudi[1], Helen Lewis[1], Dorrik Stow[1] and Andy Bell[2]
Obinna.chudi@pet.hw.ac.uk, Helen.lewis@pet.aha.ac.uk, Dorrik.stow@pet.hw.ac.uk

1- Institute of Petroleum Engineering, Heriot-Watt University, EH14 4AS, Edinburgh, UK
2- Shell Global Solutions International, The Hague

Abstract

The Niger Delta basin is one of the prolific passive margin basins in West Africa. With over 50 years of exploration, it is considered to be a mature basin. The majority of the hydrocarbon trapped has been from the Miocene and younger clastic sediments of the Agbada Formation, while the deeper untapped Oligocene sediments remain fully unexplored or at best poorly understood. A two-dimensional integrated petroleum system with diagenetic modelling was constructed with the aim of understanding the charge history of the Oligocene sediments and the influence of hydrocarbon emplacement on quartz cementation. This study provides a basin modelling perspective that would improve the understanding of the Oligocene sediments as a potential reservoir thereby reducing exploration risk associated with reservoir presence.

The two dimensional model shows that the Akata shales started charging the Oligocene sands at 20Ma with four hydrocarbon accumulations predicted at the present day. Proven hydrocarbon accumulations trapped within the Miocene sequence and penetrated by Well A1, the deepest well in the study, were also predicted. In addition, results observed from the 2D basin model simulation reveals that the timing of quartz cementation precedes the timing of oil emplacement; however, not more than 5% of the pore space was occluded by quartz cement in each of the four accumulations before peak hydrocarbon saturation (irreducible water saturation) was attained. So it is likely that the early emplacement of hydrocarbon would have slowed down the rate of quartz precipitation thereby preserving reservoir porosity.

Introduction

The deep-water western Niger Delta in the past ten years have been a centre of hydrocarbon exploration and production with giant discoveries made that straddles the shelf and the continental slope of the basin (Ofurhie et al., 2002). Good reservoir quality sands have been discovered mostly in the Miocene sediments of the Agbada Formation, occurring as turbidite sands within amalgamated channel-levee systems, with both structural and stratigraphic trapping components. The Miocene play enjoys good reservoir quality owing to the excellent porosities of up to 35% and permeability in the Darcy range, which has been encountered by most of the wells drilled (Fehintola et al., 2009).

This paper focuses on the reservoir potential of the deeper, poorly understood Oligocene Agabda formation within the study area, located across a water depth of 800-1000m in the slope part of the western Niger delta (Figure 6.1). Over 30 wells have been drilled in the study area but only one well (A1) penetrated the top of the Oligocene sequence, which is the primary interval that is being studied. The other wells were drilled to a depth within the Miocene sequence. Conventional well logs were acquired from the A1 well, including gamma ray, resistivity, sonic, neutron and density logs. The logs reveal less than 10m of sand units with a very weak resistivity profile within the Oligocene interval. The small thicknesses of sands encountered by Well A1 coupled with its low resistivity profile suggest that the Oligocene sediments of the Agbada Formation are faced with a risk of both charge and of reservoir presence.

In this paper we discuss the timing of hydrocarbon emplacement in the Oligocene reservoirs relative to the timing of quartz cementation and the corresponding effect on the reservoir quality. The effect of hydrocarbon on reservoir quality is derived from the widely accepted concept that early hydrocarbon emplacement in a reservoir can potentially stop or slow down the rate of quartz precipitation thereby preserving porosity (Taylor et al., 2010, Worden and Morad, 2000). We draw inferences from the studies of Chudi et al., (2014 in press) (Chapter 7 of this thesis) which was centred on an integrated basin modelling, diagenetic and petrophysical study of the target Oligocene sediments, aimed at predicting the degree of quartz cementation in the potential Oligocene reservoir.

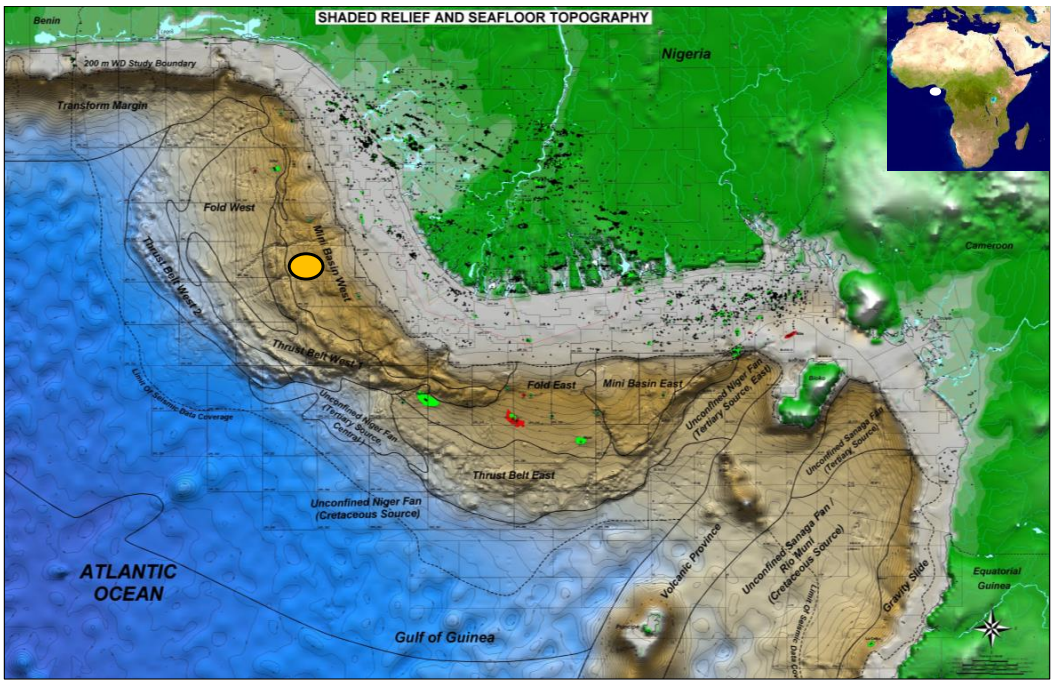

Figure 6.1: Niger Delta map showing shaded relief and sea-floor topography. Study area depicted in amber circle (Courtesy of Shell Nigeria).

Geological Setting

The hydrocarbon-prolific Niger Delta has been the centre of attraction for hydrocarbon exploration and production in the continental margin of West Africa for over five decades (Haack et al., 2000) and this is the reason that it has been extensively studied (Short and Stauble, 1967, Weber, 1971, Whiteman, 1982, Ejedawe et al., 1984, Doust and Omatsola, 1990, Damuth, 1994, Haack et al., 2000). The delta and its deep-water system is situated in the Gulf of Guinea (Doust and Omatsola 1989) and the subaerial portion covers an area of approximately 75,000km^2 with a maximum clastic sediment thickness of about 12km at the basin centre (Damuth, 1994). The evolution of the basin is linked to the separation of the South American and African plates in the Mesozoic.

Three lithrostratigraphic units have been penetrated by wells drilled mostly along the basin flank: the Benin, Agbada and the Akata Formations (Short and Stauble 1967), see Figure 6.2. The Benin formation characterised by high sand percentage is of continental fluvial depositional environment of the upper delta plain setting (Obaje, 2009) and likely to be Miocene to Recent in age (Short and Stauble 1967). Underlying the Benin Formation is the paralic sequence of the Agbada Formation representing sediments of transitional environment including delta front and deep-water slope and fan

characterised by alternating sands and shales that range from Eocene to Recent in age. The Agbada Formation constitutes the primary reservoir unit of the Delta both onshore and offshore. The hemipelagic and pelagic muds of the Akata Formation make up the deepest part of the Tertiary sedimentary sequence. The marine shales of this sequence range from Palaeocene to Holocene in age. Based on regional studies and experimental analysis of the rock samples retrieved from wells that encountered the Akata shales, they are considered as the active source rock of the Tertiary Niger delta (Evamy et al., 1978, Lambert-Aikhionbare and Ibe, 1984, Tuttle et al., 1999). In deep-water the top of the Akata is known to contain sand beds that are likely turbiditic in origin with reservoir potential.

The shelf margin of the delta is known to be modified by a number of canyons that also extend beyond the shelf into the deep-water. These canyons form major conduits for sediments deposited in the deep-water, for example the Opuama canyon located in the western arm of the basin is thought to be responsible for channelling sediments in the Oligocene times (Petters, 1984) and therefore likely to have served as a sediment conduit to the slope region in the vicinity of the study area.

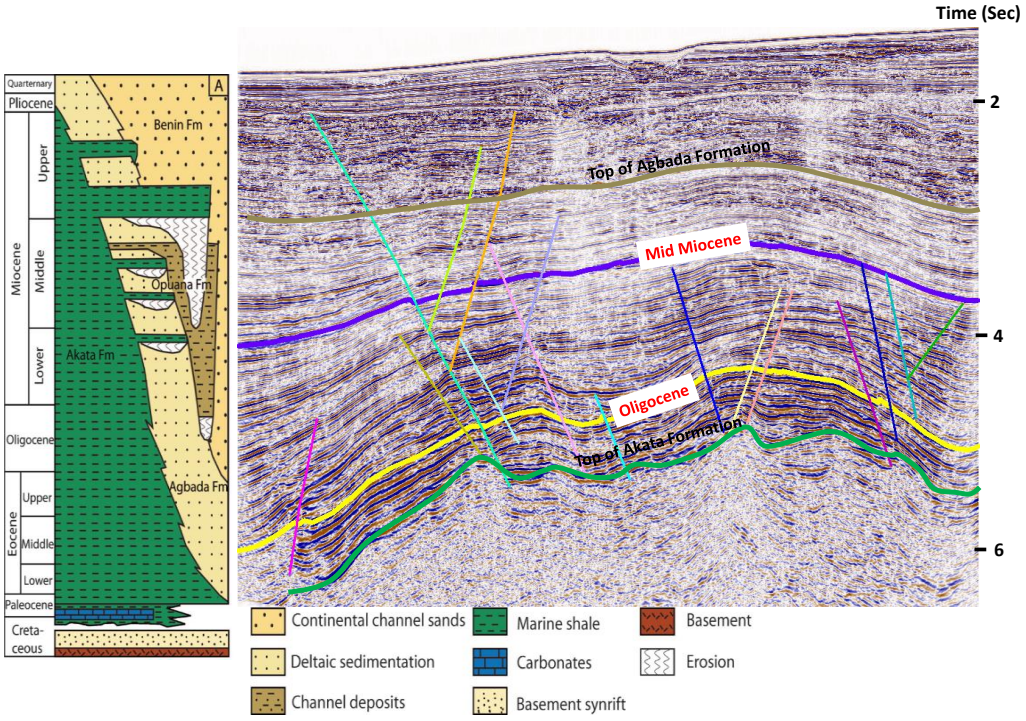

Figure 6.2: A) Regional stratigraphy of the Niger Delta and seismic transect across the deep-water western Niger Delta illustrating the main lithostratigraphic unit and fault

pattern. Mid-Miocene and Oligocene horizon of the Agbada Formation also highlighted (Modified after Corredor et al. 2005).

Controlled by gravity driven tectonics, three structural provinces define the Delta. Updip from the Shelf to the onshore part of the basin, extensional features are prevalent and are dominated by listric growth faults. The upper and middle slope is dominated by mud diapirs and folds. This zone is known as the translational zone. The lower slope is a zone of horizontal shortening triggered by downslope movement of sediment due to gravity gliding forming fold and thrust belts (Bilotti and Shaw, 2005, Corredor et al., 2005, Deptuck et al., 2007).

The study area is located in the translational province of the mid to lower slope setting (Figure 6.1). The present day reservoir packages are Miocene channel sands of the Agbada formation. Current petrophysical evaluation indicates that the reservoirs are of good quality with porosities of up to 35% and permeability in the Darcy range.

The Miocene reservoirs in the study area have been cored and are seen to be loosely consolidated sands that are moderately sorted and display a dominant grain size of medium to fine. The sands have been classed as quartz arenites and subarenites considering that they are largely composed of quartz with less than 15% feldspars. Unsurprisingly this well sorted, poorly consolidated and almost uncemented fine to medium grainsized quartz sand has the expected high porosity and permeability values.

The Oligocene interval encountered by well A1 appears to have less than 10m of sand with average calculated porosity of about 20%. The resistivity log profile appear to be of low value similar to that expected in a clean water bearing sands, although minor increase in resistivity value is noticeable but does not reflect significant hydrocarbon saturation (Figure 6.3). No core was acquired across the Oligocene interval.

Although, three source rocks have been described to be present in the Niger Delta (Haack et al., 2000) that includes the terrigenous Tertiary shales; the Upper Cretaceous-Palaeocene marine shales and the Lower Cretaceous lacustrine source rocks. The Tertiary source rocks are considered to have charged the Agbada reservoirs both

onshore and offshore. The source rock potential of the older rocks are poorly understood, largely attributed to the lack of geochemical data from these deeply buried rocks since no well have been drilled to that depth.

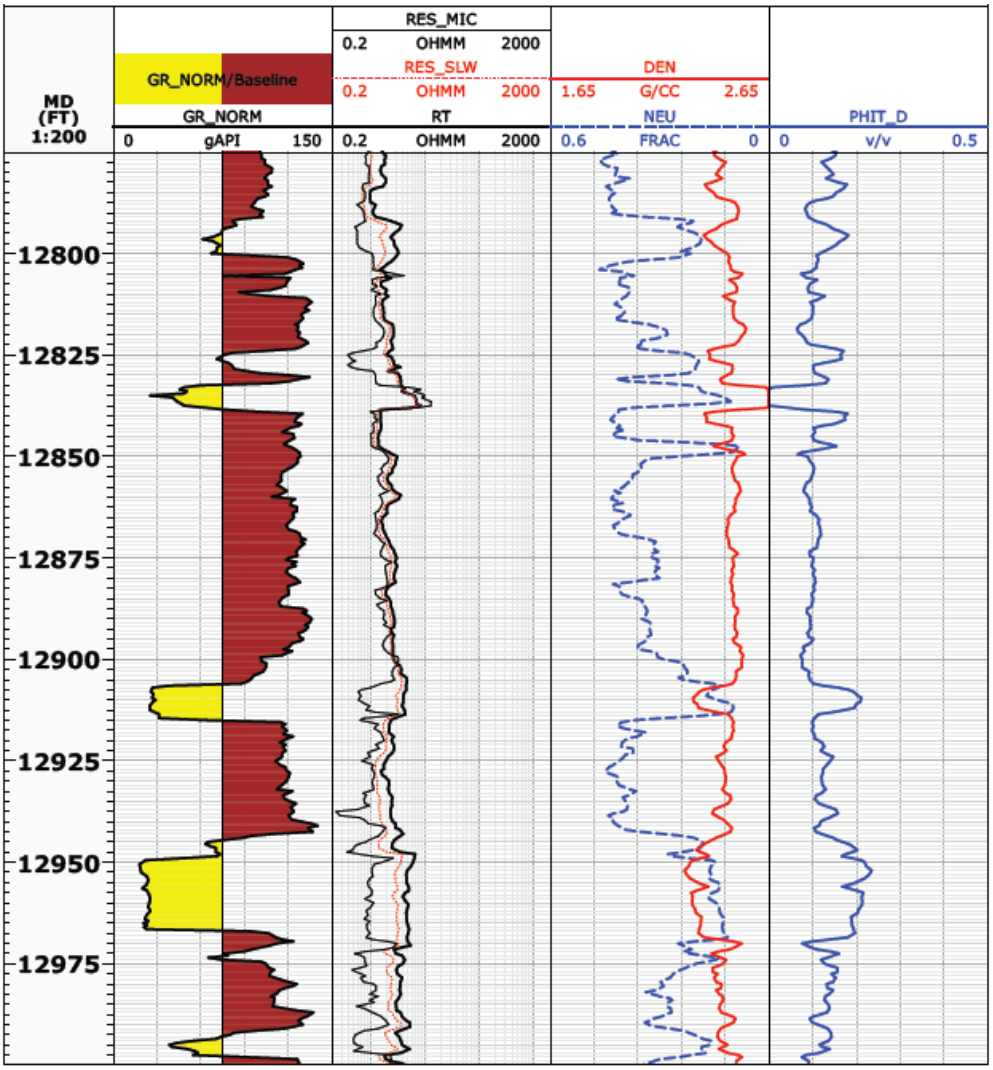

Figure 6.3: Petrophysical log across the Oligocene sequence penetrated by well A1.

Methods and Input Data

In this study, PetroMod^{TM} software of Schlumberger was used to study the temperature, maturity and charge history of the study area in relation to the Oligocene deep-water system. Basic data requirements for the modelling include but not limited to the present day geometry, lithological description of layers and their associated rock properties (thermal conductivity, porosity, permeability, etc.), and absolute ages of each of the stratigraphic layers, boundary conditions and calibration data. The general model frame work was created by digitizing the 2D seismic line provided by Shell Nigeria

(SNEPCO). This 2D transect runs NE-SW for over a distance of 160km across the extensional, translational and compressional parts of the Niger Delta basin (Bilotti and Shaw 2005, Corredor et al., 2005, Deptuck et al., 2007). Figure 6.4A shows the seismic cross section through the study area. The 2D transect intercepted the location of the deepest well in the study area which was used to (1) constrain lithology assignment of the layers, and (2) calibrate the heat flow and thermal maturity since temperature, vitrinite and porosity measurements were acquired from the well.

A

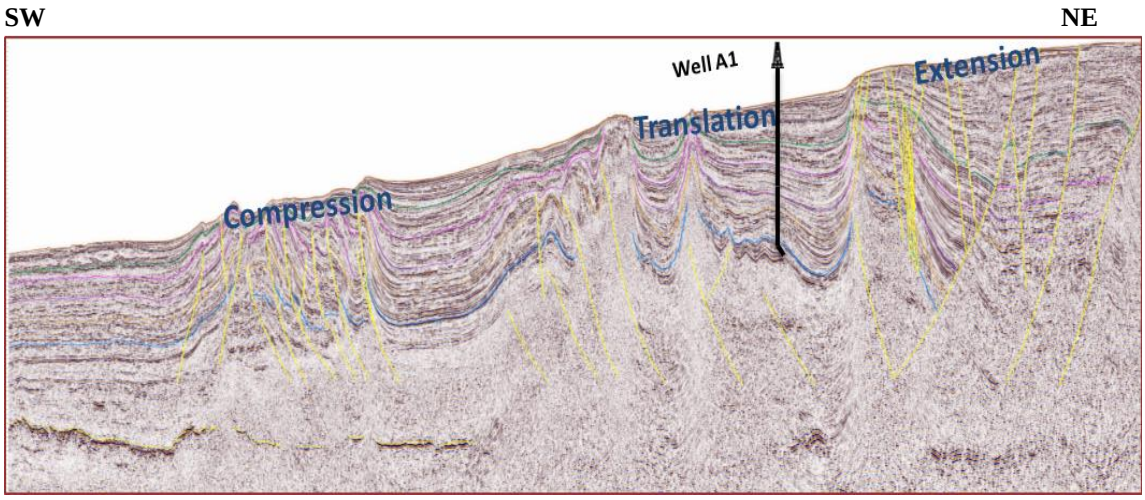

B

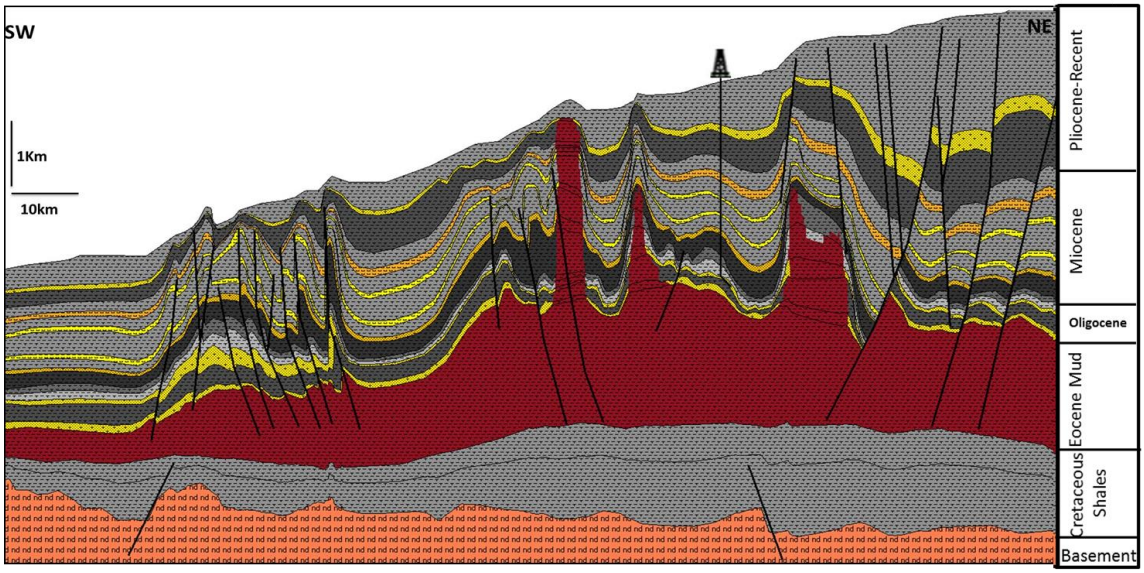

Figure 6.4: a) Interpreted regional 2D transect across the 3 structural provinces (Courtesy of Shell Nigeria); b) Digitized 2D transect.

Conceptual Model

Conceptual models derived from the conversion of geologic realism from geological data into numerical form (Welte and Yalcin 1988) were developed by adopting the principles published by Yalcin *et al*. (1997) and Hantschel & Kauerauf (2009). In this study, the conceptual models consist of depositional events with no hiatus or erosion interpreted (Table 6.1). These events are generally based on the regional geology of the study area typical of a regressive depositional system with no basin-wide hiatus or erosion (Whiteman 1982, Doust & Omatsola 1989). Stratigraphic and depth information for both 1D and 2D models was constrained from the stratigraphic interpretation of deepest well in the study location (Well A1) that was drilled to a total depth of 4100m (13475 ftss) within the Oligocene. Appendix C of this thesis shows an example of the approach adopted in determining the lithological properties for the reservoirs modelled. Beyond 4100m, the stratigraphic subdivision was extracted from literature information (Short and Stauble 1967, Doust and Omatsola 1989, Damuth 1994) and from a 3D seismic volume acquired in the study area. The amber coloured box in Table 6.1 indicates the interval not penetrated by the well.

Layer	Depo (From)	Depo (to)	Lithology	PSE	TOC	Source Rock Kinetics	HI
	Ma	Ma			%		mgHC/gTOC
Upper Pliocene-Recent	1.7	0	PliesRecent	Overburden Rock			
Mid Pliocene	2	1.7	Sd67Silt28_Sh5	Reservoir Rock			
Lower Pliocene	8	2	Shale (typical)	Overburden Rock			
Upper Miocene_SL	10.8	8	Sh85SL25	Seal Rock			
Upper Miocene_RES	12.2	10.8	Sd70Silt25_Sh5	Reservoir Rock			
Upper Miocene_SL	15	12.2	Sh85SL25	Seal Rock			
Mid Miocene_RES	15.6	15	Sd75Silt20_Sh5	Reservoir Rock			
Mid Miocene_SL	18.4	15.6	Sh90Silt5	Seal Rock			
Mid Miocene_RES	19	18.4	Sd75Silt20_Sh5	Reservoir Rock			
Lower Miocene_SL	22.05	19	Sh90Silt5	Seal Rock			
Lower Miocene_RES	23.35	22.05	Sd84Silt6_Sh10	Reservoir Rock			
Lower Miocene_SL	27.7	23.35	Sh90Silt5	Seal			
Top Oligocene SL	28.31	27.7	Sh90Silt5	Seal			
Oligocene SL	29	28.31	Sd90Silt5_Sh5	Seal Rock			
OligoceneRES_S	29.25	29	Sd84Silt6_Sh10	Reservoir Rock			
Oligocene SL	29.5	29.25	Sh90Silt5	Seal Rock			
Oligocen Res_D	35	29.5	Sd84Silt6_Sh10	Reservoir Rock			
Akata Mud	72	35	Shale (organic rich typical)	Source Rock	5	Burnham(1989)_TII	400
Upper Cretaceous_SR	79.35	72	Shale (typical)	Source Rock	4	Burnham(1989)_TII	400
Lower Cretaceous	93	79.35	Shale (typical)	Underburden Rock			
Basement	100	93	Basalt	Basement			

Table 6.1: Model stratigraphy defined in PetroMod™ showing layers, lithological composition and event timing. Percentage of sand (Sd) and shale (Sh) was constrained from well information, while basalt crust was assumed.

Interpreted faults on the 2D transect were also digitized with priority given to the faults that are likely to have a significant impact on hydrocarbon migration with the selection done by adopting similar criteria to Derks et al. (2012). Of the 39 faults originally

interpreted in the 2D line, only 26 faults were considered for model simplification based on the following criteria:

d) Regional faults that extend over a great distance cutting across most of the horizons most especially faults that connected deep seated source rocks to shallow reservoirs.

e) Where two or more faults are parallel to each other and cutting the same horizons with similar offset, then a representative fault is selected.

f) Faults that are continued by other faults are merged.

Sensitivity analysis was done on the fault property to evaluate the importance of faulting on fluid migration particularly vertical migration through faults. The influence of representing the faults as entirely open or entirely closed was assessed in the model; however, an open fault system was preferred since modelled hydrocarbon accumulation matched present day observation only when faults are open. Other fault properties such as the thermal properties, permeability and shale gouge ratio were not considered in the model building workflow as this would require further investigation and analysis beyond the scope of this work and limitation of the modelling tool used. However, the impact of the fault properties particular the influence of mud diapirs on the faults can have an impact on model results especially fluid migration.

Modelling Mud Diapirs

The study area is characterised my mud diapirs which has affected the stratigraphy encountered. The mud tectonics and mud piercing into the overlying sediments were encountered for in the model building process by using the salt tectonics and facie piercing tool in PetroMod^{TM} software package. A better definition of the mud thickness (the top and base mud) was done so that the pre-mud layers are flat again and the mud movement that occurred between 33Ma and present day is accounted for. One main assumption is this process is that the pre-mud geometries observed today have not changed since the deposition of the mud. So the present day base salt geometry was used as a reference at older time step and used to compensate for regional subsidence. The Present day salt area was calculated to be a total of 251km^2 (includes the base area of 232km^2 and a pierced area of 19.2km^2) and used as the reference layer. For every

time step (1, 1.5, 5.3, 10.9, 18, 20, 25 and 33.5Ma) defined in the model an incremental increase in mud area was calculated, building up systematically to 250.19km^2 at 33.5Ma which marks the onset of mud diapirsim (Whiteman, 1982).

Age

The 2D transect was interpreted with chronostratigraphic surfaces defined by Shell (Figure 6.4A). A total of seven horizons were interpreted that includes the sea-floor representing present day, Lower Pliocene, Upper Miocene, Middle Miocene, Lower Miocene and Oligocene. An additional surface representing the top of the basement was later mapped. The ages of the surfaces were subsequently tied to chronostrtigraphic tops interpreted in the well A1 to ensure conformity between well tops and seismic horizon picks. The seismic section was in depth domain and tied to well logs also in depth.

Lithology

Each of the stratigraphic unit defined by the chronostratigraphic tops were further subdivided into discrete layers with lithology assigned to each layer. Rock properties, for example porosity, permeability, thermal conductivity were defined for each of the layers based on mixing of the default properties provided in PetroMod^{TM}. This process was controlled by the stratigraphy and lithology as observed from log and petrographic study and generalised for modelling purpose so that away from the well where no well control was available, the lithology was assumed to be laterally continuous updip and downdip from the well location (See Figure 6.4B). This was a key assumption that was considered whilst building the model.

Source Rock Properties

Geochemical analysis of source rocks does not form part of this research, hence the two source rocks that were considered in this study and their properties – total organic carbon (TOC) and hydrogen index (HI) are average values derive from extensive studies of the Niger delta source rocks (Evamy et al., 1978, Ekweozor and Daukoru, 1984, Ejedawe et al., 1984, Lambert-Aikhionbare and Ibe, 1984, Nwachukwu and Chukwura, 1986, Doust and Omatsola, 1990, Haack et al., 2000). In addition, the kerogen kinetics which controls the rate of conversion of kerogen in the source rock to petroleum under increasing thermal stress was assumed to be based on the kinetic parameters of

Burnham and Sweeney (1989). This was built on the assumption that the shales used in his model have similar source rock properties as the Cretaceous and Tertiary source rocks in this study. Although if source rock samples were present, custom kinetic parameters measured from this samples would have been the most preferred option.

The source rocks considered in the model includes:

(1) Upper Cretaceous to Lower Palaeocene source rock of marine Type II and II/III oil prone kerogen. HI and TOC values are ca.400 mgH/g TOC and 4% respectively.

(2) A Tertiary source rocks of the Akata Formation composed of terrestrial organic matter input with both gas prone and oil prone end members. This places the organic matter of the tertiary source facies to be of Type II/III kerogen with TOC of 5% and HI of 450 mgH/g TOC respectively.

Boundary Conditions

The boundary conditions; basal heat flow representing the lower boundary condition, sediment-water interface temperature (SWIT) that characterises the upper boundary condition and the paleowater depth (Figure 6.5) were first established for the 1D model at well location and after model calibration the values were adopted for the 2D model.

Basal heat flow

The lower boundary condition which determines how much energy is introduced into the system from below (Nelskamp et al., 2008) was chosen and defined by applying the uniform stretching model of Makenzie 1978 with a maximum heat flow of 105 mW/m^2 representing the period of rifting of the South America plate and Africa at the Niger Delta location during the Mid Cretaceous (ca.100Ma). Thereafter the heat flow gradually declined to a present day value of about 53 mW/m^2 established by calibrating the calculated temperature from the model and measured bottom hole temperature (BHT) from well A1. A present day geothermal gradient of $40^{O}C/km$ is calculated in the model.

Sediment-water interface temperature (SWIT)

The upper boundary condition is set by the SWIT – a function of an assumed surface temperature and water depth. The calculation done on SWIT was based on the works of Wygrala 1988. The tool generates a global surface temperature curve based on a predefined continent of the study area. Paleowater depth is also required to calculate SWIT. The SWIT starts up at value of about 25˚ C, an assumed surface temperature before the break-up of the South American and African Plate and steadily decreases during the break-up from the Early Cretaceous and maintains a temperature of about 4˚ C from Late Cretaceous till present day (Figure 6.5B).

Paleowater Depth (PWD)

Paleo-water depths were set on the basis of paleogeographic reconstruction tool from Google Earth while a present water depth of 3382 ftss (C. 1000m) as seen in well A1 was defined in the model. For the 2D model, the present day water depth varied throughout the continental slope, so four depth points were selected at the basin shelf, upper slope mid-slope and toe of slope. These four points were based on water depth for wells drilled at these geographic positions that formed the basis for determining the PWD for the 2D model. PetroMod^{TM} interpolates water depths in between the predefined depth points. Generally, the water depth stays at a zero value before the continental drift of South America and Africa and thereafter increases to water depth of about 8000ft (2400m) in the Late Cretaceous. This value is maintained until the Cenozoic when the delta begins to build basinward with sedimentation progressively prograding towards the deep-water (Figure 6.5C) and water depth gradually reducing to present day values.

A

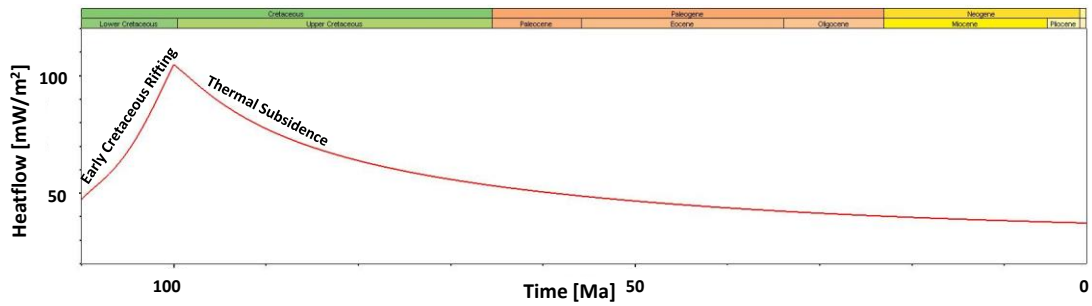

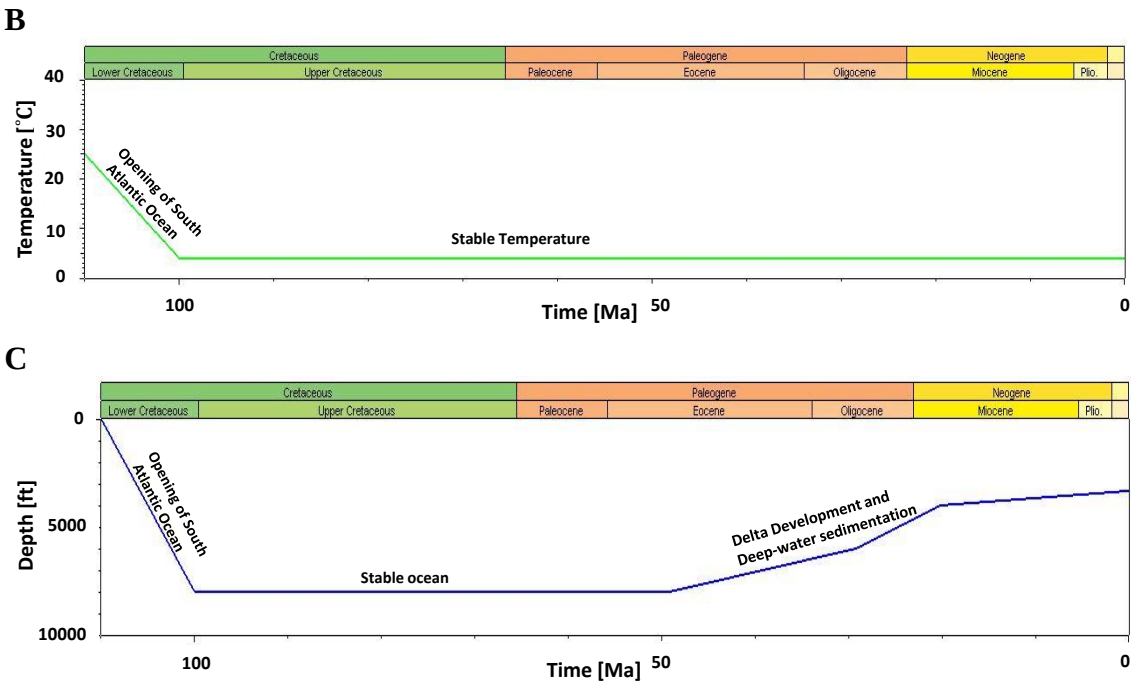

Figure 6.5: Boundary conditions for the basin modelling: A = Heat flow, B = Sediment water interface temperature (SWIFT) and C = Paleo Water Depth (PWD). All three curves are seen to respect fully the break-up of the South America and African plate in Late Cretaceous (100Ma) and subsequent delta development and progressive sedimentation in deep-water.

Model Calibration

To calibrate the present-day heat flow, corrected bottom-hole temperatures (BHT) were used. Two sets of temperature data were utilized; temperature data from Well A1 in the primary study location and bottom-hole temperature from a well updip in the shelf region located directly on the seismic line. Vitrinite reflection data that is known to have linear responses of temperature with depth was used for calibrating thermal evolution of the study area. Vitrinite measurement was only available from Well A1 and the values range from 0.3 % to 0.6%VR_o. The data distribution of the vitrinite measurement indicates that it is of good quality with no scatter that could reflect measurement from recycled vitrinite, caved in samples or oxidation due to prolonged storage of samples. The calculated vitrinite from model simulation is based on the kinetic EASY $\%R_O$ algorithm of Sweeney and Burnham (1990). This algorithm is a simplified Arrhenius reaction model that incorporates a distribution of activation energies that is used to calculate vitrinite maturation as a function of time and temperature. The model

calculates vitrinite maturation within a window of 0.3 – 4.5% $R_{O.}$ The % R_O is estimated based on the equation below:

% R_O = exp (-1.6 + 3.7F)

Where F the extent of reaction is given as:

$$F = 1 - \omega / \omega_o = 1 - \sum_i f_i \left[\omega_i / \omega_{oi} \right]$$

Where ω is the initial concentration of the total reactant, ω_{oi} is the initial concentration for component *i and* f_i *are* stoichiometric or weighting coefficient for the reaction components

The advantage of this model over other models is that 1) it uses an Arrhenius-reaction approach with a distribution of activation energies which are representative of the varying chemical reactions involved. Hence the model can be applied to laboratory heating rate of 1°C/week to geological heating rates ranging from 10°C/100yr to 1°C/my, 2) it can be used with any type of thermal history – non-deposition, uplift or cooling, thereby allowing calibration to be performed in any basin settings and depth and therefore makes this suitable for passive margin setting like the study area.

Other data that were used in calibration were average well log porosity calibrated against stressed corrected core porosity and pore pressure measurement both acquired across reservoir zones from Well A1.

By varying the peak heat flow value during rifting, the present day heat flow value and the thickness of sedimentary package particularly at deeper intervals below the well TD (total depth) a good calibration was achieved between measured values and calculated values from the model (Figure 6.6). Ground truth of the model was also achieved with calculated hydrocarbon occurrences matching present day oil accumulation at Well A1 location in the Miocene reservoirs. These Miocene reservoir are one of the prolific oil reservoirs in the deep-water western Niger Delta (Figure 6.7).

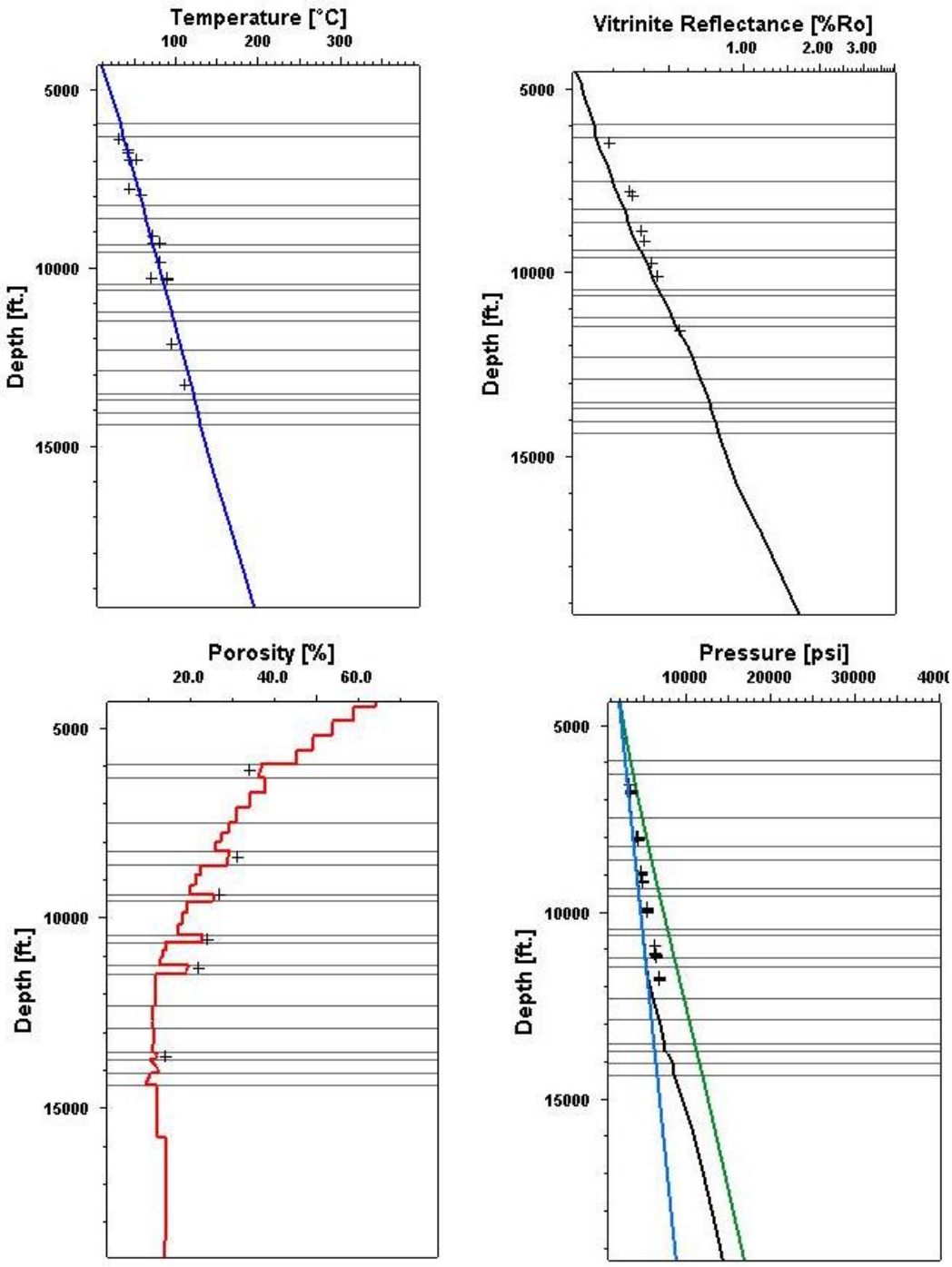

Figure 6.6: ID extraction at Well A1 location from 2D model of temperature, vitrinite, porosity and pressure. Cross = measured data, and line = calculated data. Good calibration achieved as measured values matches calculated values from simulation. Although porosity data exist in other wells within the study area, calibration was only carried using well A1 considering it's the deepest well in the study with complete suit of data.

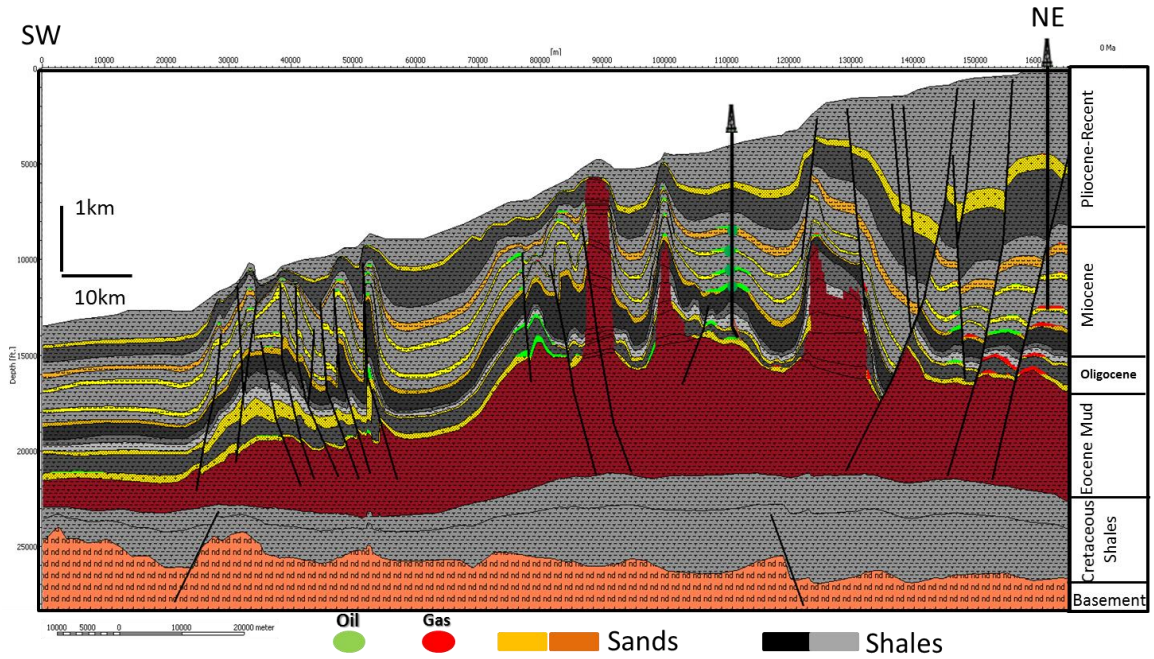

Figure 6.7: Predicted hydrocarbon occurrence matches present day observed oil accumulation in well A1.

Results

Petroleum Generation, Expulsion and Migration

The geological evolution along the 2D transect was reconstructed with the thermal and maturity history established by calibrating the modelled vitrinite reflectance and BHT data to the measured data taken from the exploration Well A-1. Therefore the temperature and hence the source rock maturation and the corresponding hydrocarbon generation can be estimated with reasonable certainty. The resulting present day temperature and thermal maturity profile along the line is seen in Figures 8 and 9. The observed present day temperature distribution indicates that the system is at equilibrium with iso-therms running almost parallel to the sediment-water interface (see Figure 6.8).

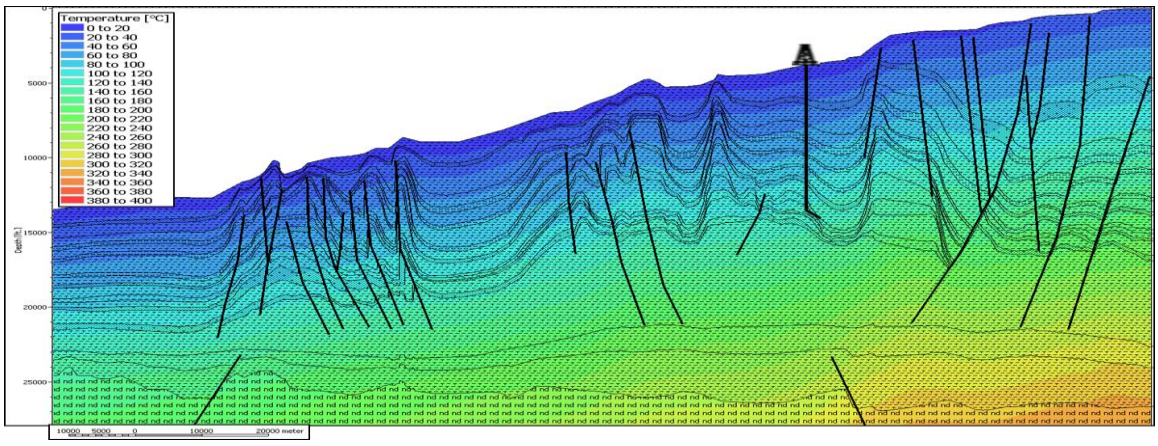

Figure 6.8: Iso-temperature overlay on cross section

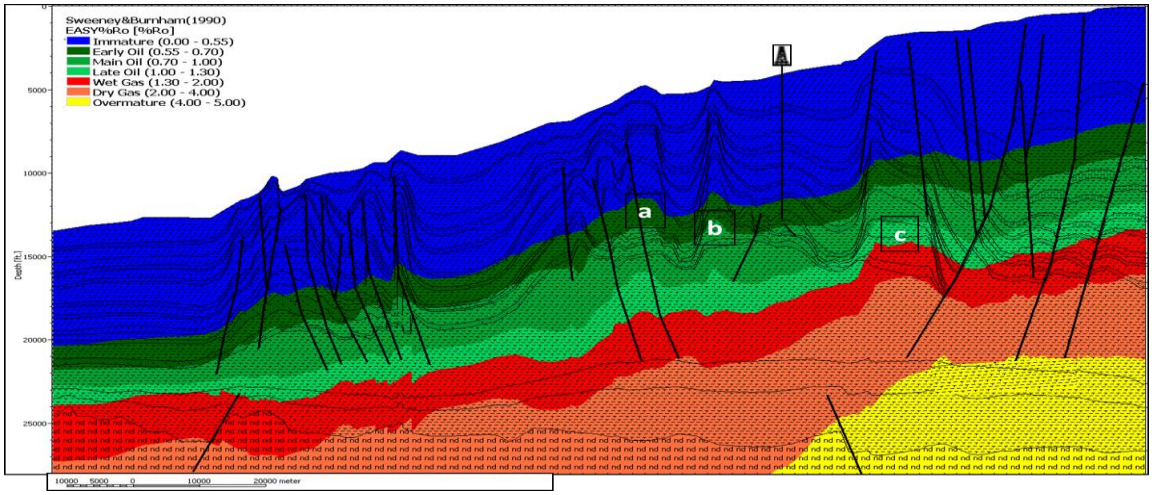

Figure 6.9: Iso-vitrinite overlay on cross section; a, b and c indicates location with mud diaper.

Overall, a decrease in in thermal maturity is obvious from north-east to southwest, basin ward of the section, which is likely related to 3 key factors:

1- A wedge shape delta which is thicker updip and thins basinward, so that for the same lithological unit the burial depth is lot deeper landward and shallower (relative to the sea-floor) moving offshore.

2- The top boundary condition – the predicted sediment water interface temperature, becomes cooler as you move from shelf to deep-water leading to a general cooler system.

3- Another factor that is seen to impact on the thermal maturity distribution is the presence of mud diapirs. In terms of thermal conductivity in a clastic setting, muds are known to have very low thermal conductivity compared to sands, so that heat is not well transmitted across the mud but retained. The implication on maturity would be a slight peak in thermal maturity around the vicinity of the mud diapir (see locations a, b and c in Figure 6.9) and away from the mud the thermal maturity returns to the expected profile. This effect is seen to diminish with increase in depth. A similar anomaly is also noted in salt diapirs but rather than a peak in maturity around the salt a drop in maturity is expected since salt is a good thermal conductor (Schwarzer and Littke, 2007).

The main sections of interest in modelling hydrocarbon generation and expulsion are the Palaeocene-Eocene Mud of the Akata Formation and the Cretaceous shales which are the principle source rocks considered in this study. A moderate to high sedimentation (<200m/Ma) rate is seen from Late Cretaceous into the Tertiary as the delta begins to build basinward and increases from Late Miocene to the present day (Figure 6.10). Due to the deep burial of the source rocks and with the moderate to high heat flow values experienced over time, thermal maturation of these source rocks has been well achieved.

The Akata source rock is presently in its peak to wet gas generation window (1– 2.3% VRo) at its top and base while the Cretaceous shale is currently in the wet gas window with an average coalification value of 2.3% VR_o (Figures 6.9). The Akata shale started generating and expelling hydrocarbon in Late Oligocene to Early Miocene with the 100% transformation ratio (TR) reached in Mid-Miocene time (12.5 Ma) while the Cretaceous shales is noted to have attained 100% TR by Late Oligocene to Early Miocene (Figures 6.11A and B).

Hydrocarbon migration was simulated using the flow simulator of PetroMod^{TM} that calculates fluid flow for the different fluid phases.

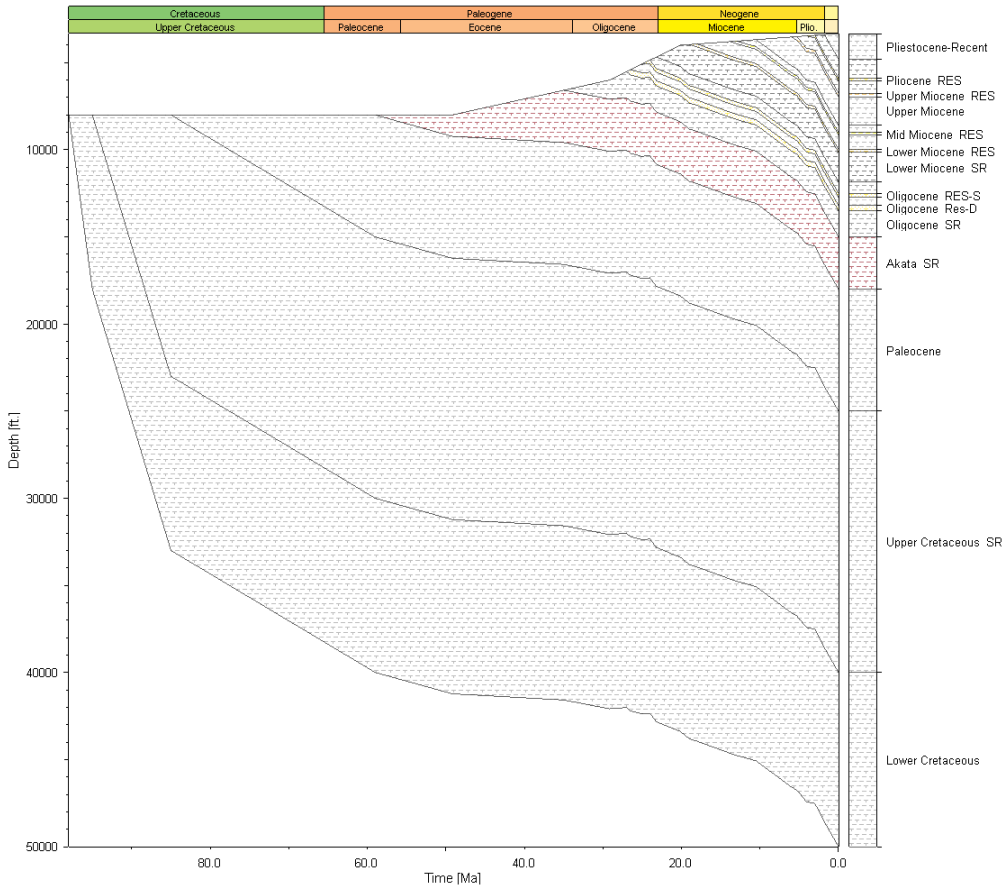

Figure 6.10: Burial history at well A1 location.

Calculated permeability is based on lithology mixing applied in PetroMod so also the capillary pressure (CP) with typical values for CP varying from 0.01 MPa in sandstones to 5MPa in tight shales. For oil migration the simulation process would require a saturation of at least 5% within an individual finite-element grid cell of the model, whereas gas does not require a critical saturation as long as other physical factors are in place (Schwarzer & Littke 2007).

A

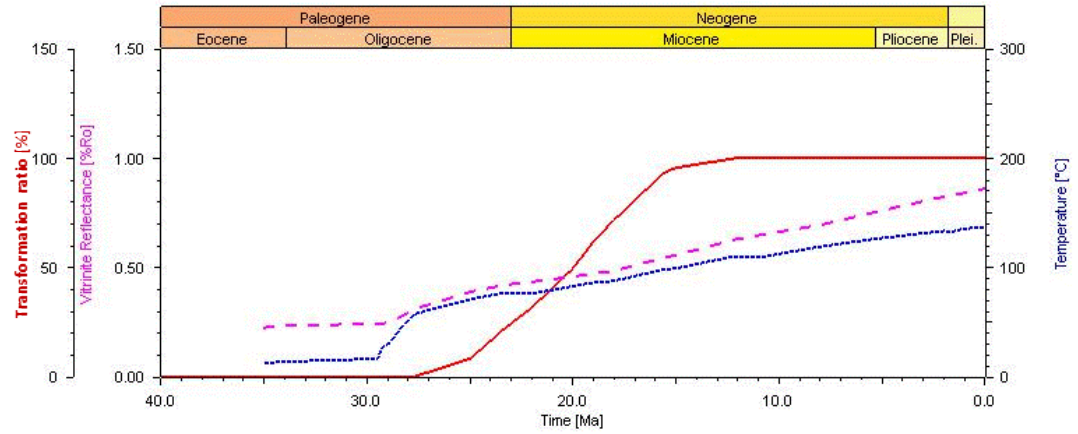

B

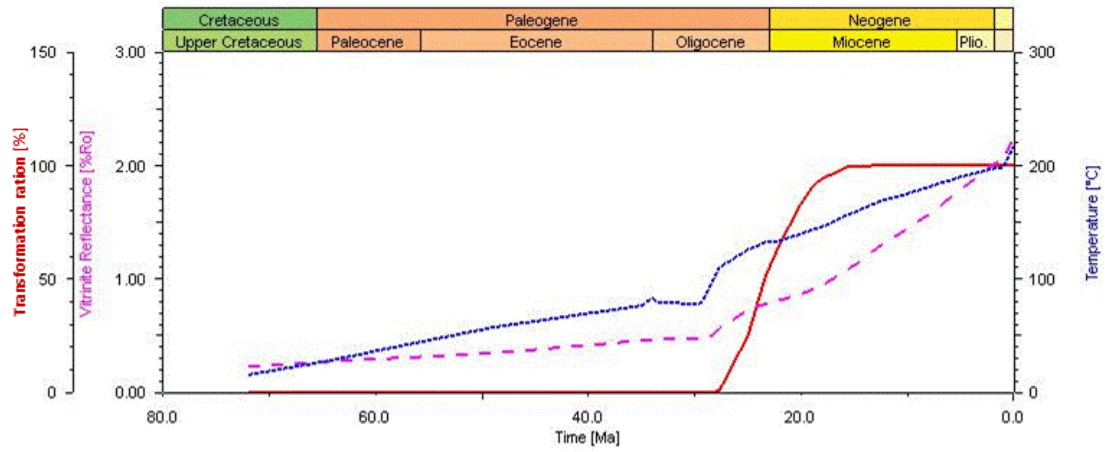

Figure 6.11: 1D extraction from 2D simulated history of Temperature (blue), maturity (pink) and transformation ratio (red) for Eocene Shales (A) and Cretaceous source rock (B) at well A1 location.

Migration modelling was done using the hybrid migration method that combines Darcy flow for rock of low permeability with buoyancy-controlled flow in high permeability layers. Vertical migration is observed to be via fault (Figure 6.12).

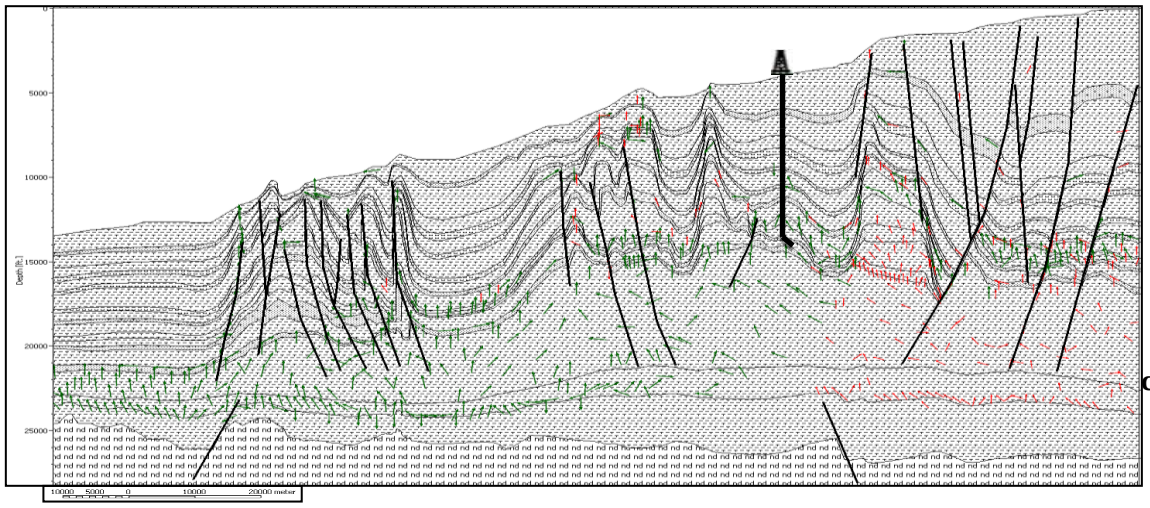

ce

Discussion

Implication on hydrocarbon prospectivity of the Oligocene reservoirs

The parameters that have been used to analyse the play potential of reservoir in the vicinity of well A1 are the TR ratio of the source rocks, the possible migration pathway from the active source rock(s) and hydrocarbon accumulations are described in their relation to the timing of trap and diagenesis. Structural traps in the form of growth faults associated with roll-over anticlines that are triggered by over pressured shales constitute the key trapping style in both Shelf and Slope regions of the Delta (Lehner and de Ruiter, 1977). The shale diapirs are thought to have been forming since at least Early Miocene (Whiteman, 1982) and have controlled sedimentation and fault development. In reconstructing the burial history in the study location, the time of onset of both the mud diapirs and growth fault that are responsible for trapping hydrocarbon was set to begin in the Miocene. In addition to structural traps, stratigraphic traps also form major traps in the slope region particular within the proven discoveries of the Miocene reservoirs in the study location occurring as turbidite channels or channel axis sands pinching out against clay rich levee walls (Chapin *et al*. 2002). Seismic studies show that the Oligocene submarine fan system appears to be encased in a mud rich system which is likely to serve as stratigraphic traps (Chudi et al., 2015: In prep.). Figures 6.11A and B show the transformation ratio of the two source rocks around the vicinity of the Well A-1 in the study location.

The TR ratio of convertible kerogen for the Akata Shale indicates to increase steadily from the onset of generation from Late Oligocene (25Ma) and attained 100%

transformation by Mid-Miocene (Figure 6.11A). The late Cretaceous source rocks on the other hand reached its generation potential in Early Miocene (Figure 6.11B). This implies that the Oligocene reservoir sands would have been ready to receive hydrocarbon from either the Eocene Akata shales or the Cretaceous source rocks. Buoyancy drive moved hydrocarbon up-dip through open faults and carrier beds to charge the Oligocene reservoirs from the Early Miocene (20Ma) to the Late Miocene (10Ma).

Four accumulations in the vicinity of the well A1are generated in the cross section basin simulation (Figure 6.13); one accumulation further south of the well within the Oligocene-shallow layer and three accumulations below the well TD in the Oligocene-deep layer which was not penetrated by well A1. Simulation results also indicate oil accumulations in shallower Miocene reservoirs that agree with present day proven oil reservoirs as seen by well A1. Over ninety percent of the accumulation in the Oligocene and also the shallow Miocene appear to be sourced from the Eocene Akata shales (Figure 6.13C). This is likely attributed to the excellent fault conduit that connects the Akata shales to both the Oligocene and Miocene reservoirs. The low volume of hydrocarbon in the reservoir from the Cretaceous source rocks could also be attributed to two factors; (1) traps were not emplaced to receive oil charge generated from the Cretaceous shales when these shales entered the oil window in the Early Oligocene (29 Ma), and (2) the Cretaceous source rocks are buried at great depth and separated from shallow potential traps by thick shales of the Akata Formation (Lehner & de Ruiter 1977), making it difficult for effective migration through the Akata shales.

A

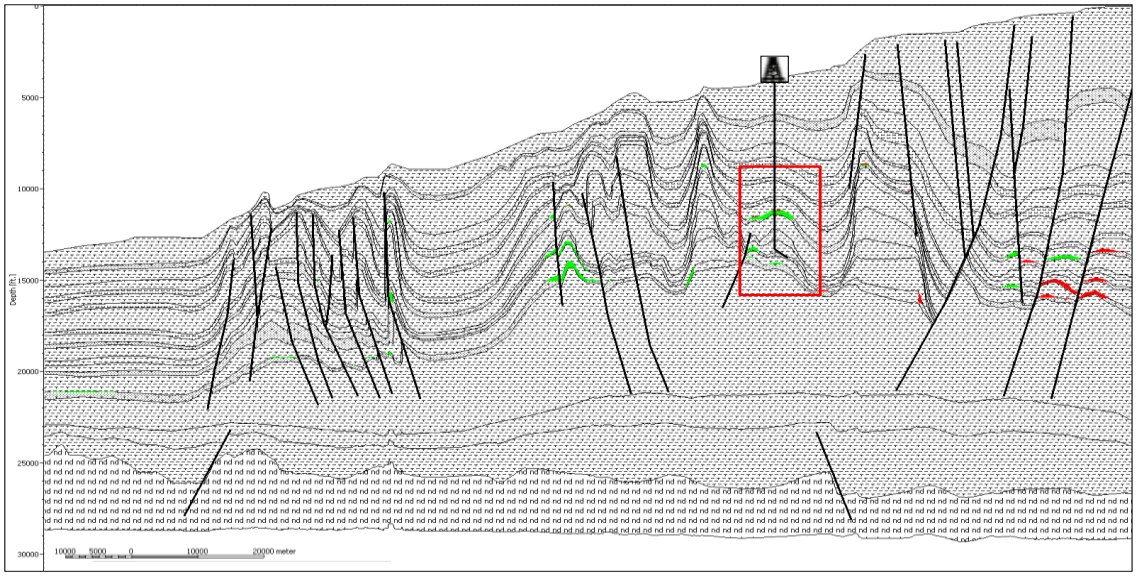
A
5000
10000
15000
20000
25000
30000
Depth (ft)
10000 5000 0 10000 20000 meter

B

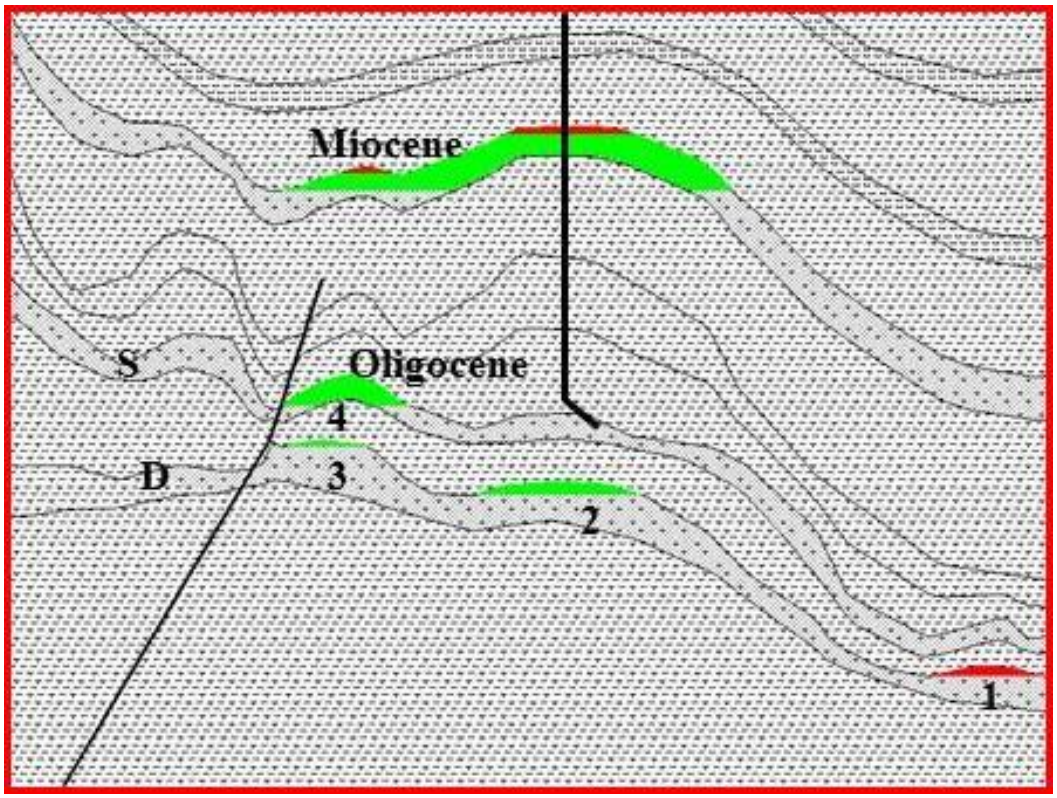
Miocene
S
Oligocene
4
D
3
2
1

C

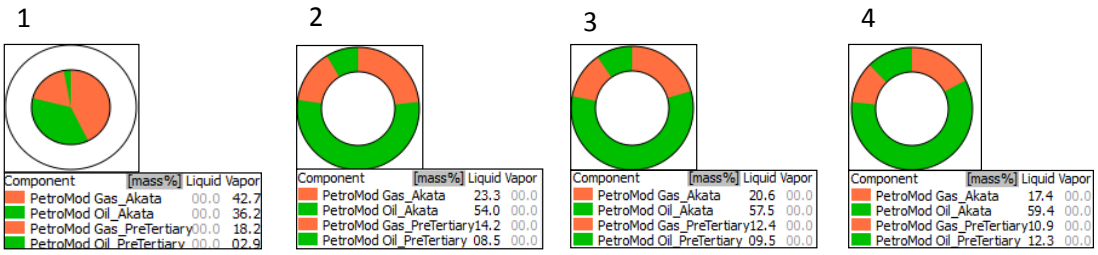

Figure 6.13: A = Predicted hydrocarbon accumulation in the vicinity of well A1 within the shallow (S) and deep (D) Oligocene reservoirs and Miocene accumulation. Depth in feet, distance in meters Calculated Miocene accumulation matches observed oil accumulation at Well A1. B = zoomed-in version across the study location clearly showing the Oligocene accumulation. C = charts that depicts the mass percentage of oil and gas in each of the four accumulations with significant percentage mass of components from the Tertiary Akata shale. The Cretaceous shale here is referred as 'PreTertiary'.

Timing of oil emplacement and quartz cementation

The concept that early hydrocarbon emplacement could influence the quality of reservoirs by halting or slowing down quartz precipitation thereby preserving intergranular porosity (Worden and Morad, 2000, Barclay and Worden, 2009, Taylor et al., 2010) is considered in this study. This is born from the observation of high porosity values at the structural crest of reservoirs and decreases towards the flank beyond the oil water contact (OWC). Where water is the wetting phase in a reservoir, as hydrocarbon saturation increases with a corresponding decrease in water saturation, the advective and diffusive transport of the chemical components (in the water) required for quartz precipitation would dramatically reduce; this would halt or at least reduce quartz precipitation.

In this study, the relative timing of quartz cementation and the time of charge in the Oligocene reservoir is considered. The result presented here could be calibrated against petrographic study of fluid inclusion to confirm both quartz homogenization temperature and the timing of charge. Both quartz cementation and hydrocarbon charge modelling were performed using the PetroMod^{TM} software. By applying the Walderhaug cementation model (see equation 6.1) in PetroMod^{TM}, documented in an earlier series of this study (Chudi et al., 2014; in prep.), cumulative quartz volume is

calculated based on the modelled thermal history of the basin, quartz grain size, volume of grain coating and the volumetric distribution of detrital mineral (see section on diagenetic modelling in Chudi et al., 2014; in prep). Figure 6.14 shows an overlay of predicted quartz cement volume across the 2D line for the Miocene and Oligocene reservoirs with quartz cement volume increasing from the Miocene reservoirs into the Oligocene potential reservoirs.

$$\frac{\delta\phi cc}{\delta t} = \frac{m}{\rho}\frac{(1-C)6f}{D}\frac{\phi}{\phi_o}Ae^{-Eo/RT} \qquad (6.1)$$

where C is the quartz grain coating factor, f is the quartz grain volume fraction, D is the average quartz grain size, A and E_o are respectively the frequency factor and activation energy of quartz precipitation. M represents the mol-mass and ρ the density of quartz (Walderhaug, 1994).

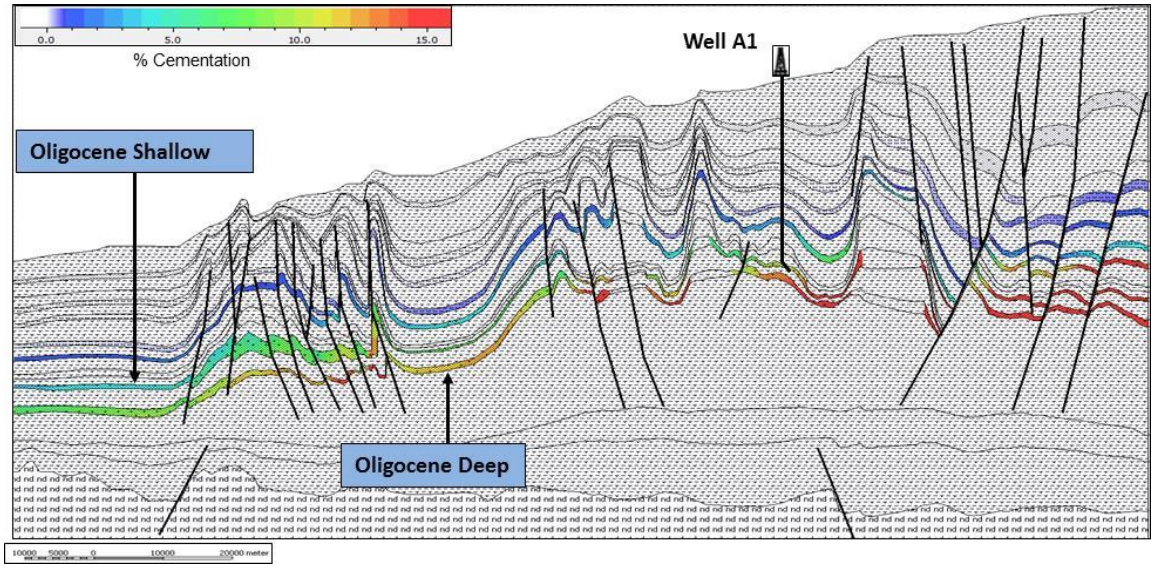

Figure 6.14: Overlay of predicted quartz volume across the 2D transect (adapted from Chudi et al., 2014: In prep.). The colour legend shows percentage of the porosity that becomes occupied by quartz cement.

Charge modelling in the potential reservoir is illustrated as change in hydrocarbon saturation through time based on the volume contribution of hydrocarbon generated from an active pod of source rock (see the above section on petroleum generation, expulsion and migration). Figures 6.15A and B illustrate the variation in hydrocarbon

saturation and the cumulative build-up of cementation through time (the time evolution of the basin in relation to hydrocarbon charge and cementation is further illustrated in Appendix D). The accumulations 1 to 4 in the vicinity of well A1 (see Figure 6.13) simulated in the Oligocene reservoirs have been considered. All accumulations have been charged at different times with accumulation 1 starting at about 20Ma, while the remaining accumulations were charged from 15Ma to 11Ma. Maximum hydrocarbon saturation, or irreducible water saturation were attained at 15.5Ma for accumulation 1 and 8Ma for accumulations 2, 3 and 4. The onset of quartz precipitation for all four accumulations is seen to be from about 20Ma synchronous with time of charge for accumulation 1 but earlier than the time of charge in accumulations 2 to 4. Although, the volume of quartz cement precipitated before peak/maximum hydrocarbon saturation is less than 5%. Therefore, considering that hydrocarbon emplacement can halt or slow down precipitation, it is likely that after peak hydrocarbon saturation was attained, the rate of quartz precipitation will have slowed down considerably and reservoir quality would have been preserved. Where well A1 encountered the Oligocene sands no hydrocarbon accumulation was modelled (see Figure 6.13) which agrees with observation from well logs. The Oligocene average porosity estimated from well log at the well location is about 20%. So if hydrocarbon emplacement has retarded the later quartz cementation, it is therefore likely that the porosity values of the Oligocene reservoirs at the accumulation locations 1-4 could be greater than 20%, most especially the reservoirs with accumulation 4 which is within the same stratigraphic layer penetrated by well A1.

A

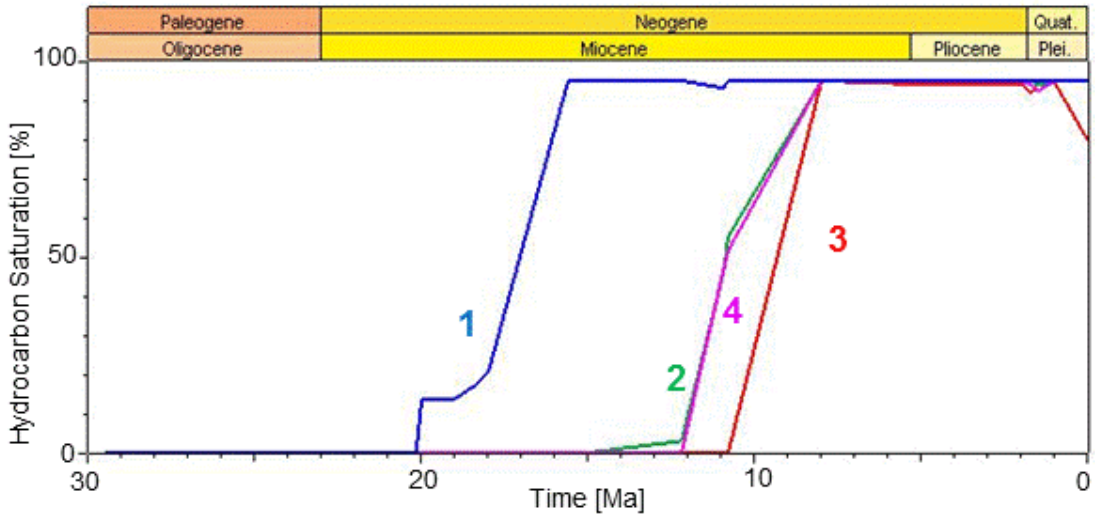

B

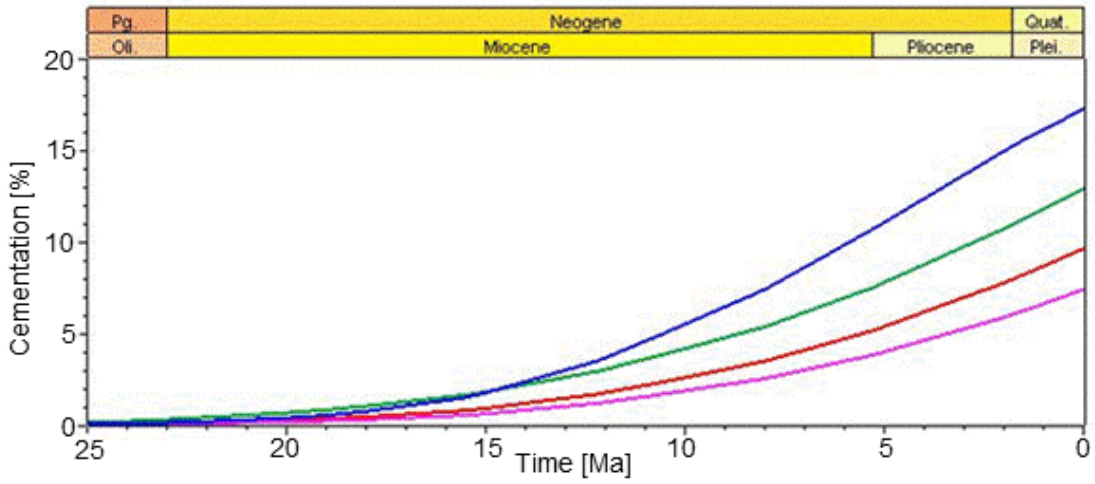

Figure 6.15: A = Hydrocarbon saturation through time for four accumulations in the Oligocene. Peak hydrocarbon saturation for accumulation 1 at 16Ma predates peak hydrocarbon saturation for accumulations 2-4 at 8Ma. B = cumulative increase in quartz cement through time. Each accumulation has been assigned distinct colour codes similar in both plots.

Conclusion

Of the two source rocks considered in this study; the Eocene Akata shales and the Cretaceous mud, the Akata shales generated more than 90% of the hydrocarbon trapped in both the Miocene and the target potential Oligocene reservoirs. The Akata shale has been simulated to have entered the oil window in Mid-Miocene (15Ma) and has achieved 100% TR of its generative potential. This implies that the Oligocene sands

were already deposited and trapping structures were formed (structural or stratigraphic traps) to receive early hydrocarbon charge from the Eocene Akata shales. The deeper Cretaceous source rocks are simulated to have been spent by Early Miocene (23Ma) and with poor faults connection to the shallower Oligocene reservoir it has contributed less than 3% of the hydrocarbon trapped in the shallow structures.

The Early Miocene (22Ma) quartz cementation proceeds the time of hydrocarbon charge, from 20Ma in the Oligocene aged sediments, present a reservoir quality risk. However, the basin model simulates peak hydrocarbon saturation being reached when less than 5% of the pore space in all 4 simulated accumulations were quartz cemented. It is quite possible that quartz precipitation would have been significantly retarded from the time of peak oil charge, thereby preserving a significant fraction of the porosity in the potential Oligocene reservoirs.

CHAPTER 7

RESERVOIR QUALITY PREDICTION

This chapter comprises Paper 3 of the thesis: “Predicting Oligocene Reservoir Potential in the Deep-Water Western Niger Delta: An integrated Basin Modelling and Diagenetic Study”.

It is based on an integrated cementation modelling, petrographic and petrophysical analysis of suites of data from the study area in the western Niger Delta. The paper has been submitted to the Geological Society Special Publication and it is currently in the first review stage.

It is reprinted here in full, although figure numbers have been replaced by chapter figure numbers (e.g. Figure 1 becomes Figure 7.1), and the references are included in the main reference list at the end of the thesis.

There is necessarily some overlap and repetition with other parts of the thesis in presenting the ‘introduction’ and ‘geological setting’. The discussion is developed further in Chapter 8.

The authorship includes my two supervisors, but the work and principal findings are entirely my own.

7.1 Paper 3

Reservoir quality prediction via integrated diagenesis, advanced petrophysics and basin modelling: Deepwater Oligocene sandstone Western Niger Delta

O.K. Chudi, Helen Lewis, D.A.V. Stow, J.O. Buckman*
Institute of Petroleum Engineering, Heriot-Watt University, EH14 4AS, Edinburgh, UK
Corresponding author-Obinna.chudi@pet.hw.ac.uk,

This paper was submitted to Geological Society Special Publications

Abstract

Hydrocarbon exploration and exploitation in the Niger Delta has mainly been focussed on the onshore, deltaic and deep-water Miocene succession. The Miocene to Recent deep-water sands above 3600m in the study area located in the basin slope show very good reservoir quality with porosities as high as 35% and permeability in the Darcy range. This study centres on predicting the petrophysical properties of the Oligocene sandstones located below 3800m, particularly the onset and amount of quartz cementation, and aims to determine their reservoir potential in comparison to the well-known Miocene reservoirs. Results from cementation modelling reveal that the Oligocene reservoirs have been exposed to conditions favourable for quartz precipitation with predictions of less than 14% quartz cement volume. This outcome is in agreement with both elemental analysis from petrophysical studies and petrographic observation of thin-sections. Only the Lower Miocene reservoirs buried at 3445m have less than 5% quartz overgrowth noticeable from petrographic studies. Based on this study the Oligocene sediments are likely to have their reservoir quality compromised by the presence of quartz overgrowths. However, it is likely that the volume of cement is not sufficient to prevent the Oligocene reservoirs from being a viable reservoir play Offshore Niger Delta.

Introduction

The Miocene clastic succession of the prolific Niger Delta province has since the 50's been the major target for reservoir play that is responsible for accommodating most of the discoveries both onshore and the offshore part of the Delta (Doust and Omatsola, 1990, Saugy and Eyer, 2003, Reijers, 2011). This has been attributed to the excellent porosities and permeabilities that characterise this sequence of poorly consolidated

sands (Weber, 1971). Porosities of up to 35% and permeability of more than 3000mD have been reported from well logs and cores across producing fields in the delta. This therefore suggests that the precipitation of authigenic minerals has not significantly degraded the reservoir quality of the Miocene interval, considering that the distribution of quartz cement can control sandstone reservoir quality by occluding pore space and pore throats–two major factors that control volume and transmissibility of hydrocarbon in reservoirs (Barclay and Worden, 2009).

As the quest for hydrocarbon reserves increases, exploration and production is gradually moving from shallow easily identifiable reservoirs of the Miocene to deeper and hotter plays that could be exposed to physio–chemical condition suitable for quartz precipitation. The aim of this work is to estimate the degree of quartz cementation of unexplored deeply buried Oligocene deep-water clastic sediments of the Niger Delta through an integration and cross-comparison of cementation modelling, petrographic analysis and petrophysical multi–mineral elemental analysis. The integration of these methods in the study of the deep-water Oligocene sediments is seen to be novel to the Niger Delta sedimentary basin. Although each approach is distinct in its workflow, they however, tend to show similar results relevant for predicting reservoir quality and the corresponding controlling factors.

Generally reservoir rock quality is controlled by variables such as the grain size, initial depositional porosity, mechanical compaction, pressure dissolution, mineralogy and volume of pore filling cement (Worden and Morad, 2000). These factors have particularly influenced the strategy and the technique adopted for petrophysical evaluation across fields within the delta system. The interplay of these factors under conditions of increased effective stress, temperature and burial, results in variable outcomes with respect to reservoir porosity and permeability (Taylor et al., 2010).

The low volume of quartz cement (less than 5%) in the Lower Miocene section of the study area located offshore Niger Delta within a water depth of 800-1300 m can be attributed to the shallow burial depth of the sediments within a temperature window below that required for significant quartz cementation. The regional geothermal gradient of the Delta ranges from 1.3 to 1.8^{O} C/100m in the centre of the basin and increases up-dip and northward to about 2.7 to 5.5^{O} C/100m (Nwachukwu, 1976, Doust and

Omatsola, 1990). These geothermal gradients puts the Miocene section particularly the Mid-Miocene to Recent succession at the study location buried to a temperature window of less than 70^{O} C and the Oligocene buried at depths greater than 4000m with temperatures exceeding 70^{O} C. Several reports have been published that suggests the temperature of quartz crystallization to be between 70-135^{O} C ((Walderhaug, 1994, Walderhaug, 2000, Worden and Morad, 2000, Taylor et al., 2010). For this study 70^{O} C has been considered to be the most likely temperature for the onset of quartz precipitation.

Geological Setting

Province

The hydrocarbon prolific Niger Delta has been the centre of attraction for hydrocarbon exploration and production in the continental margin of West Africa for over four decades (Haack et al., 2000) and this is one of the singular reason why it has been extensively studied (Short & Stauble 1967, Weber 1971, Whiteman 1982, Ejedawe et al., 1984, Damuth 1994, Haack et al., 2000). The delta is situated in the Gulf of Guinea and covers an area of approximately 140,000km^2 with a maximum clastic sediment thickness of about 12km at the basin centre (Damuth 1994).

The Niger Delta began to evolve in Palaeocene and Eocene times as sediments prograded over the subsiding continental–oceanic lithospheric transition zone. By the Oligocene the delta had fully spread over cooling oceanic crust, hence increasing sediment load on a cooling and subsiding oceanic basement, with sediment load complementing subsidence due to lithospheric cooling. From the Eocene to present day, the delta has significantly prograded in a south–west direction creating major depositional belts or depobelts that represent the most active portion of the delta at every stage of development. Sediments at this time were sourced from the Benue–Niger drainage system that fed mostly the north-western part of the delta. While the Cross River system which supplied sediments mostly to the eastern delta areas. The present day Niger Delta complex takes the form of a constructive arcuate delta, with mud diapirism playing a major role in controlling progradation and sedimentation in the Delta complex (Whiteman 1982).

Lithology

The Tertiary Niger Delta comprises three sedimentary environments (Figure 7.1); continental, transitional and marine environment. The Continental environment comprises of sediments of the fluvial and upper delta plain with predominantly sandy lithofacies with no faunal assemblages. The sediments are poorly sorted, coarse grained, granular and pebbly to very fine grained. These sands have been described as the Benin Formation that occurs onshore in the north and beyond the present coastline (Short & Stauble 1967). Based on the age of shales underlying the sandy sequence, an Oligocene to Recent age has been ascribed to the Benin Formation. The poor quality nature of the sands is responsible for its inability to be a hydrocarbon reservoir.

Underlying the Benin Formation is the paralic sequence of the transitional environment comprising of sandstone and shale couplets defined as the Agbada Formation. The shale units are seen to be more prominent with depth becoming progressively thicker than the sandstone units; this therefore illustrates the seaward advance of the Delta through time (Whiteman , 1982). The sandstone units constitute the major reservoir units of the Niger Delta Basin, having excellent reservoir quality, with reservoir to source rock communication established through growth faults. The Agbada Formation extends all through the Niger Delta with both lower delta plain and marine sediment of the continental shelf depositional environments. The interplay between subsidence and sediment supply and the relative change in sea level expressed as transgression and regression cycles are responsible of the alternating sandstones and shale sequence (Doust & Omatsola 1990). The age of the Agbada Formation ranges from Eocene to possibly Pleistocene.

The pelagic mud of the Akata Formation makes up the deepest part of the Tertiary sedimentary sequence. The marine shales of this sequence range from Paleocene to Holocene in age. Regional studies and experimental analysis places the Akata Formation as the active source rock of the Tertiary Niger delta (Evamy et al., 1978, Lambert-Aikhionbare & Ibe 1984, Tuttle et al., 1999). Although the upper part of the sequence is more sandy and believed to be turbiditic in origin with reservoir potential for the offshore part of the Niger Delta. The Akata shales are continuous and possibly extend across the whole delta area.

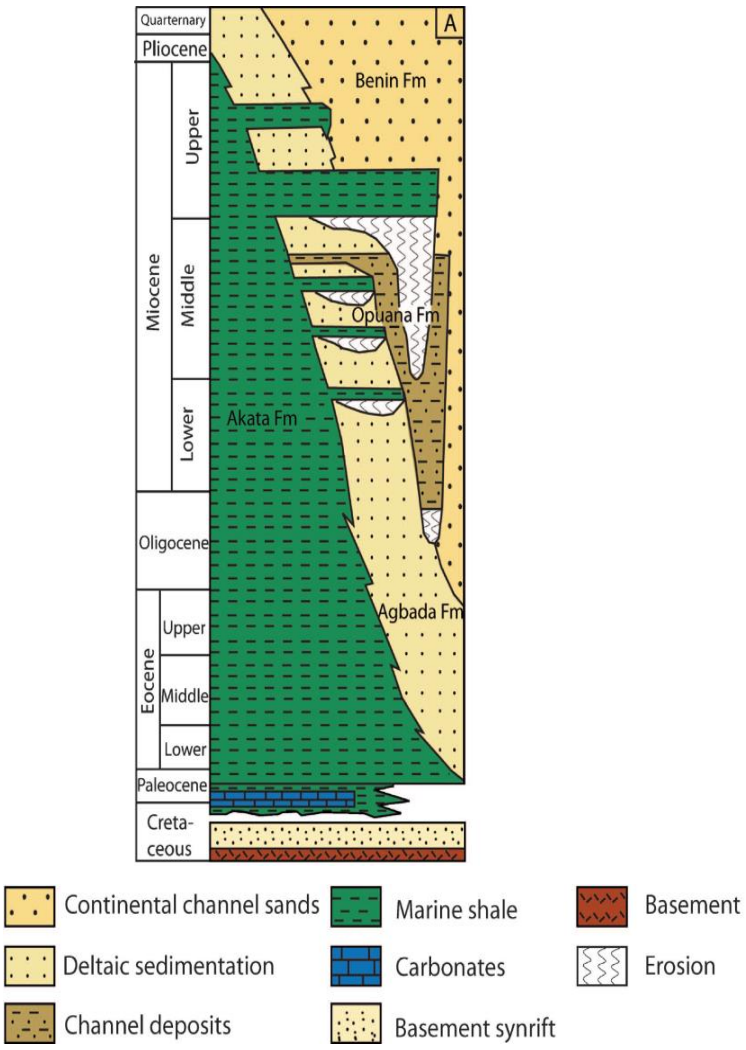

Figure 7.1: Regional stratigraphy of the Niger Delta, from (after Corredor *et al.* 2005).

Tectonics and Structure

The end of rifting in the Late Cretaceous gave way to gravity tectonism being the primary deformational process affecting Delta development. Due to burial of fine grained, low permeability hence poorly compacted, over pressured delta slope muds beneath the rapidly prograding delta system, mud diapirs developed in the fine grained sediments (Whiteman, 1982). Diapirism began in the Miocene times and is still taking place, recognised around the delta front and extending further into the deep-water area. The growth of the diapirs enabled the development of growth fault features from Miocene times (Whiteman, 1982, Damuth, 1994). The fault is seen to offset the part of the paralic formation and flatten onto the detachment layer at the top of the pelagic mud. The overall structural trend is oriented in a northwest-southeast direction (Haack et al.,

2000). Controlled by gravity driven tectonics, three structural provinces generally defines the Delta (Figure 7.2). Updip from the Shelf to Onshore part of the basin, extensional features are prevalent, represented by listric growth faults. The upper and middle slope is dominated by mud diapirs and folds. This zone is known as the translational zone. The lower slope is a zone of compressional features triggered by downslope movement of sediment due to gravity gliding with liner toe thrust feature forming fold and thrust belts (Bilotti and Shaw 2005, Corredor et al., 2005, Deptuck et al., 2007).

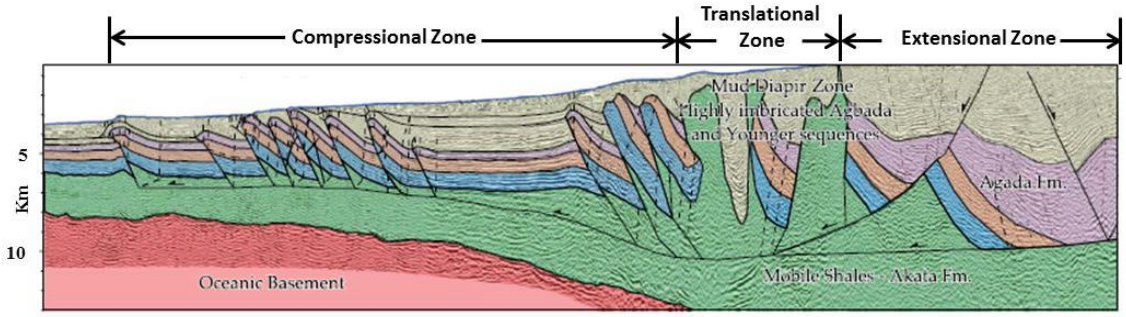

Figure 7.2: Regional cross section showing the three structural provinces of the Niger Delta (modified from Corridor et al. 2005).

The study area is located in the translational province of the mid slope setting (Figure 7.3). The reservoir package is Miocene channel sands of the Agbada Formation. The petrophysical evaluation presented here indicates that the reservoir is of good quality with porosities of greater than 30% and permeability in the darcy range. Of all the over 30 wells drilled in the study area only one well penetrated the top of the Oligocene unit of the Agbada Formation, which is the primary interval that has been studied.

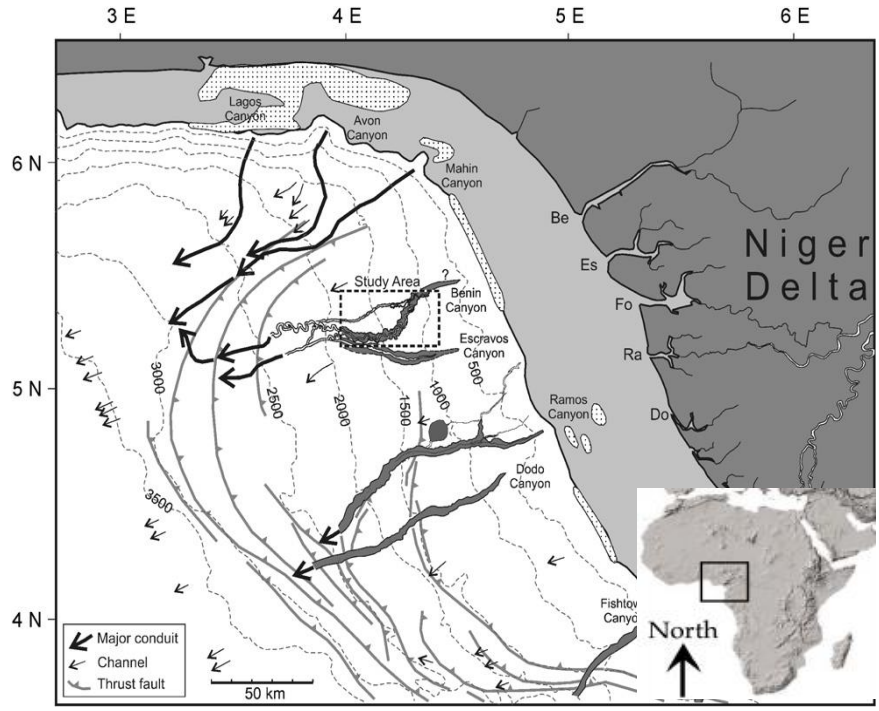

Figure 7.3: Regional location map showing the western Niger Delta and study area. Adapted from (Deptuck et al. 2007)

Methods

Petrography

Petrographic analysis was conducted on 17 samples acquired across four wells in the study area. The cored samples were taken across the Miocene interval from Middle Miocene at a depth of 2470m and lower Miocene at 3450m. Samples taken from depths shallower than 3000m were unconsolidated sands. The samples inspected were made as thin-sections and polished blocks.

Techniques used included optical microscope and Scanning Electron Microscopy (SEM) using Back Scattered Electron imaging (BSE) and Cathodoluminescence (CL) analysis. Due to the poorly consolidated nature of most the samples (excluding the Lower Miocene samples), they were not suited for polished thin-sections; therefore thin-sections with cover slips were made. The samples were dried at 38^{O}C and bulk impregnated under vacuum with epoxy resin to stabilise the samples. Ultraviolet glue was further applied to mount cover slips. For the purpose of SEM studies, samples were also made into polished blocks again drying at 38^{O}C and placed in a 25/30mm diameter

mould. The granular samples were filled with epoxy resin, mixed by stirring and placed under vacuum to remove air bubbles.

Optical microscopy was used for mineralogical identification and where optical identification of overgrowths was difficult, SEM was used. Cathodoluminescence (CL) analyses were carried out on the SEM with a Centaurus CL detector. BSE and CL combined analysis was based on the method outlined by (Evans et al., 1994) which involves the analysis of pairs of BSE and CL images from polished block samples. A set of 13 samples were selected for analysis. Cathodoluminescence is particularly useful in distinguishing detrital quartz grains from syntaxial quartz overgrowths. SEM analysis was done over the Middle and Lower Miocene intervals to investigate the likely presence of microcrystalline quartz or chlorite rims, as they are likely to impede the nucleation of quartz overgrowth (Bloch et al., 2002, Marchand et al., 2002, Taylor et al., 2010).

Petrophysical Analysis

Wireline log data from four wells within the study location were analysed to characterise the porosity and permeability of the reservoir zones penetrated. Of the four wells studied only one well penetrated the Oligocene interval. The density log was used to calculate porosity and these values were calibrated against core porosity where it was available. Permeability was estimated using the neural network technique, where sets of input logs (Gamma ray, sonic, density and neutron logs) were trained to recognise the core derived, stress corrected air permeability, acquired from routine core analysis (Sonde et al., 2011).

A multi-mineral model based on petrophysical elemental analysis (ELAN) of open-hole logs was used to compute the volume of mineralogical components within the intervals of interest. ELAN uses log curves and the response parameters of the tools to compute volumetric constituents of formation minerals and fluid. This method derives the relative quantities, or relative volumes, of the mineral components that would most probably produce the set of measurements recorded by the logging instruments. So there is a three way relationship among tools (T), response parameters (R) and formation component volume (V), as depicted in Figure 7.4.

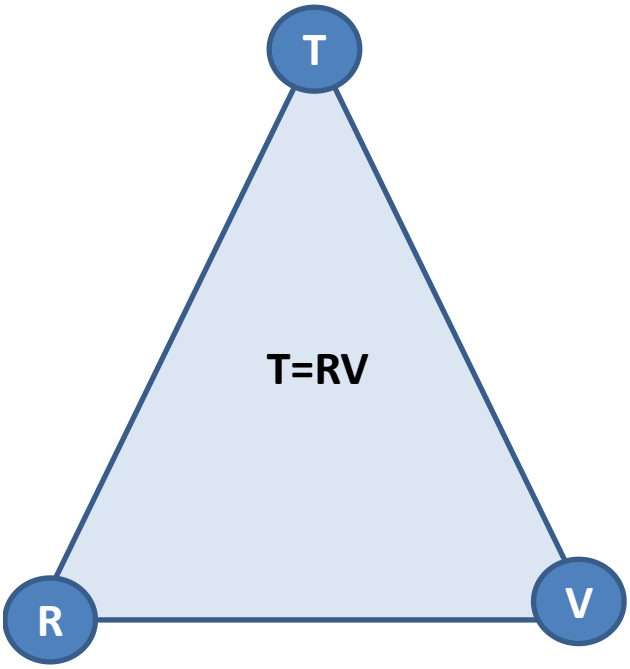

Figure 7.4: Schematic illustration of ELAN. T represents the tool vector in this case the input log data (gamma ray, resistivity, neutron, density, and calculated porosity logs), R is the response matrix, that is, a pre-defined value for the reading each tool would give for 100% of each formation component. R values were determined based on the known mineralogical responses to the physics of the different tools (Reeder et al. 2013) as defined using the Schlumberger Techlog software package. V is the volume vector–the volume of the formation components.

Given the data represented by any two corners of the triangle the third can be determined. In this study, T and R are used to compute V. For quality control, forward modelling of R and V are used to reconstruct T–the input logs. The reconstructed logs are compared against the input data to determine the quality of the volume results. Four principal minerals (quartz, feldspar, zircon and kaolinite) were modelled in ELAN based on their abundances determined in the petrographic study.

Basin Modelling

Basin modelling is a technique that has been developed since the early 1980's to study the burial and thermal history of a basin, particularly in relation to hydrocarbon generation, expulsion, migration, accumulation and preservation (Welte and Yalcin, 1988b, Wygrala, 1988, Talçin, 1991, Hermanrud, 1993, Underdown and Redfern, 2008). This technique has been adopted to study diagenetic evolution and its impact on

reservoir quality, particularly porosity (Sombra and Chang, 1997, Walderhaug, 2000). Diagenetic reactions are related to burial history with introduction of fluid, stress and temperature changes (Siever, 1983), which ultimately control reaction rates like the transformation of organic matter to hydrocarbon and quartz precipitation from silica rich fluid. Before the 80's Arthy's compaction models and similar models are used to relate sediment compaction to porosity (Lundegard, 1992, Paxton et al., 2002), although these are not able to accommodate the effect of porosity loss due to cementation. Other methods that were later adopted, related models of basin history and paleogeotherms from heat flow model to temperatures of diagenetic reactions (Siever 1983); inferring temperatures from petrographic study of fluid inclusion;–particularly chemical composition and isotopic signatures (Taylor, 1950, Marchand et al., 2002, Wilkinson et al., 2004) and utilizing time-depth index (TDI) to quantify empirically the influence of burial history on the evolution of sandstone porosity (Sombra and Chang 1997).

In this paper, forward models are constructed by taking into account quantitative evaluations of diagenetic processes in order to make reliable diagenetic predictions. Of importance is the understanding of the type of diagenetic reactions prevalent in the study area, where they take place and when these reactions occur during the history of the basin.

Results

Core Study

The Miocene reservoirs in the study area have been cored and are seen to be typically loosely consolidated sands that are moderately sorted and display a dominant grain size of medium to fine, although coarser grain sizes exist. The sands have been classed as quartz arenite (McBride, 1963) as they are largely composed of quartz with less than 15% feldspar. The excellent quality of the reservoir sands is largely attributed to the unconsolidated nature of the sands with little or no cementation present, producing high porosities.

A total of 15.1m of cores was studied; 12m across the Mid-Miocene and about 3.1m across the Lower Miocene sequence. The Mid-Miocene reservoir facies comprise of massive, unconsolidated sands that are typical of the Bouma Ta facies with minor

normal grading seen in the sands. High density turbidity current flow is the most likely depositional mechanism. Two facies have been noted in the Lower Miocene section studied; (1) light gray, very fine consolidated massive sands that are moderately to well sorted, representing deposition under high density turbidity current flow, and (2) Interlaminated very fine sands and silts characterised by millimetre scale parallel and convolute lamination. Some dark laminations are also noted and are most likely mud or organic material. These facies represents the Tcd sequence of dilute turbidity current deposition. Figure 7.5 is a schematic of the sedimentological log of the core section studied with core photographs representing sections of the facies where some of the samples for petrographic studies were taken.

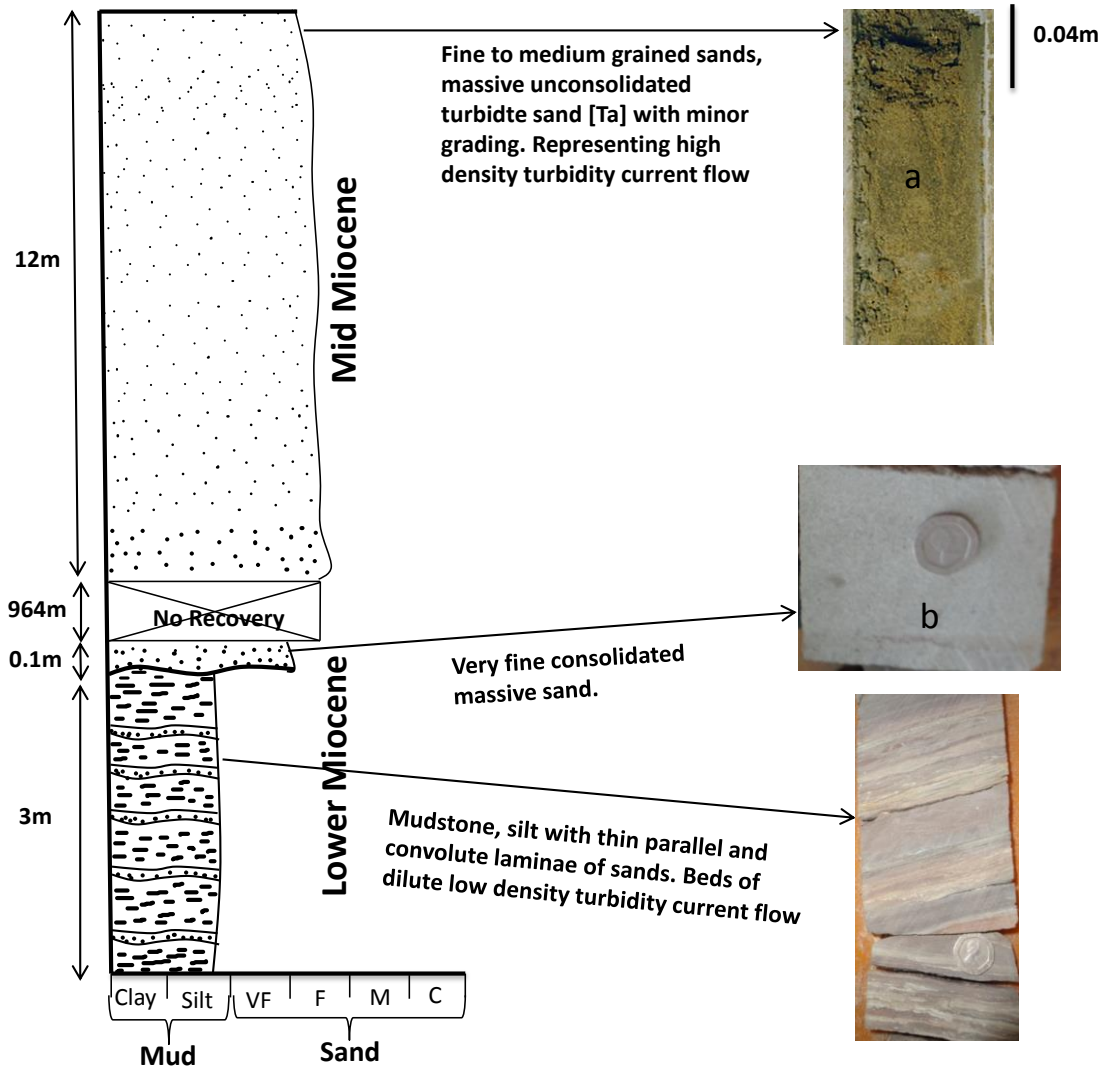

Figure 7.5: Sedimentological log of core from well A1 across the Mid-Miocene and Lower Miocene sections. Core photos represent typical section of the lithology described; some samples for petrographic study were taken from 'a' and 'b' on core photos.

Petrographic Analysis

Detrital Mineralogy

The Miocene samples from three wells examined by optical microscopy are dominantly quartz, comprising of up to 85% monocystalline grains, with minor polycrystalline quartz, 10% feldspar and 0-5% lithic fragments of possible igneous and metamorphic origin (Figure 7.6). Muscovite and heavy minerals (likely sphene, pyrite or zircon) occur in trace amounts. Heavy minerals are easily recognisable from the scanning electron microscopy (SEM) micrographs as highly luminescent grains, as depicted in Figs 7.7A-D. Grain-size ranges between fine and medium sand (125 - 500 microns), with sorting from poor to well sorted and grain roundness from subangular to angular.

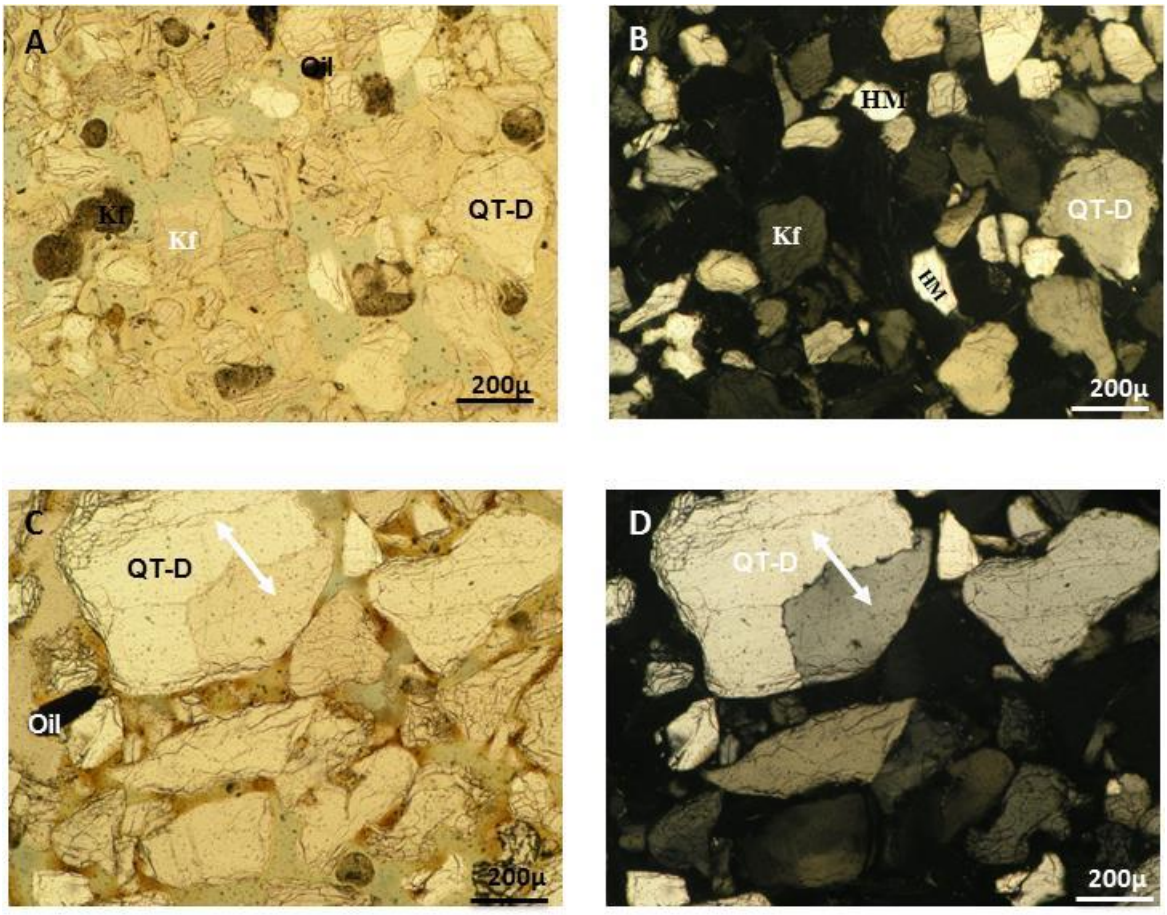

Figure 7.6: Photomicrographs in both plane polar and cross polar images of Mid-Miocene (A, B) and Lower Miocene reservoirs (C, D): Detrital quartz (QT-D), K-feldspar (Kf), arrow across a polycrystalline quartz grain

Diagenetic Mineralogy

Quartz Cement: Quartz cements are rarely present in observed thin-sections most especially in the Mid-Miocene samples located at depths of less than 3000m. However, thin-sections of samples retrieved from 3450m, from the Lower Miocene reservoirs show evidence of quartz overgrowths occurring as grain riming cement. In some cases they occur as euhedral overgrowths protruding into primary pores. The overgrowths range in size from individual small euhedral crystal growths of 3-20µ to grain rimming cements of less than 30µ thick. Overgrowths are not widespread but are patchily developed around few of the quartz grains.The cathodoluminescence (CL) and Back Scattered Electron (BSE) images allowed distinction between authigenic and detrital quartz. Authigenic quartz rims are typically less luminescent than their detrital are (Figure 7.7D). The Scanning Electron Microscopy (SEM) image reveals quartz overgrowths with well-defined crystal faces over the surface of detrital substrate (Figure 7.7E) .The BSE studies of the same sample showed no distinction as both detrital and autigenic quartz display a light grey colour (Figure 7.7C).

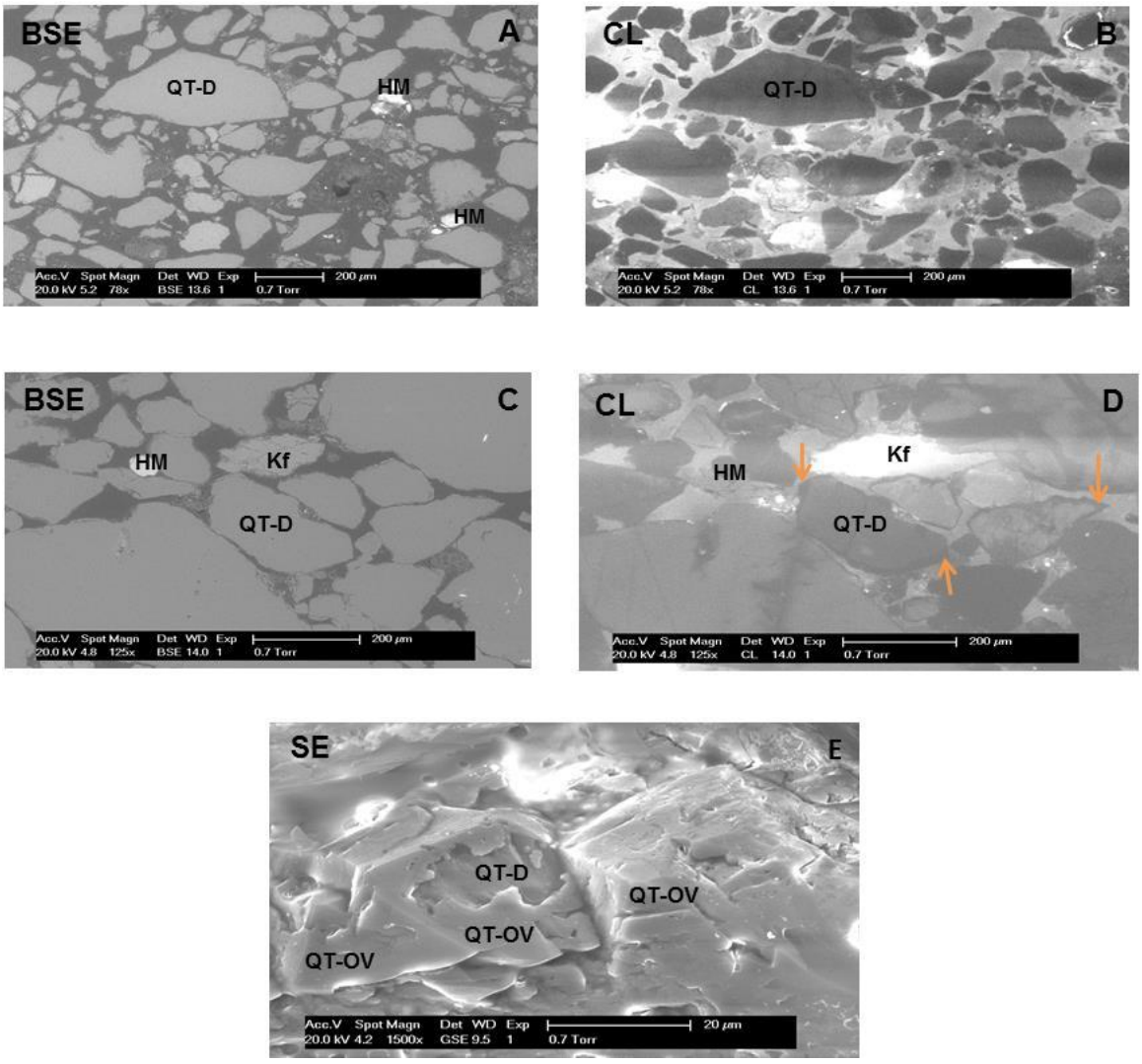

Figure 7.7: Upper Miocene polished block samples with no quartz cement as seen from both BSE and CL plates (A and B), while overgrowth (indicated by amber coloured arrow) is present in Lower Miocene (C, D and E). QT-D = detrital quartz, QT-OV = quartz overgrowth, Kf = potassium feldspar, HM = heavy mineral.

Grain Coating: The SEM analysis of the samples does not reveal the presence of any grain coating minerals like microcrystalline quartz or chlorite coatings, around detrital grains, that have the potential of preventing quartz overgrowth (such as in Taylor et al., 2010). The upper Miocene samples are seen to be coated with thick 'dead'/bituminous oil (Figure 7.8). The presence of this oil is indicative of likely biodedegradation due to exposure of the Mid-Miocene reservoir to low temperatures of less than 60^{O}C (Peters et al., 1996).

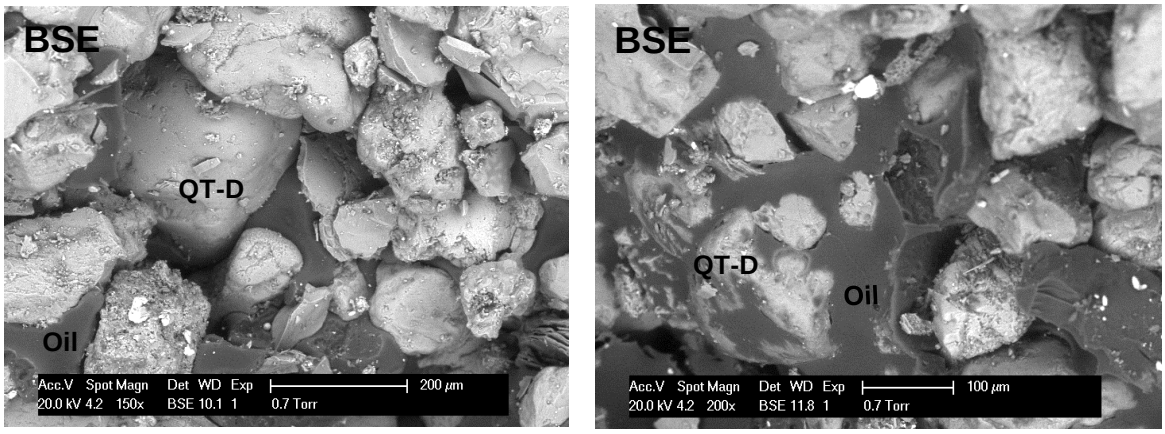

Figure 7.8: SEM picture of Upper Miocene samples showing quartz grains coated by oil.

Clay Mineralogy: SEM examination revealed the presence of kaolinite-type clay in both the Upper Miocene and the Lower Miocene successions occurring as stacked pseudohexagonal crystals of euhedral booklets (Figure 7.9A and B). For the Lower Miocene succession, kaolinite sits between some grain to grain surfaces filling primary porosities within the sandstone matrix, suggesting that the kaolinite clay developed before mechanical compaction started (Gier et al., 2008). Figure 7.9C illustrates this feature.

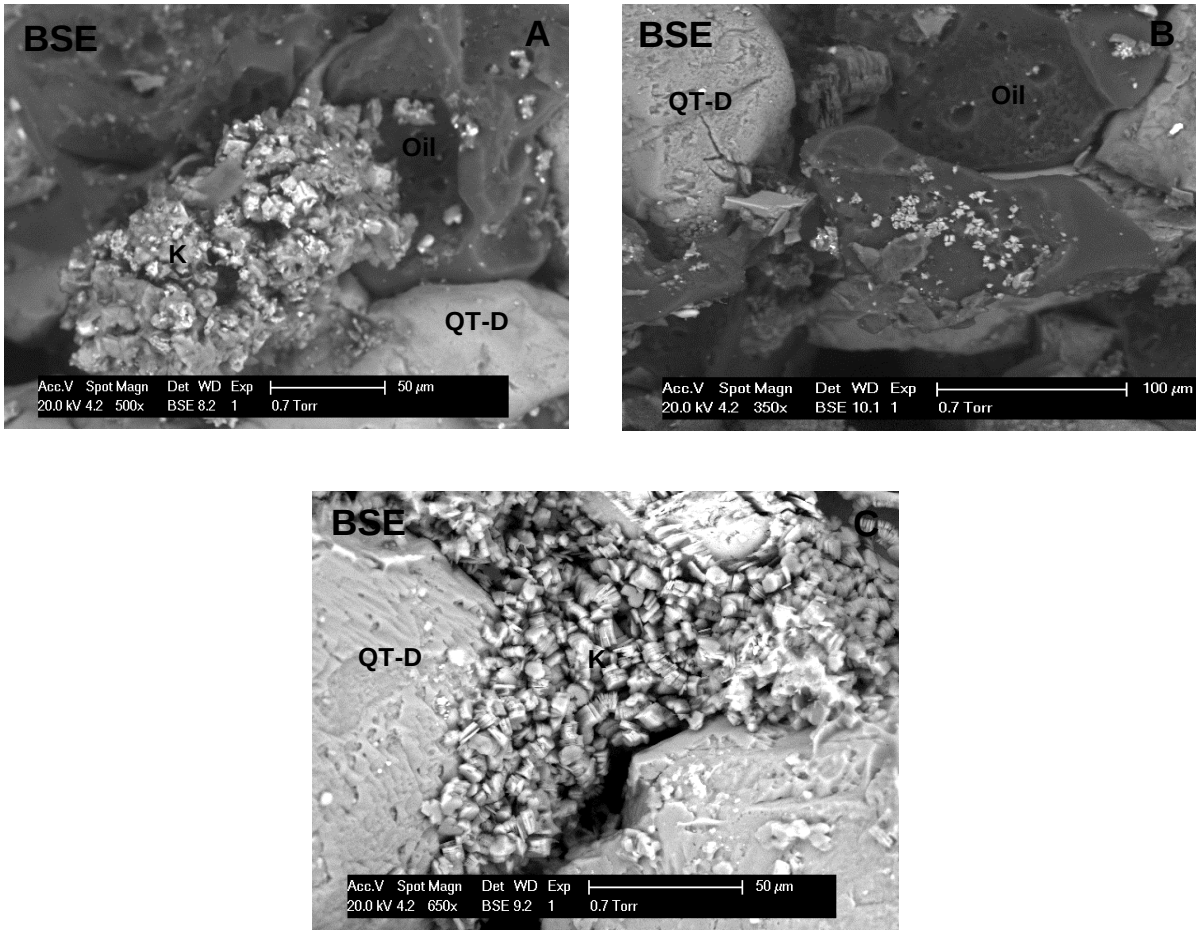

Figure 7.9: SEM images of Upper Miocene and Lower Miocene Sandstone. A and B images show autigenic kaolinite surrounded by oil coats on detrital quartz grains. C = pore filling kaolinite crystals. QT-D = detrital quartz, QT-OV = quartz overgrowth, K = Kaolinite.

Petrophysics

The estimated porosity from wire line log decreases with depth as seen from the porosity depth plot of 4 wells in the study location (Figure 7.10). The Figure also reveals that only the estimated porosities from Well A1 (represented by triangle) which is the only well that encountered the Oligocene reservoirs have average porosity values of 20 % .The porosity for the Miocene ranges from 21- 37% across all the wells, (see Figure 7.11).

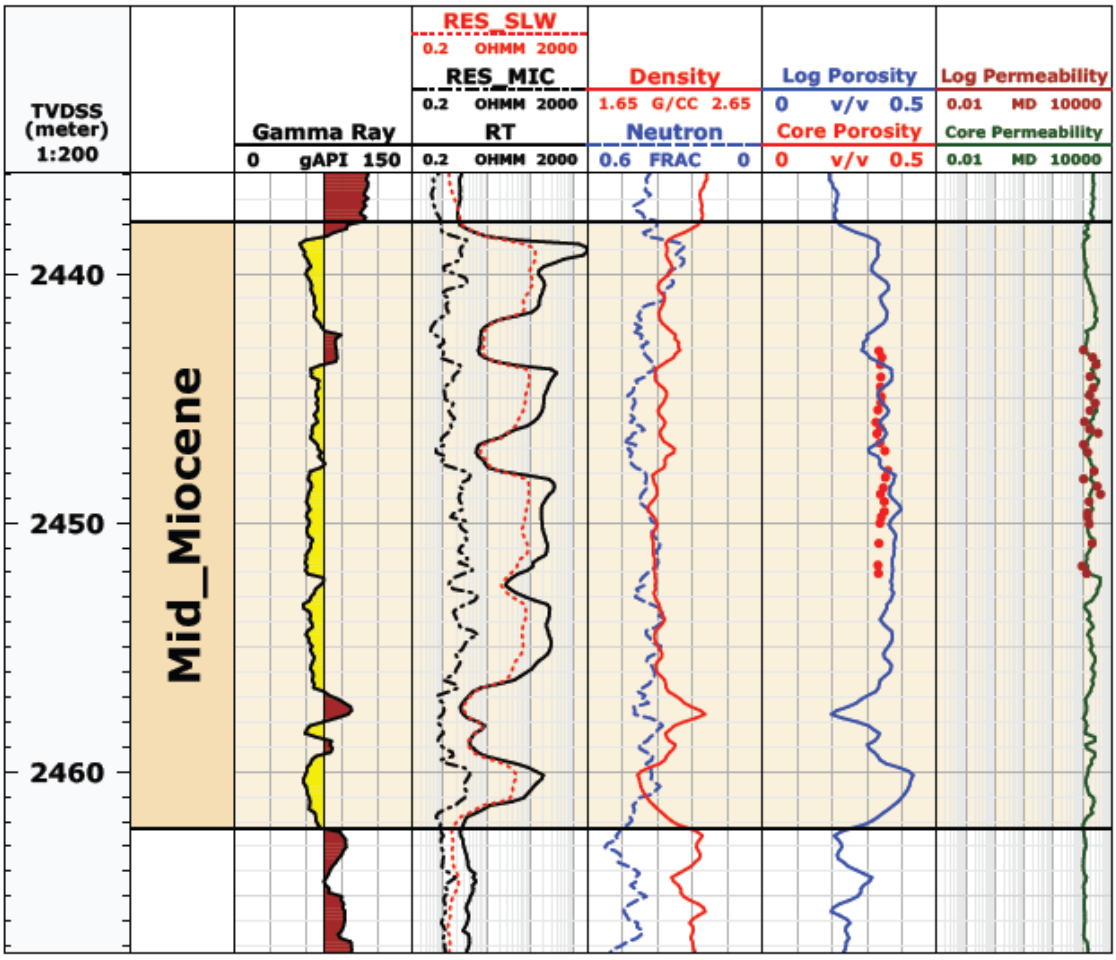

Figure 7.10: Petrophysical data log showing evaluated porosity calibrated on core porosity (track 6) and modelled permeability calibrated against core permeability (Track7).

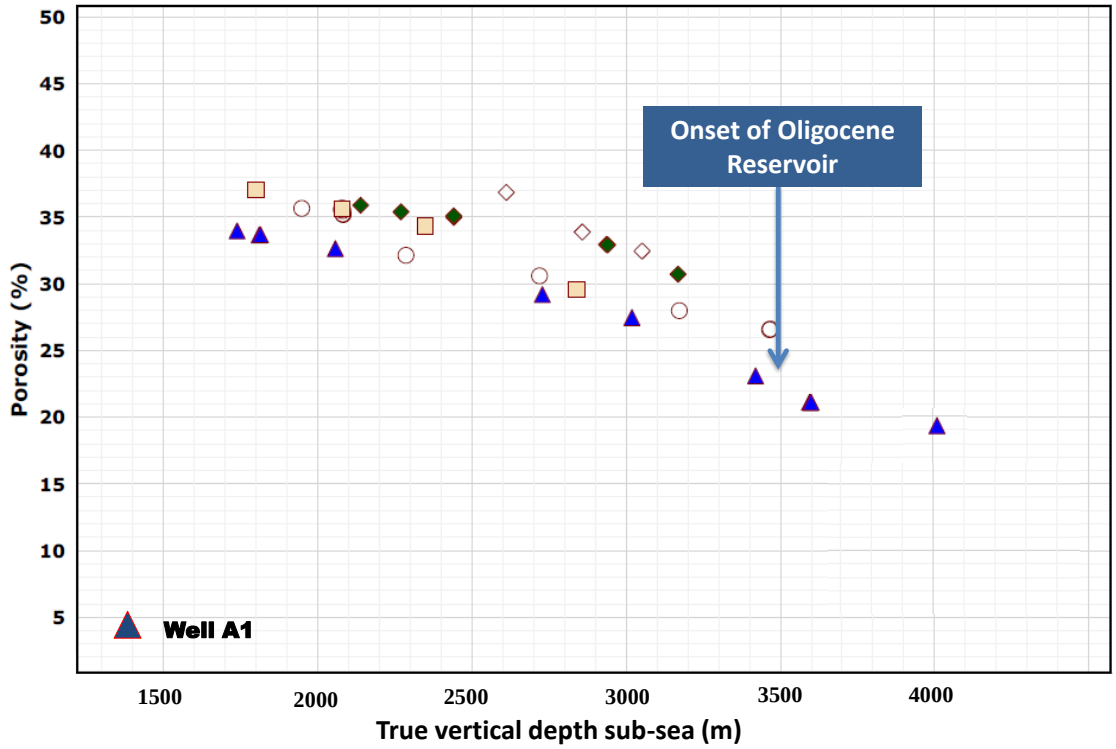

Figure 7.11: Porosity-Depth trend showing reduction in porosity for several stacked reservoirs plotted against depth for 4 wells. Well A1 the deepest well in blue triangle with Oligocene porosity starting at 3500m.

The results of the multi-mineral analysis are displayed in Figure 7.12. Tracks three to seven of Figure 7.12A show the input logs while the last track shows the multimineral model derived from the open-hole logs. The modelled quartz volume is seen to increase with depth as observed from the cross plot of quartz volume as a fraction of the total reservoir component (mineral, fluid and rock) plotted against depth (Figure 7.12B) with two trend lines seen. The first trend line 'a' indicates a steady increase with depth in quartz volume of close to 60% volume fraction from the Upper Miocene to the Middle Miocene reservoirs. An offset is seen in the second trend 'b' representing quartz volume for Lower Miocene down to the Oligocene with an estimated quartz volume of close to 80% in the Oligocene aged reservoir.

A

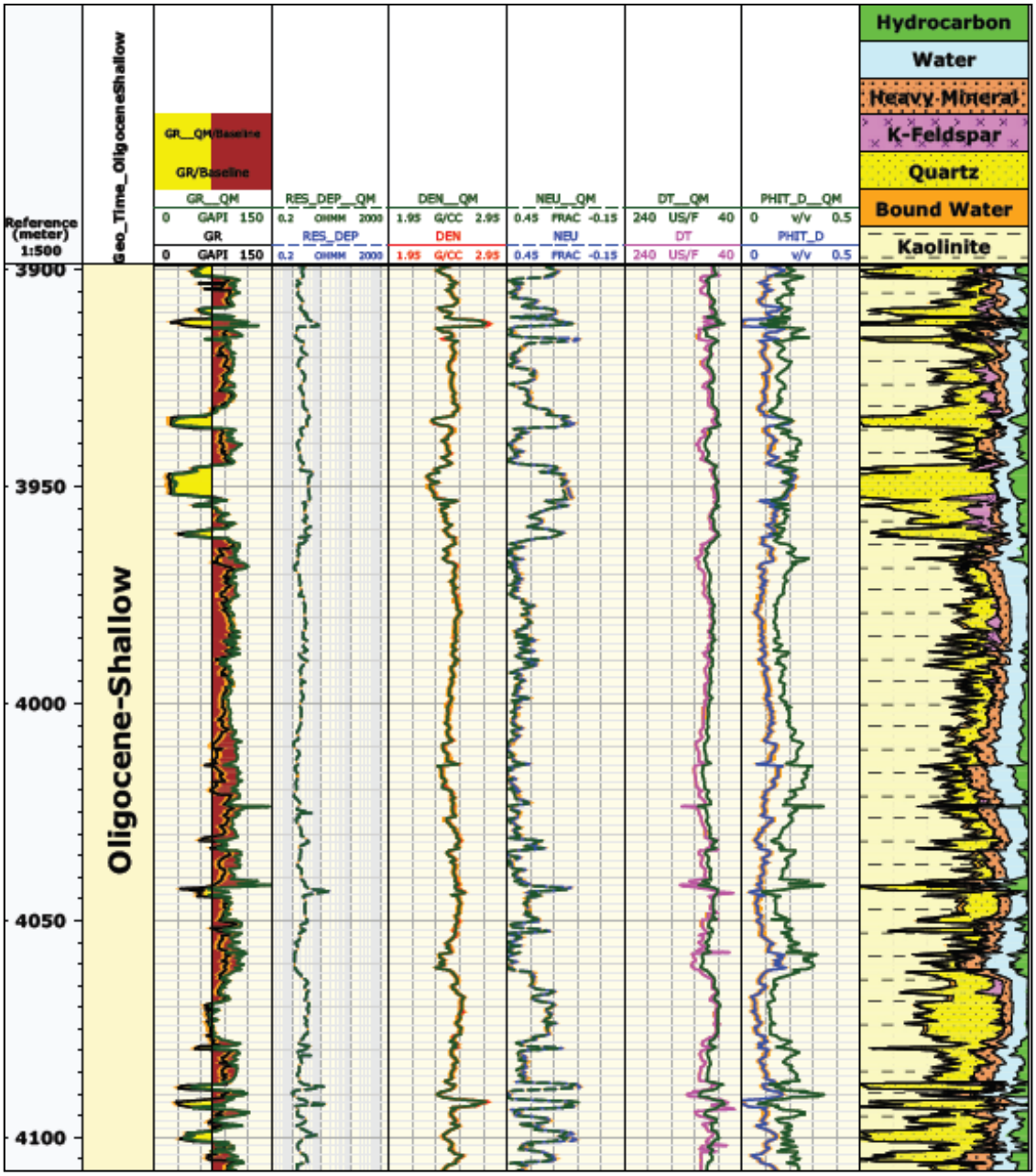
Hydrocarbon
Water
Heavy Mineral
K-Feldspar
Quartz
Bound Water
Kaolinite
Reference (meter) 1:500
Geo_Time_OligoceneShallow
GR_QM/Baseline
GR/Baseline
GR_QM
RES_DEP_QM
DEN_QM
NEU_QM
DT_QM
PHIT_D_QM
0 GAPI 150
GR
0.2 OHMM 2000
RES_DEP
1.95 G/CC 2.95
DEN
0.45 FRAC -0.15
NEU
240 US/F 40
DT
0 v/v 0.5
PHIT_D
3900
3950
4000
4050
4100
Oligocene-Shallow

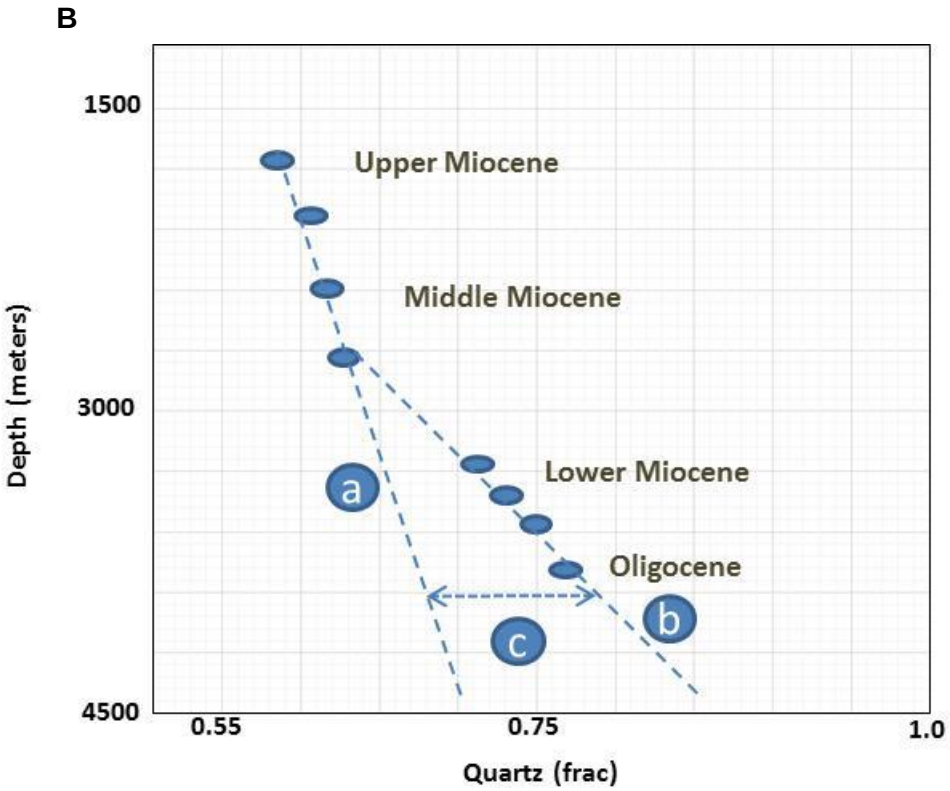

Figure 7.12: A = Modelled mineral volumes in track 8 (quartz = yellow, feldspar = pink, mica = black, kaolinite = cream with dash).Track 3;Gamma ray, track 4;resistivity;track 5; density, track 6; neutron and track 7; porosity, logs with suffix of ELAN represents back calculated logs: B = Cross plot of modelled quartz volume against depth.

Basin Modelling

Temperature and Pressure History

An interpreted regional 2D seismic section that cuts across the extensional, translational and compressional structural systems of the western part of the Niger Delta (Briggs et al., 2009) was digitized using PetroMod^{TM} and subsequently simulated (Figure 7.13). The thermal history calculated by the 2D basin model shows that the Mid-Miocene and younger reservoirs at the study location have been exposed to temperatures less than 60^{O}C (see Figure 7.14a), which is below the 70-135^{O}C quartz precipitation temperature (Walderhaug 1994, Bjørkum *et al*. 1998).

A

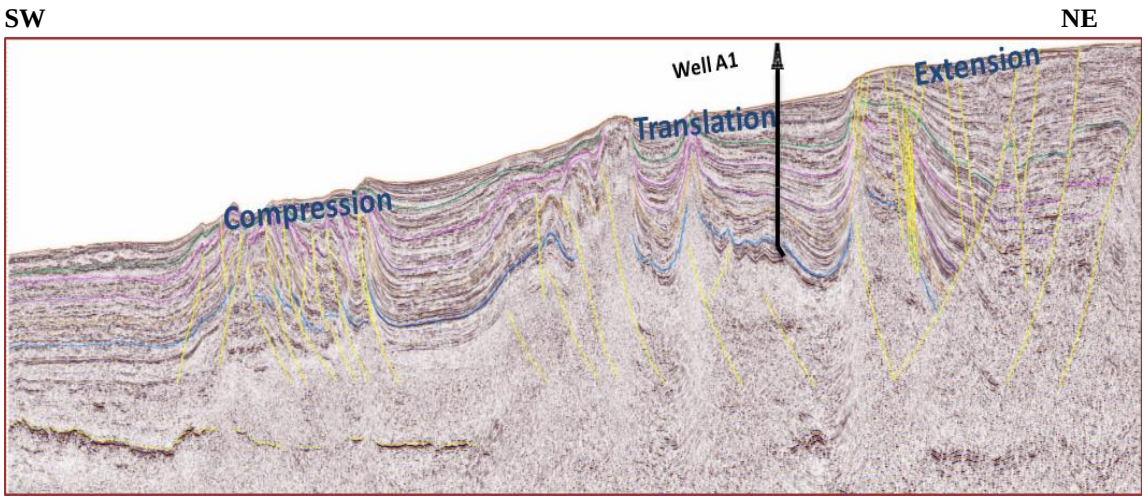

B

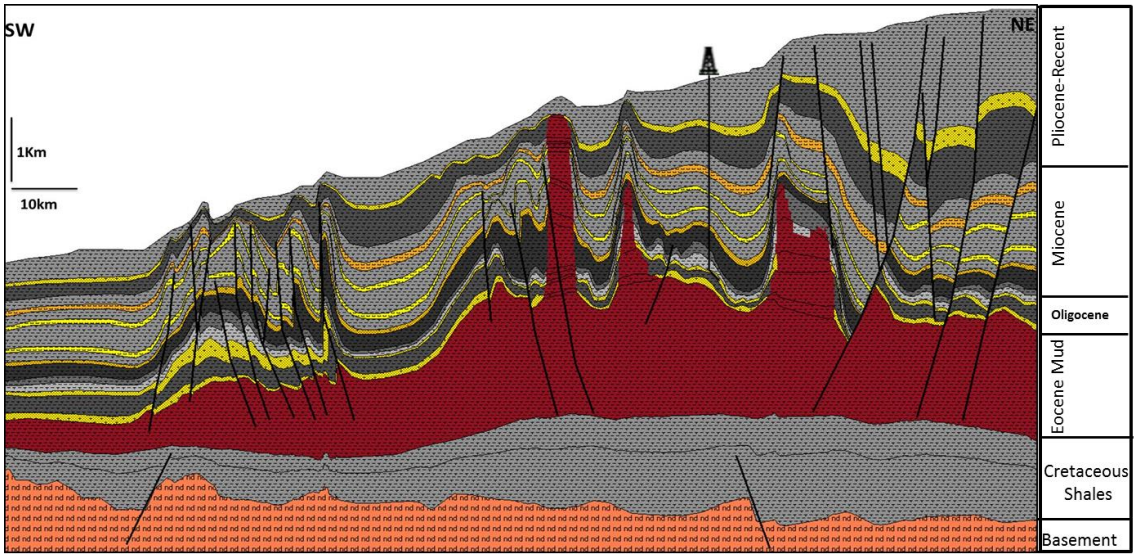

Figure 7.13: A = interpreted regional 2D transect across the 3 structural provinces (Courtesy of Shell Nigeria); B = digitized 2D transect.

On the other hand both the Late Miocene and Oligocene interval has been buried to temperatures above 70^{O}C. However, the Oligocene has been exposed to temperatures above 70^{O}C since the Early Miocene and has consistently stayed above 70^{O}C to present day (Figure 7.13A). While the Late Miocene reservoirs encountered high temperatures from Early Pliocene and reaching only about 80^{O}C at present day, hence the minor quartz overgrowth seen from petrographic observation.

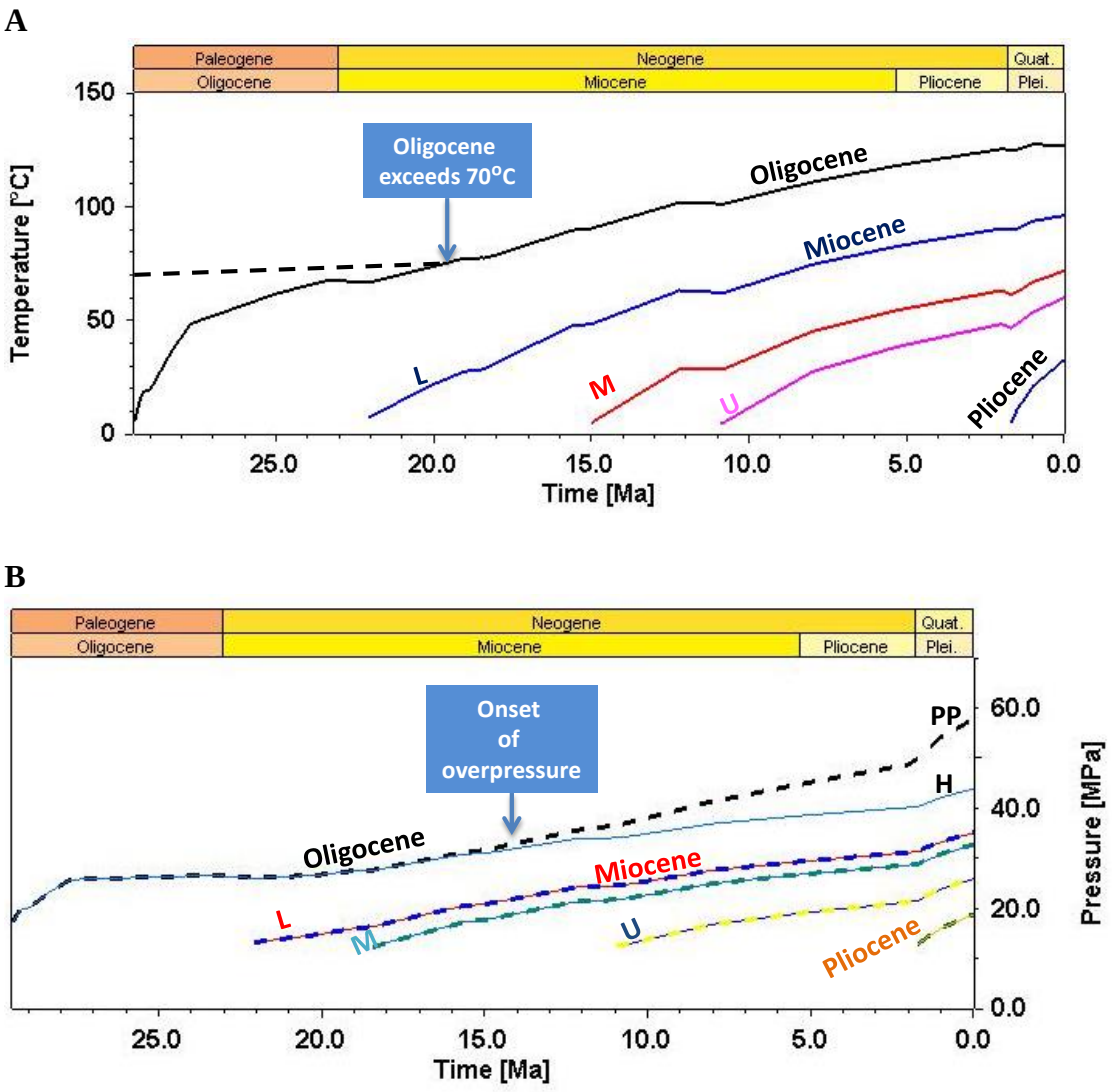

Figure 7.14: Simulated thermal (A) and pressure (B) histories for reservoirs extracted at Well A1 location. The Pressure histories (B) are plots for both hydrostatic (line) and pore pressure (dash): (L = Lower Miocene, M = Middle Miocene and U = Upper Miocene.

The simulated results also reveal that the Oligocene rocks encountered overpressure from the Mid-Miocene, which has increased to the present day to about 16MPa above hydrostatic pressure. This is seen from the separation of the pore pressure (PP) and hydrostatic pressure (H) lines (Figure 7.14B). Figures 7.15 A and B shows the simulated hydrostatic and pore pressure predictions in 2D view revealing overpressure development within the Oligocene interval and in deeper successions.

A

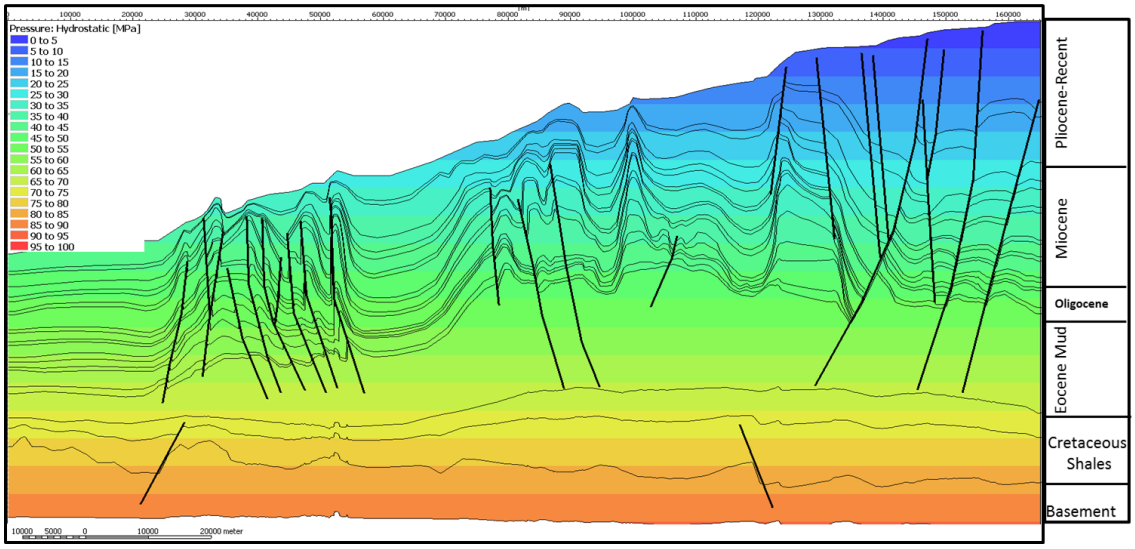

B

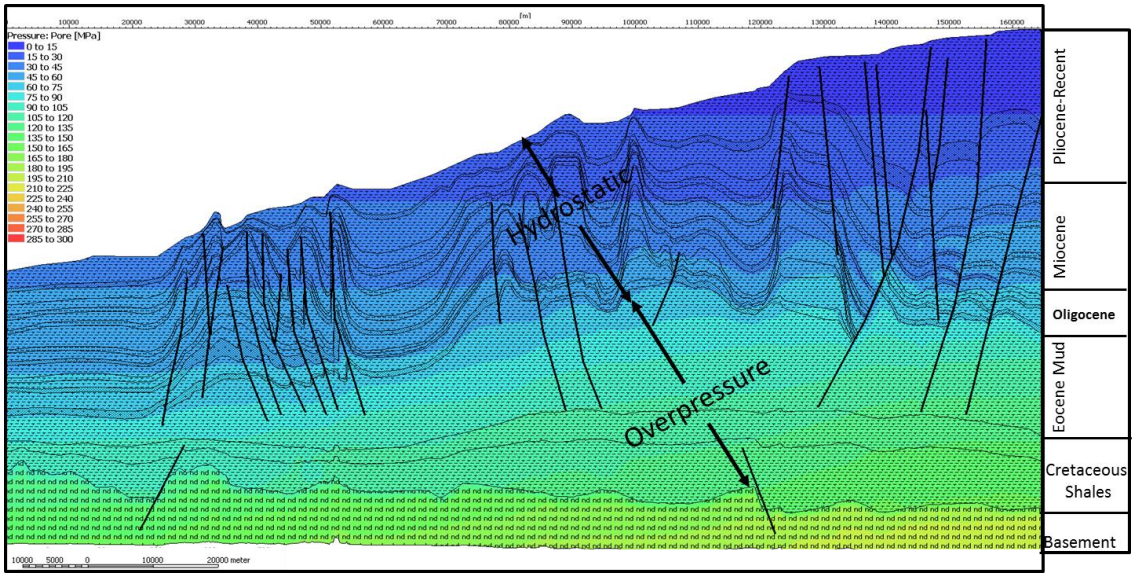

Figure 7.15: 2D pressure map (A) Iso-hydrostatic pressure map (B) Iso-pore pressure map showing hydrostatic and overpressured windows.

Quartz Cement Modelling

Basin Modelling (1D & 2D) using Schlumberger PetroMod^{TM} V.2013 has been used to predict quartz cementation which varies with temperature and fluid pressure.

A conceptual model was established to define the input parameters for the numerical model. The model was well optimized with measured data (corrected bottom hole temperature, vitrinite reflectance, pressure and porosity). Quartz cementation was then modelled using the algorithm provided in PetroMod^{TM} V.2013 based on the

Walderhaug quartz cementation model (Walderhaug, 2000). Cementation was modelled as a precipitation rate limiting reaction that is controlled by detrital mineralogy, quartz grain size, quartz grain coating abundance, temperature and quartz surface area. The porosity loss rate due to quartz cementation is therefore expressed as:

$$\frac{\delta\phi cc}{\delta t} = \frac{m}{\rho}\frac{(1-C)6f}{D}\frac{\phi}{\phi_o}Ae^{-Eo/RT} \qquad (7.1)$$

Where C is the quartz grain coating factor, f is the quartz grain volume fraction, D is the average quartz grain size, A and E_o are respectively the frequency factor and activation energy of quartz precipitation. M represents the mol-mass and ρ the density of quartz (Walderhaug 1994). The average grainsize and quartz grain volume fraction defined in the model were based on the results of the petrographic study. A dominant grain size of 125 - 500µ is seen in the Miocene. No core has yet been taken from the Oligocene interval, so it was assumed that the Oligocene reservoirs located below 3800m would have similar grain size as the Lower Miocene reservoir at 3450m, which is the deepest cored section from Well A1.

PetroMod^{TM} calculation assumes that quartz is sourced by stylolites that later diffuses as silica reach fluid into the interstylolite regions and further precipitates as overgrowths on quartz grains. In addition it is also assumed that the precipitation phase of the overall process is the slowest and hence the rate controlling step in the entire process (Walderhaug, 2000). By Implementing the Walderhaug quartz cementation model as part of the simulation, the percentage pore space occluded by cement was estimated. The result shows that cement volume tends to increase both with depth and landward in the updip direction along the regional transect (Figure 7.16) as water depth decreases and mean overburden increases. Little or no cement is seen above 3000m around the study location but cementation starts to develop from about 3450m depth within the Lower Miocene reservoirs with less than 5% of its pore cemented. The cement volume increases steadily with depth into the potential Oligocene reservoirs with values of close to 14% of available porosity being occluded. The minor quartz cement observed from the petrographic study for the Lower Miocene reservoir and the absence of quartz in Mid-Miocene agrees with this modelled result. The modelled result is also displayed as

a 1D extraction at the well location from the 2D model with cement volume plotted against depth (Figure 7.17).

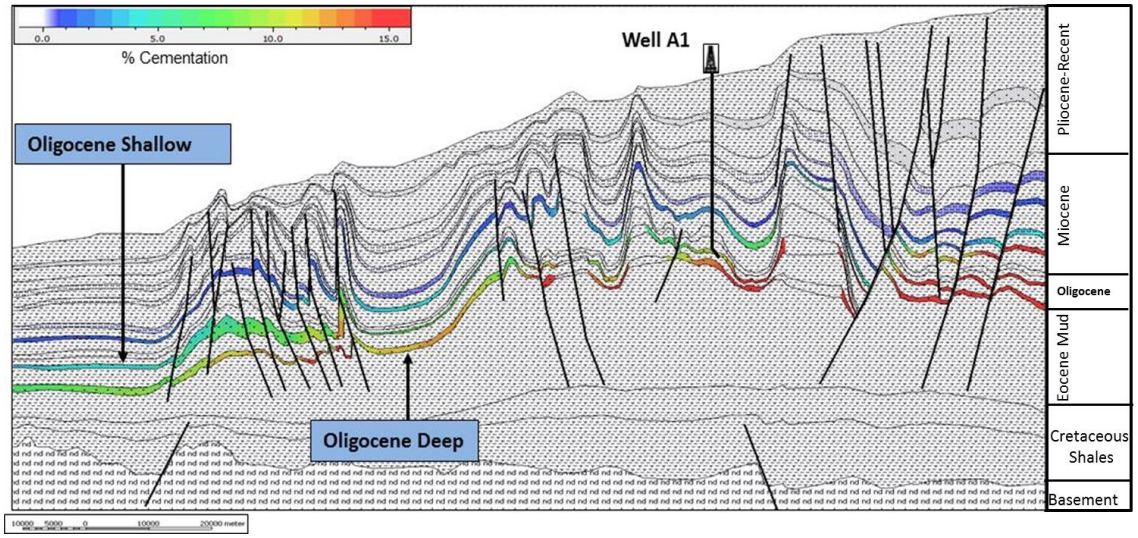

Figure 7.16: Overlay of predicted quartz cement on 2D transect. Colour spectrum show increase in cement volume from blue to red. In the vicinity of well A1 cement volume increase with depth from Miocene to Oligocene.

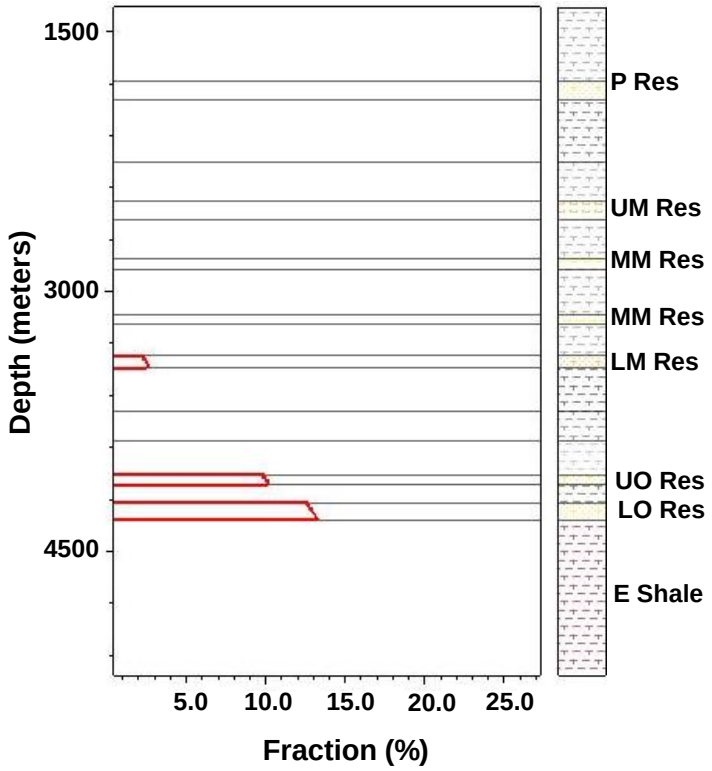

Figure 7.17: Fraction of pore space occluded by cement plotted against depth: a 1D extract at well location from 2D model in Figure 7.15. Res = reservoir, P = Pliocene, UM = Upper Miocene, MM = Mid-Miocene, LM = Lower Miocene, UO = Upper Oligocene, LO = Lower Oligocene, E =Eocene.

The observed trend from the quartz model also closely resembles the trend from the multi-mineral analysis of Figure 7.12B. A corresponding decrease in modelled porosity from Miocene to Oligocene reservoirs is seen when the modelled porosity is plotted against depth. A good match is seen between the modelled porosity and the average calculated porosity from well log (Figure 7.18).

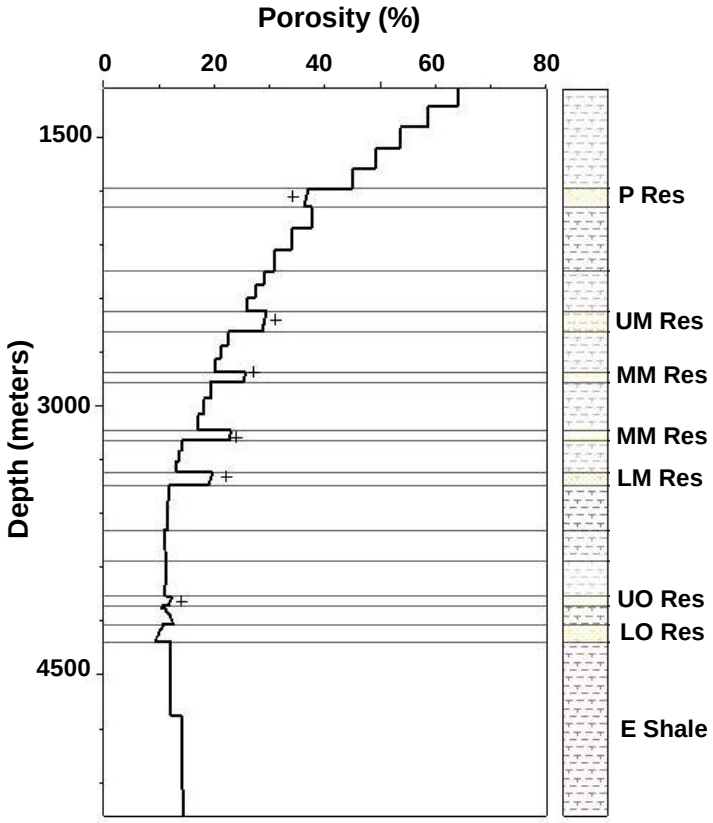

Figure 7.18: Modelled porosity (black line) versus depth, calibrated against calculated porosity from well log (black cross). Res = reservoir, P = Pliocene, UM = Upper Miocene, MM = Mid-Miocene, LM= Lower Miocene, UO= Upper Oligocene, LO= Lower Oligocene, E=Eocene

Discussion

The accurate prediction of sandstone reservoir quality has been a key challenge for hydrocarbon exploration and production. A good understanding of reservoir quality is required throughout the entire life cycle of a reservoir – at exploration phase where it is required for initial hydrocarbon reserves estimation to appraisal and development stages where porosity and permeability distribution in a reservoir are requisite for well placement optimization and to estimate economic cut off limits. These limits control

hydrocarbon pore volumes, recoverable reserves and production rates (Sneider, 1990). A fundamental control of sandstone reservoir quality is quartz cementation, itself controlled by temperature, pressure (effective stress), and surface area of quartz substrate which is a function of grain size, abundance of grain coatings and quartz clast abundance (Walderhaug 2000, Worden and Morad 2000).

We present a synthesis of petrographic, petrophysics and basin modelling studies in the characterisation of the poorly understood potential Oligocene reservoir of the offshore part of the Agbada Formation of the Niger Delta Basin. The focus of this work is to better understand and investigate the reservoir potential of the Oligocene interval buried below 3800m, most importantly its diagenetic history. The burial, temperature and pressure histories have been considered, particularly their key control on quartz cementation. Petrographic analysis of thin-sections and polished block samples of the hydrocarbon charged shallower Miocene samples were studied and inferences were deduced to predict the mineralogical distribution of the uncored Oligocene interval that was penetrated by a single well (A1) in the study location. The petrographic study was further built into the multi-mineral petrophyisical study to inversely calculate the volume percentage of the minerals based on well log responses.

The SEM images (CL) of samples from the deepest cored Lower Miocene interval at 3450m reveals the presence of syntaxial quartz overgrowths protruding into the pore space (Figure 7.7D and E). Although the thickness of the overgrowths are less than 30µ suggesting that the effect on the porosities of the Lower Miocene is likely to be minimal, which is also confirmed from the porosity calculated from the density log with an average value of about 25% (Figure 7.11). The presence of quartz overgrowths in the Lower Miocene is indicative of a possible increase in overgrowths in the potential Oligocene reservoirs, located deeper where temperature conditions would further favour the precipitation of quartz cement.

The thermal history of the studied interval calculated in the 2D basin model shows that the Miocene reservoirs especially the Mid-Miocene and younger reservoirs have consistently been, within the temperature window of 30-65^{o}C which is below the temperature required for quartz precipitation. However, the Oligocene reservoirs are

seen to have been exposed to temperatures greater than 70^{o}C since Early Miocene (19Ma) up to the present day (Figure 7.13A), suggesting the likelihood of high quartz cement in the Oligocene compared to the shallower Lower Miocene reservoirs which is presently buried to a temperature of about 80^{o}C. It has been well established that overpressured reservoirs are likely to have their porosities preserved since grain to grain contact is reduced thus improving the reservoir quality in such reservoirs (Taylor et al., 2010).

The pressure history for the reservoirs indicates that the Miocene reservoirs have not been overpressure as both pore pressure and hydrostatic curves overlap each other, but the plot for the Oligocene shows a separation of both curves indicating an overpressured system (Figure 7.14B). The pressure history plot also reveals that overpressure in the Oligocene reservoirs started developing from Mid-Miocene (14 Ma) and has steadily increased to the present day. This is also supported by the 2D pressure map in Figure 7.15 showing overpressure development within the Oligocene and deeper intervals. Although the Oligocene reservoir interval is overpressured, it is likely that the reservoir porosity wouldn't have been preserved because the reservoirs were earlier exposed to high temperatures from Early Miocene (19Ma) prior to been significantly overpressured from Late Miocene (10Ma). So the temperature required to initiate and continue quartz cementation was reached well before overpressure developed.

The degree to which quartz would have been precipitated in the reservoir prior to having been overpressured is not studied at this stage. However, two schools of thought have been put forward to address the rate of quartz cementation: (1) a continuous process that occurs slowly over a long period of time, and (2) an episodic process of short bursts of reactions punctuated with lengthy period of quiescence (Worden and Morad 2000). The adoption of either of the two would require further investigation through fluid inclusion microthermometric study, which is beyond the scope of this work. Notwithstanding, the presence of minor quartz overgrowth from the CL image of the Lower Miocene samples tends to agree with the temperature and pressure history from the model. In addition, the cementation modelling achieved by applying the Walderhaug algorithm, shows that the potential Oligocene reservoirs have had about 14% of their pore space occluded by cement while the Lower Miocene reservoir have less than 5% of pore space cement

filled (Figures 7.16 and 7.17. This agrees with the petrographic evidence of minor quartz overgrowth in the Lower Miocene. The increase in quartz cement from Lower Miocene to Oligocene is largely controlled by:

1. Temperature increase with depth, as the sediments are buried deeper they are further exposed to temperatures favouring quartz precipitation.
2. The grain size which determines the surface area available for cementation. So the smaller the grain size the larger the surface area, Since the Oligocene reservoir interval was not cored it was assumed that the grain texture of the Oligocene is similar to the deepest cored Lower Miocene.
3. The presence of grain coating which has been proven to prevent the formation of quartz overgrowth (Lander and Walderhaug, 1999, Ajdukiewicz and Larese, 2012). These coats could either be rims of chlorite or microcrystalline quartz. None of these coating agents were observed during SEM analysis, but rather we see quartz grains coated by dead oil (Figure 7.8). Considering that early oil emplacement can halt or reduce quartz cement precipitation (Taylor et al., 2010), It is therefore likely that the presence of this oil seen only in the Mid-Miocene samples would have helped in preserving the porosity.

A 1D extraction of cementation model at the well location from the 2D transect, shows a volume fraction of pore space filled with quartz cement plotted against depth (see Figure 7.16). The figure shows an increase in cement with depth; a similar trend is seen from the multi-mineral petrophysical evaluation, where fractional volumes of major rock minerals have been estimated from well log responses. A good match is seen between the original input log and the back calculated versions of the logs with a suffix of ELAN attached to the name of the curve (Figure 7.12A). This is a good quality control for the estimated volumes of quartz, feldspar, zircon and kaolinite. A cross plot of the fraction of quartz volume against depth shows an increase in quartz with depth; a clear demarcation of two trends is seen, a higher gradient from Mid-Miocene upwards (trend ‘a’) and a gentler trend from Lower Miocene down to the Oligocene (trend ‘b’). A differentiation of detrital and authigenic quartz cannot be made from this plot, although we infer that assuming a constant quartz volume input that trend ‘a’ is a function of compaction due to the weight of the overburden with the quartz volume

being a percentage of the total rock volume, while the second gentler trend 'b' is a function of both compaction and quartz volume increase due to cementation. The separation of trend 'a' and 'b', designated as line 'c', can be assumed to be additional quartz volume of about 10% due to cement. This assumption is supported by (1) the modelled quartz cement that is based on the Walderhaug algorithm that shows an onset of quartz cementation from the Lower Miocene and increasing volumetrically in the Oligocene to a cement volume of less than 14% (Figure 7.17); and (2) the presence of quartz cement rim noted from the petrographic inspection of the Lower Miocene samples (Figure 7.7D and E). No quartz cement was seen in samples from the shallower and younger reservoirs.

Comparison of the Oligocene sediments of the Niger Delta Slope system and other Oligocene turbidite systems along the South Atlantic Margin

The purpose of this section is to compare the potential Oligocene reservoir of the Niger Delta within the study location and the Oligocene turbidite system of other prolific basins along the South Atlantic Margin. Of primary importance is the quality of the reservoirs and the corresponding key controlling factors. Two passive margin basins have been considered in this study; (1) the Lower Congo Basin on the West African passive margin offshore Angola, and (2) the Campos Basin in Southeastern Brazil.

The Lower Congo basin is one of the three sub-basins (Kwanza and the Gabon Basins) developed along the West Africa passive margins, further south of the West African margin. The basin is thought to be one of the hydrocarbon prolific basins along the margin with major discoveries made within the two major deep-water turbiditic sandstones of Oligocene and Miocene age, both belonging to the Malembo Formation (Broucke et al., 2004). The Oligocene turbidite system holds the major discoveries especially in the Girassol field with estimated oil in place of 1550mmbbls and recoverable reserves placed at 725mmbbls trapped within Oligocene channel levee complex. The field is located within a water depth of 1400m (Pelleau et al., 2002). Unlike the Oligocene sediments of the Niger Delta slope system located at depth deeper than 3800m below sea level, the Oligocene reservoirs in Girassol field are located at a depth of 2400m below sea level. These suggest that the lower Congo Oligocene reservoirs have not undergone sufficient burial and therefore are minimally

compacted. This is reflected in the unconsolidated nature of the fine to very coarse sands and its excellent reservoir quality with porosity of up to 40% and permeability greater than 5 Darcy. The reservoirs are also normally pressured and with present day temperature of 58–69^{O}C (Dessus and Abreu, 2002, Pelleau et al., 2002, Delattre et al., 2004). The regional geology of the area does not suggest that the Malembo Formation had anytime been exposed to any physio-chemical conditions that would have necessitated the precipitation of any porosity occluding diagenetic minerals such as late quartz or early calcite cements (Broucke et al., 2004, Gay et al., 2006), further confirming the excellent nature of the Oligocene reservoirs in the Lower Congo Basin.

Conjugate to the basins in West Africa passive margin is the Campos Basin of the Brazil margin that lies beneath the coastal plain, continental shelf and slope of the western portion of the South Atlantic Ocean. The Campos Basin is the most prolific of the twelve eastern Brazilian basins with oil fields producing from reservoirs that range from Neocomian fractured basalts and Barremian coquinas through to Late Albian–Middle Eocene siliciclastic turbidites and to turbidites of Middle Eocene–Early Miocene Marine Regressive Megasequence (Bruhn et al., 2003).

Turbidites are the most important petroleum reservoirs in the Campos Basin with reservoirs in 37 oilfields including the Marlim Complex super giant field which encompasses the Marlim Field itself and other surrounding fields East of Marlim, West of Marlim and South of Marlim (Souza et al., 1989, Bruhn et al., 2003). The total estimated oil in place for the Marlim Complex is about 13.9 billion barrels of oil with the Marlim field accounting for over 57% of the total volume of hydrocarbon (Souza et al., 1989). The principal reservoir of the Marlin field is the Oligocene Carapebus Member of the Campos Formation, from which the study is carried out. The Marlim field was discovered by the first exploratory well drilled at a water depth of about 850m. The Oligocene reservoirs located at a depth of about 2700 m are known for three outstanding qualities; 1) predictability from seismic data, 2) good hydraulic connectivity and 3) excellent petrophysical properties. Reservoir average porosities and permeabilities typically range between 27–30%, and 1000–2000mD respectively (Pinto et al., 2001).

The sand rich reservoirs from the Marlim field are turbidite lobes, which accumulated in intra–slope, wide depressions. The reservoir facies comprises mostly of amalgamated graded beds of medium to very fine grained sandstones that are poorly consolidated, poorly sorted and with a low volume of silt, clay and diagenetic minerals. The low degree of cementation in the Oligocene reservoirs is attributed to the following factors:

1. Early oil emplacement inhibiting cementation even though the reservoirs are at present day temperature of about 80^{O}C – temperature window for early phase of quartz cementation. The exact time the oil reached the reservoirs is poorly understood, but since the Lagoa Feia Formation – the main source rock that charged the Oligocene reservoirs entered the oil window at 80Ma (Soldan et al., 1995) is directly located below the Campos Formation and with good fault connectivity, migration into the overlying reservoirs would have been timely achieved.
2. Early calcite cementation at shallower depth inhibiting the development of pressure solution and with further increase in burial depth and higher temperature, carbonate dissolution was later achieved thereby creating significant volumes of secondary porosities (Moraes, 1989).

Conclusion

1. The potential Oligocene reservoir is interpreted to have been subjected to high temperatures of above 70^{o}C from the Early Miocene to present day. This temperature is taken as the start-up temperature for quartz precipitation
2. Both petrographic evidence and petrophysical analysis of quartz overgrowths in the Lower Miocene and an increase in quartz overgrowth with depth respectively, appears as strong evidence that the Oligocene sediments are likely to be cemented.
3. The possible volume of pore space occluded by cement in the Oligocene has been estimated to be less than 14% of the pore fraction. With the presence of less than 14% of quartz cement in the Oligocene it is likely that the porosity and permeability of the Oligocene reservoir might well have been compromised
4. Despite that both modelled results and inferences deduced from both petrographic and petrophysical data, points to a possibility of quartz cementation

in the potential Oligocene reservoir, the amount of cement volume as predicted from the 2D simulation is likely not sufficient to prevent the Oligocene interval of the Agbada Formation from being a viable hydrocarbon reservoir. Also the effect of early hydrocarbon emplacement, thought to retard or slow down diagenesis, would need to be further investigated, so that the timing of hydrocarbon charge and the timing of diagenesis can be fully synthesized to further investigate the reservoir potential of the deeper untapped Oligocene sediment.

5. The reservoir properties described above for the Oligocene systems of both the Lower Congo Basin of Angola and the Campos Basin of Brazil are similar to the reservoir properties of the Miocene turbidites of amalgamated channel complex of the Niger Delta that have been buried to a depth range of 2400–3000m. It is likely that one of the major principal factors controlling reservoir quality is the depth of burial as good quality reservoirs are seen in depths of less than 3000m in all three basins (Niger Delta, Lower Congo and Campos Basins) suggesting that the physio-chemical factors controlling diagenetic cementation are prevalent in reservoirs buried deeper than 3000m. This is the case for the Oligocene reservoir of the Niger Delta fan system that is currently located at depth below 3800m, where temperature and pressure conditions are likely to favour the precipitation of authigenic quartz. Although the reservoir properties of the Oligocene fan system of the Niger Delta might not be as high as that of the shallower Miocene systems of the Delta or the Oligocene fan systems of the Lower Congo Basin and the Campos Basin, it is still capable of being a future exploration target as less than 14% cementation is not excessive and may still prove economical.

Acknowledgement

We wish to express our appreciation to Shell in Nigeria and The Hague for providing the data and particularly to Daniel Agbaire of Shell Nigeria and Andy Bell of Shell Global Solutions International, The Hague, for their expert advices. Also special thanks to Thomas Hantschel, Daniel Palmowski and Nour Koronful of Schlumberger Aachen for making possible the use of PetroMod software and for all the technical discussions which have considerably enhanced this work. This project is part of Obinna Chudi's

PhD which has been generously sponsored by the Petroleum Technology Development Fund (PTDF), Nigeria.

CHAPTER 8

DISCUSSION

Integrating basin modelling and diagenetic study, coupled with seismic interpretation and petrophysical results that are outlined in Chapters 4-7, an understanding of the Oligocene deep-water sediments in the Niger Delta slope system has been gained. The Miocene proven play reservoirs of the slope system in the study area formed a foundation upon which major inferences on the Oligocene depositional system have been made, including its depositional architecture, reservoir potential and reservoir quality. Results presented in Chapter 4 indicate that the Miocene system displays a low degree of consolidation, and includes a range of reservoir and associated facies. These ranges from structureless sands through graded sands and muds to interbedded silts, sands and mud facies. These facies are interpreted as dominantly turbidites and interbedded hemipelagites, together with rare debrites and slump deposits. There are thin and medium-bedded turbidites with partial Bouma sequences, and very thin-bedded turbidites with partial Stow sequences (Stow, 2005). Thicker sand units are similar to the deep-water massive sands of Stow and Johansson (2000), the likely result of high-concentration flows.Good reservoir properties are common in the Miocene, porosities that range from 25-37%, net-to-gross of up to 90% and permeability in the Darcy range. The Oligocene section was not cored.

In this chapter we synthesise and discuss the results presented in chapters 4-7 in relation to the reservoir quality of the Oligocene system, and where possible, project the knowledge gained from the Miocene system and extend it to infer the reservoir potential of the Oligocene succession. The wider implications of the findings will be discussed with respect to the depositional style, degree of quartz cementation and charge history in relation to the reservoir quality of the potential Oligocene reservoirs.

8.1 Characteristics of Deep-water Channel-lobe Complexes: A Seismic Interpretation Perspective

Submarine channel-lobe systems form one of the key depositional elements in the deep marine environment. Channel-lobe systems are known to be excellent hydrocarbon reservoirs across the world (Beaubouef and Friedmann, 2000, Posamentier, 2003, Anderson et al., 2012, Moscardelli et al., 2013) . Lobes themselves represent

accumulation of turbiditic deposits that are broadly lobate plan-view with their scale dependent on the accommodation space available for sedimentation, the physiographic location and volume of sediments (Wynn et al., 2002b, Deptuck et al., 2008, Savoye et al., 2009). Lobes are typically found at the downstream end of channels; these channels serve as sediment conduits for lobes. The lobes therefore record focused aggradation of coarse sediments as channelized turbidity currents decelerate and spread (Galloway, 1998). With increase in sediment deposition they are bound to pile up so that in a cross sectional view they appear as mounded features with restricted areal distribution. This mounded nature of lobes distinguishes it from the 'U' or 'V' shaped form of channels when viewed from a seismic cross section (Kolla et al., 2001, Stow and Mayall, 2000). In addition to displaying a characteristic external mounded geometry, they can also show other key recognisable characters on seismic data including: (1) the presence of pinchout geometry; (2) high amplitude continuous reflection onlapping paleobathymetric highs; and (3) bidirectionally downlapping reflections (Posamentier and Erskine, 1991). The extent to which seismic recognition criteria can be observed is dependent on the data quality and the seismic resolution – a function of rock seismic velocity and burial depth. Seismic data have been well utilized in studying lobes, particularly near sea-floor seismic that images nicely the characteristic plan view shape of lobes plus the proximal to distal changes in the stratigraphic nature of complex channel-lobe systems. Such studies have been carried out in some modern deep-water settings (Beaubouef and Friedmann, 2000, Beaubouef et al., 2003, Deptuck et al., 2008).

Modern lobes typically appear mounded in cross section and comprise relatively coarse-grained turbidites (Galloway, 1998). The mounded lobes range from a few meters to many tens of meters in thickness and are up to a few kilometres in width. Thickness and grain size of the turbidite lobes decreases down system with greater bed thickness along the lobe axis and thinner beds towards the lobe fringes (Figure 8.1). Deptuck et al., (2008) studied 20 Pleistocene submarine lobes off the northern margin of East Croatia using high resolution seismic data and noted significant variability in bed thickness and sizes in each of the lobes. Most of the lobes show downslope increase in thickness ranging from 8-40m, beyond which they progressively decrease in thickness even below seismic resolution. The lobe areas range from 3 to 70km^2 and length from

2-14km. In the South Atlantic margin, the Oligo-Miocene turbidite sequence of the Lower Congo Basin is composed of terminal lobes with massive sands over 30m thick and about 50km^2 in area. These lobes are reportedly fed by isolated elementary channels that are not connected to major erosive channels (Broucke et al., 2004). Beaubouef and Friedmann (2000) documented the presence of high amplitude channel-lobe complexes in the western Gulf of Mexico. The lobes are commonly ponded in intraslope basins and exhibit a variety of internal geometries such as highly continuous reflection character to semi-continuous facies, including onlapping and downlapping reflection termination. The width of these lobes ranges from 1-6km and a length of 3-8km. They are typically sand-rich turbidite systems and represent the most reservoir prone facies compared to other depositional elements. The high amplitude reflection character of the lobe complexes in the western Gulf of Mexico are also similar in seismic facies and geometries to the lobe units of the Amazon fan described by Pirmez et al. (1997), although the lobes of the Amazon fan range from 21km to 90km in length and from 6 to 25km in width. The Amazon fan is one of the largest river-fed submarine fan systems in the world with an annual sediment discharge at the Amazon River mouth of about 1 gigaton/y (Jegou et al., 2008). The volume of the sediment input and the corresponding large size of the Amazon fan thus results in significantly large sized lobes compared to lobes of the other basins discussed previously.

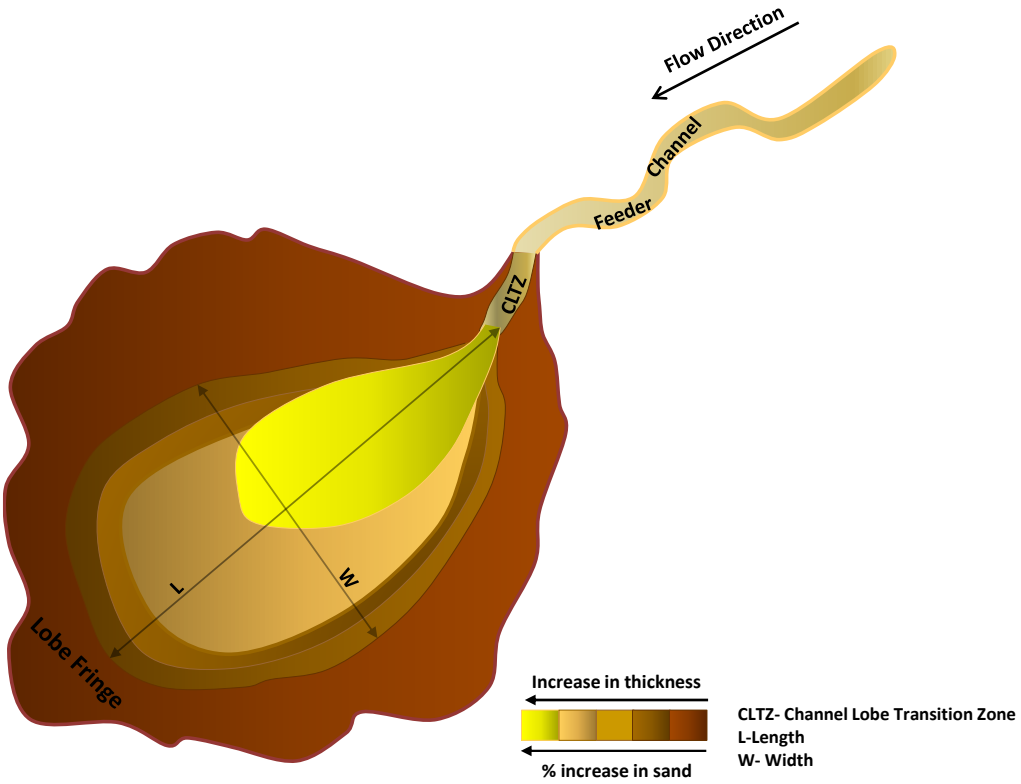

Figure 8.1: A schematic illustration of channel lobe element in plan-view showing some of the main characteristic elements.

8.1.1 Characteristics of Oligocene channel-lobe system

The majority of the channel-lobe systems discussed above are modern deep-water systems whose properties and seismic characters are well imaged from near surface measurements from either seismic or side-scan sonar. The Oligocene deep-water system of the western Niger Delta can be considered as an ancient deep-water system. Attribute maps of RMS (root mean square) and spectral decomposition-RGB (red green blue) blending techniques have been utilised to image the prevalence of lobe deposits as the main depositional element that characterises the Oligocene interval in the study. The results of this study have been presented in Chapter 5. Of the 8 lobes documented (Figure 8.2), most are interpreted to be located at the mouth of channels A – D forming channel-lobe elements. Lobe 3 and the 'Earlier Lobe' do not show a clear association to an updip feeder channel. Lobe 2 is associated with channel A, and lobe 8 with channel D.

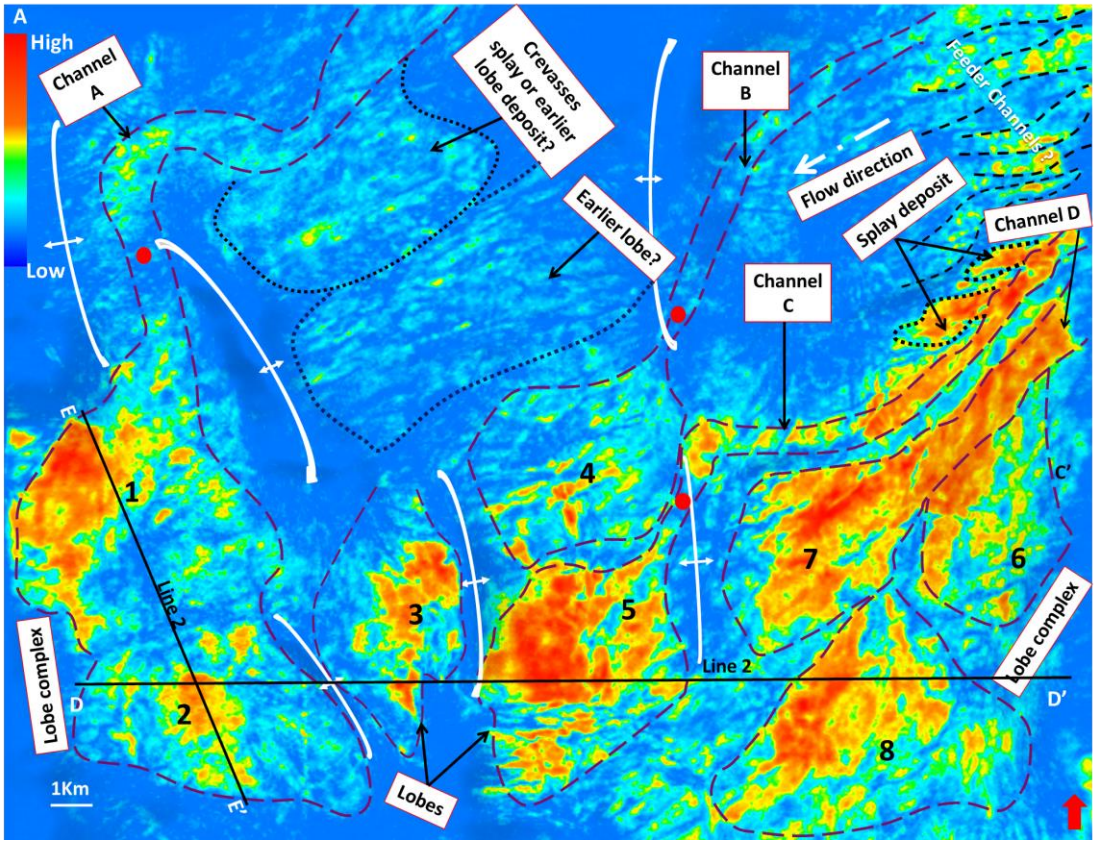

Figure 8.2: Oligocene-deep depositional elements controlled by mud highs. RMS interval amplitude mapped below the Oligocene-deep Horizon (0 to +90ms amplitude extraction window). High seismic reflection amplitude dominates the main lobes that have been identified. Locations of lines 1 and 2 of Figures 8.3 and 8.5 respectively are shown. The regional downslope trend is ENE to WSW.

Two lobe complexes composed of 5 lobe elements have been documented across the study area. The lobe complex located in the south-western part of the study area is made up of two lobe elements (lobes 1 and 2) with channel A as the main feeder channel. In the south-east, a lobe complex with three mappable lobe elements and feeder channel D were interpreted. Deep-water channel-lobe systems in this study are similar in terms of their seismic expression to the channel-lobe system of other sedimentary basins discussed previously. In cross section view the lobes show a distinctive convex-upward mounded character, in some cases mounding have been modified by growing mud diapirs (for example lobe 3 in figure 8.3c). These mounded lobes have internal bidirectionally downlapping reflections that suggest aggradational depositional style associated with stacking of discrete lobe units (Figure 8.3c). This is clearly expressed by

Lobe 8 located in the south east and characterised seismically as high amplitude lobes draped on mud induced structural high.

The axis of this lobe and other lobes in this study are likely to be: (1) a location of maximum thickness; (2) a location of maximum grain size; and (3) a site of higher net-to-gross. The lobe elements are thinner and possibly finer grained from axis to fringes. This is particularly reflected from the plan-view which shows significant high seismic amplitude at the lobe axis and further away from the axis to the lobe fringes the amplitude becomes weaker (Figure 8.2 and RGB map of Figure 5.10B in Chapter 5). Generally, within the study area most lobes have a width of 3-6km and a downslope length of 6-8km long, near similar in dimension to the hydrocarbon bearing lobes discovered in the western Gulf of Mexico. In addition, the majority of the lobes in this study, just like the Gulf of Mexico lobes are ponded within intra-slope mini-basins (Figure 8.3).

A

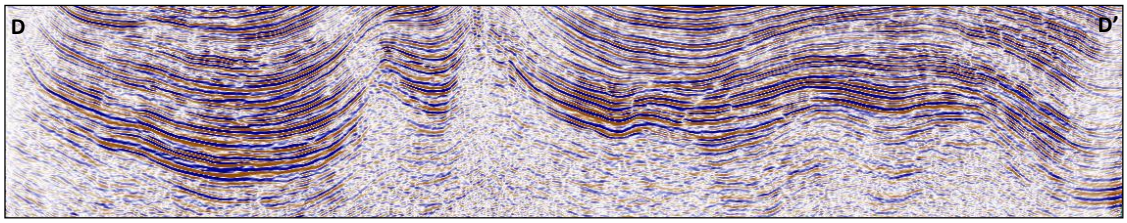

B

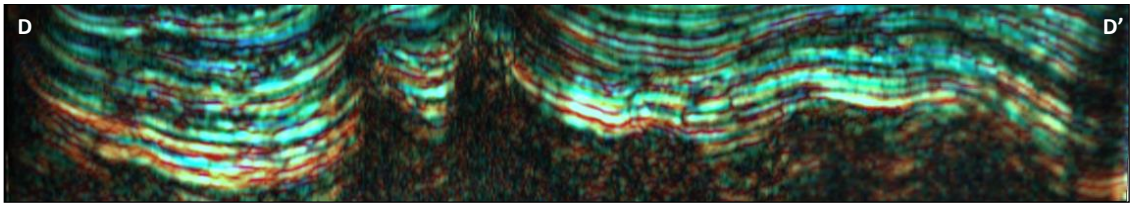

C

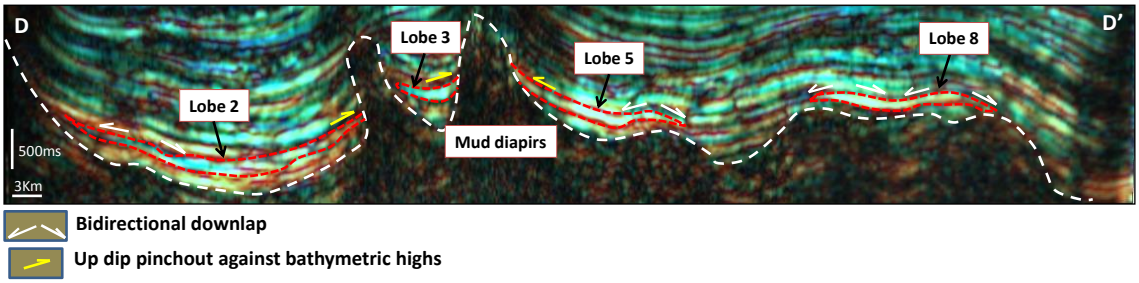

Figure 8.3: Line 1 is a strike orientation of seismic section across the key Oligocene depositional lobes showing characteristic seismic expressions. 'A' is an uninterpreted reflection amplitude seismic section. RGB blend attribute of the same line (B - uninterpreted, C - interpreted) of the Oligocene lobe deposits showing the external mounded nature with bidirectional downlapping dipping reflectors highlighted in white arrows. Note the updip pinchout geometries of the lobes (yellow arrows) against mud diapirs. The lobes are interpreted to drape on bathymetric high as well as pond within mud induced mini-basins. Line location is illustrated in Figure 8.2.

8.1.2 Role of tectonics on ponding

Submarine turbidite channels are known to transverse complex routes on slope topography, which would typically result in a change in geometry of the channels. The temporal and spatial variations in geometry of the depositional systems are mainly controlled by sea level changes, sediment flux, tectonic accommodation space and climate changes (Mayall et al., 2010). Local tectonic activity tends to modify sea-floor topography that ultimately influences sediment transport routes and the location of channel and lobe elements. This is clearly observed in passive margin basins that are characterised by high sedimentation rate and sediments underlain by mud or salt diapirs with associated fault networks. Typically the underlying substrate either salt or mud are weak and exhibit significant downslope mobility coupled with buoyancy. This is manifested in the form of complex structural features such as growth faults located updip of the slope and shelf, and folds, thrust faults, and diapirs further downslope. These features have been shown to modify slope bathymetry, so that where they are prevalent they tend to form intraslope mini-basins such as growth fault related basins, mini-basins on salt canopies, and piggyback basins behind folds (Mayall et al., 2010). Figure 8.4 below illustrates the effect of tectonics on the sediment deposition across the shelf, slope and base of slope depocentres.

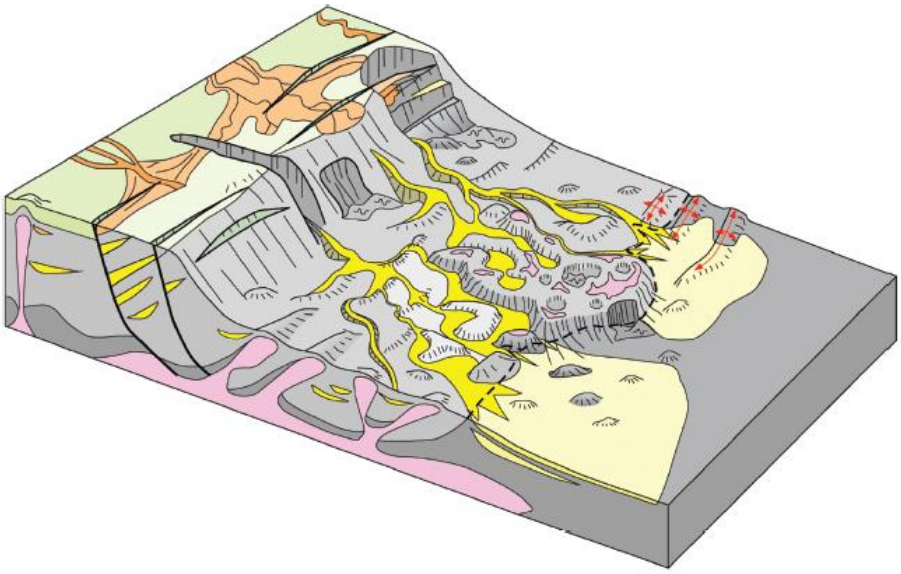

Figure 8.4: Schematic showing the structural controls on depositional systems on shelf, slope, and base of slope systems affected by tectonic. Orange represents fluvial deltaic system, sand dominated facies in yellow, basin floor fans in pale yellow, muds in grey and diapiric structures in pink. See the tortuous paths taken by slope channels around the diapiric structures (adapted from Mayall et al., 2010).

Many previous studies (Mayall et al., 2010, Dmitrieva et al., 2012, Gee and Gawthorpe, 2006, Dunlap et al., 2010, De Ruig and Hubbard, 2006, Cronin, 1995, Mayall and Stewart, 2000), have demonstrated the effects of positive relief features on the sea-floor, such as salt and mud-induced structural highs. These structural features either deflect or divert channels over tens of kiliometers, either forcing them to travel parallel to the slope axis for significant distances or simply deflecting channels locally from their downslope pathway. In some cases channels are known to cut through diapiric structures while continuing their downslope direction (Mayall et al., 2010). In either case, whether the channels are deflected away from the original course or observed to cut through structural features, their location is largely controlled by factors that include: the size, shape and orientation of the depositional slope; the erosive power of the flow; and the timing of the growth of the structural highs relative to time of channel development (Mayall et al., 2010).

The works of Mayall et al., (2010) on some Tertiary-aged channel complex systems in passive margin settings (similar to the tectonic setting of the study area), reported the

impact of structural sea-floor features on channel developments and the overall effect on timing of structural growth with respect to channel formation, where periods of growth and non-growth are recognised from onlap patterns and changes in thickness of the stratigraphy over and around the structural features. In their study they identified two groups of channel development in relation to structure: (1) channel development post-dating structures; and (2) channel development contemporaneous with structural growth. When channels post-date structural features they tend to thin and onlap against the salt wall and subsequently are deflected. On the other hand, when channel development is synchronous with structural growth, a range of channel responses can be recognised and this is significantly dictated by the rate of structural growth and the erosive power of the flows crossing the growing structures. When the energy of the channel flow cannot keep up with the rate of structural growth, the channels get deflected with the axis moving progressively away from the growing structure. Conversely, when the erosive power of the channel is significantly greater than the rate of the growing structure, the channel cuts through the growing structure and continues straight in its original downslope route. Although the examples cited above do not particularly show a change in form or geometry in channel development in relation to structural growth, abrupt change from a confined to a weakly confined or lobate morphology has been imaged in some deep-water settings.

Beaubouef and Friedmann, (2000) described successive downslope intraslope mini-basins in the Gulf of Mexico. The mini-basins were formed as a result of salt withdrawal and had become depocentres that are characterised by dramatic change in gradient. Channel geometry abruptly changes when approaching such depositional centres. Within such depositional centres, channels are noted to transit into an unconfined lobate feature that can appear either circular in salt withdrawal basins or elongate in mud induced mini-basins (Prather, 2003). An abrupt transition zone is observed between channels and lobes, where confined channels exit into slope depressions of lower gradient. At such transition zones the turbidity current expresses an erosional behaviour typically known as a hydraulic jump leading to rapid flow expansion and increased turbulence, which in turn results in erosion and sediment by pass (Wynn et al., 2002a, Gee and Gawthorpe, 2006, Prather, 2003). Hydraulic jumps are associated with a decrease in flow velocity, increase in flow depth, and a site for

possible erosion followed by rapid deposition (Gee and Gawthorpe, 2006). They are not only located at channel lobe transition zones (CLTZ) but also where canyons or channels experience a change in width and length due to sudden change in slope gradient.

Wynn et al., (2002) discovered well-developed channel lobe transition zones using side-scan sonar imagery across three different deep-water settings: the Lisbon fan off the margin of Lisbon, offshore Morocco in the Agadir Basin, and the Rhone fan in the Mediterranean Sea. All are characterised by erosional scour features of varying sizes. The images from the Lisbon canyon showed amalgamated scours at the transition of the Lisbon canyon into lobe that are deposited in the Tagus Abyssal Plain. The CLTZ of the Lisbon fan extends for over 40km. The scours are V-shaped and are generally aligned parallel with the main flow pathway. The Agadir CLTZ is up to 60km long from the canyon mouth, characterised by large scours occurring immediately downslope at a change in slope gradient. The 40km long CLTZ of the Rhone fan contains a series of erosional scours of various sizes with the largest scours being up to 20m deep and 1km long. These mostly occur in the region just downslope from the channel mouth. Smaller scours visible from the side-scan sonar image develop farther downslope about 30km from the channel mouth. Kolla and Macurda Jr (1988) documented that channel fill in the transition zones consist of abundant low amplitude discontinuous seismic facies owing to significant erosion taking place at the CLTZ.

Ponded accommodation of the Oligocene deep-water system

As documented in chapter 5, the interpreted 3D seismic data used in this study reveals that in the Oligocene, turbiditic flow in the study area was influenced and directed by mud ridges associated with locally compressional-extensional tectonics that have complicated the bathymetric relief at the seabed (Figure 5.10 of Chapter 5). Hence, lobe deposition occurred mainly in ponded mini-depressions (or mini-basins) located downslope of the channel terminus. Three channels (Channels A, B and C) of the four channels interpreted show downstream modification as they approach topographic lows induced by local mud withdrawal processes. A change from a confined channel system to an unconfined lobate morphology has been interpreted. In some cases the lobes are deposited between two mud-walls with onlap geometry against flanks even along the

downstream direction (Figure 8.3c). Based on this stratal relationship between the channel-lobe bodies and the mud cored-ridges, it is possible that the deformation of the sea-floor, related to gravity driven growth structures, modified the morphology of the slope prior to channel and lobe development. This is clearly manifested as the seismic amplitude becomes weaker from the lobe axis to margin towards the mud highs, indicating thinning of the lobes against the mud ridges (Figures 8.2 and 5.9 of Chapter 5).

Channel 'A' is oriented in an ENE-WSW downslope direction before encountering a mud ridge (top left Figure 8.2). it is therefore deflected into a N-S direction between separated mud ridges. It terminates to the south against the mud-wall shown in Figure 8.5. As the channel enters the mini-basin created by this topography it terminates as lobe deposits. These lobe deposits are ponded in accommodation space flanked by low mud ridges and a more prominent mud-wall. This mini-basin appears to be completely enclosed, so that as the accommodation space is filled with lobe 1, sediments over-spill and the depocentre moves southward leading to the deposition of lobe 2 into another mini-basin (Figure 8.5). Similar fill and spill process have been discussed by Prather (2003) as a dominant process on slopes with ponded intraslope basins particularly in the Gulf of Mexico. Highly reflective convergent-baselapping seismic facies character is diagnostic of such a fill-and-spill process, which is also prevalent across intraslope basins accommodating lobes 1 and 2 of this study. This high reflection event is thought to be indicative of high a sand:shale ratio that results from relatively high density turbidity current processes (Prather, 2003). The efficiency of such turbidity processes in sand deposition is controlled by the interplay between the heights of the flow entering the basin relative to the height of the outbound basin sill. If sill height is high relative to flow height both mud and sands would be ponded in the basin. But, where the height of the basin is shallower than the height of the flow, then sands are more likely to be confined within the basin while the finer grained silt and mud would over-top the basin sill (Prather, 2003, Posamentier and Kolla, 2003). Prather et al., (1998) and Booth et al., (2003) have both demonstrated this relationship in ponded basins in the central Gulf of Mexico.

A

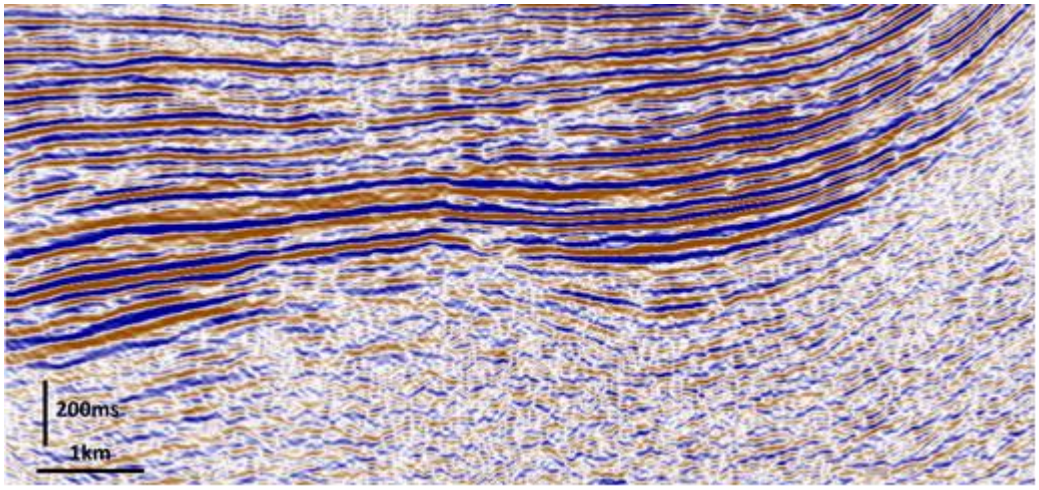

B

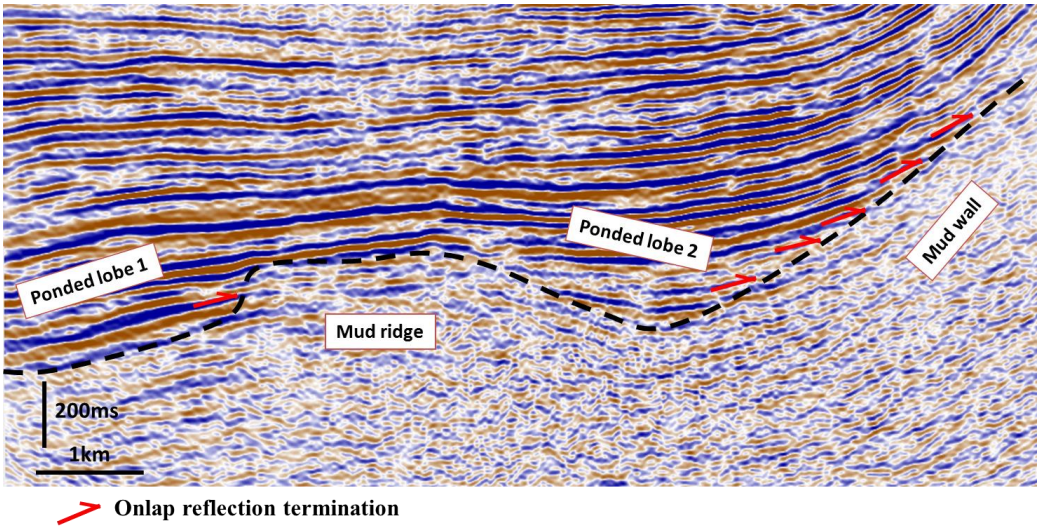

Figure 8.5: Vertical seismic profile across intraslope basins (a) uninterpreted, (b) interpreted showing lobes 1 and 2 pond. Line location is illustrated in Figure 8.2.

Also associated with channel A in the updip region, a splay-like depositional feature is seen breaching the channel wall and covering an approximate area of 30km^2. Such splay features are common along outer channel bends where flow momentum results in a high tendency for flow to overtop or breach the channel wall (Posamentier and Kolla, 2003). Defining this feature as a splay deposit is based on its stratigraphic relationship and its location being at the channel bend, which is typical of crevasse splay deposits. However, this low amplitude deposits might also be interpreted to be an earlier lobe deposit that has been eroded by the more recent channel A.

Similar to channel A, channels B and C show downslope ponding of sediments at their lower reaches (Figure 8.2). Although channel B appears to have low seismic amplitude, possibly related to a shale prone depositional fill, nevertheless it terminates in high-amplitude seismic reflection lobe sediments. Channel C on the other hand shows high amplitude features just as its downstream lobe. In addition, splay deposits covering a smaller area have been interpreted in channel C, forming updip of the channel. One key feature that characterises all three channel-lobe systems is the presence of abrupt transition zones (CLTZ) due to hydraulic jumps affecting flow between updip channels and associated downdip lobes (Prather, 2003, Haughton, 1994, Wynn et al., 2002a). Figure 8.2 shows the location of the CLTZ highlighted with a red circle marker. Deceleration coupled with spreading of sediment gravity flows beyond the CLTZ can result in fall-out of a substantial amount of entrained coarse sediment from turbulent suspension (Prather, 2003). In response to the collapse of gravity flow upon encountering a reduced slope gradient, sand deposition is likely to occur.

8.1.3 Implication of Oligocene lobe deposits for hydrocarbon exploration

Lobe complexes that occur downstream of channels are known to form good reservoir target for hydrocarbon exploration. Such plays are well known in the Gulf of Mexico (GOM) (Beaubouef et al., 2003, Beaubouef and Friedmann, 2000), the Campos Basin off the Brazilian margin (Moraes, 1989, Soldan et al., 1995) and in the Lower Congo Basin in Angola (Anka et al., 2009, Broucke et al., 2004) where they form excellent hydrocarbon reservoirs. They are known for their relatively high sand: shale ratio and being laterally extensive compared to channels. Their hydrocarbon content can be more easily produced from fewer wells or even better from horizontal wells. Ponded sands typically pinchout and onlap against diapiric walls forming updip stratigraphic traps that have been interpreted across the Oligocene depositional setting in this study (Figure 8.3C). Based on outcrop data, CLTZ are likely to be composed of amalgamated sands that connect updip channel facies to good quality sandy lobes located further downslope (Wynn et al., 2002a). The sand quality of the CLTZ is challenging to predict and coupled with being likely heterogeneous in nature, depending on the flow coming from the updip feeder channel. Hydrodynamic flow barriers are then likely to form at this CLTZ. Channels A, B and C in this study show very low seismic reflection amplitude at their CLTZ which suggests the presence of hemipelagic or shale rich area and hence the

possible compartmentalization of reservoir prone facies located both in lobes and updip feeder channels.

8.1.4 Lobe attributes

The attributes of lobes that might make them favourable reservoir targets are known to vary with the nature and scale of the submarine fan or slope apron system in which they occur (Reading and Richards, 1994, Stow et al., 1996, Shanmugam, 1998). These authors show clear differences between the lobes associated with large mud-rich fans (average lobe length 100km), mud/sand-rich fans (average lobe length 50km), sand-rich fans (average lobe length 20-40km), and gravel-rich fans (average lobe length 1-5km). The further implication is that the grain-size of individual turbidites on these lobes would be coarser on the smaller sand and gravel-rich systems and finer on the mud-rich systems. The overall net/gross ratio would also be higher in the smaller sand and gravel-rich lobes. These studies further highlight the fact that tectonic control on sea-floor topography can lead to small structurally-confined basins, which serve to focus the deposition of sand-rich lobes (e.g. Scott and Tillman, 1981, Armstrong et al., 1987).

In an effort to determine whether the Niger Delta slope-system lobes in this study may be more mud-rich or more sand-rich, a small compilation of lobe attributes has been made for comparison. The database includes four large mud-rich fans (Bengal, Laurentian, Mississippi and Amazon fans), an average of six small, coarse-grained fan-deltas (synthesis in Chough and Orton, 1995; and from Stow, pers. comm. 2015), and two examples where structural confinement of channel-lobe systems is evident (Lower Congo slope/fan and Gulf of Mexico slope basins). These lobe attribute data are shown in Figure 8.6. There are clear differences observed in the full range of lobe sizes and average values for net/gross ratios. The large mud-rich fans have *average* lobe dimensions of 55.5-90km long, 15.5-50km wide and net/gross of 0.25-0.6. By contrast the small fan-delta lobes are 0.5-2km long, 0.3-1km wide and with a net/gross of 0.85-0.9.

The Niger Delta system lobes of this study have dimensions of 6-8km long and 3-5km wide. These match closely with the other examples of confined lobes. It is reasonable to infer, therefore, that they may show a similar, relatively high net/gross ratio. This is a further positive attribute for their reservoir character potential.

Submarine Fans	High case		
	Width	Length	N/G
	km	km	
Bengal	50	90	0.3
Laurentian	40	70	0.5
Mississippi	40	80	0.6
Amazon	25	90	0.6
Fan-delta	1	2	0.9
Lower Congo	8	10	0.7
GOM	6	8	0.95
ND	5	8	?

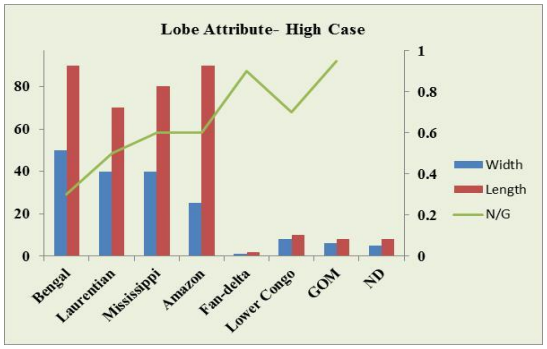

Submarine Fans	Mid case		
	Width	Length	N/G
	km	km	
Bengal	45	80	0.25
Laurentian	30	60	0.45
Mississippi	35	70	0.45
Amazon	15.5	55.5	0.45
Fan-delta	0.65	1.25	0.85
Lower Congo	6	7.5	0.55
GOM	3.5	5.5	0.7
ND	4	7	?

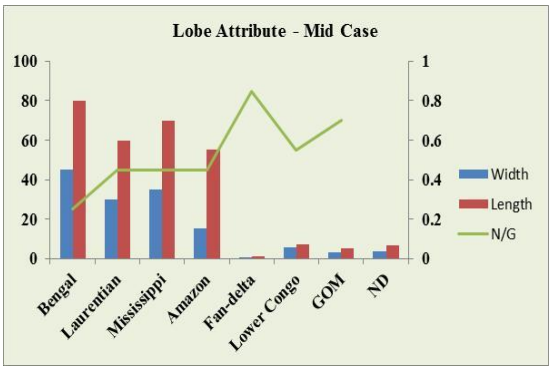

Submarine Fans	Low case		
	Width	Length	N/G
	km	km	
Bengal	40	70	0.2
Laurentian	20	50	0.4
Mississippi	30	60	0.3
Amazon	6	21	0.3
Fan-delta	0.3	0.5	0.8
Lower Congo	4	5	0.4
GOM	1	3	0.45
ND	3	6	?

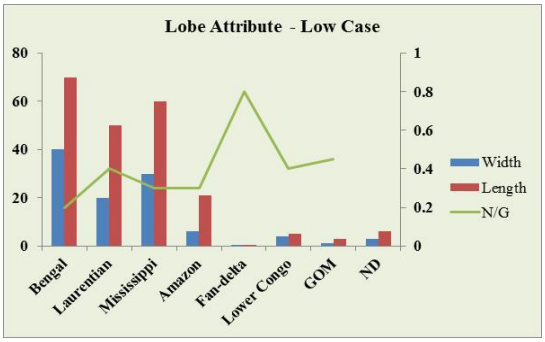

Figure 8.6: High, mid and low case lobe attribute values for three sets of lobe types: mud rich, fan delta, and confined lobes. Clearly the lobes of fan-delta and the confined lobes with smaller sizes (length and width) are characterised by high net-to-gross compared to the larger mud-rich fans.

8.1.5 Challenges with seismic interpretation within the study area

Considering that only one well penetrated the Oligocene-shallow interval and no wells have yet been drilled to test the Oligocene-deep interval, there exists some level of uncertainty. These uncertainties are mostly related to deciphering reservoir and fluid presence, which can only be confirmed with reasonable certainty from well data. Seismic mounding that has been used here as a key feature of lobe deposits can also be attributed to a variety of geomorphic features related to different geologic processes plus an array of seismic processing pitfalls. Other deposits that can also display

mounding include contourites, reefs, salt pillows, mud mounds, volcanic deposits and shelf edge deltas (Posamentier and Erskine, 1991). In addition, seismic artefacts arising from processing, such as diffractions and multiples, can also produce seismic mounding.

In comparison to other deep-water Oligocene system especially along the South Atlantic Margin, such as the Campos and Lower Congo Basin, where the Oligocene aged rocks are buried to depths of less than 2500m, the potential Oligocene reservoirs across the study area have been interpreted to be buried beyond depths of 3500m. This poses significant challenges in seismic interpretation as the resolution of seismic is known to depreciate with depth, leading to poorly resolvable stratigraphic and structural features. However, the seismic study suggests that there are potential reservoirs likely to be present within the Oligocene succession. These reservoirs occur mostly as laterally extensive lobate features with up-dip feeder channels.

8.2 Basin Modelling

Chapters 6 and 7 showed results from regional 2D basin modelling studies. Results presented in these chapters suggest that the Oligocene reservoirs have been buried to depth with temperatures in excess of 70˚ C, indicating that these sediments are within the quartz cementation window of 70-130˚ C (Taylor et al., 2010, Emery et al., 1993, Bjørkum et al., 1998). In these simulations through the application of the Walderhaug cementation algorithm (Equation 1 in Chapter 7), less than 14% of the pore volume in the Oligocene sediments have been occluded by quartz cement, leaving more than 86% of the pre-cementation pore volume available.

Since there were no cores acquired from the objective Oligocene interval even though the top of the Oligocene was penetrated by a single well (Well A1), an assumption was made that the potential Oligocene reservoirs have similar composition and textural properties as the Lower Miocene reservoirs. This has allowed the reconstruction of the burial history of the Oligocene reservoir while applying cementation processes in providing a new understanding of reservoir quality of Oligocene succession in deep-water western Niger Delta. Even though a base case present day reservoir quality for the

Oligocene succession has been predicted having less than 14% quartz volume, there still exist some uncertainties that are typically associated with the input parameters.

Considering that the key objective of the study is reservoir quality prediction, subsequent sections will show a revision of the key inputs, whose uncertainty affect the output property, and propagate the uncertainty in these input parameters throughout the model to the output property which in this case is the degree of quartz cementation.

Evaluating the sensitivity of results to the individual input parameters involves running a series of model simulations where each parameter is individually set equal to a likely maximum value and then a minimum value while keeping all the other parameter at a constant base case value. Maximum value also referred to as high case represent values of the input variable that would result in high cement volume, while minimum value or low case value would lead to a low cement volume. Base case herein represents the most likely input value that has resulted in a most likely volume of cement based on the available measured data. Four key parameters were considered, firstly because they are the main variables that control quartz cement calculations using the Walderhaug algorithm. Secondly, most of the base case input parameters such as grain size and grain coating were defined for the Oligocene reservoir by assuming similar values from the shallower Lower Miocene reservoir.

Uncertainty Range	Grain Size	Heat Flow (mW/m^2)	Grain Coating (%)	Facies
High Case	**Very Fine**	**65**	**0**	**Quartz Arenite**
Base Case	**Fine**	**53.3**	**0**	**Subarkose**
Low Case	**Very Coarse**	**35**	**1**	**Arkose**

Table 8.1: Summary of uncertainty ranges of variables considered in sensitivity study.

The variation in the amount of quartz cement present in space and time in the subsurface sediments is largely due to differences in grain size, quartz clast content, grain coating and thermal history (Walderhaug et al., 2009). These properties form the main input to the Walderhaug cementation algorithm. While sediment composition and

texture was assumed to be that of the Lower Miocene analogue, the thermal history was based on the 2D basin model that was well calibrated to measured physical properties acquired from Well A1. The initiation of quartz cementation in the Oligocene rocks began in the Early to Middle Miocene, during this time heat flow was at a constant value of about 53.3 mW/m^2. This was the heat flow utilised for the base case quartz cement volume.

Through a sensitivity study, the uncertainty in these properties has been tested, more so since there are no rock samples acquired from the Oligocene interval. The range of values (Table 8.1) considered through the sensitivity study was done objectively by constraining the values from other sedimentary basins where Oligocene reservoirs are confirmed hydrocarbon plays, particularly the Campos Basin of Brazil and the Lower Congo Basin in Angola, both of which are passive margin basins of the South Atlantic margin similar to the Niger Delta. The outcome of the uncertainty analysis is presented in the form of a tornado chart with results from the base case model as a point of reference.

8.2.1 Sensitivity analysis

Effect of grain size

Experimental evidence reveal that grain size is a major variable that influences the precipitation rate of quartz cement (Taylor et al., 2010, Lander et al., 2008). It is generally accepted that fine grained quartz undergoes more pressure dissolution than its coarser equivalent, so that where fine and coarse grained sands coexist as interbeds, then we expect that the fine grains would readily undergo pressure solution thereby sourcing silica reach pore fluid for quartz overgrowth (Worden and Morad, 2000, James et al., 1986, Porter and James, 1986). Finer grained particles are also most prone to overgrowth considering they have a larger surface area per volume exposed to quartz precipitation. Quartz surface area per volume plays a key role in controlling the net rate of quartz cementation. In addition to grain size, surface area is also controlled by the percentage of detrital quartz grains present and degree of grain coating (Lander and Walderhaug, 1999) (being discussed in subsequent sections).

The mean grain size assumed for the potential Oligocene reservoir in the base case cementation model was taken as 0.12mm indicating fine grained. This is the mean grain size value of the shallower Lower Miocene samples that formed an analogue for the un-cored Oligocene interval. Field data from the Lower Congo Basin indicates that the hydrocarbon bearing Oligocene reservoirs have grain sizes that span the spectrum of very fine to very coarse grained (0.125mm-2mm) (Delattre et al., 2004, Dessus and Abreu, 2002, Pelleau et al., 2002) while the Oligocene reservoirs of the Campos Basin are mostly medium to coarse grained (0.25mm -1mm) (Bruhn et al., 2003, Pinto et al., 2001, Souza et al., 1989). So the grain size was varied across these values as represented in Table 8.1. Grain size showed some significant control on cementation having the widest range in calculated cement (Figure 8.7 and Table 8.2). Using a grain size of 0.05mm representing a coarser silt size resulted in 19% of the pore volume filled with cement, whereas a grain size of 0.064mm (very coarse sand) corresponded to lower cement volume of 1.8% (see Figure 8.8 and Table 8.2).

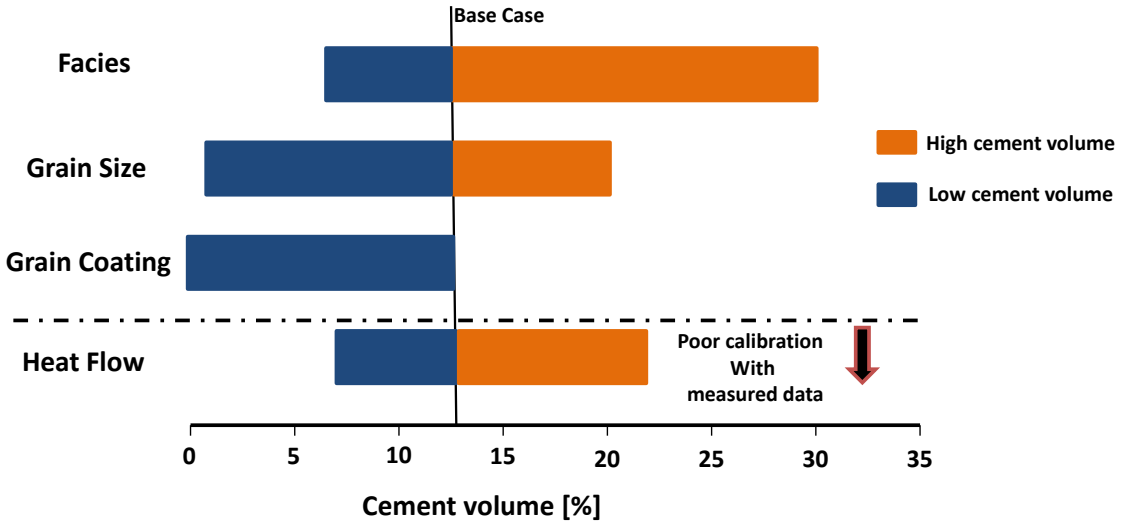

Figure 8.7: Tornado chart for total cement volume (%) within the study area. The parameters are sorted by the range of estimated average cement volume for each input parameter. Uncertainty in cement volume caused by uncertainty in heat flow shown below the horizontal dashed line has poor agreement with measured calibration data. Grain coating has a net positive effect on reservoir quality while facies has the most negative effect.

Cement Volume	Grain Size	Heat Flow (mW/m2)	Grain Coating (%)	Facies
High Case	1.8	22	0	30.6
Base Case	13.8	13.8	13.8	13
Low Case	19	8	13.8	6

Table 8.2: Summary of uncertainty in estimated cement volume based on sensitivity analysis of input parameters. Values are displayed in the form of a tornado chart in Figure 8.7.

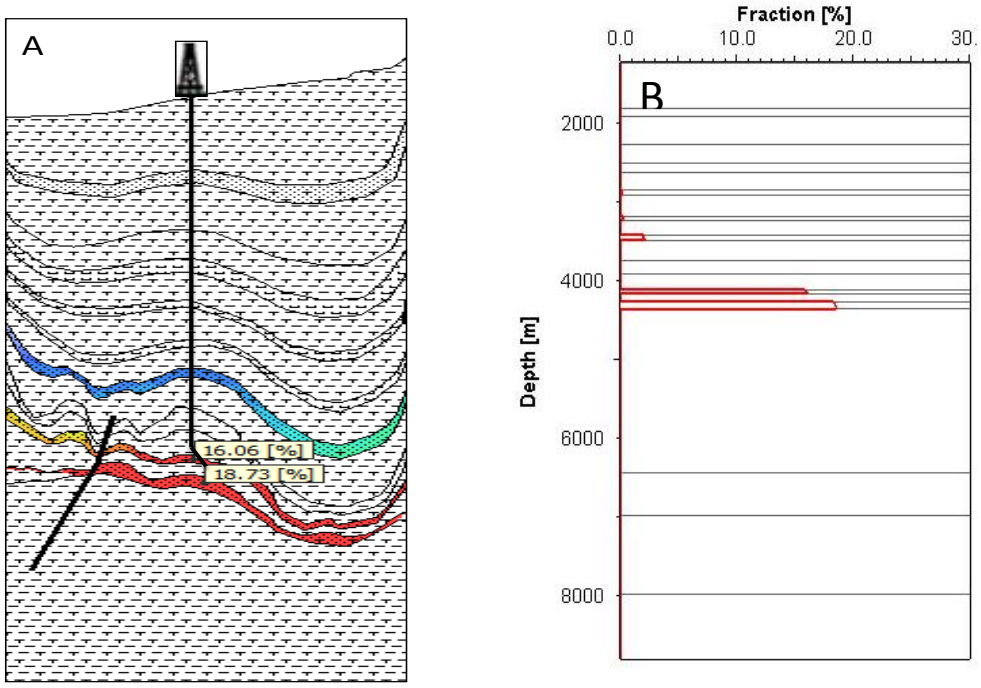

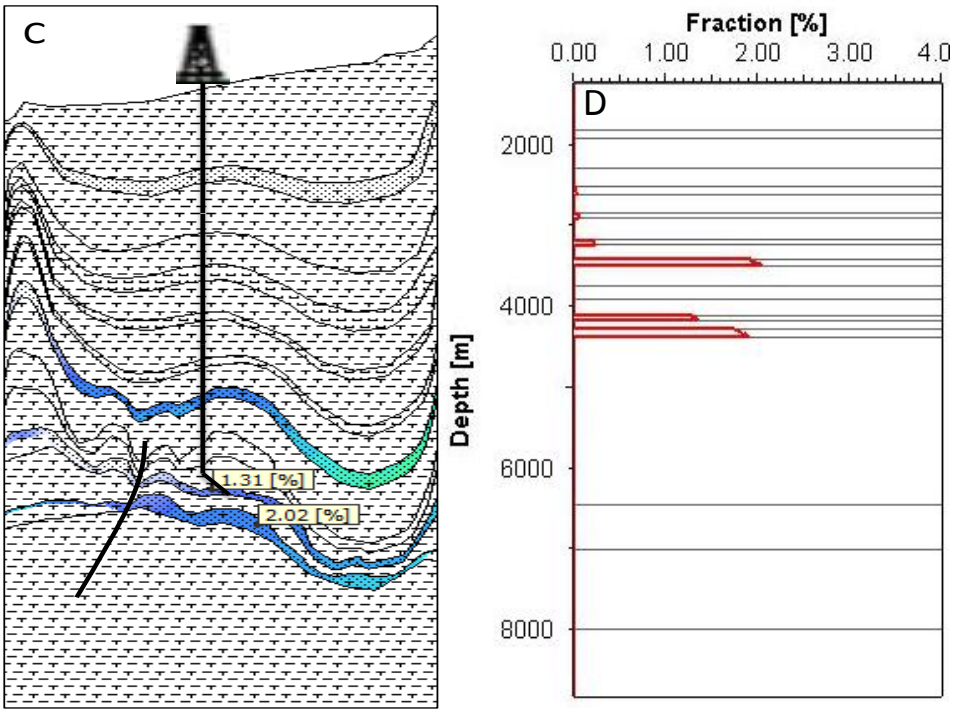

Figure 8.8: Sensitivity on grain size. A = 2D model for very fine grain size. Example of calculated cement volume for a cell is displayed in Oligocene-shallow and Oligocene-deep (lower two layers). B = 1D extraction of cement volume against depth at well location from A. C and D are the same as A and B but the sand grain size is very coarse grained. Note the decrease in cement volume from very fine to very coarse grain size.

Heat flow

The heat flow of any sedimentary basin is one of the essential requirements for any chemical transformation to occur in the subsurface as it determines the temperature window and the rate at which any given kinetic reaction occurs. Temperature thus influences quartz cementation in two main ways (Worden and Morad, 2000): (1) it is capable of affecting the stability of diagenetic assemblages resulting in geochemical reactions such as clay mineral diagenesis (for example, the conversion of kaolinite to illite) that leads to production of silica rich fluids; and (2) the rates of diffusion and precipitation of quartz, both of which are controlled by temperature. The heat flow in any sedimentary basin can be related to the basin's tectonic setting and subsidence history (Brenner et al., 1991, Worden and Morad, 2000), giving rise to a unique burial history. Hence the temperature range of quartz cementation depends on the subsidence history of the basin and the residence time of a rock unit within a certain temperature

interval. For example in a slowly subsiding cratonic basin, quartz cementation may occur during long residence times at relatively low temperatures of less than 100˚ C, while in passive margin basin with significant high sedimentation rate, cementation can take place in a short time since sediments are exposed to higher temperatures.

The heat flow history within the study area, which is in a passive margin tectonic setting, was modelled using the McKenzie heat flow model, so that peak heat flow of about 105 mW/m^2 was reached during the time of rifting (100Ma, see section X of Chapter 6). This gradually drops during thermal subsidence to a present day heat flow of about 53 mW/m^2. This was the heat flow model adopted in the base case cementation model that resulted in a cement volume of less than 14% of available pore space. Based on the work of Allen and Allen (2005), synrift heat flow values in a passive margin basin that typically range from 65 – 110 mW/m^2 were considered in the cementation model. By varying most especially the peak heat flow at 100Ma within this range, no change in cement volume was seen. However, when the heat flow was altered only during the Miocene (Figure 8.9) that marked the time of onset of quartz cementation (Figure 6.15B in Chapter 6), the calculated cement volume was significantly affected. The cement volume decreased when heat flow was dropped to 35 mW/m^2, and when heat flow was increased to 65 mW/m^2, still in the Miocene, the cement volume increased. Figure 8.10 illustrates these outcomes.

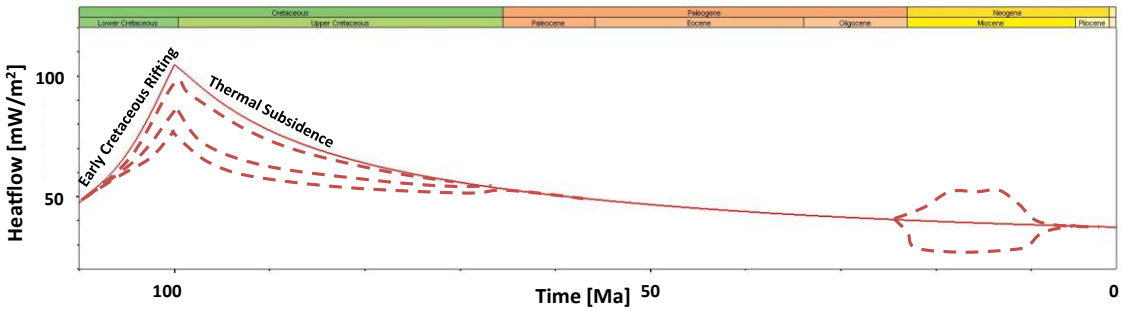

Figure 8.9: Heat flow scenarios considered (dashed curves) during sensitivity analysis. No change in calculated cement volume when heat flow is modified during the time of rifting (100Ma), since cementation did not start during this time. But significant change in cement volume is noted when heat flow is varied in the Miocene within the time of cement precipitation.

However, in either scenario whether by altering the peak heat flow at 100Ma or by adjusting in the Miocene to high or low heat flow values (relative to the base case value), they are both not justified geologically to fit a typical heat flow history of the area of the Niger Delta being studied. In addition both scenarios out-with the base case do not calibrate to measured temperature and vitirinite data. Notwithstanding, this goes on to show the significant impact of heat flow on quartz diagenesis where a change in heat flow value can result in a significant increase or decrease in calculated quartz volume.

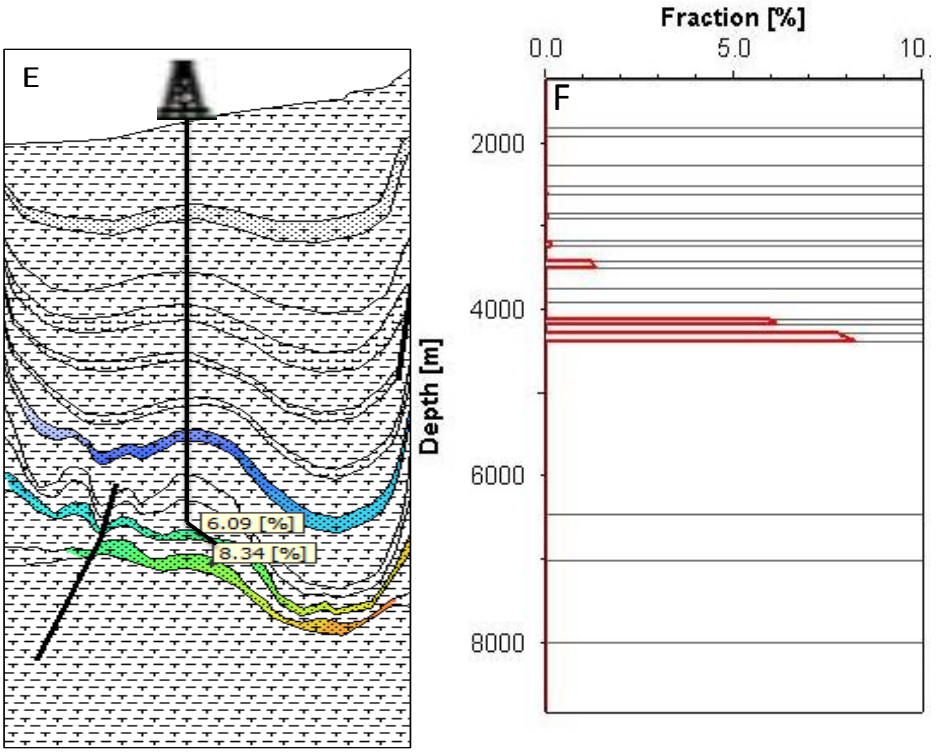

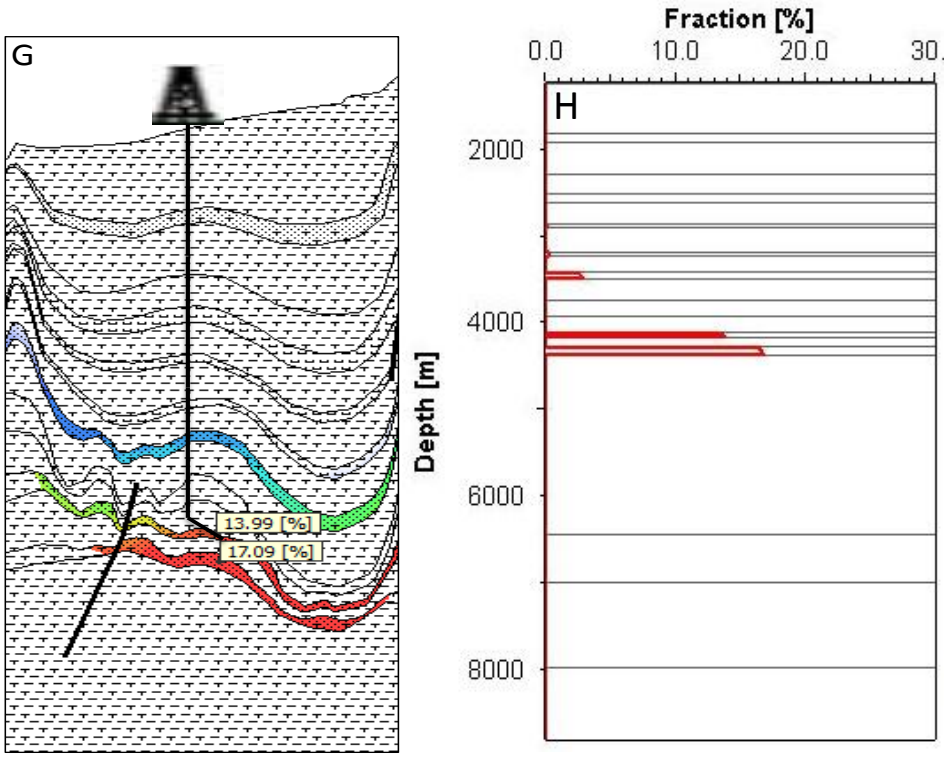

Figure 8.10: Sensitivity of quartz cementation to heat flow in the Miocene. E = basal heat flow at 35 mW/m^2. F = 1D extraction of cement volume against depth at well location from E. G and H are same as E and F but using High heat flow of 65 mW/m^2. Note the decrease in cement volume from coarse grain to very coarse grain size.

Grain coating

As discussed above under the grain size section, the quartz surface area available plays a major role in controlling the rate of quartz precipitation. The formation of grain coats on the surface of detrital quartz grain before the onset of quartz precipitation is thought to inhibit the formation of cement by forming a protective barrier or buffer that shields the detrital grain from wide spread nucleation of authigenic quartz (Taylor et al., 2010). For sandstones, the grain coating minerals that inhibit quartz precipitation the most are clay minerals and microcrystalline quartz. Iron rich authigenic chlorite coats have been reported (Bloch et al., 2002) to grow as a continuous layer that lines the interface between detrital grain and intergranular pore space. On the other hand, Aase et al. (1996) documented the presence of microcrystalline quartz in the Upper Jurassic sandstones in the Central Graben area of the North Sea that is responsible for anomalously high porosities of close to 27% at depth of c.4000m. Microcrystalline

quartz is known to be no more than 15µm thick with randomly orientated crystallographic c-axis that prevent their merging into larger syntaxial quartz overgrowths. Based on experimental analysis it is thought that growth rates of quartz overgrowth on microcrystalline quartz substrate are much slower than on a monocrystalline quartz substrate (Lander et al., 2006).

In this study, the Miocene samples observed in both scanning electron microscope (SEM) and optical microscope studies did not show any evidence of possible grain coating that would have preserved porosity, particularly in the Lower Miocene samples. Since the base case model assumes rock properties of the Lower Miocene as properties for the Oligocene, a zero coating factor in the base case model was applied. However by systematically increasing the coating factor from 0 to 1 where 1 represents grains that are 100 percent coated, the volume of quartz cement is observed to decrease steadily for each increase in coating factor. So for 100% grain coating a zero cement volume is predicted (Figure 8.11), while for zero coating, which suggests that the entire grain surface is exposed to quartz cement, less than 14% pore space is predicted to be occluded by cement (base case model).

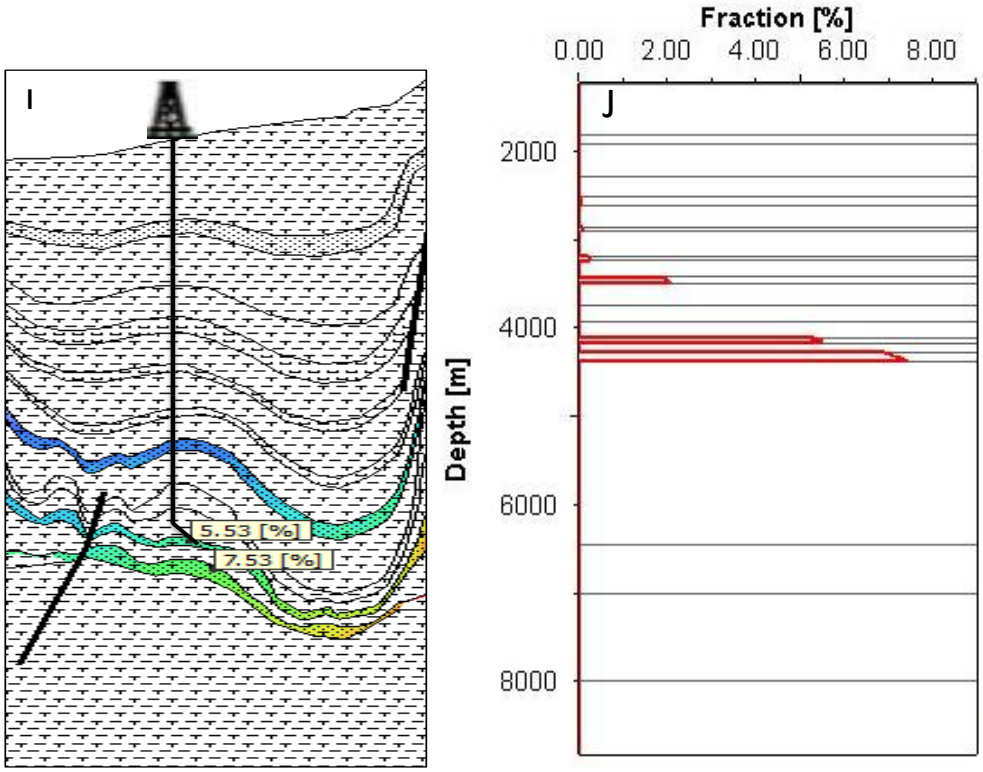

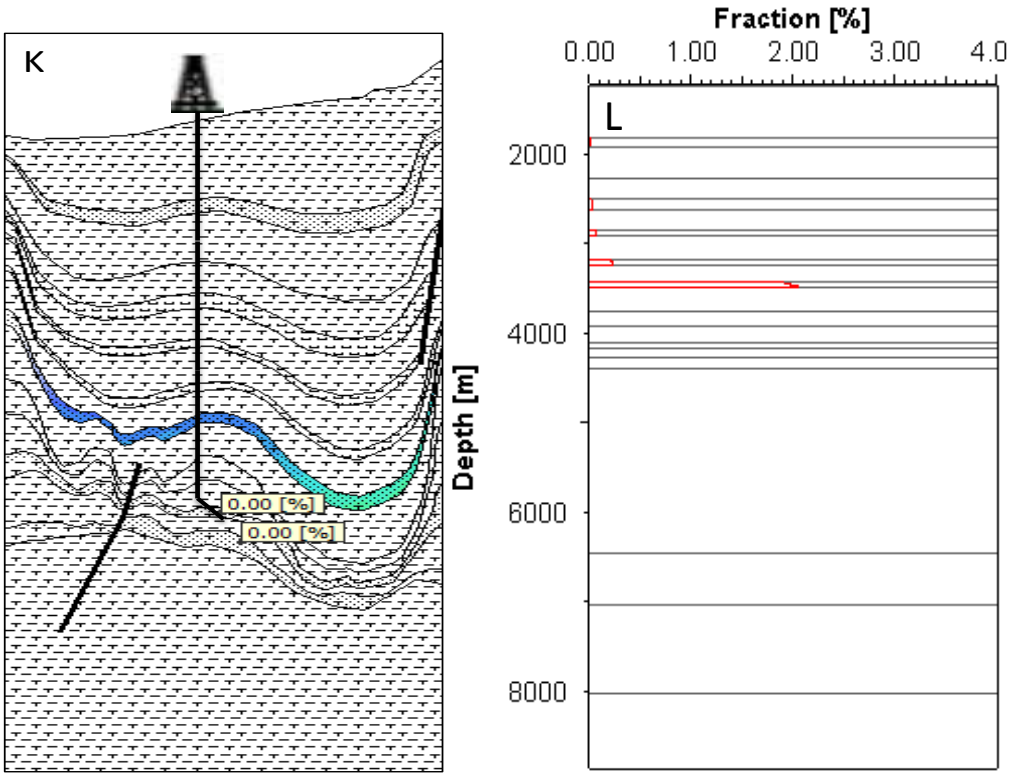

Figure 8.11: Sensitivity to grain coating. I = 50% grain coating. J = 1D extraction of cement volume against depth at well location from I. K and L are same as A and B but sensitized on 100% grain coat. Note that 100% grain coat results in 0% cement volume.

Sediment composition

A major control on authigenic quartz precipitation is the mineralogical composition of sandstone, which itself is controlled by the following factors: sediment source or provenance, depositional environment, relative sea level, extent of chemical weathering, etc. (Worden and Morad, 2000, Loucks et al., 1984, Bloch et al., 1990). The detrital composition of sand determines its chemical and physical properties. This in turn controls the pattern of diagenetic alterations both under low temperatures at near surface conditions and with increased burial depth associated with rise in temperature (Mansurbeg, 2007). For instance, mineralogically immature sands rich in micas, volcaniclastic and argillaceous rock fragments, can lead to a greater chance of minimizing quartz cement. This is because the lithic fragments are subject to ductile deformation during burial, which causes filling of pores and covering of detrital quartz grain with 'pseudo-matrix' (Primmer et al., 1997). On the other hand, an increase in original detrital quartz contents in environments where extensive reworking has produced compositionally more mature quartoze sands, can lead to a corresponding

increase of authigenic quartz cement as overgrowths. This also depends on the prevailing temperature condition, the relative absence of other pore filling cement such as early calcite cement and also the relative absence of pore filling clay minerals and grain coating authigenic minerals (Worden and Morad, 2000).

The mineralogical composition adopted for the Oligocene reservoir in the base case cementation model was based on the composition of the Lower Miocene samples being the deepest interval cored in the study area. Petrograhic evidence as highlighted in Chapters 4 and 7 reveal quartz-rich subarkoses with an average framework grain composition to be $Q_{85}F_{10}L_5$ (Q-quartz, F-feldspar and L-Lithic fragment). This composition closely matches the composition of the Oligocene reservoirs in the Lower Congo Basin of Angola, which have an average grain composition of about $Q_{80}F_{10}L_{10}$ (Delattre et al., 2004). But for the Campos Basin in Brazil the composition of the sands are noted to be feldspathic arenites (*sensu* Folk 1974 classification scheme) with QFL indices that averages $Q_{60}F_{40}L_{tr}$ (Moraes, 1989).

Since no core was acquired from the Oligocene reservoir penetrated by well A1, alternative lithological compositions were considered by adopting, for the basin simulation, the composition of deep-water Oligocene reservoirs from the Campos Basin and further assuming an extreme case of quartz arenite with about 95% quartz composition. A high dependency of the volume of quartz cement on varying facies is observed from the tornado chart (Figure 8.7) with systematic increase in calculated cement volume as the percentage of quartz increases from feldspathic arenite (typical of the Campos Basin) through subarkoses (seen in the Oligocene of the Lower Congo Basin and Lower Miocene of this study and adopted for the target Oligocene sediments) to quartz arenite (Figure 8.12).

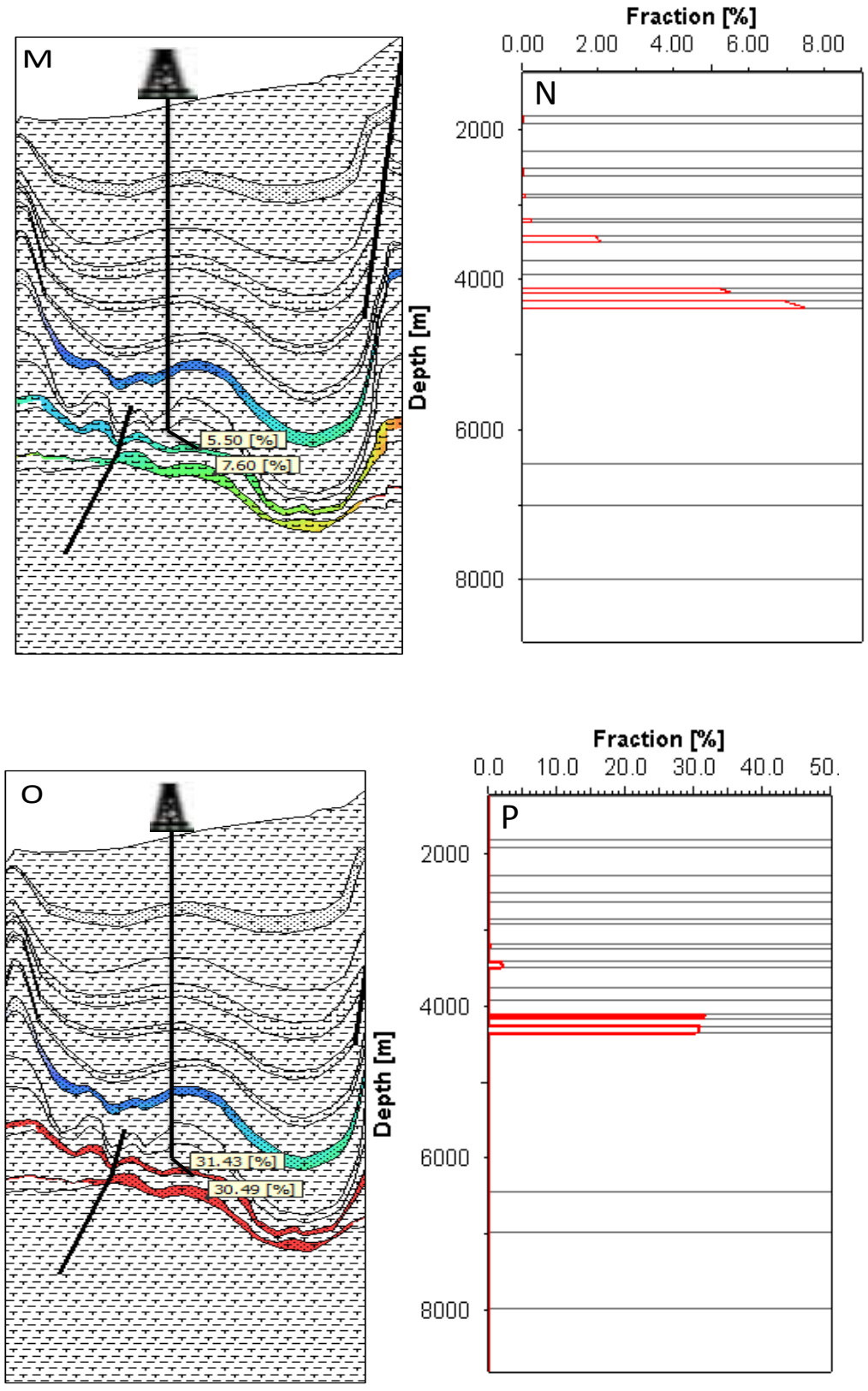

Figure 8.12: Sensitivity to sediment composition. M = 2D model with Oligocene sand of Arkosic composition. N = 1D extraction of cement volume against depth at well location

from M. O and P are same as M and N but sensitized on quartz arenite. Note the dramatic increase in cement volume from arkosic to quartz arenite composition.

Overall the parameters in the tornado plot are sorted by decreasing range of cement volume based on the uncertainty window defined for each parameter. So input parameter uncertainties producing the widest range in model results are displayed at the top of the plot, which in this case is the sediment composition/facies. However, considering that the ultimate concern is the impact of cement volume on reservoir quality, particularly porosity, another way of representation might be sorting by the minimum cement volume which relates to a likely higher estimated porosity. The degree of grain coating and grain size distribution could therefore be considered to be the most important variables that can lead to a better reservoir quality of the Oligocene sediments (Table 8.2).

Of the four parameters considered in the sensitivity analysis, only adjustments made in the heat flow produced results outside the range of the calibration data. This indicates that the heat flow changes made are not in agreement to any geological process(es) that have taken place or affected basin development or sedimentary fill over geologic time.

Facies distribution

In addition to assuming that the target Oligocene reservoir has the same sedimentological properties (facies, grain size, etc.) as the deepest cored Lower Miocene reservoirs, another major assumption is that the reservoir facies defined in all stratigraphic levels in the 2D model were laterally extensive upslope and downslope of the well A1 location. The lack of well control away from the main study area was the major factor responsible for applying this assumption, not being sufficient to establish a detailed facies model. However, the assumption allowed inferences to be made on the possible reservoir quality if sandstones were present outwith well A1 location. A simulation run was carried out based on a scenario where sand pockets are defined laterally at regularly intervals while maintaining the reservoir presence at well location (Figure 13). This approach was particularly considered in the section that covers the deep marine realm beyond the shelf where it is expected that sediment remobilization processes would lead to punctuated-type distribution of sediments.

This model still showed good calibration at well A1 location with calculated parameters matching nicely with measure data from the well. This is actually expected as lithological distribution has not changed at the well location between model types (that is, the model with lateral continuous reservoirs and the sand pocket model). In addition, modelled cement volume at the well location also remains very much like the initial base case model. But away from the well, where sands have been replaced by shales, no obvious quartz cement is seen. However, the consequence of having shales adjacent to sand pockets is a higher volume of calculated quartz cement in the sands. Shales affect the distribution of heat and so temperature by acting as a poor conductor of heat. The heat retained in shales is easily dissipated to the neighbouring sands thereby promoting an increase in quartz cement. For example, downslope of well A1, reservoir pockets of the Oligocene deep have a calculated higher cement volume compared to the base case (Figure 8.13B and C).

A

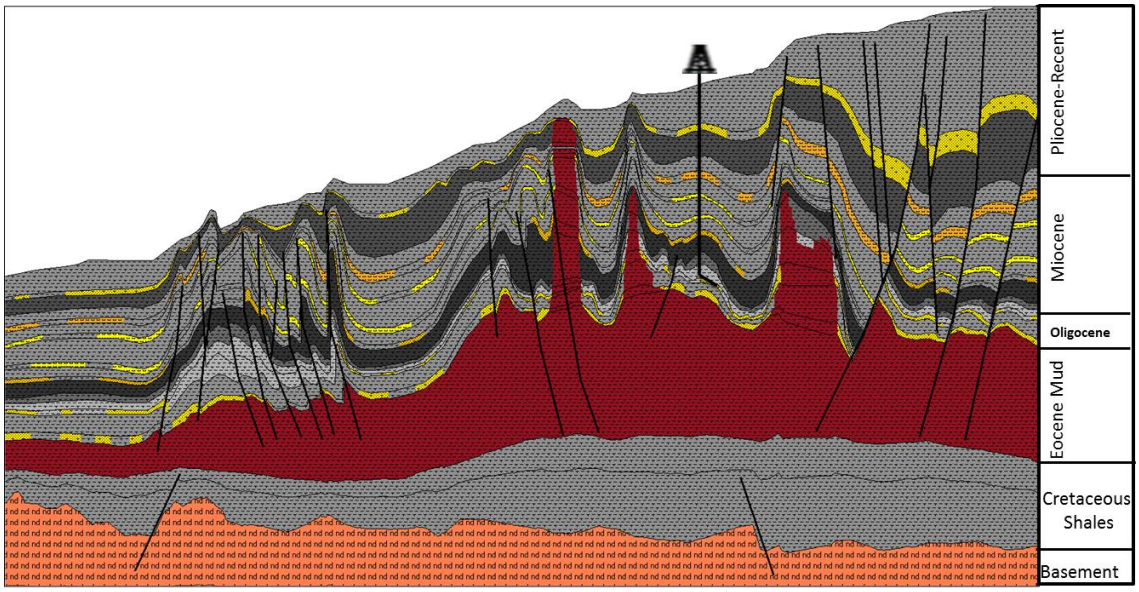

B

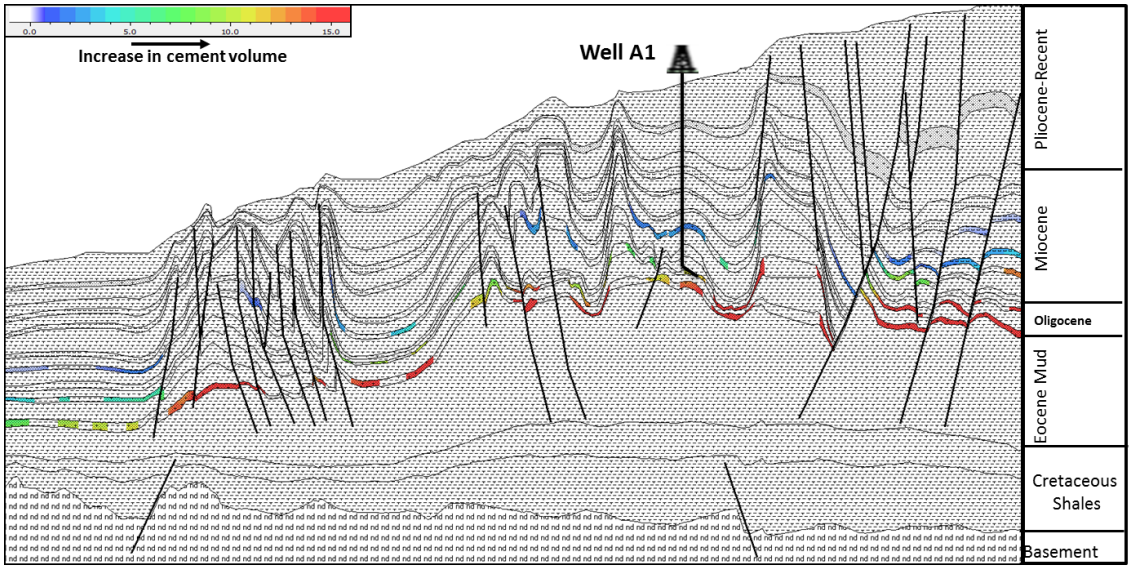

C

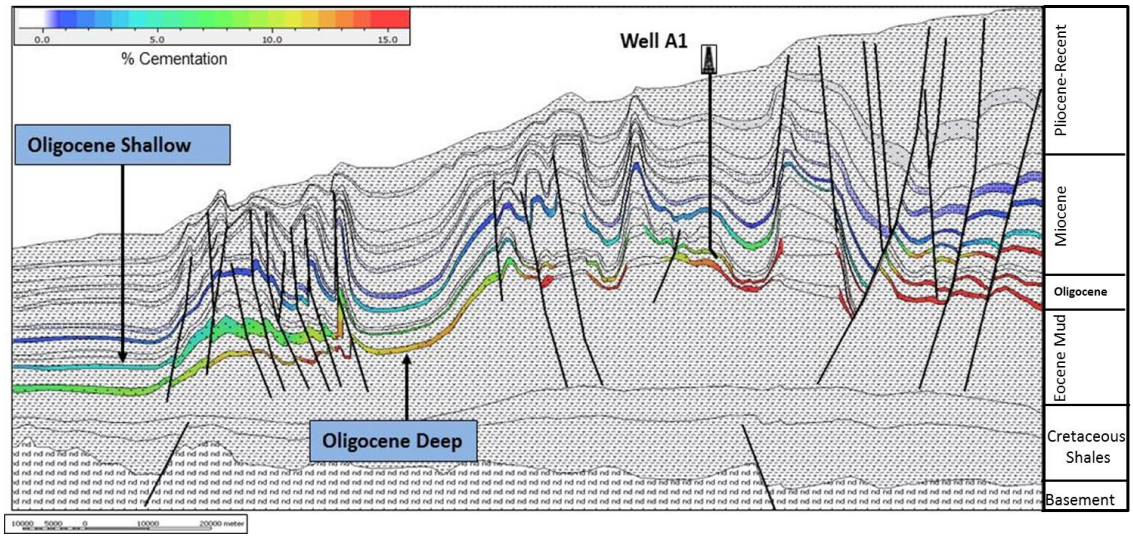

Figure 8.13: Model modified with sand distributed as pockets. A = Input model; sands are in amber and yellow colour. B = Simulated model showing calculated volume of cement. Calculated cement volume at well location is similar to base case model. C = Base case model shows lower cement volume calculated in Oligocene-deep reservoir. For example reservoirs located where the 'Oligocene Deep' arrows points, the cement colour map at that location reveals a lower cement volume than that calculated at the same location in the sand pocket model.

8.2.2 Hydrocarbon emplacement

The concept of early hydrocarbon emplacement slowing down or completely halting the precipitation of autigenic cement thereby preserving porosity has been widely debated. One school of thought agrees with this hypothesis based on numerical (Walderhaug, 1994) and theoretical models (Worden et al., 1998) plus field observations (Neilson et al., 1996). Their argument is based on the assumption that the invasion of a reservoir by hydrocarbon results in the displacement of water from the reservoir so that the advective transport of silica to sand essentially stops due to low relative permeability to water (Taylor et al., 2010, Honarpour et al., 1986). They support this argument with evidence of higher porosities observed in oil (gas) legs of reservoirs compared with extensive cementation below the oil water contact of the same sand reservoir (Neilson et al., 1996).

Evidence of hydrocarbon bearing fluid inclusions in quartz, albite and carbonate cement is noted as an evidence to the contrary (Taylor et al., 2010), proving that cementation continues to some extent in the presence of hydrocarbon. Ehrenberg and Nadeau (1989) reported the presence of illite showing no significant change in abundance across several oil water contacts. This suggests that the precipitation of illite still continuous even after hydrocarbon emplacement. The difficulty in adequately establishing the effect of hydrocarbon emplacement on reservoir quality can be traceable to the lack of conventional core from the water leg. This prevents adequate comparison of cement volumes, porosity types, grain size and sorting and sand composition between the oil and water intervals of a reservoir (Taylor et al., 2010, Bloch et al., 2002). The likely difference in the burial and thermal histories across the two compartments is also a major factor that needs to be considered.

An initial step in linking reservoir quality to hydrocarbon presence is to understand the relative timing of quartz cementation and maturation of source rocks since both processes rely heavily on the degree of thermal exposure. While the initiation of quartz precipitation begins from about 70˚ C, the rate of conversion of kerogen to oil typically starts from about 60˚ C and peaks at approximately 110-140˚ C, but this is largely a function of source rock types (Pepper and Corvi, 1995).

A base case model was built in this study that considered the relative timing of hydrocarbon emplacement to quartz cementation in the Oligocene reservoirs. This model reveals that quartz cementation predates hydrocarbon charge for most of the accumulations (accumulations 1 to 4) that were predicted in the basin model, except for "accumulation 1". In this case the hydrocarbon charge is synchronous with cementation at approximately 20Ma (Figure 8.3A and B). However, by considering the time of peak hydrocarbon charge, herein portrayed as peak hydrocarbon saturation, it is observed that the time of peak hydrocarbon saturation at 16Ma (accumulation 1) and 8Ma (accumulations 2-4) predates the time of significant volume of precipitated cement (Figure 8.14A). Hence no more than 5% of the pore space would have been cemented when peak hydrocarbon saturation was reached (Figure 8.14B). Thus, if we assume that under conditions of high hydrocarbon saturation, advective transport of silica into sands stops or slows down as the relative permeability to water reduces (Taylor et al., 2010, Honarpour et al., 1986). It implies that the Oligocene reservoirs are likely to have their porosities preserved because of early hydrocarbon emplacement. Sensitivity analysis was not done on parameters that are tied to petroleum systems modelling, especially source rock properties, since these parameters have no one-to-one relationship on quartz cement prediction. Therefore, building scenario models centred on the timing of hydrocarbon charge was not considered. Furthermore, the current version of PetroMod^{TM} software mathematically simulates hydrocarbon emplacement and cementation modelling as two independent processes so that the effect of one process does not in any way result in a corresponding effect on the other process. Although a sensitivity study on source rock properties and maturity was not considered in this study, its impact on time, volume of hydrocarbon generated and subsequently charged to reservoir still plays a significant role in assessing the reservoir potential of the Oligocene succession. For example, the age of Akata shales have been defined as Eocene, however, based on the diachronous nature of the Niger Delta Stratigraphy (Doust and Omatsola, 1990), it is likely that this source could be younger, possibly Oligocene age. If the Akata shales are modelled as Oligocene in age, with the thermal history of the basin remaining constant, it likely the Akata shales would not be buried sufficiently into the oil window to have sourced the volume of hydrocarbon seen today. And the effect of early hydrocarbon emplacement preserving porosity might be minimal.

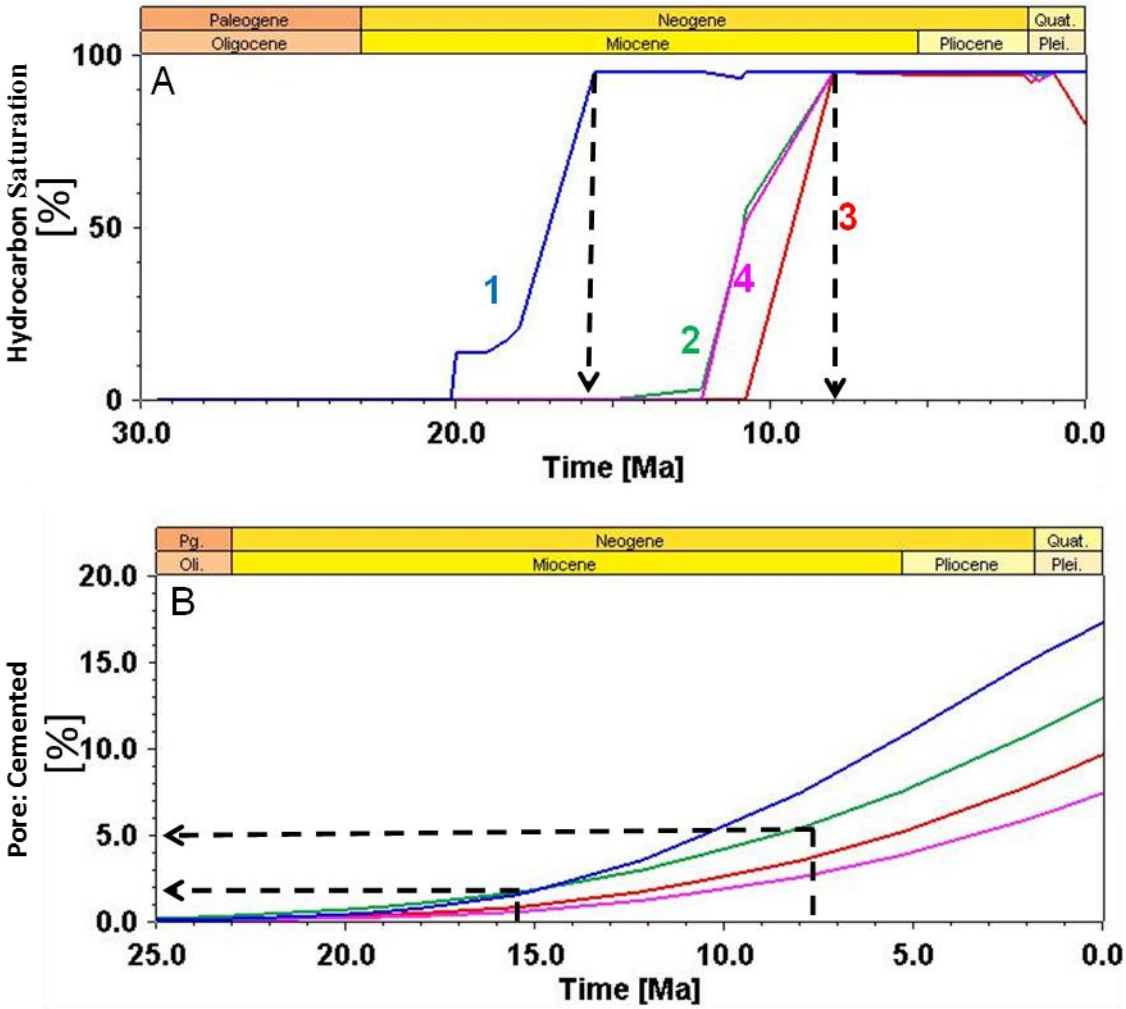

Figure 8.14: Illustrates a comparison between time of charge and time of cementation. A = time of hydrocarbon emplacement showing peak hydrocarbon saturation at 16 and 8Ma. B = time of cementation. Superimposing both plot suggests that peak hydrocarbon saturation (downward pointing arrows) predates time of significant quartz cementation. Not more than 5% (arrows in B) volume is likely to be precipitated at peak saturation.

8.3 Diagenetic Analysis

A diagenetic assessment across the study area has been conducted on samples acquired from the Miocene section. Optical microscopy and SEM formed the main techniques that were used. In addition, to further characterise the mineralogical assemblage present in the sample, EDX (Energy-dispersive X-ray spectroscopy) technology was used for elemental analysis of the samples, which further confirmed the mineralogical constituents of the sampled intervals.

With limited samples from the Miocene reservoir available for diagenetic analysis plus absence of rock samples from the target Oligocene sediment, there exists a significant level of uncertainty, which can only be reduced as more information or data becomes available. Hence, to fine tune the results of the model predictions discussed in previous sections, the sections below will be considering the wider implications of the diagenetic signatures observed in the study, particularly how the observations in this study align to the diagenetic (paragenetic) sequence expected in similar tectonic settings eleswhere.

All of the samples subjected to petrographic analysis were from the quartz-rich Miocene section, for which the average mineralogical composition across is noted to be $Q_{85}F_{10}L_5$. Minor heavy minerals were also detected.

8.3.1 Deep-water diagenesis

Studies show that the type, extent and distribution of diagenetic alterations in deep-water turbiditic sandstones are significantly controlled by the type of tectonic setting whether in a passive margin or active margin setting. Sediments in these two settings would experience different diagenetic processes (Brenner et al., 1991, Mansurbeg, 2007, Mansurbeg et al., 2006, Galloway, 1984, Primmer et al., 1997). In either situation the type of diagenetic product is known to differ with depth as temperature and pore fluid chemistry changes, particularly in a clastic depositional environment. Morad et al. (2000)**,** define two diagenetic realms that are characterised by suites of diagenetic products, these include the eodiagenesis and mesodiagenesis realms. Eodiagenesis is defined as the zone at or near the surface of sedimentation where the chemistry of interstitial water is dominated by surface meteoric water prior to being completely sealed off after effective burial has been achieved (Schmidt and Mcdonald, 1979). The eodiagenesis realm is characterised by temperatures below 70˚ C and burial depth of less than 2km. Mesodiagenesis occurs at depths and temperatures beyond 2km and 70˚ C respectively (Salem et al., 2000).

This classification is also similar to the classification of Galloway (1984) that distinguished three hydrogeologic regimes: meteoric, compactional and thermobaric. The meteoric regime is in constant contact with meteoric water and therefore is considered to be an open system. The compactional regime is characterised by

continuous expulsion of water during compaction with no continuous source of water recharge, hence this zone is considered a closed system. So also is the thermobaric regime a closed system as it is characterised by the release of mostly water expelled from diagenetic processes such as during clay mineral alteration (Brenner et al., 1991). Both classification schemes appear to be similar, and both highlight the influence of changes in pore fluid chemistry with depth on diagenetic products. However, the Morad et al., (2000) classification tends to merge the meteoric and compactional regimes of Galloway (1984) as a single eodiagenesis realm, while the thermobaric is akin to the mesodiagenesis realm. The Morad et al., (2000) classification is adopted in this study due to its simplicity and direct relationship to deep-water systems.

Diagenetic alteration in passive margins

In the eodiagenesis realm, key phases of diagenetic style characterise tubidites in a passive margin setting (Mansurbeg, 2007, Morad et al., 2010). These include:

1) Mechanical compaction expressed by grain rearrangement and breakage, plus plastic deformation of ductile minerals such as micas.
2) Dissolution and kaolinitization of detrital silicates, primarily feldspar and micas mostly occurring in channel and basin floor sands. Where these deep-water sediments form in response to fall in sea level, dissolution and kaolinitization are abundantly manifested in lowstand system tracts (LST) of passive margin basins, where the influx of meteoric water into deep-water turbidites is supported by major sea level fall (Figure 8.15). Meteoric water incursion into sandstones is known to induce eodiagenetic dissolution of framework minerals and is commonly associated with the formation of kaolinite (Mansurbeg et al., 2006, Giles et al., 1992).
3) Calcite cementation of sandstones, particularly below marine flooding or maximum flooding surfaces as a result of the long residence time of sediments below the flooding surfaces. This results in enhanced diffusion of dissolved carbon and calcium ions from overlaying seawater.
4) Development of secondary porosity in sandstones by the dissolution of calcite cement, promoted by the influx of meteoric water. This preferentially occurs in coarser and more permeable sandstones than in finer grained and less permeable ones.

5) Formation of grain coating minerals like microquartz, siderite and some clay minerals such as chlorite. As discussed in previous sections, the presence of grain coating preserves primary porosity by inhibiting cementation.
6) Formation of glauconite just below the sea-floor, enhanced by relatively low sedimentation rates. There is debate as to whether glauconite is formed within the deeper basin or in the outer shelf region and then remobilized downslope.

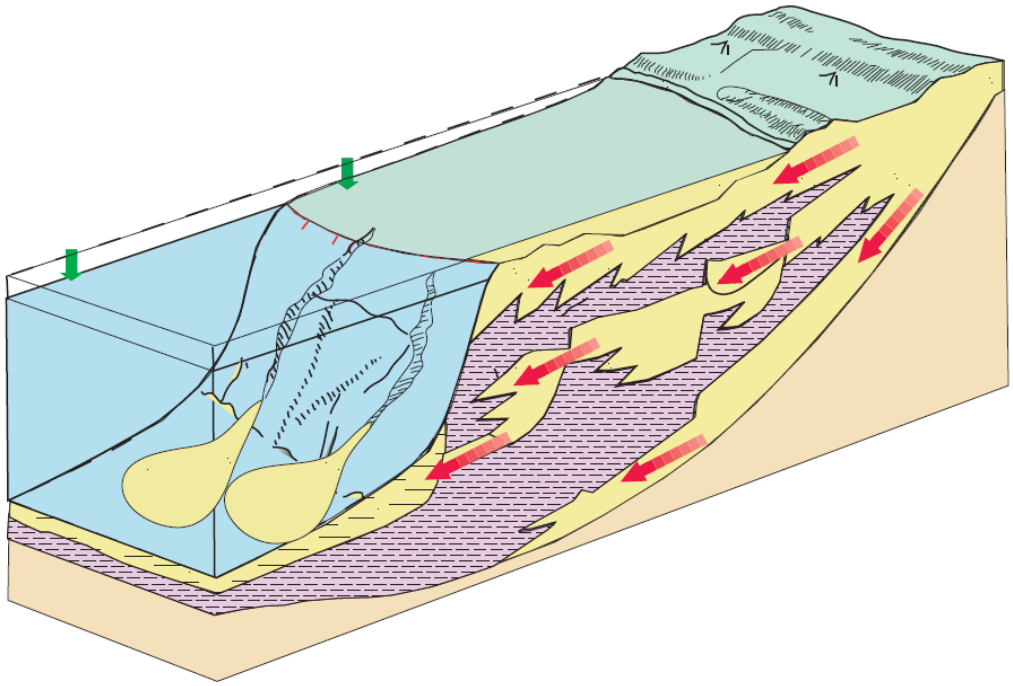

Figure 8.15: A schematic model illustrating the influence of meteoric water incursion (red arrow) into deep-water sediments during major sea level fall in a passive margin basin (adapted from Mansurbeg 2007).

The diagenetic pattern within the mesodiagenetic realm is influenced to an extent by the initial eodiagenetic influences on the sandstone prior to deep burial into the mesodiagenetic zone. Typically the main diagenetic processes prevalent in the mesodiagenetic realm for passive margin basins include the following:

1) Alteration of clay minerals such as the transformation of kaolinite into dickite and the illitization of smectite. This conversion takes place under increase in burial depth and temperature and is usually enhanced by acidic water originating from maturation of kerogen (Morad et al., 1994).
2) Precipitation of quartz cement as overgrowth and porefilling, with pressure dissolution being a key source of dissolved silica required for quartz

cementation. Both quartz cementation and pressure solution are known to be significant at a temperature range of about 90 - 130˚ C (Walderhaug, 1996), although quartz precipitation is known to begin from about 70˚ C.

3) Albitization of detrital plagioclase and potassium feldspar grains. Albitization of these minerals is known to commence at a temperature window of 70-80˚ C.

Diagenetic alteration in active margin settings

In comparison to passive margins, active margin basins display the following diagenetic processes and products in the eodiagenetic realm:

1) Mechanical compaction of ductile sedimentary and metamorphic rock fragments that can completely destroy depositional porosity and permeability.
2) Formation of minor amounts of non-ferroan dolomite cement, pyrite and calcite cement. Carbonate cementation is significant in the presence of detrital calcite and would normally take place below marine flooding surfaces.
3) Absence of glauconite in turbidites due to high sedimentation rates that would establish an iron reducing geochemical zone below the sea-floor (Mansurbeg, 2007).

Typical diagenetic alteration for turbidite sandstone in the mesodiagenitic realm includes albitization of detrital plagioclase and the precipitation of quartz, calcite and Fe-dolomite cement.

8.3.2 Diagenetic sequence of the study area

The results presented in Chapter 4 of this thesis show that most of the samples acquired from the Miocene reservoirs have all undergone a similar diagenetic history. Understanding what the diagenetic sequence is in the Miocene, will aid in understanding the likely diagenetic alterations in the target Oligocene interval. This is also supported by adopting the Morad et al., (2000) classification scheme of diagenetic alteration processes and associated products across the eodiagenetic and mesodiagenetic realm of a passive margin basin as summarised above.

Samples subjected to petrographic examination were from the Middle and Lower Miocene reservoirs that are buried within a depth range of 2470 to 3450m. The majority of the samples analysed were from the Middle Miocene intervals, drilled at

depths between 2470m to 2784m. The depth at which diagenetic products first occur differ across Middle and Lower Miocene reservoirs with some samples having unique features. Major diagenetic events in the burial history of the Miocene turbidite sandstone of the studied interval are: (a) mica and feldspar dissolution and precipitation of kaolinite; (b) siderite cementation; (c) mechanical compaction, and (d) quartz cementation (see Section 4.3, Chapter 4).

Kaolinite is present in both Mid-Miocene and Lower Miocene samples in small quantities particularly in the Lower Miocene sample (less than 5%). Although speculative, based on SEM study (Chapter 7 of this thesis) it appears that kaolinite occurrence in the Mid-Miocene reservoir was synchronous with oil charge. This inference is supported by the co-occurrence of both oil and kaolinite over detrital quartz grains. In the Lower Miocene the kaolinite occurs as a pore filling authigenic mineral that appears to compromise primary reservoir porosity (Chapter 7).

A first and only occurrence of siderite is noted at c.2540m (8333 ft) in the Middle Miocene within distinct laminae (Figure 8.16). In some instances, siderite occurs between mica laminae aiding the preservation of micro-porosity within fibrous strands of mica, through prevention of mechanical compaction (Figure 8.17A and B). In addition, siderite is seen as grain coats rimmed around detrital quartz grains (Figure 8.17A and C) capable of preventing the nucleation of quartz overgrowths. Siderite precipitation is thought to be triggered by anaerobic bacteria methanogenesis through the consumption of organic matter and reducing Fe^{3+} in the unconsolidated sediment and producing Fe^{2+} and HCO_3^- required for siderite precipitation (Dution et al., 1996). Hence siderite occurrence is evidence of an early diagenetic mineral phase. Duiton et al., (1996) reported the presence of siderite in submarine fan sandstones of the Sonora Canyon gas play in Verde Basin Texas. Their work reveals significant preservation of intergranular porosity to early siderite occurrence on quartz grains, which would have inhibited mechanical compaction and precipitation of quartz cement.

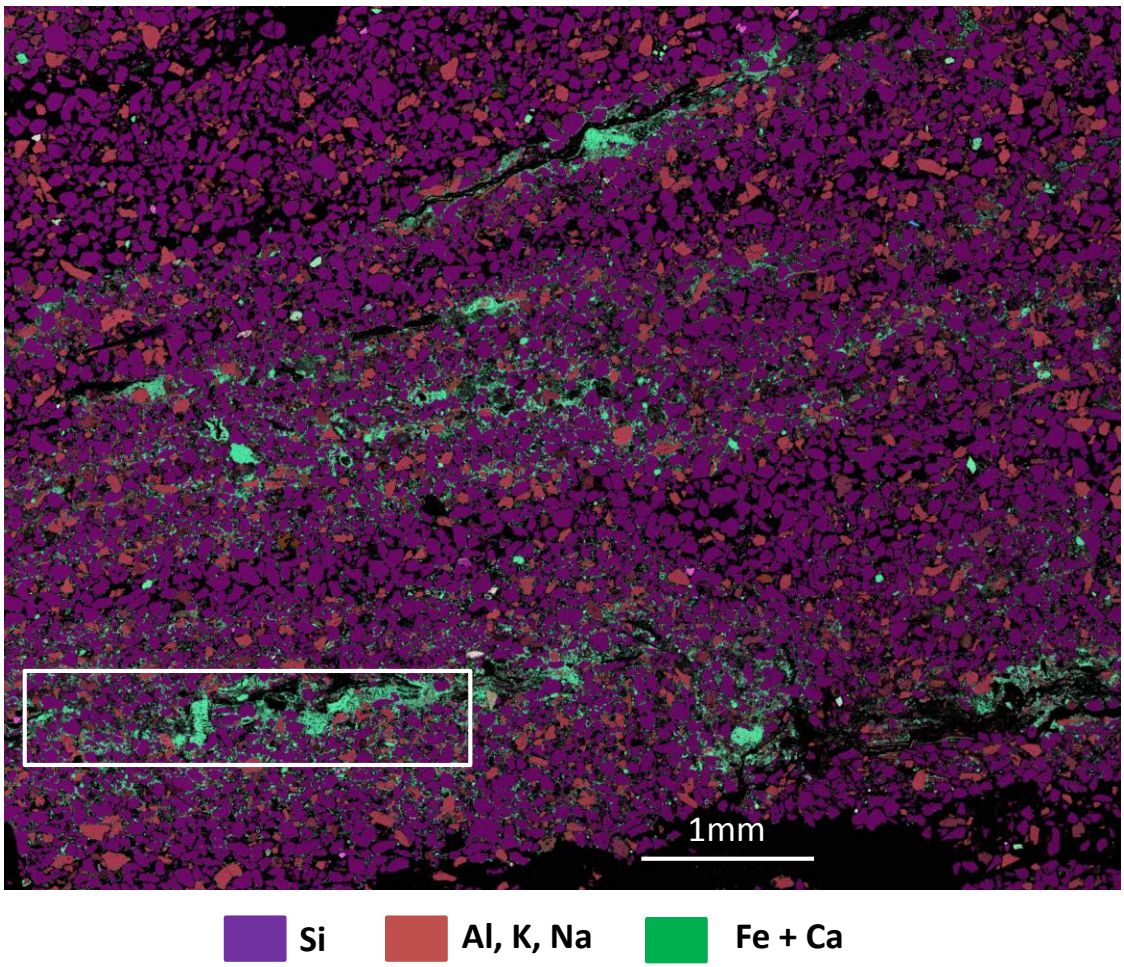

Figure 8.16: EDX map showing the distribution of quartz and feldspar with siderite laminae. EDX shows the distribution of elements contained in each of the minerals. Silicon (Si) indicates quartz in purple; brown represents a combination of Al, K and Na (Aluminium, Potassium and Sodium), which are the major constituents of feldspar; green indicates the presence of iron (Fe) and some calcium (Ca) representing siderite. Black represents resin or uncharacterised particles. The area in the white square represents the section analysed using the BSE image (Figures 8.16A-C).

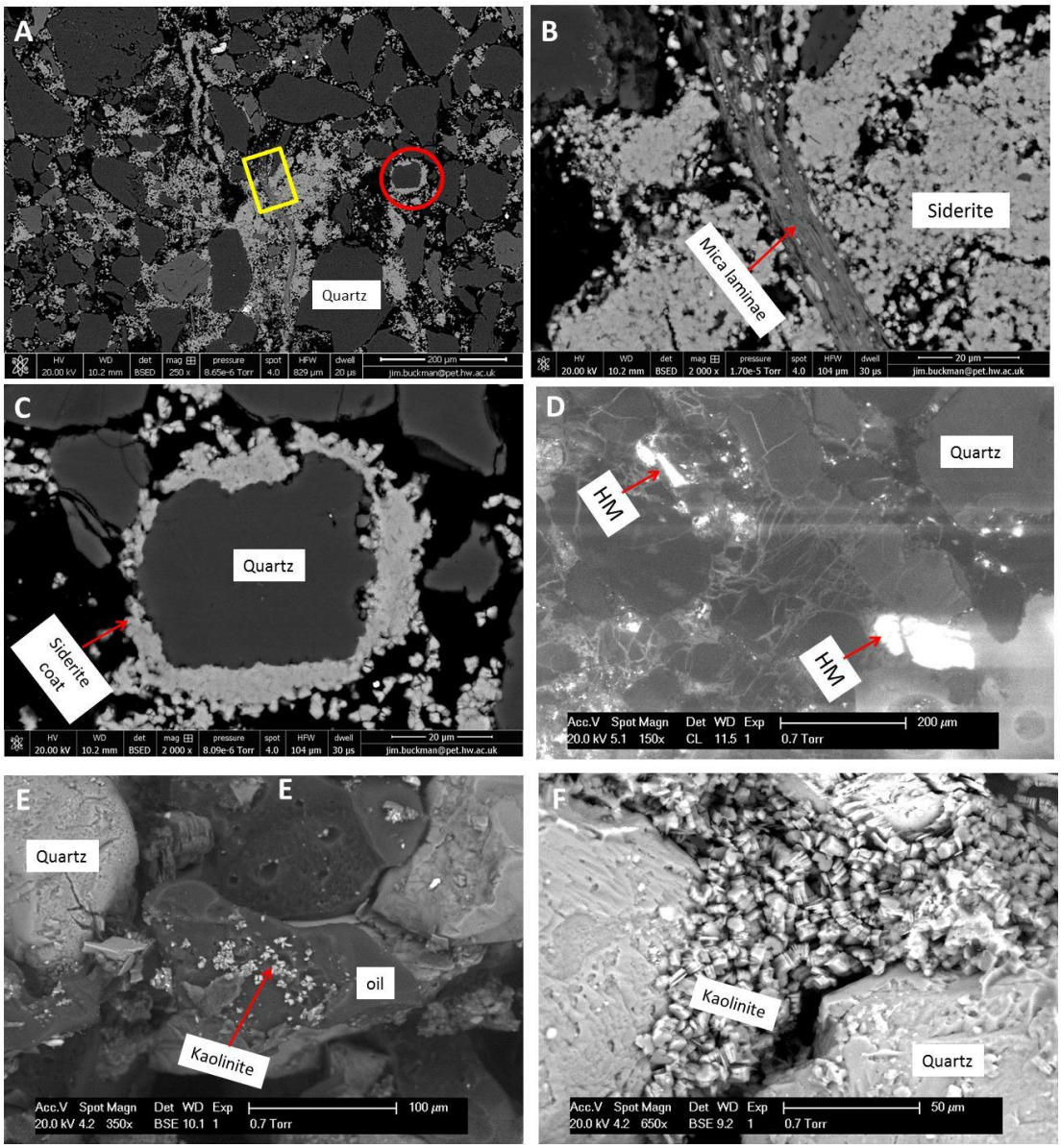

Figure 8.17: Photomicrograph showing the main authigenic mineral assemblages in the eodiagenetic realm. Photos A-E represents Mid-Miocene samples while F is from the Lower Miocene reservoir. A = BSE image showing detrital quartz grain with abundance of mirco sized particles of siderite plus mica. B = zoomed in area of the yellow square from 'A' showing authigenic siderite between bent mica laminae. C = zoomed in version of area in red circle from 'A' illustrating quartz grain coated with siderite. D = CL image showing intense fracturing of detrital quartz and highly fluorescent heavy minerals (HM). E = SEM image showing oil and kaolinite on quartz grain. F = Pore space filled with kaolinite.

Quartz cement in the sandstones is very minimal in the studied samples, occurring as patchy syntaxial overgrowths that extend into surrounding pore space of the Lower Miocene reservoirs. This reservoir is located at a depth of c.3450m (11320ft). Quartz

overgrowth, as shown in Figure 8.18, varies in extent from incipient to pervasive that fully covers the detrital quartz. A rare occurrence of quartz overgrowth is also detected in the Mid-Miocene sample that is located at c. 2470m (8130ft.). Figure 8.19 illustrates the presence of overgrowth in the Mid-Miocene sands using superposition of BSE and CL imaging techniques. Solely relying on the BSE image does not fully characterise the mineralogical constituents of the sample. By using the CL technique the presence of quartz overgrowth protruding into pore spaces is clearly demonstrated. The images tagged 'MIX' integrate both CL and BSE images; here a good demarcation is made between quartz and feldspar and also between oil and resin (area within the blue border).

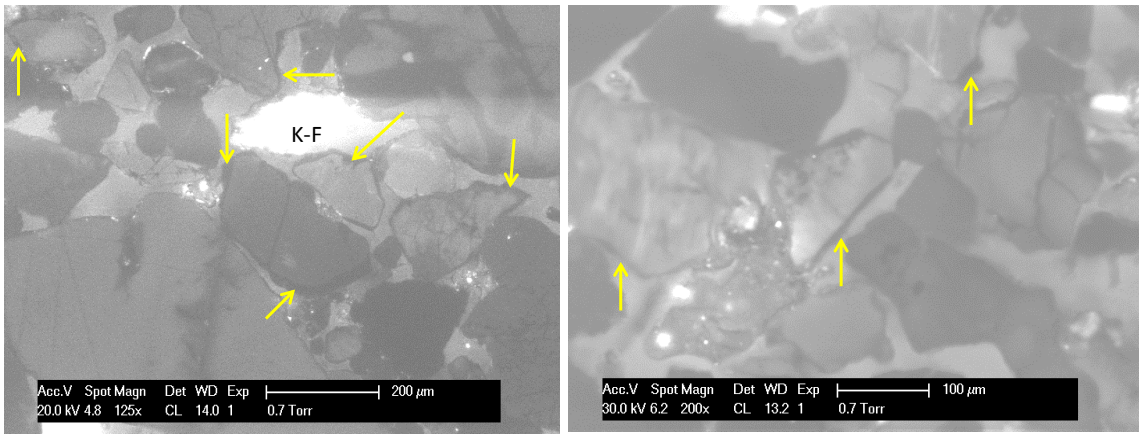

Figure 8.18: CL images of the Lower Miocene showing locations of overgrowths with yellow arrows.

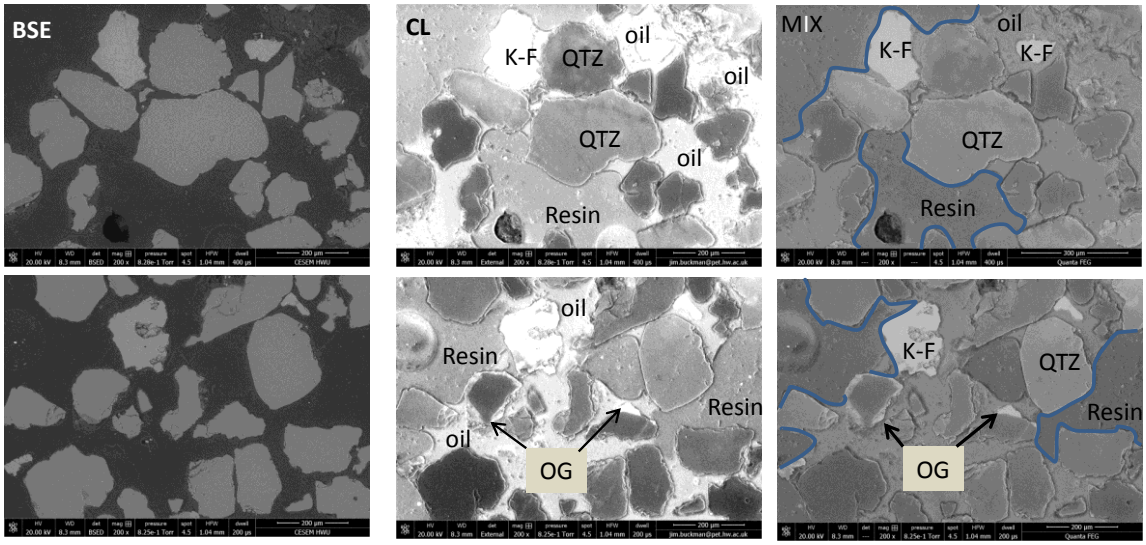

Figure 8.19: Mineralogical discrimination of Mid-Miocene reservoir using the BSE and CL imaging techniques. KF = potassium feldspar, QTZ = detrital quartz, OG =

overgrowth, MIX = CL+BSE. Blue boundary defines the area covered by resin, nicely illustrated on the MIX image.

Overall the samples analysed indicate the reservoirs have mostly been subjected to early diagenetic conditions of the eodiagenetic realm, yielding sparsely distributed diagenetic alteration products. This suggests that mechanical compaction is the main porosity reducing process. The effect of mechanical compaction is indicated by the bending of mica grains and grain fracturing (Figures 8.16B and D), particularly obvious in the Middle Miocene reservoir. The greater abundance of quartz overgrowth in deeper sandstone is consistent with the cementation modelling studies documented in chapter 7 that highlights the importance of temperature as one of the key factors necessary for quartz precipitation. In most sedimentary basins, considerable amounts of quartz overgrowths are precipitated during deep burial diagenesis within the mesodiagenetic realm at temperatures greater than 70˚ C (Worden and Morad, 2000, McBride, 1989). However, one of the samples of the Mid-Miocene reservoir examined using an integrated CL and BSE approach reveals the presence of quartz overgrowths at an unusual depth of 2480m at temperatures of less than 50˚ C. The actual cause of a rare occurrence of quartz cement at this temperature is beyond the scope of this work, however, similar observations have been made by McBride et al., (1988) documenting the precipitation of quartz overgrowths at temperatures of less than 50˚ C in Miocene sandstones located offshore Louisiana.

8.3.3 Implication of diagenetic sequence on the potential Oligocene reservoir

The overall diagenetic signature that is revealed from the studied samples indicates that eodiagenetic alteration processes typical of a passive margin setting characterise the Miocene reservoirs. The Miocene reservoirs have been buried to depths of less than 3500m, where mechanical compaction is the main driving force of reservoir quality. As burial depth increases it is likely that mechanical compaction would give way to more chemically driven diagenetic processes. This is particularly noted with the increase in quartz overgrowth from Mid-Miocene to Lower Miocene which thus suggests that the potential Oligocene reservoirs are within the mesodiagenetic realm where temperature conditions are suitable for significant quartz precipitation and therefore could be affected by quartz overgrowth. Basin and cementation modelling discussed in the

section above also supports this claim revealing from the burial history that the Oligocene reservoirs have been exposed to temperatures above 70˚ C suitable for quartz cementation. This claim does not however, take into cognisance other diagenetic alteration processes like grain coating that can preserve porosity even at great depth. But this would depend on the eodiagenetic processes that the Oligocene sediments have been subjected to prior to being buried within the mesodiagenetic window, since grain coats are typically products of early diagenesis. In addition, the influence of overpressure and hydrocarbon emplacement is not really reflected in the Miocene reservoir, although with a burial depth of less than 3500m and temperatures of less than 70˚ C, quartz precipitation is thought not to be a major problem and therefore overpressure and early hydrocarbon emplacement might not play a significant role in the reservoir quality of the Miocene. However, for the Oligocene that is buried at greater depths with a higher probability of quartz cementation, the effect of early hydrocarbon emplacement, if present, is likely to preserve the reservoir quality of the Oligocene sediments. The effect of early hydrocarbon charge has been discussed in Section 8.2.2 above. Similarly, if the Oligocene sediments have been subjected to early overpressure during its burial history, then higher than expected porosity can be encountered.

8.4 PETROPHYSICAL CHARACTERIZATION

The petrophysical evaluation conducted in this study involves the estimation of derived rock properties aimed at assessing reservoir quality. Such reservoir properties include net-to-gross (N/G) evaluation, porosity (Ø), water saturation (S_w), permeability (k) and elemental mineral estimates. Reservoir properties for the Miocene were constrained from core data and well logs acquired from 8 wells (See Figure 3.7 of Chapter 3 for well locations), while the petrophysical evaluation of the objective Oligocene sequence were based only on one well (Well A1) that penetrated the top of the Oligocene.

8.4.1 Miocene reservoir properties

Generally, the Mid-Miocene interval is noted to be of very good reservoir quality, with N/G based on log analysis of about 90% and net thickness of about 25m (80ft) (Figure 8.20A). This is also confirmed from the density-neutron cross-plot (Figure 8.20B). Density-neutron cross plot forms a strong lithological identification tool based on three pre-defined end member lithologies: sandstone, limestone and dolomite (see Section 4.5

of Chapter 4). The plot shows most of the data plotting in the vicinity the sandstone lithology line (Figure 18.9B). Following the interpretation of the seismic data (Chapter 5) revealing the Miocene play as a channel complex system, the thick sand units encountered by the well is typical of channel axis deposits. Continuous core acquired across the Miocene permitted the calibration of evaluations done on wireline logs. Estimated average log porosity weighted on reservoir thickness as encountered by each well varies from 25% in the Lower Miocene to 35% in the Mid-Miocene. The clean nature of the Miocene sands seen from core information and log data allowed the use of Archie model in calculating water saturation with a weighted average value of 12% (S_w). Hence it was not necessary to apply a shaly sand model in estimating water saturation. Average S_w was weighted on porosity and thickness of the reservoir as encountered by each of the wells. The water saturation plus porosity formed a major input to the calculation of permeability based on the Wyllie and Rose algorithm (See Equation 3, Chapter 4). The calculated porosity and permeability from well logs showed good agreement to the conventional core permeability (See Figure 8.20A-tracks 6 and 7).

A

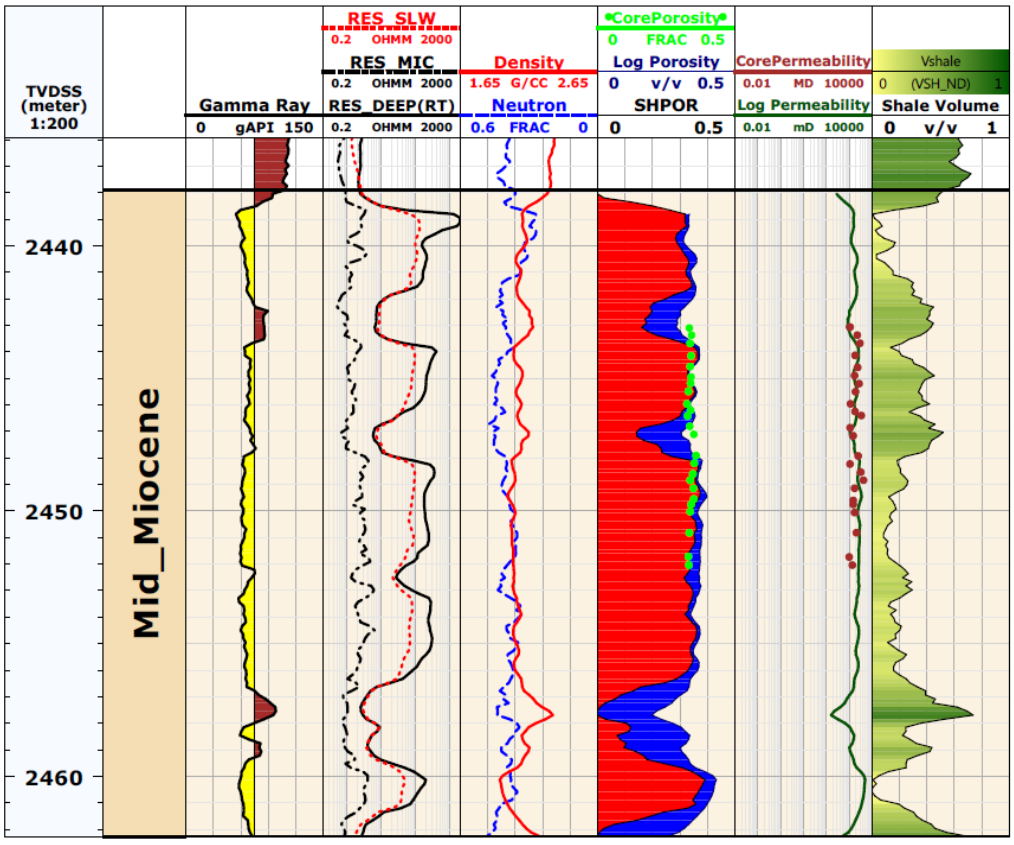

B

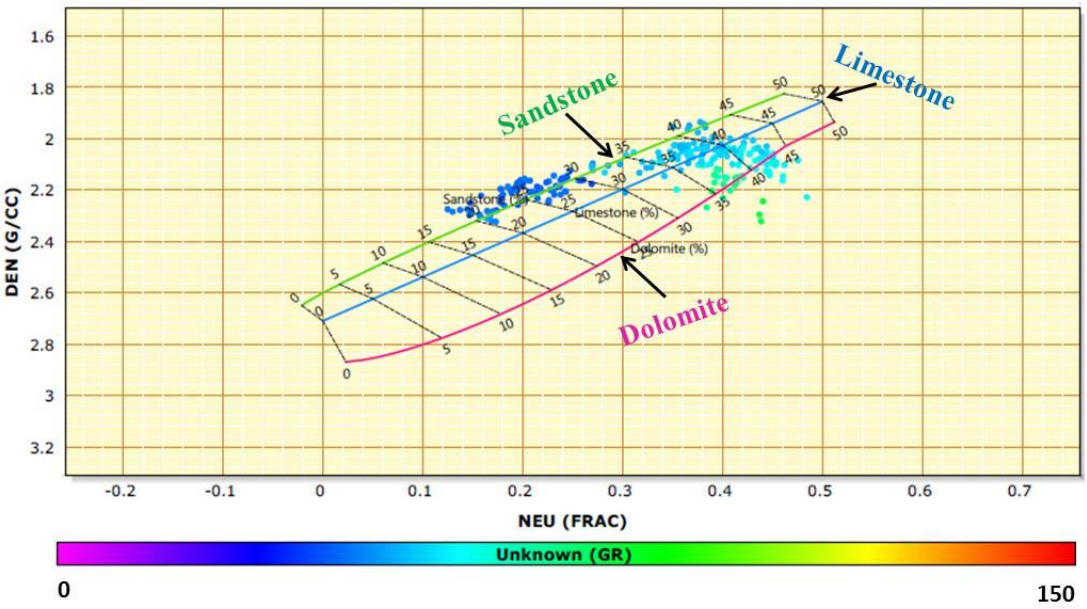

Figure 8.20: A) composite log of Mid-Miocene showing the raw logs (Tracks 3-5: track 1 = gamma ray; track 4 = shallow, mid and deep resistivity logs; track 5 = density and neutron logs) and evaluated logs (Tracks 6-9: track 6 = log porosity, core porosity (green dots) and SHPOR – fraction of pore space filled with hydrocarbon; track 7 = log permeability and core permeability (red dots); track 8 = volume of shale). B is the density-neutron cross-plot showing most of the Miocene data plotted in the vicinity of the sand-line (green line) indicating clean sands with minor shale as some data plots away from the sand-line.

8.4.2 Oligocene reservoir properties

Well A1 encountered the Oligocene succession from 3835m (12580ft) to the total depth of the well at 4180m (13700ft) (Figure 8.21). Of the 7 units of sand penetrated within this interval (identified by the green and yellow arrows in Figure 8.21). Units L1-L4 are the most permeable sand units. The unit with the largest sand thickness of 6m (20ft) is L2, while the remainder are thinner units of less than 3m (10ft) in thickness that are not easily resolvable by some logs, particularly the resistivity logs. Three of the other sand units (location of red arrows in Figure 8.21) penetrated are poorly developed and most likely to be highly consolidated and tight, as reflected in the anomalously high values of measured density. In addition to high density, slightly high resistivity values (shallow, mid and deep resistivity logs) are seen across these tight zones that are not necessary due to an effect of hydrocarbon but rather a response to the rock matrix that is acting essentially as an insulator to the flow of current. Since these intervals are tight with very

low permeability, all three resistivity logs are noted to have similar high resistivity readings. Where reservoir rocks display high permeability, the suite of resistivity logs would measure formation resistivity at different regions around the borehole based on their various depths of investigation. The shallow resistivity log would measure resistivity around the near wellbore region also known as the flushed zone (region of conductive mud filtrate); the mid resistivity would measure the transition zone (mixture of conductive mud and hydrocarbon); and the deep resistivity log records resistivity in the uninvaded zone (hydrocarbon-bearing and uncontaminated by mud filtrate). The integration of all three logs provides a qualitative indication of permeability and movable hydrocarbon (Track 4 in Figure 8.20, showing the highly permeable Miocene reservoir that illustrates this concept).

Units L1, L2, L3 and L4 (Figure 8.21) are interpreted to have good porosity with each unit having average values of about 20%. High N/G also characterises this unit with an estimated value of up to 95%, indicating the low volume of shale present in the sand packages. The estimated volume of shale based on two different methods – gamma ray log and a combination of neutron and density logs – also yields V_{sh} of less than 10%.

Since there was no core acquired in this section an electrofacies model was developed in order to understand the facies class across the logged Oligocene section based on variation in well log values with depth. The electrofacies was constructed from the density-neutron cross plot (Figure 4.4 of Chapter 4). Four facies classes, each uniquely colour coded, have been interpreted across the Oligocene interval; these include clean sands (units L1-4), tight sands, shaly sands and pure shales (Figure 4.13 of Chapter 4 and Figure 8.21 of this chapter). Sand units L1 to 4 fall within the clean sand domain of the cross plot that further confirms the high N/G initially calculated.

Permeability estimates across the clean sand units are between 100 and 180mD, being significantly lower than the Miocene. Of course this is expected considering that the Oligocene sediments are located almost 1500m (5000ft) deeper than the Miocene reservoir. Therefore under normal conditions reservoir properties are expected to reduce with depth. Cores were not acquired across the Oligocene data to calibrate log derived reservoir properties; hence some uncertainty remains in the estimated values. Higher

than expected permeability values are noted, mostly across the shale facies, but these should be disregarded due to poor borehole conditions across most of the shale interval. This has been highlighted as a grey colour fill to the right of the actual borehole size measured from the calliper log (Track 3, Figure 8.21) reflecting borehole enlargement due to the slurry nature of shales. Typically, the density tool would record a lower density value and a corresponding higher porosity across such areas and the estimated porosity is a key input to permeability calculation. Table 8.3 shows the average rock properties for unit L2, the thickest sand unit with the greatest hydrocarbon saturation (S_h).

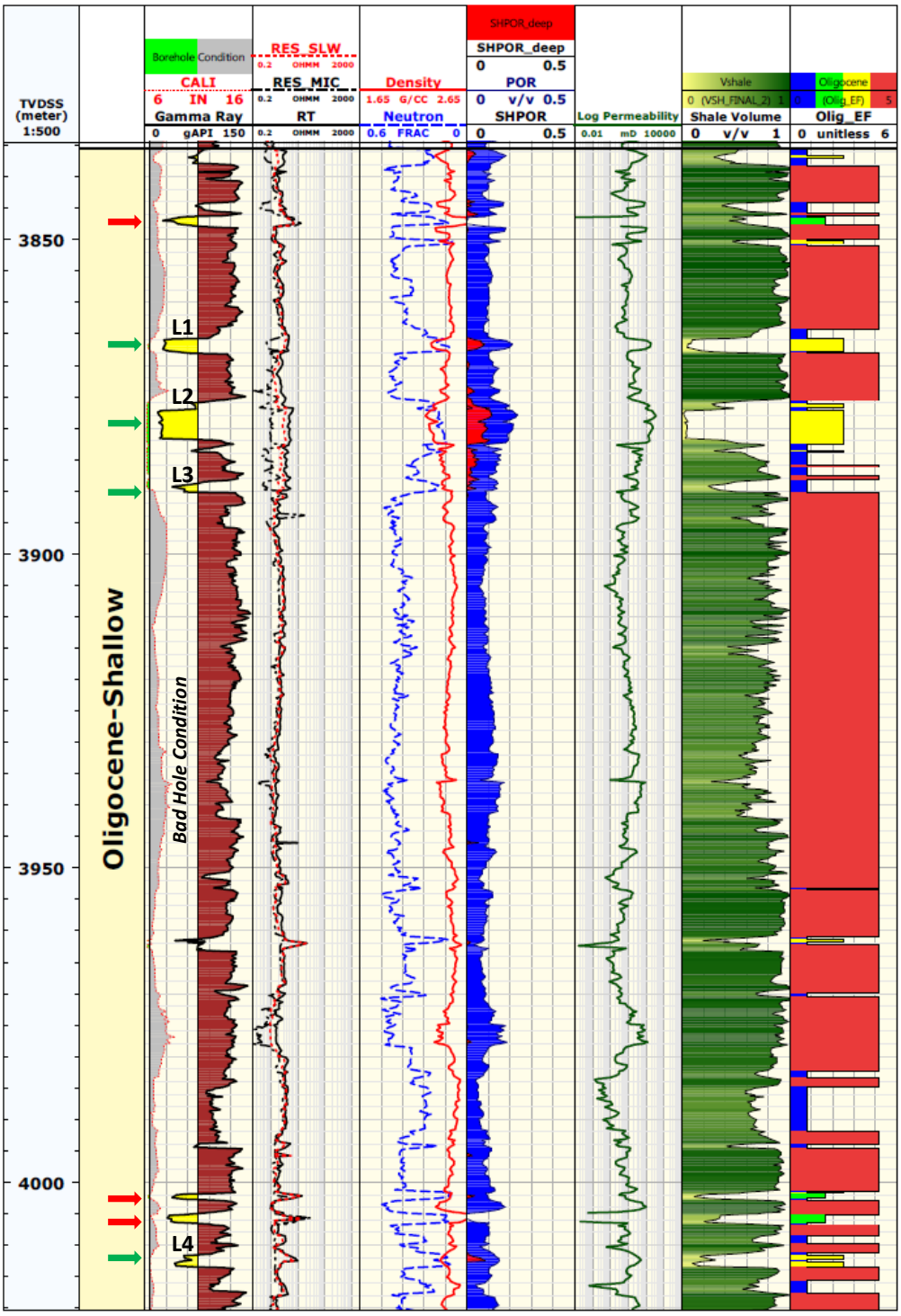

Figure 8.21: Composite log of Oligocene-Shallow showing the raw logs (Tracks 3-5: track 1 = gamma ray and calliper; track 4 = shallow, mid and deep resistivity logs; track 5 = density and neutron logs) and evaluated logs (Tracks 6-9: track 6 = porosity and SHPOR – fraction of pore filled with hydrocarbon; track 7 = log permeability; track 8 = volume of shale and track 9 = electrofacies). Note the locations of green arrows (permeable units L1, L2, L3 and L4) and red arrows (highly consolidated units).

Despite the relatively good quality of these reservoir sands, the resistivity logs across the Oligocene units are seen to be low compared to the resistivity readings of the Miocene sands, with values no more than 5 ohm-m occurring mostly in unit L2. Using the resistivity logs in the Archie water saturation model, calculated irreducible water saturation (S_{wirr}) across unit L2 is 56% (hydrocarbon saturation S_h of 44%), whereas units L1, L3 and L4 have a significantly lower hydrocarbon saturation and can be considered water bearing. Applying an alternative method of determining water saturation using the Waxman-Smith equation, which accounts for extra conductivity from shale (as the presence of shale can mask hydrocarbon effects in reservoir sands), also gives a similar result as the Archie model, thus further confirming the relatively shale-free nature of the sands and a greater certainty in the estimated hydrocarbon saturation. The low hydrocarbon saturation estimated in the Oligocene reservoir could be linked to any of the following factors:

1) Oligocene reservoirs received very low hydrocarbon charge from the source rocks, or were charged with hydrocarbon that later leaked off due to a poor seal leaving relics of hydrocarbon at the present day. The basin model result indicates that the Oligocene reservoir at the well location is not hydrocarbon bearing. The actual cause is not known at this time, but poor seal integrity is a suspect.

2) The thickness of the sand units are possibly lower than the resolution of the resistivity tool, so that the true resistivity of the hydrocarbon bearing sands has been masked by the high conductivity reading from the adjacent shale beds. The shale beds are easily detected by the tool. To resolve this problem, although beyond the scope of this study, the logs would need to be reprocessed to enhance the result of the measured data.

3) The Oligocene sands are probably mostly fine-grained with a larger surface area to attract formation water thereby preventing significant build-up of hydrocarbon and in turn a higher irreducible water saturation (S_{wirr}).

Reservoirs	Thickness (m)	N/G (Frac)	Porosity (%)	Hydrocarbon Saturation (%)	Permeability (mD)
Oligocene	**6**	**0.98**	**20**	**44**	**180**
Mid-Miocene	**25**	**0.9**	**35**	**88**	**2300**

Table 8.3: Average rock properties for the Oligocene (L2 sand) and the Mid-Miocene reservoir.

8.4.3 Implication of petrophysical evaluation on quartz diagenesis

The porosity-depth plot (D-Porosity) of the sequence encountered by well A1 follows the normal porosity-depth trend where reservoir porosity is observed to reduce with depth (Figure 8.22). Generally this has always been linked to the effect of mechanical compaction and can therefore to an extent be applied in predicting pre-drill reservoir porosity (Taylor et al., 2010, Taylor, 1950, Bloch et al., 1990, Athy, 1930). The porosity-depth trend from five wells, including well A1, shows two clusters of data – the first is a group of data from about 1650m (c.5500 ft) to 3178m (10500ft) and the second from 3178m (10500ft) to 4000m (c. 13400ft). The first cluster is characterised by a wide range in porosity values from 10% to 43% (0.1 - 0.43) while the lower group have a narrower range of 5% to 21% (0.05 – 0.22). The first group is described here as the zone where porosity reduction is largely controlled by compaction. The high mineralogical maturity of the rocks (based on petrographic analysis) yields a rigid framework of mainly quartz grains that reduces the effect of mechanical compaction on porosity. Hence a high range in porosity values is seen in this group. This zone corresponds to the depth window of the Mid-Miocene and younger aged rocks that are known for their high reservoir porosity and permeability. Below 3178m a sharp transition is noted where the porosity range dramatically reduces, this is interpreted as the depth where the effect of mechanical compaction reduces and marks the onset of quartz cementation. The Lower Miocene and deeper Oligocene reservoirs fall within this category.

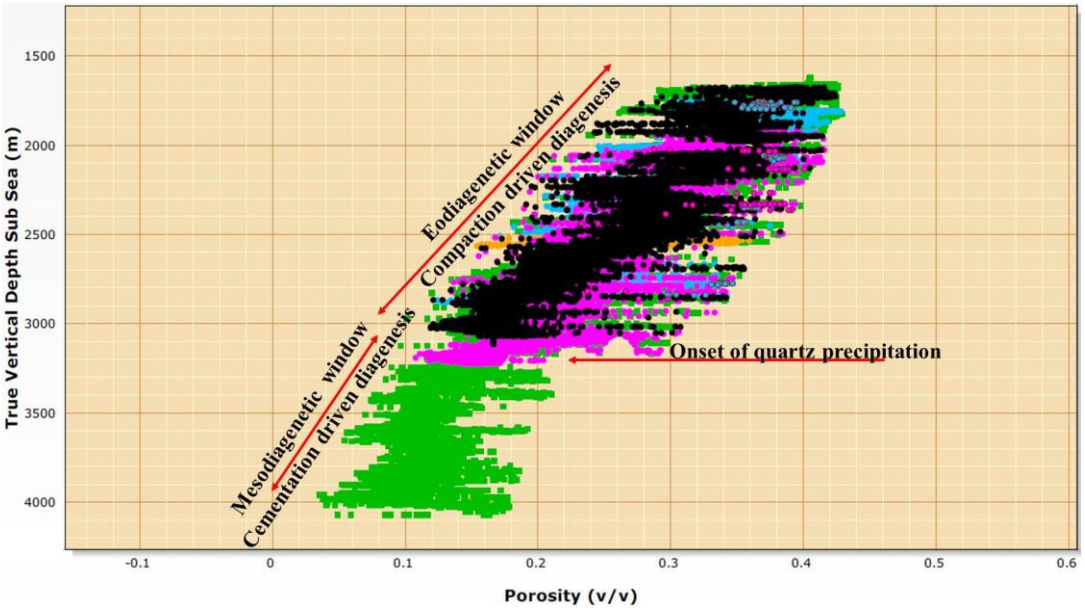

Figure 8.22: Porosity-depth plot of five wells in the study area (Well A1 data in green and the other 4 wells are represented in black, pink, blue and amber colours). The plot illustrates the diagenetic realms and associated processes that control porosity. A clear distinction in porosity distribution is observed with the narrower range in porosity from about 3178m defining the onset depth of quartz cementation.

A porosity versus present day temperature (T-porosity) plot of the reservoirs encountered in this well has also been constructed (Figure 8.23) and reveals striking similarity to the porosity-depth plot. The T-porosity plot also shows two groups of data, the first group falls within a temperature window of 25-70˚ C and porosity range of 17% to 43% (0.17 – 0.43). The porosity in this zone is also noted to maintain a near constant range with temperature increase, suggesting the low influence of mechanical compaction and little or no porosity reducing diagenetic processes. On the other hand the second zone is limited to temperatures ranging from 75 to 100˚ C and a corresponding porosity of 2 to 24% (0.02 - 0.24). Unlike the upper zone, this zone is characterised by a constant reduction in porosity with increase in temperature.

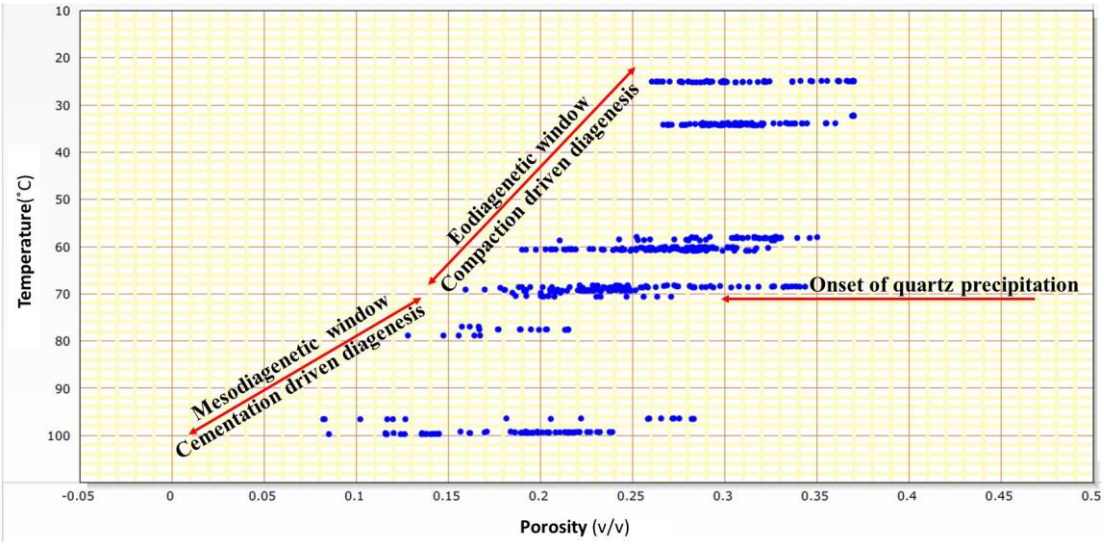

Figure 8.23: Porosity-Temperature plot of well A1 illustrating the diagenetic realms and associated processes that control porosity. A gradually reduction in porosity within a temperature window of 25° C to 70° C. This reflects the minimal effect of mechanical compaction on porosity. A significant decrease in porosity is noted as temperature increases from 70° C to 100° C suggesting the progressively build-up of quartz cementation as temperature increases.

The first group can be classed as zone of low temperature not conducive for quartz cementation but only influenced by compaction, while the second group falls within the temperature window suitable for quartz cementation. Hence the characteristically constant decrease in measured porosity within this zone. These two groups correspond respectively to the group 1 and 2 of the D-Porosity trend. The presence of early diagenetic siderite detected from the petrographic inspections of samples retrieved from c.2540m located in group 1 of both plots could also be responsible for the preservation of porosity.

The interpretation achieved from these two cross plots are in agreement with the elemental mineral analysis that also shows a step change in estimated volume of quartz, increasing from the Lower Miocene down into the Oligocene reservoirs penetrated by well A1 (Figure 7.12B in Chapter 7). Petrographic evidence that shows the rare occurrence of quartz in the Mid-Miocene, reservoir but that appears to increase in the deeper Lower Miocene reservoir, is thus in agreement with the prediction of quartz diagenesis made from the petrophysical model. In addition, the five sand units identified

from the wireline logs as compacted can be attributed to quartz cementation being buried to the depth window of group 2 described in the D-porosity and T-porosity plots. However, Units L1, L2 and L3 that are sandwiched between the compacted units and the L4-the deepest sand unit display a significantly higher porosity of about 20%, the question is what is then responsible for such high porosity in the midst of other sand packages that have little or no porosity. I propose the preservation of porosity due to early hydrocarbon emplacement considering that petrophysical evaluation reveals the presence of hydrocarbon in units L1-4.

CHAPTER 9

CONCLUSION AND FUTURE WORK

9.1 Conclusion

This study has integrated four different techniques to provide a new understanding of the reservoir potential, particularly the degree of quartz cementation, in the poorly understood, untapped, deep-water Oligocene succession of the Niger Delta slope system. An interpretation of the Oligocene depositional system based on 3D seismic volume was presented in Chapter 5, focusing on the depositional architecture and sand prediction in the study area. Petroleum systems modelling was conducted and results presented in Chapter 6, with the aim of predicting the charge history of the potential Oligocene sands and, most importantly, assessing the interplay between the time of charge and time of quartz cementation in reservoir quality prediction. An integrated result of petrographic study, petrophysical analysis and cementation modelling was documented in Chapter 7, with emphasis placed on harmonizing results from these techniques in understanding the controls of quartz cementation and the likely volume of quartz cement in the deeply buried Oligocene sediments. Finally, in order to draw some broader conclusions from the inferred reservoir potential of the Oligocene deep-water system in the study area, the reservoir quality of Oligocene sediments in the Niger Delta slope system is compared to other proven Oligocene deep-water systems located in other sedimentary basins that have similar tectonic settings as the Niger Delta slope system. This synthesis and discussion was presented in Chapter 8.

The following principal conclusions can be drawn from this research:

- Based on the interpreted 3D seismic data, the Oligocene depositional system in the slope of the Niger Delta Basin within the study area is dominated by lobe and channel-lobe depositional systems. The presence of the lobe deposits are significantly controlled by sea-floor topography that has been modified by tectonically induced, mud highs. These mud highs are inferred to be associated with mobile mud withdrawal that has resulted in the development of mini-basins, within which sediments pond. In the study area, channels are up to 1km wide and 10-15km long, feeding lobes that are 3-5km wide and 6-8km long.

- The morphology of the depositional lobes indicates that the structural highs are likely to predate the depositional elements. This is evidently manifested as seismic amplitude becomes weaker from lobe axis to margin towards the mud highs indicating thinning of the lobes against the mud ridge. Such stratal relationship between the channel-lobe bodies and the mud highs suggest possible sites for good stratigraphic traps for hydrocarbon.

- As only one well penetrated the top Oligocene succession, this study has used the excellent well to seismic calibration across the shallower Miocene proven reservoir as an analogue. The deeper Oligocene succession, with high reflection amplitude is interpreted as sand prone and hydrocarbon bearing. The calculated sweetness seismic attribute was instrumental in achieving this result.

- Basin modelling results predict that the Oligocene sediments and associated traps were in place to receive an early hydrocarbon charge from the Eocene Akata shales – a known source rock. Results from the simulation study reveal that four hydrocarbon accumulations are present in the Oligocene interval studied.

- Burial and thermal history models show that the Oligocene succession has been buried to depths where temperatures are greater than 70˚ C which favours quartz cementation. Cementation models of the Oligocene sediments indicate that less than 14% of the total porosity has been occluded by quartz cement. In addition, evidence that the Oligocene sediments are likely to be cemented are also linked to: (1) the petrographic evidence of a rare occurrence of quartz overgrowths in the Mid-Miocene that increases into the Lower Miocene reservoir, and (2) the petrophysical multi-mineral analysis conducted in Well A1, which shows the calculated quartz volume increasing by about 10% from Upper Miocene to the logged Oligocene interval.

- On the basis of the burial history model, the Oligocene system is inferred to have been overpressured from late Miocene to the present-day. It is unlikely that overpressure would have resulted in preserving porosity since the modelled thermal history shows that the Oligocene sediments encountered temperatures greater than 70˚ C predating the time of overpressure development.

- Despite that both modelled results and inferences deduced from both petrographic and petrophysical data, points to a possibility of quartz cementation in the potential Oligocene reservoir, the amount of cement volume as predicted from the 2D simulation is not likely to be sufficient to prevent the Oligocene interval from being a viable hydrocarbon reservoir. Also, the effect of early hydrocarbon emplacement, thought to retard or slow down diagenesis has been modelled. The basin model simulates peak hydrocarbon saturation being reached when less than 5% of the pore space in all 4 simulated accumulations were quartz cemented. It is quite possible that quartz precipitation would have been significantly retarded from the time of peak oil charge, thereby preserving a significant fraction of the porosity in the potential Oligocene reservoirs.

- In order to de-risk exploration targets, as well as aiding field and reservoir development, accurate reservoir quality prediction for deeply buried sediments is essential. Reservoir quality prediction is at its best when different techniques are integrated that result in similar findings. This has proved particularly useful in this study, were seismic interpretation, basin modelling, petrographic and petrophysical analysis have all been combined to provide a new understanding of the reservoir quality of the deep-water Oligocene sediments in the slope system of the Niger Delta Basin.

9.2 Future Work

- This study represents the very early stage of assessing a deeper reservoir play in the already productive deep-water Niger Delta slope system. The modelling and simulation undertaken in this thesis and the predictions made with regard to play potential provide a positive impetus for further exploration in the area. Any new exploration should be followed by further integrated reservoir quality prediction in the light of new data. This will allow further refinement of the methodology and results presented herein.
- The depositional architecture of the channel-lobe system proposed for this region of the Niger Delta slope presents a new perspective on the deep-water sedimentary system and its controls. In particular, the structurally-controlled mini-basins developed by mud-ridge confinement and the small, sand-rich turbidite lobes they

contain, need further study. This is important for better understanding the nature and controls on turbidite sedimentation and architecture in the deep-water Niger Delta slope. It also has more general implications and application to other deep-water systems worldwide.

- The integrated reservoir quality prediction methodology developed in this study has much wider application. Further work should be undertaken to apply this methodology in a range of similar sedimentary basins around the South Atlantic continental margins. Important information will be gained for refinement of the methodology from studying successions where a greater degree of quartz cementation has taken place and from where it has been retarded in deeper reservoir units.
- As more data becomes available coupled with reliable technology, risk to hydrocarbon exploration and future development can be minimised. Therefore, further work in the following areas can be considered:
    1) This study was largely dependent on 2D basin modelling of a regional 2D seismic line across the key study area. This can be improved with basin modelling conducted on multiple regional 2D seismic lines and/or 3D modelling approach. This would allow: (a) better modelling of petroleum migration and in turn better prediction of hydrocarbon accumulation, (b) better distribution of physical properties such as temperature, pressure, lithology that would lead to an improved prediction of cementation both spatially and temporally.

    2) Integrating the results from this study with seismic inversion analysis would be helpful to better understand the spatial distribution of reservoir properties. This can be achieved when acoustic seismic amplitude is inverted to generate specific rock properties like impedance, density, Vp/Vs (Vp-compressional velocity, Vs-shear velocity), etc. So that by integrating seismic inversion with seismic attribute analysis, it is possible to generate reservoir parameters that are directly used to estimate spatially, and temporally the absolute values of reservoir properties such as porosity.

    3) The basin model assumes a simple lithological description and their corresponding petrophysical properties for all the reservoirs defined in the 2D model. Both the lithology and their associated petrophysical properties were

calibrated to well logs and petrographic analysis from well A1. The use of one well for calibration purpose is not entirely sufficient for a robust basin model. So that for example, intervals that were deposited under high sedimentation rate and prone to being overpressured and not fully captured in the 2D model. Further investigation is required especially for the Plio-Pleistocene succession that are characterised with high sedimentation rate and therefore susceptible to overpressure but not captured in the model.

4) The Oligocene reservoir penetrated by the well shows very low resistivity profile across the thin reservoir interval, although slightly higher than the response of a water bearing rock. It is therefore likely that these intervals are low resistivity pay zones possibly due to thin beds with bed thickness below the resistivity tool resolution. Hence, thin bed analysis of the encountered Oligocene interval be carried out by post processing the available log or using more advanced resistivity logging tools like 3DEX or RTScanner that are capable of providing higher resolution resistivity measurements.

REFERENCES

AASE, N. E., BJORKUM, P. A. & NADEAU, P. H. 1996. The effect of grain-coating microquartz on preservation of reservoir porosity. *AAPG bulletin,* 80**,** 1654-1673.

ADEOGBA, A. A. 2003. Architecture and depositional controls of deep-water deposits as imaged by near-surface 3-D seismic data, Nigeria. Stanford University, United States.

ADEOGBA, A. A., MCHARGUE, T. R. & GRAHAM, S. A. 2005. Transient fan architecture and depositional controls from near-surface 3-D seismic data, Niger Delta continental slope. *AAPG bulletin,* 89**,** 627-643.

AHMAD, M. N. & ROWELL, P. 2012. Application of spectral decomposition and seismic attributes to understand the structure and distribution of sand reservoirs within Tertiary rift basins of the Gulf of Thailand. *The Leading Edge,* 31**,** 630-634.

AJDUKIEWICZ, J. M. & LARESE, R. E. 2012. How clay grain coats inhibit quartz cement and preserve porosity in deeply buried sandstones: Observations and experiments. *AAPG bulletin,* 96**,** 2091-2119.

AL-HAJERI, M. M., AL SAEED, M., DERKS, J., FUCHS, T., HANTSCHEL, T., KAUERAUF, A., NEUMAIER, M., SCHENK, O., SWIENTEK, O. & TESSEN, N. 2009. Basin and petroleum system modeling. *Oilfield Review,* 21**,** 14-29.

ALLEN, P. A. & ALLEN, J. R. 1990. *Basin analysis: principles and applications,* Cornwall, Wiley-Blackwell.

ANDERSON, A. V., SICKAFOOSE, D. K., FAHRER, T. R. & GOTTSCHALK, R. R. 2012. Interaction of Oligocene–Miocene deep-water depositional systems with actively evolving structures: The Lower Congo Basin, offshore Angola.

ANDERSON, J., CARTWRIGHT, J., DRYSDALL, S. & VIVIAN, N. 2000. Controls on turbidite sand deposition during gravity-driven extension of a passive margin: examples from Miocene sediments in Block 4, Angola. *Marine and Petroleum Geology,* 17**,** 1165-1203.

ANKA, Z., SÉRANNE, M., LOPEZ, M., SCHECK-WENDEROTH, M. & SAVOYE, B. 2009. The long-term evolution of the Congo deep-sea fan: A basin-wide view of the interaction between a giant submarine fan and a mature passive margin (ZaiAngo project). *Tectonophysics,* 470**,** 42-56.

ARMSTRONG, L., TEN HAVE, A. & JOHNSON, H. 1987. The geology of the Gannet fields, central North Sea, UK sector. *Petroleum geology of north-west Europe: London, Graham and Trotman***,** 533-548.

ATHY, L. F. 1930. Density, porosity, and compaction of sedimentary rocks. *AAPG Bulletin,* 14**,** 1-24.

AVBOVBO, A. A. 1978. Tertiary Lithostratigraphy of Niger Delta: GEOLOGIC NOTES. *AAPG Bulletin,* 62**,** 295-300.

BADLEY, M. E. 1985. *Practical seismic interpretation,* United States of America, D. Reidel Publishing Company.

BANDELE, V. A. & CLAUDEL, G. Leading Edge Subsurface Technologies for AKPO A Complex Condensate Field. Offshore Technology Conference, 2010. Offshore Technology Conference.

BARCLAY, S. & WORDEN, R. 2009. Petrophysical and petrographical analysis of quartz cement volumes across oil–water contacts in the Magnus Field, northern North Sea. *Quartz Cementation in Sandstones: Special Publication 29 of the IAS,* 14**,** 147.

BARKER, C. 1996. *Thermal modeling of petroleum generation: theory and application,* Netherlands, Elservier.

BEAUBOUEF, R. & FRIEDMANN, S. High resolution seismic/sequence stratigraphic framework for the evolution of Pleistocene intra slope basins, western Gulf of Mexico: depositional models and reservoir analogs. Deep-water reservoirs of the world: Gulf Coast Section SEPM 20th Annual Research Conference, 2000. SEPM, 40-60.

BEAUBOUEF, R., VAN WAGONER, J. & ADAIR, N. 2003. Ultra-high resolution 3-d characterization of deep-water deposits—II: Insights into the evolution of a submarine fan and comparisons with river deltas. *Extended Abstracts, May*, 11-14.

BEGLINGER, S. E., DOUST, H. & CLOETINGH, S. 2012. Relating petroleum system and play development to basin evolution: West African South Atlantic basins. *Marine and Petroleum Geology,* 30, 1-25.

BILOTTI, F. & SHAW, J. H. 2005. Deep-water Niger Delta fold and thrust belt modeled as a critical-taper wedge: The influence of elevated basal fluid pressure on structural styles. *AAPG bulletin,* 89, 1475-1491.

BJORKUM, P. A. 1996. How important is pressure in causing dissolution of quartz in sandstones? *Journal of Sedimentary Research,* 66.

BJØRKUM, P. A., OELKERS, E. H., NADEAU, P. H., WALDERHAUG, O. & MURPHY, W. M. 1998. Porosity prediction in quartzose sandstones as a function of time, temperature, depth, stylolite frequency, and hydrocarbon saturation. *AAPG Bulletin-American Association of Petroleum Geologists,* 82, 637.

BJØRLYKKE, K. & HØEG, K. 1997. Effects of burial diagenesis on stresses, compaction and fluid flow in sedimentary basins. *Marine and Petroleum Geology,* 14, 267-276.

BLOCH, S., DUNCAN, J. M. J. & BRIZZOLARA, D. 1990. Porosity Prediction, Prior to Drilling, in Sandstones of the Kekiktuk Formation (Mississippian), North Slope of Alaska (1). *AAPG Bulletin,* 74, 1371-1385.

BLOCH, S., LANDER, R. H. & BONNELL, L. 2002. Anomalously high porosity and permeability in deeply buried sandstone reservoirs: Origin and predictability. *AAPG bulletin,* 86, 301-328.

BLUNDELL, D. 1991. Some observations on basin evolution and dynamics. *Journal of the Geological Society,* 148, 789-800.

BOGGS, S., JR. 1987. *Principles of sedimentology and stratigraphy,* New York, Macmillan.

BOUMA, A. H. & RAVENNE, C. 2004. The Bouma Sequence (1962) and the resurgence of geological interest in the French Maritime Alps (1980s): the influence of the Grès d'Annot in developing ideas of turbidite systems. *Geological Society, London, Special Publications,* 221, 27-38.

BREDEHOEFT, J. D. & HANSHAW, R. B. 1968. On the maintenance of anomalous fluid pressures: I. Thick sedimentary sequences. *Geological Society of America Bulletin,* 79, 1097-1106.

BRENNER, R. L., LUDVIGSON, G. A., SEAL, R. & DOGAN, A. U. 1991. Diagenetic modeling of siliciclastic systems: Status report. *Kansas Geological Survey, Bulletin,* 233, 123-137.

BRIGGS, S. E., CARTWRIGHT, J. & DAVIES, R. J. 2009. Crustal structure of the deepwater west Niger Delta passive margin from the interpretation of seismic reflection data. *Marine and Petroleum Geology,* 26, 936-950.

BROUCKE, O., TEMPLE, F., ROUBY, D., ROBIN, C., CALASSOU, S., NALPAS, T. & GUILLOCHEAU, F. 2004. The role of deformation processes on the geometry of mud-dominated turbiditic systems, Oligocene and Lower–Middle Miocene of the Lower Congo basin (West African Margin). *Marine and Petroleum Geology,* 21, 327-348.

BROWN, A. R. 2011. Interpretation of three-dimensional seismic data. *AAPG Memoir,* 42, 295-308.

BRUHN, C. H., GOMES, J. A. T., LUCCHESE JR, C. & JOHANN, P. R. Campos basin: reservoir characterization and management–Historical overview and future challenges. Offshore Technology Conference, Houston, Texas, USA, 2003. 5-8.

BURKE, K. 1972. Longshore drift, submarine canyons, and submarine fans in development of Niger Delta. *AAPG Bulletin,* 56, 1975-1983.

BURKE, K., DESSAUVAGIE, T. & WHITEMAN, A. 1971. Opening of the Gulf of Guinea and geological history of the Benue Depression and Niger Delta. *Nature,* 233, 51-55.

BURKE, K., MACGREGOR, D. & CAMERON, N. 2003. Africa's petroleum systems: four tectonic 'Aces' in the past 600 million years. *Geological Society, London, Special Publications,* 207**,** 21-60.

BURNHAM, A. K. & SWEENEY, J. J. 1989. A chemical kinetic model of vitrinite maturation and reflectance. *Geochimica et Cosmochimica Acta,* 53**,** 2649-2657.

BUSTIN, R. 1988. Sedimentology and characteristics of dispersed organic matter in Tertiary Niger Delta: origin of source rocks in a deltaic environment. *AAPG Bulletin,* 72**,** 277-298.

CAMERON, N. & WHITE, K. 1999. Exploration Opportunities in Offshore Deepwater Africa. *IBC 'Oil and Gas Developments in West Africa', London, UK***,** 25-26.

CHAPIN, M., SWINBURN, P., VAN DER WEIDEN, R., SKALOUD, D., ADESANYA, S., STEVENS, D., VARLEY, C., WILKIE, J., BRENTJENS, E. & BLAAUW, M. 2002. Integrated seismic and subsurface characterization of Bonga Field, offshore Nigeria. *The Leading Edge,* 21**,** 1125-1131.

CHEN, B., WEI, X.-D., REN, D.-Z., ZHANG, Y.-Z., WANG, Y.-N. & LI, J.-H. 2010. Small fault identification based on spectrum decomposition technique. *Shiyou Diqiu Wuli Kantan(Oil Geophysical Prospecting),* 45**,** 890-894.

CHOPRA, S. & MARFURT, K. J. 2008. Emerging and future trends in seismic attributes. *The Leading Edge,* 27**,** 298-318.

CHOPRA, S. & MARFURT, K. J. 2012. Evolution of seismic interpretation during the last three decades. *The Leading Edge,* 31**,** 654-676.

CHOUGH, S. K. & ORTON, G. J. 1995. Fan deltas - depositional styles and controls-PREFACE. *Sedimentary Geology,* 98 (1-4).

CHUDI, O., LEWIS, H. & STOW, D. A. 2015. 3D seismic interpretation of depositional architecture and reservoir potential of deep-water untapped Oligocene sequence of the western Niger Delta. Heriot Watt University, Edinburgh, United Kingdom.

CHUDI, O., LEWIS, H., STOW, D. A. & BUCKMAN, J. O. 2014. Reservoir quality prediction via integrated diagenesis, advanced petrophysics and basin modelling: Deepwater Oligocene sandstone Western Niger Delta. Heriot Watt University, Edinburgh, United Kingdom.

CHUDI, O. & SIMON, R. 2012. Petrophysical Characterization of Radioactive Sands - Integrating Well Logs and Core Information: A Case Study in the Niger Delta. Society of Petroleum Engineers.

COHEN, H. A. & MCCLAY, K. 1996. Sedimentation and shale tectonics of the northwestern Niger Delta front. *Marine and Petroleum Geology,* 13**,** 313-328.

COOKE, N., SZAFIAN, P., GRUENWALD, R. & SCHULER, L. 2014. Forward modelling to understand colour responses in an HDFD RGB blend around a gas discovery. *first break,* 32**,** 87-97.

CORREDOR, F., SHAW, J. H. & BILOTTI, F. 2005. Structural styles in the deep-water fold and thrust belts of the Niger Delta. *AAPG bulletin,* 89**,** 753-780.

CRONIN, B. T. 1995. Structurally-controlled deep sea channel courses: examples from the Miocene of southeast Spain and the Alboran Sea, southwest Mediterranean. *Geological Society, London, Special Publications,* 94**,** 115-135.

DA COSTA, J. L., SCHIRMER, T. & LAWS, B. 2001. AAPG Memoir 74, Chapter 25: Lower Congo Basin, Deep-Water Exploration Province, Offshore West Africa.

DAILLY, P., HENDERSON, T., HUDGENS, E., KANSCHAT, K. & LOWRY, P. 2013. Exploration for Cretaceous stratigraphic traps in the Gulf of Guinea, West Africa and the discovery of the Jubilee Field: a play opening discovery in the Tano Basin, Offshore Ghana. *Geological Society, London, Special Publications,* 369**,** 235-248.

DAMUTH, J. E. 1994. Neogene gravity tectonics and depositional processes on the deep Niger Delta continental margin. *Marine and Petroleum Geology,* 11**,** 320-346.

DE RUIG, M. J. & HUBBARD, S. M. 2006. Seismic facies and reservoir characteristics of a deep-marine channel belt in the Molasse foreland basin, Puchkirchen Formation, Austria. *AAPG bulletin,* 90**,** 735-752.

DELATTRE, E., AUTHIER, J. F., RODOT, F., PETIT, G. & ALFENORE, J. Review of sand control results and performance on a deep water development-A case study from the Girassol Field Angola. SPE Annual Technical Conference and Exhibition, 2004. Society of Petroleum Engineers.

DEMING, D. 1994. Overburden rock, temperature, and heat flow. *AGE (Ma),* 200**,** 100.

DEPTUCK, M. E., PIPER, D. J., SAVOYE, B. & GERVAIS, A. 2008. Dimensions and architecture of late Pleistocene submarine lobes off the northern margin of East Corsica. *Sedimentology,* 55**,** 869-898.

DEPTUCK, M. E., SYLVESTER, Z., PIRMEZ, C. & O'BYRNE, C. 2007. Migration–aggradation history and 3-D seismic geomorphology of submarine channels in the Pleistocene Benin-major Canyon, western Niger Delta slope. *Marine and Petroleum Geology.*

DERKS, J., SWIENTEK, O., FUCHS, T., KAUERAUF, A., AL-QUATTAN, M. & AL-SAEED, M. 2012. Three-Dimensional Basin and Petroleum System Model of the Cretaceous Burgan Formation, Kuwait: Model-in-Model, High-Resolution Charge Modeling. *Basin Modeling: New Horizons in Research and Applications, AAPG Hedberg Series, No. 4,* 4**,** 159.

DESSUS, J. L. & ABREU, J. 2002. Girassol: Drilling and Completion Experience gained through first 12 wells. *OTC,* 14168**,** 6-9.

DMITRIEVA, E., JACKSON, C. A., HUUSE, M. & MCCARTHY, A. 2012. Paleocene deep-water depositional systems in the North Sea Basin a 3D seismic and well data case study, offshore Norway. *Petroleum Geoscience,* 18**,** 97-114.

DOUST, H. & OMATSOLA, E. 1990. Niger Delta. In:Edwards,J.D., Santogrossi, P.A (Eds), Divergent/Passive Margin Basins. *American Assoiciation of Petroleum Geologist,* 4**,** 239-248.

DUNLAP, D. B., WOOD, L. J., WEISENBERGER, C. & JABOUR, H. 2010. Seismic geomorphology of offshore Moroccos east margin, Safi Haute Mer area. *AAPG bulletin,* 94**,** 615-642.

DUTION, S. P., HAMLIN, H. S., FOLK, R. L. & CLIFT, S. J. 1996. Early siderite cementation as a control on reservoir quality in submarine fan sandstones, Sonora Canyon gas play, Val Verde Basin, Texas. *Society of Sedimentary Geology (SEPM),* 55**,** 115-127.

EHRENBERG, S. & NADEAU, P. 1989. Formation of diagenetic illite in sandstones of the Garn Formation, Haltenbanken area, mid-Norwegian continental shelf. *Clay Minerals,* 24**,** 233-253.

EJEDAWE, J., COKER, S., LAMBERT-AIKHIONBARE, D., ALOFE, K. & ADOH, F. 1984. Evolution of oil-generative window and oil and gas occurrence in Tertiary Niger Delta Basin. *AAPG Bulletin,* 68**,** 1744-1751.

EKWEOZOR, C. & DAUKORU, E. 1984. Petroleum source-bed evaluation of Tertiary Niger Delta: reply. *AAPG Bulletin,* 68**,** 390-394.

EKWEOZOR, C. M. & OKOYE, N. V. 1980. Petroleum Source-Bed Evaluation of Tertiary Niger Delta: GEOLOGIC NOTES. *AAPG Bulletin,* 64**,** 1251-1259.

EKWEOZOR, C. & UDO, O. T. 1988. The oleananes: Origin, maturation and limits of occurence in southern Nigeria sedimentary basins. *Organic Geochemistry,* 13**,** 131-140.

EMERY, D., SMALLEY, P., OXTOBY, N., RAGNARSDOTTIR, K., AAGAARD, P., HALLIDAY, A., COLEMAN, M. & PETROVICH, R. 1993. Synchronous Oil Migration and Cementation in Sandstone Reservoirs Demonstrated by Quantitative Description of Diagenesis [and

Discussion]. *Philosophical Transactions of the Royal Society of London. Series A: Physical and Engineering Sciences,* 344**,** 115-125.

EVAMY, B. D., HAREMBOURE, J., KAMERLING, P., KNAAP, W. A., MOLLY, F. A. & ROWLANDS, P. H. 1978. Hydrocarbon habitat of Tertiary Niger Delta. *American Association of Petroleum Geologists Bulletin,* 62**,** 1-39.

EVANS, J., HOGG, A. J., HOPKINS, M. S. & HOWARTH, R. J. 1994. Quantification of quartz cements using combined SEM, CL, and image analysis. *Journal of Sedimentary Research,* 64.

FEHINTOLA, T., AL-MANDHARY, I. & WEAVER, S. Probabilistic Inversion of Complex Channelised Reservoirs in Deep Water Niger Delta. Nigeria Annual International Conference and Exhibition, 2009. Society of Petroleum Engineers.

FRANKL, E. & CORDRY, E. The Niger Delta oil province: Recent developments onshore and offshore. 7th World Petroleum Congress, 1967. World Petroleum Congress.

GALLOWAY, W. 1984. Hydrogeologic regimes of sandstone diagenesis. *Clastic diagenesis: AAPG Memoir,* 37**,** 3-13.

GALLOWAY, W. E. 1975. Process framework for describing the morphologic and stratigraphic evolution of deltaic depositional systems.

GALLOWAY, W. E. 1998. Siliciclastic slope and base-of-slope depositional systems: component facies, stratigraphic architecture, and classification. *AAPG bulletin,* 82**,** 569-595.

GAY, A., LOPEZ, M., COCHONAT, P., SÉRANNE, M., LEVACHÉ, D. & SERMONDADAZ, G. 2006. Isolated seafloor pockmarks linked to BSRs, fluid chimneys, polygonal faults and stacked Oligocene–Miocene turbiditic palaeochannels in the Lower Congo Basin. *Marine Geology,* 226**,** 25-40.

GEE, M. & GAWTHORPE, R. 2006. Submarine channels controlled by salt tectonics: Examples from 3D seismic data offshore Angola. *Marine and Petroleum Geology,* 23**,** 443-458.

GENIK, G. 1993. Petroleum geology of cretaceous-Tertiary rift basins in Niger, Chad, and central African republic. *AAPG Bulletin,* 77**,** 1405-1434.

GIER, S., WORDEN, R. H., JOHNS, W. D. & KURZWEIL, H. 2008. Diagenesis and reservoir quality of Miocene sandstones in the Vienna Basin, Austria. *Marine and Petroleum Geology,* 25**,** 681-695.

GILES, M., STEVENSON, S., MARTIN, S., CANNON, S., HAMILTON, P., MARSHALL, J. & SAMWAYS, G. 1992. The reservoir properties and diagenesis of the Brent Group: a regional perspective. *Geological Society, London, Special Publications,* 61**,** 289-327.

GLUYAS, J. & CADE, C. A. 1998. Prediction of porosity in compacted sands. *MEMOIRS-AMERICAN ASSOCIATION OF PETROLEUM GEOLOGISTS***,** 19-28.

GRAUE, K. 2000. Mud volcanoes in deepwater Nigeria. *Marine and Petroleum Geology,* 17**,** 959-974.

HAACK, R. C., SUNDARARAMAN, P., DIEDJOMAHOR, J. O., XIAO, H., GANT, N. J., MAY, E. D. & KELSCH, K. 2000. AAPG Memoir 73, Chapter 16: Niger Delta Petroleum Systems, Nigeria.

HANTSCHEL, T. & KAUERAUF, A. 2009a. *Fundamentals of basin and petroleum systems modeling,* Berlin, Springer.

HANTSCHEL, T. & KAUERAUF, A. I. 2009b. *Fundamentals of basin and petroleum systems modeling*, Springer.

HART, B. S. 2008. Channel detection in 3-D seismic data using sweetness. *AAPG bulletin,* 92**,** 733-742.

HAUGHTON, P. D. 1994. Deposits of deflected and ponded turbidityents, currents, Sorbas Basin, southeast Spain. *Journal of Sedimentary Research,* 64.

HEGARTY, K. A., WEISSEL, J. K. & MUTTER, J. C. 1988. Subsidence history of Australia's southern margin: constraints on basin models. *AAPG Bulletin,* 72**,** 615-633.

HEMPTON, M., MARSHALL, J., SADLER, S., HOGG, N., CHARLES, R. & HARVEY, C. Turbidite reservoirs of the Sele Formation, Central North Sea: geological challenges for improving production. Geological Society, London, Petroleum Geology Conference series, 2005. Geological Society of London, 449-459.

HERMANRUD, C. 1993. Basin modelling techniques-an overview. *Basin modelling: advances and applications: Norwegian Petroleum Society (NPF) Special Publication,* 3**,** 1-34.

HIGLEY, D. K., LEWAN, M., ROBERTS, L. N. & HENRY, M. E. 2006. Petroleum system modeling capabilities for use in oil and gas resource assessments.

HONARPOUR, M., KOEDERITZ, F. & HERBERT, A. 1986. Relative permeability of petroleum reservoirs.

HOUSEKNECHT, D. W. 1984. Influence of grain size and temperature on intergranular pressure solution, quartz cementation, and porosity in a quartzose sandstone. *Journal of Sedimentary Research,* 54.

JAMES, W., WILMAR, G. C. & DAVIDSON, B. G. 1986. Role of quartz type and grain size in silica diagenesis, Nugget Sandstone, south-central Wyoming. *Journal of Sedimentary Research,* 56.

JEGOU, I., SAVOYE, B., PIRMEZ, C. & DROZ, L. 2008. Channel-mouth lobe complex of the recent Amazon Fan: the missing piece. *Marine Geology,* 252**,** 62-77.

JIAN-PING, L., PAN, X.-H., JUN, M., TIAN, Z.-J., CHEN, Y.-J. & WAN, L.-K. 2008. Petroleum geology and resources in West Africa: An overview. *Petroleum Exploration and Development,* 35**,** 378-384.

KOLLA, V., BOURGES, P., URRUTY, J.-M. & SAFA, P. 2001. Evolution of deep-water Tertiary sinuous channels offshore Angola (west Africa) and implications for reservoir architecture. *AAPG bulletin,* 85**,** 1373-1405.

KOLLA, V. & MACURDA JR, D. 1988. Sea-level changes and timing of turbidity-current events in deep-sea fan systems. *Wilgus, CK, Hastings, BS, Kendall,., CG, St., C., Posamentier, HW, Ross, CA, Van Wagoner, JC (Eds.), Sea-level Changes e An Integrated Approach. SEPM Special Publication,* 42**,** 381e392.

LAMBERT-AIKHIONBARE, D. & IBE, A. 1984. Petroleum source-bed evaluation of Tertiary Niger delta: discussion. *AAPG Bulletin,* 68**,** 387-389.

LANDER, R. H., LARESE, R. E. & BONNELL, L. M. 2006. Why do microquartz coatings preserve sandstone reservoir quality? *American Association of Petroleum Geologists***,** 60.

LANDER, R. H., LARESE, R. E. & BONNELL, L. M. 2008. Toward more accurate quartz cement models: The importance of euhedral versus noneuhedral growth rates. *AAPG bulletin,* 92**,** 1537-1563.

LANDER, R. H. & WALDERHAUG, O. 1999. Predicting porosity through simulating sandstone compaction and quartz cementation. *AAPG bulletin,* 83**,** 433-449.

LEFFLER, W. L., PATTAROZZI, R. & STERLING, G. 2011. *Deepwater petroleum exploration & production: A nontechnical guide*, PennWell Books.

LEHNER, P. & DE RUITER, P. A. C. 1977. Structural history of Atlantic margin of Africa. *AAPG Bulletin,* 61**,** 961-981.

LOUCKS, R. G., DODGE, M. M. & GALLOWAY, W. E. 1984. Regional controls on diagenesis and reservoir quality in lower Tertiary sandstones along the Texas Gulf Coast: Part 1. Concepts and principles.

LUNDEGARD, P. D. 1992. Sandstone Porosity Loss--A. *Journal of Sedimentary Research,* 62.

MACGREGOR, D. Petroleum Basins of Sub-Saharan Africa. 12th PESGB/HGS Conference on African E & P Review, 2013 London, United Kingdom. 1-218.

MANSURBEG, H. 2007. Diagenesis and Reservoir-Quality Evolution of Deep-Water Turbidites: Links to Basin Setting, Depositional Facies, and Sequence Stratigraphy.

MANSURBEG, H., EL-GHALI, M. A., MORAD, S. & PLINK-BJÖRKLUND, P. 2006. The impact of meteoric water on the diagenetic alterations in deep-water, marine siliciclastic turbidites. *Journal of Geochemical Exploration,* 89**,** 254-258.

MARCHAND, A. M., SMALLEY, P. C., HASZELDINE, R. S. & FALLICK, A. E. 2002. Note on the importance of hydrocarbon fill for reservoir quality prediction in sandstones. *AAPG bulletin,* 86**,** 1561-1572.

MATTHEW, O. S., WON, J., UDOEKONG, G., IBIOLA, O. & DIXON, D. 2010. Resolving the Structural Complexities in the Deepwater Niger-Delta Fold and Thrust Belt: A Case Study from the Western Lobe, Nigerian Offshore Depobelt. *AAPG Search and Discovery Article* [Online].

MAYALL, M., LONERGAN, L., BOWMAN, A., JAMES, S., MILLS, K., PRIMMER, T., POPE, D., ROGERS, L. & SKEENE, R. 2010. The response of turbidite slope channels to growth-induced seabed topography. *AAPG bulletin,* 94**,** 1011-1030.

MAYALL, M. & STEWART, I. The architecture of turbidite slope channels. Deep-Water Reservoirs of the World: SEPM, Gulf Coast Section, 20th Annual Research Conference, 2000. SEPM, 578-586.

MCBRIDE, E. F. 1963. A classification of common sandstones. *Journal of Sedimentary Research,* 33.

MCBRIDE, E. F. 1989. Quartz cement in sandstones: a review. *Earth-Science Reviews,* 26**,** 69-112.

MCDONNELL, A., LOUCKS, R. G. & GALLOWAY, W. E. 2008. Paleocene to Eocene deep-water slope canyons, western Gulf of Mexico: Further insights for the provenance of deep-water offshore Wilcox Group plays. *AAPG bulletin,* 92**,** 1169-1189.

MITCHELL, M. I. 2012. GHANA'S OFFSHORE OIL: RESOURCE CURSE OR BLESSING? *Africa Portal Backgrounder,* 44**,** 1-8.

MORAD, S., AL-RAMADAN, K., KETZER, J. M. & DE ROS, L. 2010. The impact of diagenesis on the heterogeneity of sandstone reservoirs: A review of the role of depositional facies and sequence stratigraphy. *AAPG bulletin,* 94**,** 1267-1309.

MORAD, S., ISMAIL, H. B., ROS, L. D., AL-AASM, I. & SERRHINI, N. E. 1994. Diagenesis and formation water chemistry of Triassic reservoir sandstones from southern Tunisia. *Sedimentology,* 41**,** 1253-1272.

MORAD, S., KETZER, J. & DE ROS, L. F. 2000. Spatial and temporal distribution of diagenetic alterations in siliciclastic rocks: implications for mass transfer in sedimentary basins. *Sedimentology,* 47**,** 95-120.

MORAES, M. A. 1989. Diagenetic evolution of Cretaceous-Tertiary turbidite reservoirs, Campos Basin, Brazil. *AAPG Bulletin,* 73**,** 598-612.

MORLEY, C. K., KING, R., HILLIS, R., TINGAY, M. & BACKE, G. 2011. Deepwater fold and thrust belt classification, tectonics, structure and hydrocarbon prospectivity: A review. *Earth-Science Reviews,* 104**,** 41-91.

MOSCARDELLI, L., RAMNARINE, S. K., WOOD, L. & DUNLAP, D. B. 2013. Seismic geomorphological analysis and hydrocarbon potential of the Lower Cretaceous Cromer Knoll Group, Heidrun field, Norway. *AAPG bulletin,* 97**,** 1227-1248.

NEILSON, J. E., OXTOBY, N. H. & SIMMONS, M. D. 1996. Effect of Petroleum Emplacement on Reservoir Quality in the Thamama Reservoirs ofAbu Dhabi. *Society of Petroleum Engineers***,** 989-1000.

NELSKAMP, S., DAVID, P. & LITTKE, R. 2008. A comparison of burial, maturity and temperature histories of selected wells from sedimentary basins in The Netherlands. *International journal of earth sciences,* 97**,** 931-953.

NIELSEN, S. B. 1996. Sensitivity analysis in thermal and maturity modelling. *Marine and Petroleum Geology,* 13**,** 415-425.

NWACHUKWU, J. I. & CHUKWURA, P. I. 1986. Organic matter of Agbada formation, Niger delta, Nigeria. *AAPG Bulletin,* 70**,** 48-55.

NWACHUKWU, S. 1976. Approximate geothermal gradients in Niger Delta Sedimentary Basin. *AAPG Bulletin,* 60**,** 1073-1077.

OBAJE, N. G. 2009. *Geology and mineral resources of Nigeria*, Springer.

OFURHIE, M. A., AGHA, U. G., LUFADEJU, A. O. & INEH, G. C. 2002. Turbidite Depositional Environment In Deepwater Of Nigeria. *Offshore Technology Conference.* Houston, Texas U.S.A: Offshore Technology Conference.

OKOH, E., SATHYAMOORTHY, S. & EBITU, S. Modelling High Rate Fractured Injection in the Bonga Field. Nigeria Annual International Conference and Exhibition, 2010. Society of Petroleum Engineers.

PARTYKA, G., GRIDLEY, J. & LOPEZ, J. 1999. Interpretational applications of spectral decomposition in reservoir characterization. *The Leading Edge,* 18**,** 353-360.

PAXTON, S., SZABO, J., AJDUKIEWICZ, J. & KLIMENTIDIS, R. 2002. Construction of an intergranular volume compaction curve for evaluating and predicting compaction and porosity loss in rigid-grain sandstone reservoirs. *AAPG bulletin,* 86**,** 2047-2067.

PELLEAU, R., SERCEAU, A. & TOTALFINAELF 2002. The Girassol development: project challenges.

PENNINGTON, W. D., ACEVEDO, H., GREEN, A., HAATAJA, J., LEN, S., MINAEVA, A. & XIE, D. 2002. Calibration of seismic attributes for reservoir characterization. *Final Report MTU, Houghton*.

PEPPER, A. S. & CORVI, P. J. 1995. Simple kinetic models of petroleum formation. Part I: oil and gas generation from kerogen. *Marine and Petroleum Geology,* 12**,** 291-319.

PETERS, K. E., MOLDOWAN, J. M., MCCAFFREY, M. A. & FAGO, F. J. 1996. Selective biodegradation of extended hopanes to 25-norhopanes in petroleum reservoirs. Insights from molecular mechanics. *Organic Geochemistry,* 24**,** 765-783.

PETTERS, S. 1984. An ancient submarine canyon in the Oligocene-Miocene of the western Niger Delta. *Sedimentology,* 31**,** 805-810.

PINTO, C., ANTONIO, C., GUEDES, S. S., BRUHN, C. H., GOMES, J. A. T. & NETTO, J. Marlim complex development: a reservoir engineering overview. SPE Latin American and Caribbean Petroleum Engineering Conference, 2001. Society of Petroleum Engineers.

PIOVESANEL, E., CLAUDEL, G., ATEWOLOGUN, A., ADEYEMI, A. & YUH, S. AKPO Condensate Field Case Study, Nigeria: 4D Seismic Monitoring of a Complex Deepwater Turbidite Reservoir. IPTC 2013: International Petroleum Technology Conference, 2013.

PIRMEZ, C., HISCOTT, R. N. & KRONEN, J. Sandy turbidite successions at the base of channel-levee systems of the Amazon Fan revealed by FMS logs and cores: unraveling the facies architecture of large submarine fans. Proceedings of the Ocean Drilling Program. Scientific results, 1997. Ocean Drilling Program, 7-33.

PORTER, E. & JAMES, W. 1986. Influence of pressure, salinity, temperature and grain size on silica diagenesis in quartzose sandstones. *Chemical geology,* 57**,** 359-369.

POSAMENTIER, H. & ERSKINE, R. 1991. Seismic expression and recognition criteria of ancient submarine fans. *Seismic facies and sedimentary processes of submarine fans and turbidite systems.* Springer.

POSAMENTIER, H. W. 2003. Depositional elements associated with a basin floor channel-levee system: case study from the Gulf of Mexico. *Marine and Petroleum Geology,* 20**,** 677-690.

POSAMENTIER, H. W. & KOLLA, V. 2003. Seismic geomorphology and stratigraphy of depositional elements in deep-water settings. *Journal of Sedimentary Research,* 73**,** 367-388.

PRATHER, B. E. 2003. Controls on reservoir distribution, architecture and stratigraphic trapping in slope settings. *Marine and Petroleum Geology,* 20**,** 529-545.

PRATHER, B. E., BOOTH, J. R., STEFFENS, G. S. & CRAIG, P. A. 1998. Classification, lithologic calibration, and stratigraphic succession of seismic facies of intraslope basins, deep-water Gulf of Mexico. *AAPG bulletin,* 82**,** 701-728.

PRIMMER, T. J., CADE, C. A., EVANS, J., GLUYAS, J. G., HOPKINS, M. S., OXTOBY, N. H., SMALLEY, P. C., WARREN, E. A. & WORDEN, R. H. 1997. Global patterns in sandstone diagenesis: their application to reservoir quality prediction for petroleum exploration.

RAISSON, F. & TEMPLE, F. Impact of Sedimentary Heterogeneity on Reservoir Monitoring in a Turbiditic Channel Complex–Angolan Deep Offshore Girassol Field Case. 66th EAGE Conference & Exhibition, 2004.

READING, H. G. & RICHARDS, M. 1994. Turbidite systems in deep-water basin margins classified by grain size and feeder system. *AAPG bulletin,* 78**,** 792-822.

REEDER, S. L. A Multi-Measurement Core-Log Integration for Advanced Formation Evaluation of Source Rock Formations: A Green River Case study. 2013. Unconventional Resources Technology Conference (URTEC).

REIJERS, T. 2011. Stratigraphy and sedimentology of the Niger Delta. *Geologos,* 17.

ROSALES, I. & PEREZ-GARCIA, A. 2010. Porosity development, diagenesis and basin modelling of a Lower Cretaceous (Albian) carbonate platform from northern Spain. *Geological Society, London, Special Publications,* 329**,** 317-342.

SALEM, A. M., MORAD, S., MATO, L. F. & AL-AASM, I. 2000. Diagenesis and reservoir-quality evolution of fluvial sandstones during progressive burial and uplift: Evidence from the Upper Jurassic Boipeba Member, Reconcavo Basin, Northeastern Brazil. *AAPG bulletin,* 84**,** 1015-1040.

SAMUEL, O. J., CORNFORD, C., JONES, M., ADEKEYE, O. A. & AKANDE, S. O. 2009. Improved understanding of the petroleum systems of the Niger Delta Basin, Nigeria. *Organic Geochemistry,* 40**,** 461-483.

SAUGY, L. & EYER, J. A. 2003. Fifty years of exploration in the Niger Delta (West Africa).

SAVOYE, B., BABONNEAU, N., DENNIELOU, B. & BEZ, M. 2009. Geological overview of the Angola–Congo margin, the Congo deep-sea fan and its submarine valleys. *Deep Sea Research Part II: Topical Studies in Oceanography,* 56**,** 2169-2182.

SCHMIDT, V. & MCDONALD, D. 1979. The role of secondary porosity in the course of sandstone diagenesis. *The Society of Economic Paleontologists and Mineralogists (SPEM),* 26**,** 175-207.

SCHMOKER, J. W. & GAUTIER, D. L. 1988. Sandstone porosity as a function of thermal maturity. *Geology,* 16**,** 1007-1010.

SCHWARZER, D. & LITTKE, R. 2007. Petroleum generation and migration in the 'Tight Gas' area of the German Rotliegend natural gas play: a basin modelling study. *Petroleum Geoscience,* 13**,** 37-62.

SCOTT, R. M. & TILLMAN, R. W. 1981. Stevens Sandstone (Miocene), San Joaquin Basin, California.

SHANMUGAM, G. 1998. Dimensions and geometries of the components of deepwater systems. *Spec.Publ.Mobil Technology Co., Dallas, Tx***,** 110pp.

SHANMUGAM, G. & MOIOLA, R. 1991. Types of Submarine Fan Lobes: Models and Implications (1). *AAPG Bulletin,* 75**,** 156-179.

SHORT, K. & STAUBLE, A. 1967. Outline of geology of Niger Delta. *AAPG bulletin,* 51**,** 761-779.

SIEVER, R. 1983. Burial history and diagenetic reaction kinetics. *AAPG Bulletin,* 67**,** 684-691.

SNEIDER, R. M. 1990. Reservoir Description of Sandstones. *Sandstone Petroleum Reservoirs.* Springer.

SOLDAN, A., CERQUEIRA, J., FERREIRA, J., TRINDADE, L., SCARTON, J. & CORÁ, C. 1995. Giant Deep Water Oil Fields in Campos Basin, Brazil: A Geochemical Approach. *Revista Latino-Americana de Geoquimica Organica,* 1**,** 14-27.

SOMBRA, C. L. & CHANG, H. K. 1997. Burial history and porosity evolution of Brazilian Upper Jurassic to Tertiary sandstone reservoirs.

SONDE, A., OMOBUDE, O., CHUDI, O., OGHENE, U. & COKER, T. Integrated 3D Modelling in a Structurally Complex Brown Field: A Foundation for Improved Reservoir Management and Optimisation of Further Development. Nigeria Annual International Conference and Exhibition, 2011. Society of Petroleum Engineers.

SOUZA, J., SCARTON, J., CANDIDO, A., CRUZ, C. & CORA, C. The Marlim and Albacora Fields: Geophysical Geological and Reservoir Aspects. Offshore Technology Conference, 1989. Offshore Technology Conference.

STONELEY, R. 1966. The Niger delta region in the light of the theory of continental drift. *Geological Magazine,* 103**,** 385-397.

STOW, D., READING, H. & COLLINSON, J. 1996. Deep seas. *Sedimentary environments: processes, facies and stratigraphy,* 3**,** 395-453.

STOW, D. A. & JOHANSSON, M. 2000. Deep-water massive sands: nature, origin and hydrocarbon implications. *Marine and Petroleum Geology,* 17**,** 145-174.

STOW, D. A. & MAYALL, M. 2000. Deep-water sedimentary systems: new models for the 21st century. *Marine and Petroleum Geology,* 17**,** 125-135.

STOW, D. A. & SHANMUGAM, G. 1980. Sequence of structures in fine-grained turbidites: comparison of recent deep-sea and ancient flysch sediments. *Sedimentary Geology,* 25**,** 23-42.

STOW, D. A. V. 2005. *Sedimentary rocks in the field: a colour guide*, CRC Press.

SWEENEY, J. J. & BURNHAM, A. K. 1990. Evaluation of a Simple Model of Vitrinite Reflectance Based on Chemical Kinetics (1). *AAPG Bulletin,* 74**,** 1559-1570.

TADA, R. & SIEVER, R. 1989. Pressure solution during diagenesis. *Annual Review of Earth and Planetary Sciences,* 17**,** 89.

TALÇIN, M. N. 1991. Basin modeling and hydrocarbon exploration. *Journal of Petroleum Science and Engineering,* 5**,** 379-398.

AASE, N. E., BJORKUM, P. A. & NADEAU, P. H. 1996. The effect of grain-coating microquartz on preservation of reservoir porosity. *AAPG bulletin,* 80**,** 1654-1673.

ADEOGBA, A. A. 2003. Architecture and depositional controls of deep-water deposits as imaged by near-surface 3-D seismic data, Nigeria. Stanford University, United States.

ADEOGBA, A. A., MCHARGUE, T. R. & GRAHAM, S. A. 2005. Transient fan architecture and depositional controls from near-surface 3-D seismic data, Niger Delta continental slope. *AAPG bulletin,* 89**,** 627-643.

AHMAD, M. N. & ROWELL, P. 2012. Application of spectral decomposition and seismic attributes to understand the structure and distribution of sand reservoirs within Tertiary rift basins of the Gulf of Thailand. *The Leading Edge,* 31**,** 630-634.

AJDUKIEWICZ, J. M. & LARESE, R. E. 2012. How clay grain coats inhibit quartz cement and preserve porosity in deeply buried sandstones: Observations and experiments. *AAPG bulletin,* 96**,** 2091-2119.

AL-HAJERI, M. M., AL SAEED, M., DERKS, J., FUCHS, T., HANTSCHEL, T., KAUERAUF, A., NEUMAIER, M., SCHENK, O., SWIENTEK, O. & TESSEN, N. 2009. Basin and petroleum system modeling. *Oilfield Review,* 21**,** 14-29.

ALLEN, P. A. & ALLEN, J. R. 1990. *Basin analysis: principles and applications,* Cornwall, Wiley-Blackwell.

ANDERSON, A. V., SICKAFOOSE, D. K., FAHRER, T. R. & GOTTSCHALK, R. R. 2012. Interaction of Oligocene–Miocene deep-water depositional systems with actively evolving structures: The Lower Congo Basin, offshore Angola.

ANDERSON, J., CARTWRIGHT, J., DRYSDALL, S. & VIVIAN, N. 2000. Controls on turbidite sand deposition during gravity-driven extension of a passive margin: examples from Miocene sediments in Block 4, Angola. *Marine and Petroleum Geology,* 17**,** 1165-1203.

ANKA, Z., SÉRANNE, M., LOPEZ, M., SCHECK-WENDEROTH, M. & SAVOYE, B. 2009. The long-term evolution of the Congo deep-sea fan: A basin-wide view of the interaction between a giant submarine fan and a mature passive margin (ZaiAngo project). *Tectonophysics,* 470**,** 42-56.

ARMSTRONG, L., TEN HAVE, A. & JOHNSON, H. 1987. The geology of the Gannet fields, central North Sea, UK sector. *Petroleum geology of north-west Europe: London, Graham and Trotman***,** 533-548.

ASQUITH, G. B. & KRYGOWSKI, D. 2004. Basic Well Log Analysis. *American Association of Petroleum Geologists,*.

ATHY, L. F. 1930. Density, porosity, and compaction of sedimentary rocks. *AAPG Bulletin,* 14**,** 1-24.

AVBOVBO, A. A. 1978. Tertiary Lithostratigraphy of Niger Delta: GEOLOGIC NOTES. *AAPG Bulletin,* 62**,** 295-300.

BADLEY, M. E. 1985. *Practical seismic interpretation,* United States of America, D. Reidel Publishing Company.

BANDELE, V. A. & CLAUDEL, G. Leading Edge Subsurface Technologies for AKPO A Complex Condensate Field. Offshore Technology Conference, 2010. Offshore Technology Conference.

BARCLAY, S. & WORDEN, R. 2009. Petrophysical and petrographical analysis of quartz cement volumes across oil–water contacts in the Magnus Field, northern North Sea. *Quartz Cementation in Sandstones: Special Publication 29 of the IAS,* 14**,** 147.

BARKER, C. 1996. *Thermal modeling of petroleum generation: theory and application,* Netherlands, Elservier.

BEAUBOUEF, R. & FRIEDMANN, S. High resolution seismic/sequence stratigraphic framework for the evolution of Pleistocene intra slope basins, western Gulf of Mexico: depositional models and reservoir analogs. Deep-water reservoirs of the world: Gulf Coast Section SEPM 20th Annual Research Conference, 2000. SEPM, 40-60.

BEAUBOUEF, R., VAN WAGONER, J. & ADAIR, N. 2003. Ultra-high resolution 3-d characterization of deep-water deposits—II: Insights into the evolution of a submarine fan and comparisons with river deltas. *Extended Abstracts, May***,** 11-14.

BEGLINGER, S. E., DOUST, H. & CLOETINGH, S. 2012. Relating petroleum system and play development to basin evolution: West African South Atlantic basins. *Marine and Petroleum Geology,* 30**,** 1-25.

BILOTTI, F. & SHAW, J. H. 2005. Deep-water Niger Delta fold and thrust belt modeled as a critical-taper wedge: The influence of elevated basal fluid pressure on structural styles. *AAPG bulletin,* 89**,** 1475-1491.

BJORKUM, P. A. 1996. How important is pressure in causing dissolution of quartz in sandstones? *Journal of Sedimentary Research,* 66.

BJØRKUM, P. A., OELKERS, E. H., NADEAU, P. H., WALDERHAUG, O. & MURPHY, W. M. 1998. Porosity prediction in quartzose sandstones as a function of time, temperature, depth, stylolite frequency, and hydrocarbon saturation. *AAPG Bulletin-American Association of Petroleum Geologists,* 82**,** 637.

BJØRLYKKE, K. & HØEG, K. 1997. Effects of burial diagenesis on stresses, compaction and fluid flow in sedimentary basins. *Marine and Petroleum Geology,* 14**,** 267-276.

BLOCH, S., DUNCAN, J. M. J. & BRIZZOLARA, D. 1990. Porosity Prediction, Prior to Drilling, in Sandstones of the Kekiktuk Formation (Mississippian), North Slope of Alaska (1). *AAPG Bulletin,* 74**,** 1371-1385.

BLOCH, S., LANDER, R. H. & BONNELL, L. 2002. Anomalously high porosity and permeability in deeply buried sandstone reservoirs: Origin and predictability. *AAPG bulletin,* 86**,** 301-328.

BLUNDELL, D. 1991. Some observations on basin evolution and dynamics. *Journal of the Geological Society,* 148**,** 789-800.

BOGGS, S., JR. 1987. *Principles of sedimentology and stratigraphy,* New York, Macmillan.

BOUMA, A. H. & RAVENNE, C. 2004. The Bouma Sequence (1962) and the resurgence of geological interest in the French Maritime Alps (1980s): the influence of the Grès d'Annot in developing ideas of turbidite systems. *Geological Society, London, Special Publications,* 221**,** 27-38.

BREDEHOEFT, J. D. & HANSHAW, R. B. 1968. On the maintenance of anomalous fluid pressures: I. Thick sedimentary sequences. *Geological Society of America Bulletin,* 79**,** 1097-1106.

BRENNER, R. L., LUDVIGSON, G. A., SEAL, R. & DOGAN, A. U. 1991. Diagenetic modeling of siliciclastic systems: Status report. *Kansas Geological Survey, Bulletin,* 233**,** 123-137.

BRIGGS, S. E., CARTWRIGHT, J. & DAVIES, R. J. 2009. Crustal structure of the deepwater west Niger Delta passive margin from the interpretation of seismic reflection data. *Marine and Petroleum Geology,* 26**,** 936-950.

BROUCKE, O., TEMPLE, F., ROUBY, D., ROBIN, C., CALASSOU, S., NALPAS, T. & GUILLOCHEAU, F. 2004. The role of deformation processes on the geometry of mud-dominated turbiditic systems, Oligocene and Lower–Middle Miocene of the Lower Congo basin (West African Margin). *Marine and Petroleum Geology,* 21**,** 327-348.

BROWN, A. R. 2011. Interpretation of three-dimensional seismic data. *AAPG Memoir,* 42**,** 295-308.

BRUHN, C. H., GOMES, J. A. T., LUCCHESE JR, C. & JOHANN, P. R. Campos basin: reservoir characterization and management–Historical overview and future challenges. Offshore Technology Conference, Houston, Texas, USA, 2003. 5-8.

BURKE, K. 1972. Longshore drift, submarine canyons, and submarine fans in development of Niger Delta. *AAPG Bulletin,* 56**,** 1975-1983.

BURKE, K., DESSAUVAGIE, T. & WHITEMAN, A. 1971. Opening of the Gulf of Guinea and geological history of the Benue Depression and Niger Delta. *Nature,* 233**,** 51-55.

BURKE, K., MACGREGOR, D. & CAMERON, N. 2003. Africa's petroleum systems: four tectonic 'Aces' in the past 600 million years. *Geological Society, London, Special Publications,* 207**,** 21-60.

BURNHAM, A. K. & SWEENEY, J. J. 1989. A chemical kinetic model of vitrinite maturation and reflectance. *Geochimica et Cosmochimica Acta,* 53**,** 2649-2657.

BUSTIN, R. 1988. Sedimentology and characteristics of dispersed organic matter in Tertiary Niger Delta: origin of source rocks in a deltaic environment. *AAPG Bulletin,* 72**,** 277-298.

CAMERON, N. & WHITE, K. 1999. Exploration Opportunities in Offshore Deepwater Africa. *IBC 'Oil and Gas Developments in West Africa', London, UK***,** 25-26.

CHAPIN, M., SWINBURN, P., VAN DER WEIDEN, R., SKALOUD, D., ADESANYA, S., STEVENS, D., VARLEY, C., WILKIE, J., BRENTJENS, E. & BLAAUW, M. 2002. Integrated seismic and subsurface characterization of Bonga Field, offshore Nigeria. *The Leading Edge,* 21**,** 1125-1131.

CHEN, B., WEI, X.-D., REN, D.-Z., ZHANG, Y.-Z., WANG, Y.-N. & LI, J.-H. 2010. Small fault identification based on spectrum decomposition technique. *Shiyou Diqiu Wuli Kantan(Oil Geophysical Prospecting),* 45**,** 890-894.

CHOPRA, S. & MARFURT, K. J. 2008. Emerging and future trends in seismic attributes. *The Leading Edge,* 27**,** 298-318.

CHOPRA, S. & MARFURT, K. J. 2012. Evolution of seismic interpretation during the last three decades. *The Leading Edge,* 31**,** 654-676.

CHOUGH, S. K. & ORTON, G. J. 1995. Fan deltas - depositional styles and controls-PREFACE. *Sedimentary Geology,* 98 (1-4).

CHUDI, O., LEWIS, H. & STOW, D. A. 2015. 3D seismic interpretation of depositional architecture and reservoir potential of deep-water untapped Oligocene sequence of the western Niger Delta. Heriot Watt University, Edinburgh, United Kingdom.

CHUDI, O., LEWIS, H., STOW, D. A. & BUCKMAN, J. O. 2014. Reservoir quality prediction via integrated diagenesis, advanced petrophysics and basin modelling: Deepwater Oligocene sandstone Western Niger Delta. Heriot Watt University, Edinburgh, United Kingdom.

CHUDI, O. & SIMON, R. 2012. Petrophysical Characterization of Radioactive Sands - Integrating Well Logs and Core Information: A Case Study in the Niger Delta. Society of Petroleum Engineers.

COHEN, H. A. & MCCLAY, K. 1996. Sedimentation and shale tectonics of the northwestern Niger Delta front. *Marine and Petroleum Geology,* 13**,** 313-328.

COOKE, N., SZAFIAN, P., GRUENWALD, R. & SCHULER, L. 2014. Forward modelling to understand colour responses in an HDFD RGB blend around a gas discovery. *first break,* 32**,** 87-97.

CORREDOR, F., SHAW, J. H. & BILOTTI, F. 2005. Structural styles in the deep-water fold and thrust belts of the Niger Delta. *AAPG bulletin,* 89**,** 753-780.

CRONIN, B. T. 1995. Structurally-controlled deep sea channel courses: examples from the Miocene of southeast Spain and the Alboran Sea, southwest Mediterranean. *Geological Society, London, Special Publications,* 94**,** 115-135.

DA COSTA, J. L., SCHIRMER, T. & LAWS, B. 2001. AAPG Memoir 74, Chapter 25: Lower Congo Basin, Deep-Water Exploration Province, Offshore West Africa.

DAILLY, P., HENDERSON, T., HUDGENS, E., KANSCHAT, K. & LOWRY, P. 2013. Exploration for Cretaceous stratigraphic traps in the Gulf of Guinea, West Africa and the discovery of the Jubilee Field: a play opening discovery in the Tano Basin, Offshore Ghana. *Geological Society, London, Special Publications,* 369**,** 235-248.

DAMUTH, J. E. 1994. Neogene gravity tectonics and depositional processes on the deep Niger Delta continental margin. *Marine and Petroleum Geology,* 11**,** 320-346.

DE RUIG, M. J. & HUBBARD, S. M. 2006. Seismic facies and reservoir characteristics of a deep-marine channel belt in the Molasse foreland basin, Puchkirchen Formation, Austria. *AAPG bulletin,* 90**,** 735-752.

DELATTRE, E., AUTHIER, J. F., RODOT, F., PETIT, G. & ALFENORE, J. Review of sand control results and performance on a deep water development-A case study from the Girassol Field Angola. SPE Annual Technical Conference and Exhibition, 2004. Society of Petroleum Engineers.

DEMING, D. 1994. Overburden rock, temperature, and heat flow. *AGE (Ma),* 200**,** 100.

DEPTUCK, M. E., PIPER, D. J., SAVOYE, B. & GERVAIS, A. 2008. Dimensions and architecture of late Pleistocene submarine lobes off the northern margin of East Corsica. *Sedimentology,* 55**,** 869-898.

DEPTUCK, M. E., SYLVESTER, Z., PIRMEZ, C. & O'BYRNE, C. 2007. Migration–aggradation history and 3-D seismic geomorphology of submarine channels in the Pleistocene Benin-major Canyon, western Niger Delta slope. *Marine and Petroleum Geology.*

DERKS, J., SWIENTEK, O., FUCHS, T., KAUERAUF, A., AL-QUATTAN, M. & AL-SAEED, M. 2012. Three-Dimensional Basin and Petroleum System Model of the Cretaceous Burgan

Formation, Kuwait: Model-in-Model, High-Resolution Charge Modeling. *Basin Modeling: New Horizons in Research and Applications, AAPG Hedberg Series, No. 4,* 4**,** 159.

DESSUS, J. L. & ABREU, J. 2002. Girassol: Drilling and Completion Experience gained through first 12 wells. *OTC,* 14168**,** 6-9.

DMITRIEVA, E., JACKSON, C. A., HUUSE, M. & MCCARTHY, A. 2012. Paleocene deep-water depositional systems in the North Sea Basin a 3D seismic and well data case study, offshore Norway. *Petroleum Geoscience,* 18**,** 97-114.

DOUST, H. & OMATSOLA, E. 1990. Niger Delta. In:Edwards,J.D., Santogrossi, P.A (Eds), Divergent/Passive Margin Basins. *American Assoiciation of Petroleum Geologist,* 4**,** 239-248.

DUNLAP, D. B., WOOD, L. J., WEISENBERGER, C. & JABOUR, H. 2010. Seismic geomorphology of offshore Moroccos east margin, Safi Haute Mer area. *AAPG bulletin,* 94**,** 615-642.

DUTION, S. P., HAMLIN, H. S., FOLK, R. L. & CLIFT, S. J. 1996. Early siderite cementation as a control on reservoir quality in submarine fan sandstones, Sonora Canyon gas play, Val Verde Basin, Texas. *Society of Sedimentary Geology (SEPM),* 55**,** 115-127.

EHRENBERG, S. & NADEAU, P. 1989. Formation of diagenetic illite in sandstones of the Garn Formation, Haltenbanken area, mid-Norwegian continental shelf. *Clay Minerals,* 24**,** 233-253.

EJEDAWE, J., COKER, S., LAMBERT-AIKHIONBARE, D., ALOFE, K. & ADOH, F. 1984. Evolution of oil-generative window and oil and gas occurrence in Tertiary Niger Delta Basin. *AAPG Bulletin,* 68**,** 1744-1751.

EKWEOZOR, C. & DAUKORU, E. 1984. Petroleum source-bed evaluation of Tertiary Niger Delta: reply. *AAPG Bulletin,* 68**,** 390-394.

EKWEOZOR, C. & UDO, O. T. 1988. The oleananes: Origin, maturation and limits of occurence in southern Nigeria sedimentary basins. *Organic Geochemistry,* 13**,** 131-140.

EKWEOZOR, C. M. & OKOYE, N. V. 1980. Petroleum Source-Bed Evaluation of Tertiary Niger Delta: GEOLOGIC NOTES. *AAPG Bulletin,* 64**,** 1251-1259.

EMERY, D., SMALLEY, P., OXTOBY, N., RAGNARSDOTTIR, K., AAGAARD, P., HALLIDAY, A., COLEMAN, M. & PETROVICH, R. 1993. Synchronous Oil Migration and Cementation in Sandstone Reservoirs Demonstrated by Quantitative Description of Diagenesis [and Discussion]. *Philosophical Transactions of the Royal Society of London. Series A: Physical and Engineering Sciences,* 344**,** 115-125.

EVAMY, B. D., HAREMBOURE, J., KAMERLING, P., KNAAP, W. A., MOLLY, F. A. & ROWLANDS, P. H. 1978. Hydrocarbon habitat of Tertiary Niger Delta. *American Association of Petroleum Geologists Bulletin,* 62**,** 1-39.

EVANS, J., HOGG, A. J., HOPKINS, M. S. & HOWARTH, R. J. 1994. Quantification of quartz cements using combined SEM, CL, and image analysis. *Journal of Sedimentary Research,* 64.

FEHINTOLA, T., AL-MANDHARY, I. & WEAVER, S. Probabilistic Inversion of Complex Channelised Reservoirs in Deep Water Niger Delta. Nigeria Annual International Conference and Exhibition, 2009. Society of Petroleum Engineers.

FRANKL, E. & CORDRY, E. The Niger Delta oil province: Recent developments onshore and offshore. 7th World Petroleum Congress, 1967. World Petroleum Congress.

GALLOWAY, W. 1984. Hydrogeologic regimes of sandstone diagenesis. *Clastic diagenesis: AAPG Memoir,* 37**,** 3-13.

GALLOWAY, W. E. 1975. Process framework for describing the morphologic and stratigraphic evolution of deltaic depositional systems.

GALLOWAY, W. E. 1998. Siliciclastic slope and base-of-slope depositional systems: component facies, stratigraphic architecture, and classification. *AAPG bulletin,* 82**,** 569-595.

GAY, A., LOPEZ, M., COCHONAT, P., SÉRANNE, M., LEVACHÉ, D. & SERMONDADAZ, G. 2006. Isolated seafloor pockmarks linked to BSRs, fluid chimneys, polygonal faults and stacked Oligocene–Miocene turbiditic palaeochannels in the Lower Congo Basin. *Marine Geology,* 226**,** 25-40.

GEE, M. & GAWTHORPE, R. 2006. Submarine channels controlled by salt tectonics: Examples from 3D seismic data offshore Angola. *Marine and Petroleum Geology,* 23**,** 443-458.

GENIK, G. 1993. Petroleum geology of cretaceous-Tertiary rift basins in Niger, Chad, and central African republic. *AAPG Bulletin,* 77**,** 1405-1434.

GIER, S., WORDEN, R. H., JOHNS, W. D. & KURZWEIL, H. 2008. Diagenesis and reservoir quality of Miocene sandstones in the Vienna Basin, Austria. *Marine and Petroleum Geology,* 25**,** 681-695.

GILES, M., STEVENSON, S., MARTIN, S., CANNON, S., HAMILTON, P., MARSHALL, J. & SAMWAYS, G. 1992. The reservoir properties and diagenesis of the Brent Group: a regional perspective. *Geological Society, London, Special Publications,* 61**,** 289-327.

GLUYAS, J. & CADE, C. A. 1998. Prediction of porosity in compacted sands. *MEMOIRS-AMERICAN ASSOCIATION OF PETROLEUM GEOLOGISTS***,** 19-28.

GRAUE, K. 2000. Mud volcanoes in deepwater Nigeria. *Marine and Petroleum Geology,* 17**,** 959-974.

HAACK, R. C., SUNDARARAMAN, P., DIEDJOMAHOR, J. O., XIAO, H., GANT, N. J., MAY, E. D. & KELSCH, K. 2000. AAPG Memoir 73, Chapter 16: Niger Delta Petroleum Systems, Nigeria.

HANTSCHEL, T. & KAUERAUF, A. 2009a. *Fundamentals of basin and petroleum systems modeling,* Berlin, Springer.

HANTSCHEL, T. & KAUERAUF, A. I. 2009b. *Fundamentals of basin and petroleum systems modeling*, Springer.

HART, B. S. 2008. Channel detection in 3-D seismic data using sweetness. *AAPG bulletin,* 92**,** 733-742.

HAUGHTON, P. D. 1994. Deposits of deflected and ponded turbidityents, currents, Sorbas Basin, southeast Spain. *Journal of Sedimentary Research,* 64.

HEGARTY, K. A., WEISSEL, J. K. & MUTTER, J. C. 1988. Subsidence history of Australia's southern margin: constraints on basin models. *AAPG Bulletin,* 72**,** 615-633.

HEMPTON, M., MARSHALL, J., SADLER, S., HOGG, N., CHARLES, R. & HARVEY, C. Turbidite reservoirs of the Sele Formation, Central North Sea: geological challenges for improving production. Geological Society, London, Petroleum Geology Conference series, 2005. Geological Society of London, 449-459.

HERMANRUD, C. 1993. Basin modelling techniques-an overview. *Basin modelling: advances and applications: Norwegian Petroleum Society (NPF) Special Publication,* 3**,** 1-34.

HIGLEY, D. K., LEWAN, M., ROBERTS, L. N. & HENRY, M. E. 2006. Petroleum system modeling capabilities for use in oil and gas resource assessments.

HONARPOUR, M., KOEDERITZ, F. & HERBERT, A. 1986. Relative permeability of petroleum reservoirs.

HOUSEKNECHT, D. W. 1984. Influence of grain size and temperature on intergranular pressure solution, quartz cementation, and porosity in a quartzose sandstone. *Journal of Sedimentary Research,* 54.

JAMES, W., WILMAR, G. C. & DAVIDSON, B. G. 1986. Role of quartz type and grain size in silica diagenesis, Nugget Sandstone, south-central Wyoming. *Journal of Sedimentary Research,* 56.

JEGOU, I., SAVOYE, B., PIRMEZ, C. & DROZ, L. 2008. Channel-mouth lobe complex of the recent Amazon Fan: the missing piece. *Marine Geology,* 252**,** 62-77.

JIAN-PING, L., PAN, X.-H., JUN, M., TIAN, Z.-J., CHEN, Y.-J. & WAN, L.-K. 2008. Petroleum geology and resources in West Africa: An overview. *Petroleum Exploration and Development,* 35**,** 378-384.

KOLLA, V., BOURGES, P., URRUTY, J.-M. & SAFA, P. 2001. Evolution of deep-water Tertiary sinuous channels offshore Angola (west Africa) and implications for reservoir architecture. *AAPG bulletin,* 85**,** 1373-1405.

KOLLA, V. & MACURDA JR, D. 1988. Sea-level changes and timing of turbidity-current events in deep-sea fan systems. *Wilgus, CK, Hastings, BS, Kendall,., CG, St., C., Posamentier, HW, Ross, CA, Van Wagoner, JC (Eds.), Sea-level Changes e An Integrated Approach. SEPM Special Publication,* 42**,** 381e392.

LAMBERT-AIKHIONBARE, D. & IBE, A. 1984. Petroleum source-bed evaluation of Tertiary Niger delta: discussion. *AAPG Bulletin,* 68**,** 387-389.

LANDER, R. H., LARESE, R. E. & BONNELL, L. M. 2006. Why do microquartz coatings preserve sandstone reservoir quality? *American Association of Petroleum Geologists***,** 60.

LANDER, R. H., LARESE, R. E. & BONNELL, L. M. 2008. Toward more accurate quartz cement models: The importance of euhedral versus noneuhedral growth rates. *AAPG bulletin,* 92**,** 1537-1563.

LANDER, R. H. & WALDERHAUG, O. 1999. Predicting porosity through simulating sandstone compaction and quartz cementation. *AAPG bulletin,* 83**,** 433-449.

LEFFLER, W. L., PATTAROZZI, R. & STERLING, G. 2011. *Deepwater petroleum exploration & production: A nontechnical guide*, PennWell Books.

LEHNER, P. & DE RUITER, P. A. C. 1977. Structural history of Atlantic margin of Africa. *AAPG Bulletin,* 61**,** 961-981.

LOUCKS, R. G., DODGE, M. M. & GALLOWAY, W. E. 1984. Regional controls on diagenesis and reservoir quality in lower Tertiary sandstones along the Texas Gulf Coast: Part 1. Concepts and principles.

LUNDEGARD, P. D. 1992. Sandstone Porosity Loss--A. *Journal of Sedimentary Research,* 62.

MACGREGOR, D. Petroleum Basins of Sub-Saharan Africa. 12th PESGB/HGS Conference on African E & P Review, 2013 London, United Kingdom. 1-218.

MANSURBEG, H. 2007. Diagenesis and Reservoir-Quality Evolution of Deep-Water Turbidites: Links to Basin Setting, Depositional Facies, and Sequence Stratigraphy.

MANSURBEG, H., EL-GHALI, M. A., MORAD, S. & PLINK-BJÖRKLUND, P. 2006. The impact of meteoric water on the diagenetic alterations in deep-water, marine siliciclastic turbidites. *Journal of Geochemical Exploration,* 89**,** 254-258.

MARCHAND, A. M., SMALLEY, P. C., HASZELDINE, R. S. & FALLICK, A. E. 2002. Note on the importance of hydrocarbon fill for reservoir quality prediction in sandstones. *AAPG bulletin,* 86**,** 1561-1572.

MATTHEW, O. S., WON, J., UDOEKONG, G., IBIOLA, O. & DIXON, D. 2010. Resolving the Structural Complexities in the Deepwater Niger-Delta Fold and Thrust Belt: A Case Study from the Western Lobe, Nigerian Offshore Depobelt. *AAPG Search and Discovery Article* [Online].

MAYALL, M., LONERGAN, L., BOWMAN, A., JAMES, S., MILLS, K., PRIMMER, T., POPE, D., ROGERS, L. & SKEENE, R. 2010. The response of turbidite slope channels to growth-induced seabed topography. *AAPG bulletin,* 94**,** 1011-1030.

MAYALL, M. & STEWART, I. The architecture of turbidite slope channels. Deep-Water Reservoirs of the World: SEPM, Gulf Coast Section, 20th Annual Research Conference, 2000. SEPM, 578-586.

MCBRIDE, E. F. 1963. A classification of common sandstones. *Journal of Sedimentary Research,* 33.

MCBRIDE, E. F. 1989. Quartz cement in sandstones: a review. *Earth-Science Reviews,* 26**,** 69-112.

MCDONNELL, A., LOUCKS, R. G. & GALLOWAY, W. E. 2008. Paleocene to Eocene deep-water slope canyons, western Gulf of Mexico: Further insights for the provenance of deep-water offshore Wilcox Group plays. *AAPG bulletin,* 92**,** 1169-1189.

MITCHELL, M. I. 2012. GHANA'S OFFSHORE OIL: RESOURCE CURSE OR BLESSING? *Africa Portal Backgrounder,* 44**,** 1-8.

MORAD, S., AL-RAMADAN, K., KETZER, J. M. & DE ROS, L. 2010. The impact of diagenesis on the heterogeneity of sandstone reservoirs: A review of the role of depositional facies and sequence stratigraphy. *AAPG bulletin,* 94**,** 1267-1309.

MORAD, S., ISMAIL, H. B., ROS, L. D., AL-AASM, I. & SERRHINI, N. E. 1994. Diagenesis and formation water chemistry of Triassic reservoir sandstones from southern Tunisia. *Sedimentology,* 41**,** 1253-1272.

MORAD, S., KETZER, J. & DE ROS, L. F. 2000. Spatial and temporal distribution of diagenetic alterations in siliciclastic rocks: implications for mass transfer in sedimentary basins. *Sedimentology,* 47**,** 95-120.

MORAES, M. A. 1989. Diagenetic evolution of Cretaceous-Tertiary turbidite reservoirs, Campos Basin, Brazil. *AAPG Bulletin,* 73**,** 598-612.

MORLEY, C. K., KING, R., HILLIS, R., TINGAY, M. & BACKE, G. 2011. Deepwater fold and thrust belt classification, tectonics, structure and hydrocarbon prospectivity: A review. *Earth-Science Reviews,* 104**,** 41-91.

MOSCARDELLI, L., RAMNARINE, S. K., WOOD, L. & DUNLAP, D. B. 2013. Seismic geomorphological analysis and hydrocarbon potential of the Lower Cretaceous Cromer Knoll Group, Heidrun field, Norway. *AAPG bulletin,* 97**,** 1227-1248.

NEILSON, J. E., OXTOBY, N. H. & SIMMONS, M. D. 1996. Effect of Petroleum Emplacement on Reservoir Quality in the Thamama Reservoirs ofAbu Dhabi. *Society of Petroleum Engineers***,** 989-1000.

NELSKAMP, S., DAVID, P. & LITTKE, R. 2008. A comparison of burial, maturity and temperature histories of selected wells from sedimentary basins in The Netherlands. *International journal of earth sciences,* 97**,** 931-953.

NIELSEN, S. B. 1996. Sensitivity analysis in thermal and maturity modelling. *Marine and Petroleum Geology,* 13**,** 415-425.

NWACHUKWU, J. I. & CHUKWURA, P. I. 1986. Organic matter of Agbada formation, Niger delta, Nigeria. *AAPG Bulletin,* 70**,** 48-55.

NWACHUKWU, S. 1976. Approximate geothermal gradients in Niger Delta Sedimentary Basin. *AAPG Bulletin,* 60**,** 1073-1077.

OBAJE, N. G. 2009. *Geology and mineral resources of Nigeria*, Springer.

OFURHIE, M. A., AGHA, U. G., LUFADEJU, A. O. & INEH, G. C. 2002. Turbidite Depositional Environment In Deepwater Of Nigeria. *Offshore Technology Conference.* Houston, Texas U.S.A: Offshore Technology Conference.

OKOH, E., SATHYAMOORTHY, S. & EBITU, S. Modelling High Rate Fractured Injection in the Bonga Field. Nigeria Annual International Conference and Exhibition, 2010. Society of Petroleum Engineers.

PARTYKA, G., GRIDLEY, J. & LOPEZ, J. 1999. Interpretational applications of spectral decomposition in reservoir characterization. *The Leading Edge,* 18**,** 353-360.

PAXTON, S., SZABO, J., AJDUKIEWICZ, J. & KLIMENTIDIS, R. 2002. Construction of an intergranular volume compaction curve for evaluating and predicting compaction and porosity loss in rigid-grain sandstone reservoirs. *AAPG bulletin,* 86**,** 2047-2067.

PELLEAU, R., SERCEAU, A. & TOTALFINAELF 2002. The Girassol development: project challenges.

PENNINGTON, W. D., ACEVEDO, H., GREEN, A., HAATAJA, J., LEN, S., MINAEVA, A. & XIE, D. 2002. Calibration of seismic attributes for reservoir characterization. *Final Report MTU, Houghton*.

PEPPER, A. S. & CORVI, P. J. 1995. Simple kinetic models of petroleum formation. Part I: oil and gas generation from kerogen. *Marine and Petroleum Geology,* 12**,** 291-319.

PETERS, K. E., MOLDOWAN, J. M., MCCAFFREY, M. A. & FAGO, F. J. 1996. Selective biodegradation of extended hopanes to 25-norhopanes in petroleum reservoirs. Insights from molecular mechanics. *Organic Geochemistry,* 24**,** 765-783.

PETTERS, S. 1984. An ancient submarine canyon in the Oligocene-Miocene of the western Niger Delta. *Sedimentology,* 31**,** 805-810.

PINTO, C., ANTONIO, C., GUEDES, S. S., BRUHN, C. H., GOMES, J. A. T. & NETTO, J. Marlim complex development: a reservoir engineering overview. SPE Latin American and Caribbean Petroleum Engineering Conference, 2001. Society of Petroleum Engineers.

PIOVESANEL, E., CLAUDEL, G., ATEWOLOGUN, A., ADEYEMI, A. & YUH, S. AKPO Condensate Field Case Study, Nigeria: 4D Seismic Monitoring of a Complex Deepwater Turbidite Reservoir. IPTC 2013: International Petroleum Technology Conference, 2013.

PIRMEZ, C., HISCOTT, R. N. & KRONEN, J. Sandy turbidite successions at the base of channel-levee systems of the Amazon Fan revealed by FMS logs and cores: unraveling the facies architecture of large submarine fans. Proceedings of the Ocean Drilling Program. Scientific results, 1997. Ocean Drilling Program, 7-33.

PORTER, E. & JAMES, W. 1986. Influence of pressure, salinity, temperature and grain size on silica diagenesis in quartzose sandstones. *Chemical geology,* 57**,** 359-369.

POSAMENTIER, H. & ERSKINE, R. 1991. Seismic expression and recognition criteria of ancient submarine fans. *Seismic facies and sedimentary processes of submarine fans and turbidite systems.* Springer.

POSAMENTIER, H. W. 2003. Depositional elements associated with a basin floor channel-levee system: case study from the Gulf of Mexico. *Marine and Petroleum Geology,* 20**,** 677-690.

POSAMENTIER, H. W. & KOLLA, V. 2003. Seismic geomorphology and stratigraphy of depositional elements in deep-water settings. *Journal of Sedimentary Research,* 73**,** 367-388.

PRATHER, B. E. 2003. Controls on reservoir distribution, architecture and stratigraphic trapping in slope settings. *Marine and Petroleum Geology,* 20**,** 529-545.

PRATHER, B. E., BOOTH, J. R., STEFFENS, G. S. & CRAIG, P. A. 1998. Classification, lithologic calibration, and stratigraphic succession of seismic facies of intraslope basins, deep-water Gulf of Mexico. *AAPG bulletin,* 82**,** 701-728.

PRIMMER, T. J., CADE, C. A., EVANS, J., GLUYAS, J. G., HOPKINS, M. S., OXTOBY, N. H., SMALLEY, P. C., WARREN, E. A. & WORDEN, R. H. 1997. Global patterns in sandstone diagenesis: their application to reservoir quality prediction for petroleum exploration.

RAISSON, F. & TEMPLE, F. Impact of Sedimentary Heterogeneity on Reservoir Monitoring in a Turbiditic Channel Complex–Angolan Deep Offshore Girassol Field Case. 66th EAGE Conference & Exhibition, 2004.

READING, H. G. & RICHARDS, M. 1994. Turbidite systems in deep-water basin margins classified by grain size and feeder system. *AAPG bulletin,* 78**,** 792-822.

REIJERS, T. 2011. Stratigraphy and sedimentology of the Niger Delta. *Geologos,* 17.

RIDER, M. H. 1986. The geological interpretation of well logs.

ROSALES, I. & PEREZ-GARCIA, A. 2010. Porosity development, diagenesis and basin modelling of a Lower Cretaceous (Albian) carbonate platform from northern Spain. *Geological Society, London, Special Publications,* 329**,** 317-342.

SALEM, A. M., MORAD, S., MATO, L. F. & AL-AASM, I. 2000. Diagenesis and reservoir-quality evolution of fluvial sandstones during progressive burial and uplift: Evidence from the Upper Jurassic Boipeba Member, Reconcavo Basin, Northeastern Brazil. *AAPG bulletin,* 84**,** 1015-1040.

SAMUEL, O. J., CORNFORD, C., JONES, M., ADEKEYE, O. A. & AKANDE, S. O. 2009. Improved understanding of the petroleum systems of the Niger Delta Basin, Nigeria. *Organic Geochemistry,* 40**,** 461-483.

SAUGY, L. & EYER, J. A. 2003. Fifty years of exploration in the Niger Delta (West Africa).

SAVOYE, B., BABONNEAU, N., DENNIELOU, B. & BEZ, M. 2009. Geological overview of the Angola–Congo margin, the Congo deep-sea fan and its submarine valleys. *Deep Sea Research Part II: Topical Studies in Oceanography,* 56**,** 2169-2182.

SCHMIDT, V. & MCDONALD, D. 1979. The role of secondary porosity in the course of sandstone diagenesis. *The Society of Economic Paleontologists and Mineralogists (SPEM),* 26**,** 175-207.

SCHMOKER, J. W. & GAUTIER, D. L. 1988. Sandstone porosity as a function of thermal maturity. *Geology,* 16**,** 1007-1010.

SCHWARZER, D. & LITTKE, R. 2007. Petroleum generation and migration in the 'Tight Gas' area of the German Rotliegend natural gas play: a basin modelling study. *Petroleum Geoscience,* 13**,** 37-62.

SCOTT, R. M. & TILLMAN, R. W. 1981. Stevens Sandstone (Miocene), San Joaquin Basin, California.

SHANMUGAM, G. 1998. Dimensions and geometries of the components of deepwater systems. *Spec.Publ.Mobil Technology Co., Dallas, Tx***,** 110pp.

SHANMUGAM, G. & MOIOLA, R. 1991. Types of Submarine Fan Lobes: Models and Implications (1). *AAPG Bulletin,* 75**,** 156-179.

SHORT, K. & STAUBLE, A. 1967. Outline of geology of Niger Delta. *AAPG bulletin,* 51**,** 761-779.

SIEVER, R. 1983. Burial history and diagenetic reaction kinetics. *AAPG Bulletin,* 67**,** 684-691.

SNEIDER, R. M. 1990. Reservoir Description of Sandstones. *Sandstone Petroleum Reservoirs.* Springer.

SOLDAN, A., CERQUEIRA, J., FERREIRA, J., TRINDADE, L., SCARTON, J. & CORÁ, C. 1995. Giant Deep Water Oil Fields in Campos Basin, Brazil: A Geochemical Approach. *Revista Latino-Americana de Geoquimica Organica,* 1**,** 14-27.

SOMBRA, C. L. & CHANG, H. K. 1997. Burial history and porosity evolution of Brazilian Upper Jurassic to Tertiary sandstone reservoirs.

SONDE, A., OMOBUDE, O., CHUDI, O., OGHENE, U. & COKER, T. Integrated 3D Modelling in a Structurally Complex Brown Field: A Foundation for Improved Reservoir Management and Optimisation of Further Development. Nigeria Annual International Conference and Exhibition, 2011. Society of Petroleum Engineers.

SOUZA, J., SCARTON, J., CANDIDO, A., CRUZ, C. & CORA, C. The Marlim and Albacora Fields: Geophysical Geological and Reservoir Aspects. Offshore Technology Conference, 1989. Offshore Technology Conference.

STONELEY, R. 1966. The Niger delta region in the light of the theory of continental drift. *Geological Magazine,* 103**,** 385-397.

STOW, D., READING, H. & COLLINSON, J. 1996. Deep seas. *Sedimentary environments: processes, facies and stratigraphy,* 3**,** 395-453.

STOW, D. A. & JOHANSSON, M. 2000. Deep-water massive sands: nature, origin and hydrocarbon implications. *Marine and Petroleum Geology,* 17**,** 145-174.

STOW, D. A. & MAYALL, M. 2000. Deep-water sedimentary systems: new models for the 21st century. *Marine and Petroleum Geology,* 17**,** 125-135.

STOW, D. A. & SHANMUGAM, G. 1980. Sequence of structures in fine-grained turbidites: comparison of recent deep-sea and ancient flysch sediments. *Sedimentary Geology,* 25**,** 23-42.

STOW, D. A. V. 2005. *Sedimentary rocks in the field: a colour guide*, CRC Press.

SWEENEY, J. J. & BURNHAM, A. K. 1990. Evaluation of a Simple Model of Vitrinite Reflectance Based on Chemical Kinetics (1). *AAPG Bulletin,* 74**,** 1559-1570.

TADA, R. & SIEVER, R. 1989. Pressure solution during diagenesis. *Annual Review of Earth and Planetary Sciences,* 17**,** 89.

TALÇIN, M. N. 1991. Basin modeling and hydrocarbon exploration. *Journal of Petroleum Science and Engineering,* 5**,** 379-398.

TANER, M. & SHERIFF, R. E. 1977. Application of amplitude, frequency, and other attributes to stratigraphic and hydrocarbon determination: section 2. Application of seismic reflection configuration to stratigraphic interpretation.

TAYLOR, J. M. 1950. Pore-space reduction in sandstones. *AAPG Bulletin,* 34**,** 701-716.

TAYLOR, T. R., GILES, M. R., HATHON, L. A., DIGGS, T. N., BRAUNSDORF, N. R., BIRBIGLIA, G. V., KITTRIDGE, M. G., MACAULAY, C. I. & ESPEJO, I. S. 2010. Sandstone diagenesis and reservoir quality prediction: Models, myths, and reality. *AAPG bulletin,* 94**,** 1093-1132.

TOBIN, R. 1997. Porosity prediction in frontier basins: a systematic approach to estimating subsurface reservoir quality from outcrop samples. In: Kupecz, J.A., Gluyas, J., Bloch, S. (Eds), Reservoir quality prediction in sandstones and carbonates. *American Association of Petroleum Geologists Memoir,* 69**,** 1-18.

TUTTLE, M. L., CHARPENTIER, R. R. & BROWNFIELD, M. E. 1999. *The Niger Delta Petroleum System: Niger Delta Province, Nigeria, Cameroon, and Equatorial Guinea, Africa*, US Department of the Interior, US Geological Survey.

UJJAL KR, D., PANT, D. C., PARIDA, G., RAKESH, R. & BHARDWAJ, A. Application of multi-attribute and spectral decomposition with RGB blending for understanding the strati-structural features: A case study. 10th Biennial International Conference & Exposition, 2013 Kochi, India. Society of Petroleum Geophysicist, 1-8.

UNDERDOWN, R. & REDFERN, J. 2008. Petroleum generation and migration in the Ghadames Basin, north Africa: A two-dimensional basin-modeling study. *AAPG bulletin,* 92**,** 53-76.

WALDERHAUG, O. 1994. Precipitation rates for quartz cement in sandstones determined by fluid-inclusion microthermometry and temperature-history modeling. *Journal of Sedimentary Research,* 64**,** 324-333.

WALDERHAUG, O. 1996. Kinetic modeling of quartz cementation and porosity loss in deeply buried sandstone reservoirs. *AAPG bulletin,* 80**,** 731-745.

WALDERHAUG, O. 2000. Modeling quartz cementation and porosity in Middle Jurassic Brent Group sandstones of the Kvitebjørn field, northern North Sea. *AAPG bulletin,* 84**,** 1325-1339.

WALDERHAUG, O., LANDER, R., BJØRKUM, P., OELKERS, E., BJØRLYKKE, K. & NADEAU, P. 2009. Modelling quartz cementation and porosity in reservoir sandstones: examples from the Norwegian continental shelf. *Quartz cementation in sandstones***,** 39-49.

WAPLES, D. 1998. Basin modelling: how well have we done? *Geological Society, London, Special Publications,* 141**,** 1-14.

WAPLES, D. & COUPLES, G. 1998. Some thoughts on porosity reduction—rock mechanics, overpressure and fluid flow. *Geological Society, London, Special Publications,* 141**,** 73-81.

WAPLES, D. W., KAMATA, H. & SUIZU, M. 1992. The art of maturity modeling. Part 1: Finding a satisfactory geologic model. *AAPG Bulletin (American Association of Petroleum Geologists);(United States),* 76.

WEBER, K. 1971. Sedimentological aspects of oil fields in the Niger Delta. *Geologie en Mijnbouw,* 50**,** 559-576.
WEI, X. Interpretational Applications of Spectral Decomposition in Identifying Minor Faults. 72nd EAGE Conference & Exhibition, 2010.
WELTE, D. & YALCIN, M. 1988a. Basin modelling--a new comprehensive method in petroleum geology. *Organic geochemistry,* 13**,** 141-151.
WELTE, D. & YALCIN, M. 1988b. Basin modelling—a new comprehensive method in petroleum geology. *Organic Geochemistry,* 13**,** 141-151.
WELTE, D. H., HORSFIELD, B. & BAKER, D. R. 1997. *Petroleum and basin evolution: insights from petroleum geochemistry, geology and basin modeling,* Verlag Berling Heidelberg, Springer.
WESTWOOD, J. & KNIGHT, R. 2001. West African Deep Water: Development Prospects In A Global Context.
WHITE, R. & SIMM, R. 2003. Tutorial: Good practice in well ties. *First Break,* 21.
WHITEMAN, A. 1982. Nigeria: Its petroleum geology, resources and potential vol 1.
WILKINSON, M., STUART HASZELDINE, R., ELLAM, R. M. & FALLICK, A. 2004. Hydrocarbon filling history from diagenetic evidence: Brent Group, UK North Sea. *Marine and petroleum geology,* 21**,** 443-455.
WOOD, J. R. & BRYRNES, A. P. 1994. Alternate and emerging methodologies in geochemical and empirical modeling. *The Society for Sedimentary Geology (SEPM),* SC30.
WOOD, L. J. & MIZE-SPANSKY, K. L. 2009. Quantitative seismic geomorphology of a Quaternary leveed-channel system, offshore eastern Trinidad and Tobago, northeastern South America. *AAPG Bulletin,* 93**,** 101-125.
WORDEN, R. & MORAD, S. 2000. Quartz cementation in oil field sandstones: a review of the key controversies. *Quartz cementation in sandstones,* 29**,** 1-20.
WORDEN, R. H., OXTOBY, N. H. & SMALLEY, P. C. 1998. Can oil emplacement prevent quartz cementation in sandstones? *Petroleum Geoscience,* 4**,** 129-137.
WYGRALA, B. 1988. Integrated computer-aided basin modeling applied to analysis of hydrocarbon generation history in a Northern Italian oil field. *Organic geochemistry,* 13**,** 187-197.
WYNN, R. B., KENYON, N. H., MASSON, D. G., STOW, D. A. & WEAVER, P. P. 2002a. Characterization and recognition of deep-water channel-lobe transition zones. *AAPG bulletin,* 86.
WYNN, R. B., WEAVER, P. P., MASSON, D. G. & STOW, D. A. 2002b. Turbidite depositional architecture across three interconnected deep-water basins on the north-west African margin. *Sedimentology,* 49**,** 669-695.
YALCIN, N. M. 1991. Basin modeling and hydrocarbon exploration. *Journal of Petroleum Science and Engineering,* 5**,** 379-398.

TAYLOR, J. M. 1950. Pore-space reduction in sandstones. *AAPG Bulletin,* 34**,** 701-716.
TAYLOR, T. R., GILES, M. R., HATHON, L. A., DIGGS, T. N., BRAUNSDORF, N. R., BIRBIGLIA, G. V., KITTRIDGE, M. G., MACAULAY, C. I. & ESPEJO, I. S. 2010. Sandstone diagenesis and reservoir quality prediction: Models, myths, and reality. *AAPG bulletin,* 94**,** 1093-1132.
TOBIN, R. 1997. Porosity prediction in frontier basins: a systematic approach to estimating subsurface reservoir quality from outcrop samples. In: Kupecz, J.A., Gluyas, J., Bloch, S. (Eds), Reservoir quality prediction in sandstones and carbonates. *American Association of Petroleum Geologists Memoir,* 69**,** 1-18.
TUTTLE, M. L., CHARPENTIER, R. R. & BROWNFIELD, M. E. 1999. *The Niger Delta Petroleum System: Niger Delta Province, Nigeria, Cameroon, and Equatorial Guinea, Africa*, US Department of the Interior, US Geological Survey.

UNDERDOWN, R. & REDFERN, J. 2008. Petroleum generation and migration in the Ghadames Basin, north Africa: A two-dimensional basin-modeling study. *AAPG bulletin,* 92**,** 53-76.

WALDERHAUG, O. 1994. Precipitation rates for quartz cement in sandstones determined by fluid-inclusion microthermometry and temperature-history modeling. *Journal of Sedimentary Research,* 64**,** 324-333.

WALDERHAUG, O. 1996. Kinetic modeling of quartz cementation and porosity loss in deeply buried sandstone reservoirs. *AAPG bulletin,* 80**,** 731-745.

WALDERHAUG, O. 2000. Modeling quartz cementation and porosity in Middle Jurassic Brent Group sandstones of the Kvitebjørn field, northern North Sea. *AAPG bulletin,* 84**,** 1325-1339.

WALDERHAUG, O., LANDER, R., BJØRKUM, P., OELKERS, E., BJØRLYKKE, K. & NADEAU, P. 2009. Modelling quartz cementation and porosity in reservoir sandstones: examples from the Norwegian continental shelf. *Quartz cementation in sandstones***,** 39-49.

WAPLES, D. 1998. Basin modelling: how well have we done? *Geological Society, London, Special Publications,* 141**,** 1-14.

WAPLES, D. & COUPLES, G. 1998. Some thoughts on porosity reduction—rock mechanics, overpressure and fluid flow. *Geological Society, London, Special Publications,* 141**,** 73-81.

WAPLES, D. W., KAMATA, H. & SUIZU, M. 1992. The art of maturity modeling. Part 1: Finding a satisfactory geologic model. *AAPG Bulletin (American Association of Petroleum Geologists);(United States),* 76.

WEBER, K. 1971. Sedimentological aspects of oil fields in the Niger Delta. *Geologie en Mijnbouw,* 50**,** 559-576.

WEI, X. Interpretational Applications of Spectral Decomposition in Identifying Minor Faults. 72nd EAGE Conference & Exhibition, 2010.

WELTE, D. & YALCIN, M. 1988a. Basin modelling--a new comprehensive method in petroleum geology. *Organic geochemistry,* 13**,** 141-151.

WELTE, D. & YALCIN, M. 1988b. Basin modelling—a new comprehensive method in petroleum geology. *Organic Geochemistry,* 13**,** 141-151.

WELTE, D. H., HORSFIELD, B. & BAKER, D. R. 1997. *Petroleum and basin evolution: insights from petroleum geochemistry, geology and basin modeling,* Verlag Berling Heidelberg, Springer.

WESTWOOD, J. & KNIGHT, R. 2001. West African Deep Water: Development Prospects In A Global Context.

WHITEMAN, A. 1982. Nigeria: Its petroleum geology, resources and potential vol 1.

WILKINSON, M., STUART HASZELDINE, R., ELLAM, R. M. & FALLICK, A. 2004. Hydrocarbon filling history from diagenetic evidence: Brent Group, UK North Sea. *Marine and petroleum geology,* 21**,** 443-455.

WOOD, J. R. & BRYRNES, A. P. 1994. Alternate and emerging methodologies in geochemical and empirical modeling. *The Society for Sedimentary Geology (SEPM),* SC30.

WOOD, L. J. & MIZE-SPANSKY, K. L. 2009. Quantitative seismic geomorphology of a Quaternary leveed-channel system, offshore eastern Trinidad and Tobago, northeastern South America. *AAPG Bulletin,* 93**,** 101-125.

WORDEN, R. & MORAD, S. 2000. Quartz cementation in oil field sandstones: a review of the key controversies. *Quartz cementation in sandstones,* 29**,** 1-20.

WORDEN, R. H., OXTOBY, N. H. & SMALLEY, P. C. 1998. Can oil emplacement prevent quartz cementation in sandstones? *Petroleum Geoscience,* 4**,** 129-137.

WYGRALA, B. 1988. Integrated computer-aided basin modeling applied to analysis of hydrocarbon generation history in a Northern Italian oil field. *Organic geochemistry,* 13**,** 187-197.

WYNN, R. B., KENYON, N. H., MASSON, D. G., STOW, D. A. & WEAVER, P. P. 2002a. Characterization and recognition of deep-water channel-lobe transition zones. *AAPG bulletin,* 86.

WYNN, R. B., WEAVER, P. P., MASSON, D. G. & STOW, D. A. 2002b. Turbidite depositional architecture across three interconnected deep-water basins on the north-west African margin. *Sedimentology,* 49**,** 669-695.

YALCIN, N. M. 1991. Basin modeling and hydrocarbon exploration. *Journal of Petroleum Science and Engineering,* 5**,** 379-398.